PB94-181773

30272-101

REPORT DOCUMENTATION PAGE	1. REPORT NO. NCEER-93-0019	2.	

4. Title and Subtitle
Development of an Earthquake Motion Simulator and its Application in Dynamic Centrifuge Testing

5. Report Date
October 23, 1993

6.

7. Author(s)
I. Krstelj (supervised by J.H. Prevost)

8. Performing Organization Rept. No.

9. Performing Organization Name and Address
Princeton University
School of Engineering and Applied Sciences
Department of Civil Engineering and Operations Research
Princeton, New Jersey

10. Project/Task/Work Unit No.

11. Contract(C) or Grant(G) No.
(C) BCS-89-22869
BCS 90-25010
(G) NEC-91029

12. Sponsoring Organization Name and Address
National Center for Earthquake Engineering Research
State University of New York at Buffalo
Red Jacket Quadrangle
Buffalo, New York 14261

13. Type of Report & Period Covered
Technical Report

14.

15. Supplementary Notes
This research was conducted at Princeton University and was partially supported by the National Science Foundation under Grant No. BCS 90-25010 and the New York State Science and Technology Foundation under Grant No. NEC-91029.

16. Abstract (Limit: 200 words)
Centrigue model studies of dynamics effects in soils are dependent upon the capability to simulate the excitation due to earthquakes. Various efforts have been made by experimentalists to design and develop such capabilities for existing geotechnical centrifuges. This study reports on the development of an electro-hydraulic earthquake motion simulator for the Princeton University geotechnical centrifuge. The success of the Princeton ground motion simulator indicates that application of electro-hydraulic shaker technology in centrifuge dynamic testing does not necessarily require high investments. The first group of tests performed with the electro-hydraulic ground motion simulator are part of the VELACS (Verification of Liquefaction Analysis by Centrifuge Studies) project. A soil deposit constructed with two layers, sand and silt, was tested to study dynamic behavior of non-uniform horizontal soil deposits. Next, an experimental study of soil-structure interaction effects was performed with geometry of the test corresponding to one of the collapsed Niigata apartments, damaged due to the liquefaction induced by 1964 Niigata earthquake. The experimental results are compared with results obtained from different methods of numerical analysis encompassed in computer codes DYNA1D and DYNA-FLOW developed at Princeton University.

17. Document Analysis a. Descriptors

b. Identifiers/Open-Ended Terms
Geotechnical centrifuges. Verification of Liquefaction Analysis by Centrifuge Studies (VELACS). Ground motion simulators. Electrohydraulic shakers. Servovalves. Hydraulic systems. Testing methods. Earthquake engineering.

c. COSATI Field/Group

18. Availability Statement
Release Unlimited

19. Security Class (This Report)
Unclassified

20. Security Class (This Page)
Unclassified

21. No. of Pages
218

22. Price

(See ANSI-Z39.18) See Instructions on Reverse OPTIONAL FORM 272 (4-77) (Formerly NTIS-35)

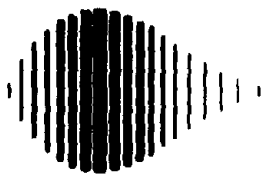

NATIONAL CENTER FOR EARTHQUAKE
ENGINEERING RESEARCH
State University of New York at Buffalo

PB94-181773

Development of an Earthquake Motion Simulator and its Application in Dynamic Centrifuge Testing

by
I. Krstelj

Supervised by J.H. Prevost

Princeton University
School of Engineering and Applied Sciences
Department of Civil Engineering and Operations Research
Princeton, New Jersey 08544

Technical Report NCEER-93-0019

October 23, 1993

REPRODUCED BY:
U.S. Department of Commerce
National Technical Information Service
Springfield, Virginia 22161

This research was conducted at Princeton University and was partially supported by the National Science Foundation under Grant No. BCS 90-25010 and the New York State Science and Technology Foundation under Grant No. NEC-91029.

NOTICE

This report was prepared by Princeton University as a result of research sponsored by the National Center for Earthquake Engineering Research (NCEER) through grants from the National Science Foundation, the New York State Science and Technology Foundation, and other sponsors. Neither NCEER, associates of NCEER, its sponsors, Princeton University, nor any person acting on their behalf:

a. makes any warranty, express or implied, with respect to the use of any information, apparatus, method, or process disclosed in this report or that such use may not infringe upon privately owned rights; or

b. assumes any liabilities of whatsoever kind with respect to the use of, or the damage resulting from the use of, any information, apparatus, method, or process disclosed in this report.

Any opinions, findings, and conclusions or recommendations expressed in this publication are those of the author(s) and do not necessarily reflect the views of NCEER, the National Science Foundation, the New York State Science and Technology Foundation, or other sponsors.

Development of an Earthquake Motion Simulator and its Application in Dynamic Centrifuge Testing

by

I. Krstelj[1]

Supervised by J.H. Prevost[2]

October 23, 1993

Technical Report NCEER-93-0019

NCEER Project Number 89-1504
and
NSF Velacs Contract Number BSC-89-22869

NSF Master Contract Number BCS 90-25010
and
NYSSTF Grant Number NEC-91029

1 Graduate Student, Department of Civil Engineering and Operations Research, Princeton University
2 Professor, Department of Civil Engineering and Operations Research, Princeton University

NATIONAL CENTER FOR EARTHQUAKE ENGINEERING RESEARCH
State University of New York at Buffalo
Red Jacket Quadrangle, Buffalo, NY 14261

PREFACE

The National Center for Earthquake Engineering Research (NCEER) was established to expand and disseminate knowledge about earthquakes, improve earthquake-resistant design, and implement seismic hazard mitigation procedures to minimize loss of lives and property. The emphasis is on structures in the eastern and central United States and lifelines throughout the country that are found in zones of low, moderate, and high seismicity.

NCEER's research and implementation plan in years six through ten (1991-1996) comprises four interlocked elements, as shown in the figure below. Element I, Basic Research, is carried out to support projects in the Applied Research area. Element II, Applied Research, is the major focus of work for years six through ten. Element III, Demonstration Projects, have been planned to support Applied Research projects, and will be either case studies or regional studies. Element IV, Implementation, will result from activity in the four Applied Research projects, and from Demonstration Projects.

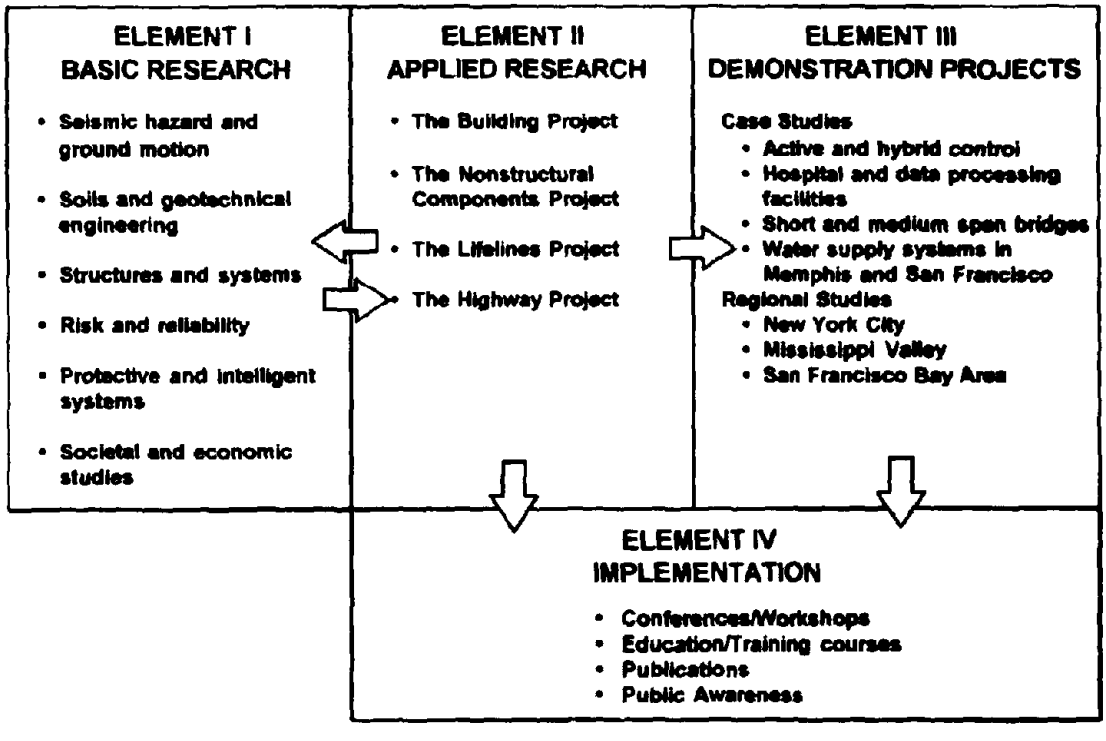

Tasks in Element I, **Basic Research,** include research in seismic hazard and ground motion; soils and geotechnical engineering; structures and systems; risk and reliability; protective and intelligent systems; and societal and economic impact.

The soils and geotechnical engineering program constitutes one of the important areas of research in Element I, **Basic Research**. Major tasks are described as follows:

1. Perform site response studies for code development.
2. Develop a better understanding of large lateral and vertical permanent ground deformations associated with liquefaction, and develop corresponding simplified engineering methods.
3. Continue U.S. - Japan cooperative research in liquefaction, large ground deformation, and effects on buried pipelines.
4. Perform soil-structure interaction studies on soil-pile-structure interaction and bridge foundations and abutments, with the main focus on large deformations and the effect of ground failure on structures.
5. Study small earth dams and embankments.

This report describes the development of an earthquake motion simulator for centrifuge testing and its application to studying the dynamic response of saturated soil deposits. Two groups of tests were performed. The first tests were part of the Verification of Liquefaction Analysis by Centrifuge Studies (VELACS) project sponsored by the National Science Foundation. The results from these tests were used to study the validity of the liquefaction analysis programs DYNA1D and DYNAFLOW. It was confirmed that both programs can closely simulate the details of the experimental centrifuge liquefaction test.

A second set of tests were performed to investigate soil-structure interaction. The results were correlated with numerical simulations from the DYNAFLOW computer program. Comparisons of computed versus recorded structure accelerations and pore water pressure variations were found to be in good agreement.

ABSTRACT

Centrifuge model studies of dynamics effects in soils are dependent upon the capability to simulate the excitation due to earthquakes. Various efforts have been made by experimentalists to design and develop such capabilities for existing geotechnical centrifuges. This study reports on the development of an electro-hydraulic earthquake motion simulator for the Princeton University geotechnical centrifuge. The success of the Princeton ground motion simulator indicates that application of electro-hydraulic shaker technology in centrifuge dynamic testing does not necessarily require high investments.

The first group of tests performed with the electro-hydraulic ground motion simulator are part of the VELACS (Verification of Liquefaction Analysis by Centrifuge Studies) project. A soil deposit constructed with two layers, sand and silt, was tested to study dynamic behavior of non-uniform horizontal soil deposits.

Next, an experimental study of soil-structure interaction effects was performed with geometry of the test corresponding to one of the collapsed Niigata apartments, damaged due to the liquefaction induced by 1964 Niigata earthquake.

The experimental results are compared with results obtained from different methods of numerical analysis encompassed in computer codes DYNA1D and DYNAFLOW developed at Princeton University.

ACKNOWLEDGMENT

This report documents research performed at Princeton University which was supported in part by National Science Foundation grants No. BCS-89-22869 (VELACS Project, Dr. C. Astill Manager), and by National Center for Earthquake Engineering Research subcontract No. NCEER 89-1504 under NSF grant No. ECE 86-07591. The report is based on the master thesis by Igor Krstelj submitted in October, 1992 to the Department of Civil Engineering and Operations Research at Princeton University in partial fulfillment of the requirements for the M.S. degree.

TABLE OF CONTENTS

SECTION	TITLE	PAGE
1	**INTRODUCTION**	1-1
2	**BACKGROUND**	2-1
2.1	Liquefaction	2-1
2.2	History of Centrifugal Modelling	2-4
2.3	Principles of Centrifugal Modelling	2-5
2.4	Princeton University Geotechnical Centrifuge Facility	2-8
3	**GROUND MOTION SIMULATOR**	3-1
3.1	Introduction	3-1
3.2	Types of Ground Motion Simulators	3-1
3.3	Princeton University Designs	3-3
3.4	Electro-Hydraulic Shaker	3-5
3.4.1	Hydraulic Subsystem	3-5
3.4.2	Electronic Subsystem	3-7
3.4.3	Slip Table	3-12
3.5	Instrumentation and Data Acquisition System	3-14
4	**VELACS PROJECT**	4-1
4.1	Introduction	4-1
4.2	Standard Model Check Test	4-2
4.3	100*g* Tests	4-3
4.3.1	100*g* Tests Comparison	4-5
4.4	75*g* Tests	4-9
4.4.1	75*g* Tests Comparison	4-9
4.5	Comparison Between the 100*g* and the 75*g* Tests (Modelling of Models Concept)	4-13
4.6	Vertical Displacements	4-14
4.7	Numerical Simulation	4-22
4.7.1	Introduction and Background	4-22
4.7.2	One-Dimensional Finite Element Discretization	4-23
4.7.3	Two-Dimensional Finite Element Discretization	4-24
4.7.4	Material Properties	4-26
4.7.5	Test Results	4-35
4.8	Appendix	4-48
5	**SOIL-STRUCTURE INTERACTION**	5-1
5.1	Introduction	5-1
5.2	Soil Structure Interaction Centrifuge Tests	5-2
5.2.1	Sample Preparation	5-2
5.2.2	Test Procedure	5-3
5.3	Numerical Analysis	5-4

TABLE OF CONTENTS (Cont'd)

SECTION	TITLE	PAGE
5.3.1	Simulation Procedure	5-4
5.3.2	Material Properties	5-11
5.4	Test Results and Comparisons	5-13
6	**CONCLUSIONS**	6-1
7	**REFERENCES**	7-1
APPENDIX A	**SUMMARY OF THE MODEL TESTS**	A-1
APPENDIX B	**VELACS 100*g* TESTS**	B-1
B.1	Test 100*g/I*	B-1
B.2	Test 100*g/II*	B-11
APPENDIX C	**VELACS 75*g* TESTS**	C-1
C.1	Test 75*g/I*	C-1
C.2	Test 75*g/II*	C-13
C.3	Test 75*g Glycerin/I*	C-25
C.4	Tests With the Bonnie Silt (Bonnie/I & Bonnie/II)	C-31
APPENDIX D	**SOIL-STRUCTURE INTERACTION TESTS**	D-1
D.1	Test #1	D-1
D.2	Test #2	D-8

LIST OF ILLUSTRATIONS

FIGURE	TITLE	PAGE
1.1	Damage Caused by 1964 Niigata Earthquake	1-2
2.1	Prototype Model	2-6
2.2	P.U. Geotechnical Centrifuge Laboratory	2-9
2.3	P.U. Geotechnical Centrifuge Operating Range	2-10
2.4	P.U. Geotechnical Centrifuge Schematic	2-11
3.1	Old Hammer-Exciter Shaker on P.U. Geotechnical Centrifuge	3-4
3.2	Shaker Hydraulic Subsystem on the Princeton Geotechnical Centrifuge	3-8
3.3	Team Assembly Head and Moog Servovalve Mounted on the Swing Platform	3-9
3.4	Team Assembly Head and Moog Servovalve	3-10
3.5	Electronic Subsystem of the Ground Motion Simulator	3-11
3.6	Horizontal and Vertical Acceleration Time History Comparison	3-13
4.1	Comparison of the Measured Acceleration Time Histories of the 100*g* Tests	4-6
4.2	Comparison of the Measured Pore Water Pressure Time Histories of the 100*g* Tests	4-7
4.3	Comparison of the Measured Pore Water Pressure Time Histories (Long-Term) of the 100*g* Tests	4-8
4.4	Comparison of the Measured Horizontal Acceleration Time Histories of the 75*g* Tests	4-10
4.5	Comparison of the Measured Pore Water Pressure Time Histories of the 75*g* Tests	4-11
4.6	Comparison of the Measured Pore Water Pressure Time Histories (Long Term) of the 75*g* Tests	4-12
4.7	Standard VELACS Model Test Acceleration Time Histories Comparison Between 100*g* and 75*g* Tests	4-15
4.8	Standard VELACS Model Test Short Term Pore Pressure Ratio Time Histories Comparison Between 100*g* and 75*g* Tests	4-16
4.9	Standard VELACS Model Test Long Term Pore Pressure Ratio Time Histories Comparison Between 100*g* and 75*g* Tests	4-17
4.10	Short Term Vertical Displacement Comparisons of the Two 75*g* Tests With the Bonnie Silt	4-19
4.11	Long Term Vertical Displacement Comparisons of the Two 75*g* Tests With the Bonnie Silt	4-20
4.12	Long Term Vertical Displacements and Long Term Pore Water Pressure Time History of the Test Bonnie/1	4-21
4.13	1D Numerical Model for the VELACS Standard Test	4-25
4.14	2D Numerical Model for the VELACS Standard Test	4-27

LIST OF ILLUSTRATIONS (Cont'd)

FIGURE	TITLE	PAGE
4.15	Drucker-Prager and Mohr-Coulomb Criteria	4-32
4.16	Mobilized Friction Angle From the 'Triaxial' Compression Tests	4-33
4.17	Mobilized Friction Angle From the 'Triaxial' Extension Tests	4-34
4.18	Equivalent Friction Angle (Plain Strain) Versus Friction Angle (Axial Compression)	4-35
4.19	Comparison of the Measured and Computed Acceleration Time Histories on the Silt Surface	4-38
4.20	Comparison of the Measured and Computed Acceleration Time Histories on the Silt Layer	4-39
4.21	Comparison of the Measured and Computed Pore Pressure Time Histories in the Sand Layer	4-40
4.22	Comparison of the Measured and Computed Pore Pressure Time Histories in the Sand Layer	4-41
4.23	Comparison of the Measured and Computed Pore Pressure Time Histories in the Sand Layer With Permeabilities Increased 75 Times	4-42
4.24	Comparison of the Measured and Computed Pore Pressure Time Histories in the Sand Layer With Permeabilities Increased 10 Times	4-43
4.25	Comparison of the Measured and Computed Pore Pressure Time Histories in the Sand Layer With 1D and 2D Analysis	4-44
4.26	Comparison of the Measured Pore Pressure Time Histories in the Sand Layer on the Side of the Box With Corresponding Results of the 1D Analysis	4-45
4.27	Comparison of the Computed Pore Pressure Time Histories in the Sand Layer With 1D and 2D Analysis on the Side of the Box	4-46
4.28	Comparison of the Measured and Computed Pore Pressure Time Histories in the Sand Layer With 1D and 2D Analysis on the Side of the Box	4-47
4.29	Comparison of the Pore Pressure Time Histories in the Sand Layer Obtained With DYNA1D and DYNAFLOW 1D Analysis	4-49
4.30	Comparison of the Pore Pressure Time Histories in the Sand Layer Obtained With DYNAFLOW 1D Analysis and 2D Analysis of 1D Elements	4-50
4.31	Comparison of the Pore Pressure Time Histories in the Sand Layer Obtained With DYNAFLOW 1D and DYNAFLOW 2D with Free Field B.C. Analysis	4-51
4.32	Comparison of the Pore Pressure Time Histories in the Sand Layer Obtained With DYNAFLOW 1D and DYNAFLOW 2D with Rigid Box B.C. Analysis	4-52

LIST OF ILLUSTRATIONS (Cont'd)

FIGURE	TITLE	PAGE
5.1	Soil-Structure Interaction Model Test # I, Before and After the Event	5-5
5.2	Acceleration Time Histories Comparisons	5-6
5.3	Comparisons of the Excessive Pore Pressure Time Histories Below the Structure	5-7
5.4	Comparisons of the Excessive Pore Pressure Time Histories, Free Field Versus Below the Structure	5-8
5.5	Soil-Structure Finite Element Mesh	5-10
5.6	Comparison Between the Computed With DYNAFLOW and the Recorded Acceleration Time Histories of the Structure (Test II)	5-14
5.7	Comparison Between the Computed With DYNAFLOW and the Recorded Excessive Pore Pressure Time Histories	5-15
5.8	Deformed Finite Element Mesh	5-16
5.9	Computed Structure Vertical Displacement Time Histories	5-17
B.1	Standard VELACS Model Test 100*g/I*	B-2
B.2	Standard VELACS Model Test 100*g/I* Horizontal Acceleration of the Base	B-4
B.3	Standard VELACS Model Test 100*g/I* Vertical Acceleration of the Base	B-5
B.4	Standard VELACS Model Test 100*g/I* Horizontal Acceleration in the Silt Layer	B-6
B.5	Standard VELACS Model Test 100*g/I* Short Term Pore Pressure Ratio Time Histories	B-7
B.6	Standard VELACS Model Test 100*g/I* Long Term Pore Pressure Ratio Time Histories	B-8
B.7	Standard VELACS Model Test 100*g/I* Stress and Pore Pressure Variations With Depth	B-9
B.8	Standard VELACS Model Test 100*g/I* Vertical Displacement of the Silt Surface	B-10
B.9	Standard VELACS Model Test 100*g/II*	B-12
B.10	Standard VELACS Model Test 100*g/II* Horizontal Acceleration of the Base	B-13
B.11	Standard VELACS Model Test 100*g/II* Vertical Acceleration of the Base	B-14
B.12	Standard VELACS Model Test 100*g/II* Horizontal Acceleration in the Silt Layer	B-15
B.13	Standard VELACS Model Test 100*g/II* Horizontal Acceleration on the Silt Surface	B-16
B.14	Standard VELACS Model Test 100*g/II* Short Term Pore Pressure Ratio Time Histories	B-17

LIST OF ILLUSTRATIONS (Cont'd)

FIGURE	TITLE	PAGE
B.15	Standard VELACS Model Test 100*g*/*II* Long Term Pore Pressure Ratio Time Histories	B-18
B.16	Standard VELACS Model Test 100*g*/*II* Stress and Pore Pressure Variations With Depth	B-19
C.1	Standard VELACS Model Test 75*g*/*I*	C-2
C.2	Standard VELACS Model Test 75*g*/*I* Horizontal Acceleration of the Base	C-4
C.3	Standard VELACS Model Test 75*g*/*I* Vertical Acceleration of the Base	C-5
C.4	Standard VELACS Model Test 75*g*/*I* Horizontal Acceleration in the Silt Layer	C-6
C.5	Standard VELACS Model Test 75*g*/*I* Vertical Acceleration in the Silt Layer	C-7
C.6	Standard VELACS Model Test 75*g*/*I* Horizontal Acceleration on the Silt Surface	C-8
C.7	Standard VELACS Model Test 75*g*/*I* Vertical Acceleration on the Silt Surface	C-9
C.8	Standard VELACS Model Test 75*g*/*I* Short Term Pore Pressure Ratio Time Histories	C-10
C.9	Standard VELACS Model Test 75*g*/*I* Long Term Pore Pressure Ratio Time Histories	C-11
C.10	Standard VELACS Model Test 75*g*/*I* Stress and Pore Pressure Variations With Depth	C-12
C.11	Standard VELACS Model Test 75*g*/*II*	C-14
C.12	Standard VELACS Model Test 75*g*/*II* Horizontal Acceleration of the Base	C-15
C.13	Standard VELACS Model Test 75*g*/*II* Vertical Acceleration of the Base	C-16
C.14	Standard VELACS Model Test 75*g*/*II* Horizontal Acceleration in the Silt Layer	C-17
C.15	Standard VELACS Model Test 75*g*/*II* Vertical Acceleration in the Silt Layer	C-18
C.16	Standard VELACS Model Test 75*g*/*II* Horizontal Acceleration on the Silt Surface	C-19
C.17	Standard VELACS Model Test 75*g*/*II* Vertical Acceleration on the Silt Surface	C-20
C.18	Standard VELACS Model Test 75*g*/*II* Short Term Pore Pressure Ratio Time Histories	C-21
C.19	Standard VELACS Model Test 75*g*/*II* Short Term Pore Pressure Ratio Time Histories Comparison Between the Side and the Center of the Testing Box	C-22

LIST OF ILLUSTRATIONS (Cont'd)

FIGURE	TITLE	PAGE
C.20	Standard VELACS Model Test 75*g/II* Long Term Pore Pressure Ratio Time Histories	C-23
C.21	Standard VELACS Model Test 75*g/II* Stress and Pore Pressure Variations With Depth	C-24
C.22	Standard VELACS Model Test 75*g Glycerin/I*	C-26
C.23	Standard VELACS Model Test 75*g Glycerin/I* Input Acceleration Time Histories	C-27
C.24	Standard VELACS Model Test 75*g Glycerin/I* Horizontal Acceleration Time Histories	C-28
C.25	Standard VELACS Model Test 75*g Glycerin/I* Vertical Acceleration Time Histories	C-29
C.26	Standard VELACS Model Test 75*g Glycerin/I* Pore Fluid Pressure Ratio Time Histories	C-30
C.27	Standard VELACS Model Test 75*g Bonnie/I*	C-33
C.28	Standard VELACS Model Test 75*g Bonnie/I* Horizontal Acceleration Time Histories	C-34
C.29	Standard VELACS Model Test 75*g Bonnie/I* Short Term Pore Water Pressure Time Histories	C-35
C.30	Standard VELACS Model Test 75*g Bonnie/I* Long Term Pore Water Pressure Time Histories	C-36
C.31	Standard VELACS Model Test 75*g Bonnie/I* Short Term Vertical Displacement Time Histories	C-37
C.32	Standard VELACS Model Test 75*g Bonnie/I* Long Term Vertical Displacement Time Histories	C-38
C.33	Standard VELACS Model Test 75*g Bonnie/II*	C-39
C.34	Standard VELACS Model Test 75*g Bonnie/II* Horizontal Acceleration Time Histories	C-40
C.35	Standard VELACS Model Test 75*g Bonnie/II* Short Term Pore Water Pressure Time Histories	C-41
C.36	Standard VELACS Model Test 75*g Bonnie/II* Long Term Pore Water Pressure Time Histories	C-42
C.37	Standard VELACS Model Test 75*g Bonnie/II* Short Term Vertical Displacement Time Histories	C-43
C.38	Standard VELACS Model Test 75*g Bonnie/II* Long Term Vertical Displacement Time Histories	C-44
D.1	Soil-Structure Model Test I	D-3
D.2	Soil-Structure Interaction Test I, Horizontal Acceleration Time Histories	D-4
D.3	Soil-Structure Interaction Test I, Vertical Acceleration Time Histories	D-5

LIST OF ILLUSTRATIONS (Cont'd)

FIGURE	TITLE	PAGE
D.4	Soil-Structure Interaction Test I, Excessive Pore Pressure Time Histories Below the Structure	D-6
D.5	Soil-Structure Interaction Test I, Excessive Pore Pressure Time Histories Comparison, Free Field Versus Below the Structure	D-7
D.6	Soil-Structure Model Test II	D-10
D.7	Soil-Structure Interaction Test II, Horizontal Acceleration Time Histories	D-11
D.8	Soil-Structure Interaction Test II, Vertical Acceleration Time Histories	D-12
D.9	Soil-Structure Interaction Test II, Excessive Pore Pressure Time Histories Below the Structure	D-13
D.10	Soil-Structure Interaction Test II, Excessive Pore Pressure Time Histories Comparison, Free Field Versus Below the Structure	D-14

LIST OF TABLES

TABLE	TITLE	PAGE
2.1	Scaling Relations	2-7
2.2	Available and Used Connections Through the Centrifuge Axis	2-12
3.1	Comparison of Various Methods for Simulating Earthquake Ground Motions on Centrifuge	3-2
4.1	Standard VELACS Model Tests Performed on Princeton Geotechnical Centrifuge	4-3
4.2	Material Properties Used in Numerical Analysis	4-28
5.1	Material Properties Used in Numerical Analysis	5-12

Section 1

Introduction

Earthquakes can so often be violent, and so far they have been unpredictable. Their activity produces injury, damage, and helplessness, so people have always feared them. Popular legends in many countries attributed earthquakes to underground monsters and gods. In Japanese ancient folklore a great catfish (*namazu*) causes earthquakes by thrashing its body; its activity can only be restrained by a god (*dainyojin*). But when the attention of the *dainyojin* wanders the *namazu* moves and the ground shakes.

Most of the modern world today uses what are believed to be more scientific approaches. Because of the complex nature of earthquake effects, current investigations encompass many disciplines, including those of the both physical and social sciences.

The engineering part is in employing appropriate countermeasures to decrease the hazard to urban and rural areas that can lead to disasters, and in providing an adequate degree of safety at an affordable cost. That requires an extensive knowledge and high level of expertise in earthquake engineering.

The influence of saturated soils on the behavior of structures received little or no attention from engineers until the early 1960's. However, a series of catastrophic failures, such as landslides during the 1964 Alaska earthquake, and extreme liquefaction during the Niigata earthquake in 1964 (Figure 1.1) brought scientist's interest

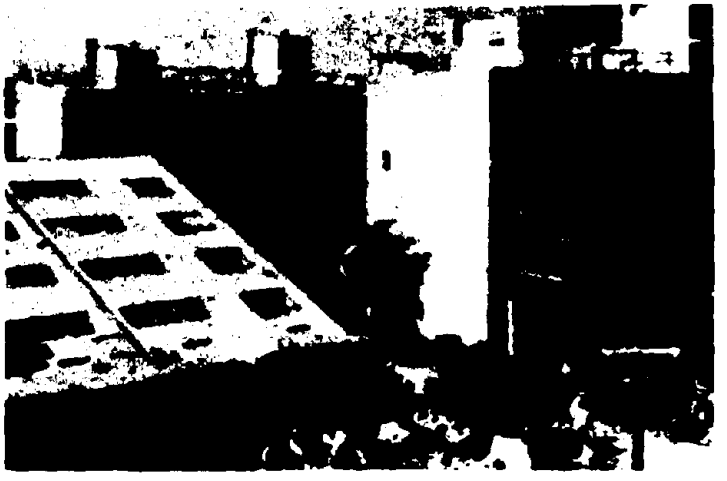

Figure 1.1: **Damage caused by 1964 Niigata Earthquake**

to the field of soil dynamics.

In recent years, there have been a number of model studies of the earthquake response of saturated soils, and soil-structure interaction using geotechnical centrifuges. Still, there is a need for further model studies, and new equipment that would enable systematic and careful experimental methods.

This study includes the development of a centrifuge earthquake motion simulator, and its use in small-scale modelling of soil liquefaction and soil-structure interaction.

The report provides a review of liquefaction phenomenon, centrifuge testing and the Princeton University centrifuge facility (Section 2).

The structure of the shaker system is presented in Section 3 together with its

performance and ability to maintain desired earthquake-like excitation on a testing model.

First geotechnical testing, performed with the Princeton University hydraulic ground motion simulator was a part of the Verification of Liquefaction Analysis by Centrifuge Studies project (VELACS). A brief introduction to the VELACS project and a description of performed tests and numerical simulations are presented in Section 4 .

Section 5 details the soil-structure interaction model tests and numerical simulation with DYNAFLOW code.

Section 6 provides conclusions and some recommendations for future work.

Apendix A presents a summary of the all centrifuge model tests performed on the Princeton University Geotechnical Centrifuge.

Appendices B to D provide detailed descriptions and results of the performed centrifuge tests.

Section 2

Background

2.1 Liquefaction

During earthquakes, the shaking of ground may cause a loss of strength or stiffness that results in landslides, dam failures, settlements of structures, or other damage (Figure 1.1). The process leading to such loss of strength and stiffness is called soil *liquefaction*.

This is a phenomenon primarily associated with saturated sands. Soil liquefaction has been observed in almost all large earthquakes, and in many cases it has caused serious damage. The destructive effects of soil liquefaction were brought to the attention of engineers by the 1964 earthquake in Niigata, Japan. This earthquake caused more than one billion dollars in damages, due mostly to widespread soil liquefaction.

For critical structures, such as nuclear power plants and large earth dams, the possibility of liquefaction presents a serious engineering problem. Knowledge concerning liquefaction and its effects has come mainly from three distinct efforts:

- field observations during and following earthquakes,
- theoretical studies (employing numerical procedures),

- experiments in the laboratory on soil samples and models of foundations and earth structures (including small scale models).

In the first case, one has to wait for earthquakes of sufficient magnitude to occur to obtain the required data. As the time and place of an earthquake cannot be predicted, it is necessary to install instrumentation on many structures in many locations in the hope of eventually acquiring some data.

However, careful field studies identified sandy soils to be most likely to liquefy, and provided some information and correlations of great value to engineering practice. With a certain confidence, the occurrence or nonoccurrence of liquefaction relating to the intensity of ground motion can be obtained from in-situ evaluation of soil characteristics.

Numerical analysts, even if they have good modelling procedures, face problems with determining the properties of soil deposits in non-homogeneous layers and lenses. In addition, the boundary conditions are often difficult to define. Still, theoretical analysis made good progress in formulating constitutive relations that describe the physical behavior of soil as a continuum.

Soils laboratory testing showed that cyclic straining of a saturated soil can cause pore pressure to build up as a result of rearrangement of soil particles. In an undrained environment, gravity loading is transferred from soil skeleton to the pore water, with reduction in the soil capacity to resist loading.

These tests have also demonstrated influence of size, shape, and gradation of particles on the ability of soils to liquefy. Saturated uniform granular soils without cohesive fines are most susceptible to the pore pressure build-up. Other factors affecting the level of pore pressure build-up include the amplitude of straining, the density, the history of stressing, the confining pressure, and the overconsolidation ratio of the soil [5].

- experiments in the laboratory on soil samples and models of foundations and earth structures (including small scale models).

In the first case, one has to wait for earthquakes of sufficient magnitude to occur to obtain the required data. As the time and place of an earthquake cannot be predicted, it is necessary to install instrumentation on many structures in many locations in the hope of eventually acquiring some data.

However, careful field studies identified sandy soils to be most likely to liquefy, and provided some information and correlations of great value to engineering practice. With a certain confidence, the occurrence or nonoccurrence of liquefaction relating to the intensity of ground motion can be obtained from in-situ evaluation of soil characteristics.

Numerical analysts, even if they have good modelling procedures, face problems with determining the properties of soil deposits in non-homogeneous layers and lenses. In addition, the boundary conditions are often difficult to define. Still, theoretical analysis made good progress in formulating constitutive relations that describe the physical behavior of soil as a continuum.

Soils laboratory testing showed that cyclic straining of a saturated soil can cause pore pressure to build up as a result of rearrangement of soil particles. In an undrained environment, gravity loading is transferred from soil skeleton to the pore water, with reduction in the soil capacity to resist loading.

These tests have also demonstrated influence of size, shape, and gradation of particles on the ability of soils to liquefy. Saturated uniform granular soils without cohesive fines are most susceptible to the pore pressure build-up. Other factors affecting the level of pore pressure build-up include the amplitude of straining, the density, the history of stressing, the confining pressure, and the overconsolidation ratio of the soil [5].

Model tests of foundation and earth structures performed on large shake-table devices, used by some experimentalists, have been useful to study the complex distribution of pore pressure and deformations. However, these tests suffer from the disadvantage of having much lower effective stresses in the laboratory model than those encountered in the field.

One experimental technique that offers the ability to create relatively realistic full-scale stress states together with measurable soil properties is centrifuge model testing. Centrifuge testing of dynamic problems has been widely employed by geotechnical investigators in recent years, in a variety of test configurations, including liquefaction studies.

Several test facilities, besides Princeton University Centrifuge, now have capability of dynamic model testing to simulate seismic loads. Hydraulics shakers similar to the Princeton shaker are operational at U.C. Davis, Caltech, RPI, and at the University of Colorado Boulder. Cambridge University has been operating a centrifuge shaking table, known as the "Bumpy Road Simulator" since 1980. With the development of these facilities, it is now possible to study the effects of simulated earthquakes on the behavior of the variety of structures built of or on liquefiable soils.

2.2 History of Centrifugal Modelling

The idea of the small scale modelling in the centrifuge was presented for the first time in 1869 by E. Phillips in France [6]. Using the equilibrium differential equations for elastic solids, Phillips derived the relationship which had to be satisfied for the prototype and the small scale model, to exhibit the same behavior. He briefly gave some general principles for the design of centrifuges, and proposed using a centrifuge for testing models of a metal bridge for spanning the British Channel.

Sixty years would pass before this idea would be implemented. In the early thirties, this idea was re-discovered independently in the former USSR and in the US. Pokrovski in the former USSR, and Bucky in the US used the idea to study stability of slopes in river banks and deformation of rock beams in underground chambers, respectively. The centrifuge model testing has been used ever since in civil and military projects. In the US, use was confined to mining applications [8].

In the following thirty years, more than twenty centrifuges have been built in various research organizations specially for geotechnical studies, but it took almost forty years for centrifuge tests to become something other than an exotic scientific undertaking. Finally, one can consider the establishment of an International Technical Committee on Centrifuge Testing in 1981 to be an 'official' recognition by the geotechnical community of the value of the centrifuge experiments.

Recent developments in the electronic fields provided some fancy features in the measuring, and the data acquisition systems. Miniature transducers and powerful data acquisition oriented computers opened a new dimension in the centrifuge testing approach.

2.3 Principles of Centrifugal Modelling

The basic principle concerns the question of *weight*. In Figure 2.1, 1/100 scale model of mass 5 $[Kg]$ (of soil), in flight in centrifuge with radius of 1.1 $[m]$, at a speed of 30 $[radians/s]$ (286 $[RPM]$), has a tangential acceleration of 990 $[m/s^2]$, which will cause the 5 $[Kg]$ mass to experience an inertial force of $\sim$ 5 $[kN]$ force radially inwards. Viewed externally, the model appears to be constantly accelerating in the direction of the arrow, but on the television screen, the block will appear to be at rest relative to the camera [19].

The centrifuge arm has to be strong, because the block of soil will be trying to accelerate through the bottom with an equal and opposite relative acceleration of 990 $[m/s^2]$ ($\sim$ 100 times earth's gravity). If the frame of reference is the basket (viewed internally), then the direction of the force field is pointed outwards.

A large prototype exposed to the earth's gravity field experiences the same pressures across its volume as a small model in a centrifuge, exposed to the force field due to the centrifuge acceleration. In both cases, the upper surface of the body is unstressed and the pressure builds up through the depth of the body. Hence, the stress-strain behavior of a point in the model is the same as that of the homologous point in the prototype. This technique allows various tests to be performed at a conveniently reduced scale, and provides data applicable to full-scale problems. Further, the tests can be performed on any particular soil type and/or deposit, and/or for any structure configuration.

The modelling technique leads to a set of scaling relationships, or scaling laws, that affect time, physical dimensions, and the many derivatives of these combinations such as velocity, acceleration, force etc. These scaling relations are listed in Table 2.1.

The centrifuge approach promises to be an invaluable aid for studying a variety

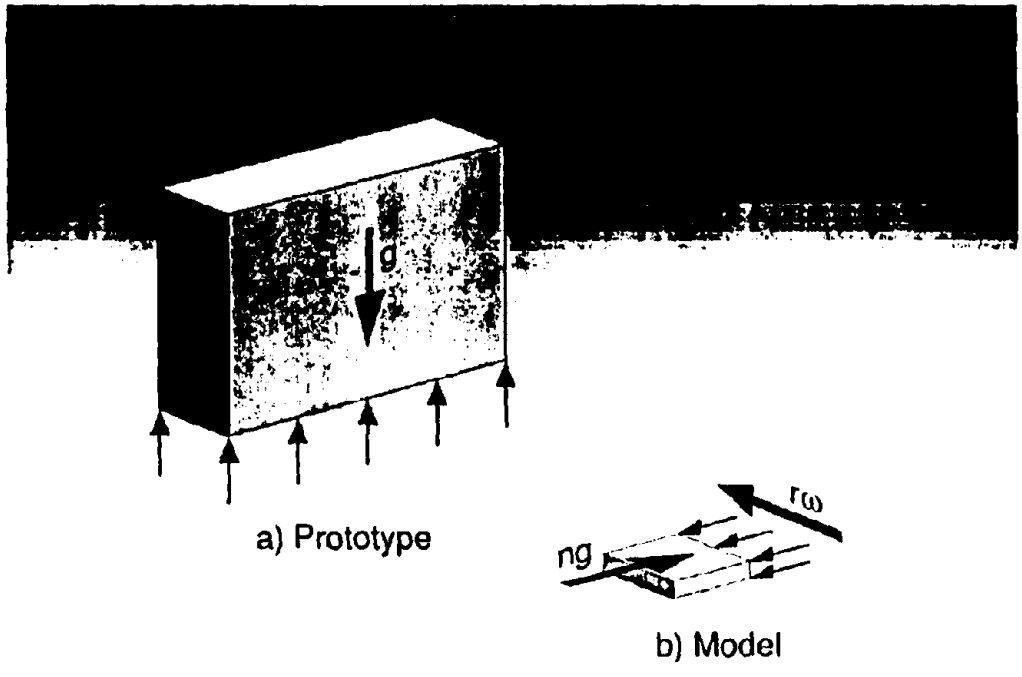

Figure 2.1: **Prototype - Model**

of complex geotechnical problems and in particular, for studying soil liquefaction, and soil-structure liquefaction problems.

Finally, a model tested at Ng should have a geometry that is $1/N$ times the geometry of the prototype to reproduce prototype stresses. For correct scaling of inertial effects, the model horizontal acceleration time history should have accelerations magnitudes N times the prototype accelerations, with a frequency equal to N times the prototype frequency.

Unfortunately, not all effects behave like experimentalists would like them to

Quantity	Full Scale Prototype	Centrifugal Model at ng
Linear Dimension, Displacement	1	$1/n$
Area	1	$1/n^2$
Volume	1	$1/n^3$
Stress	1	1
Strain	1	1
Force	1	$1/n^2$
Mass	1	$1/n^3$
Acceleration	1	n
Energy	1	$1/n^3$
Density	1	1
Energy Density	1	1
Velocity	1	1
Time		
In Dynamic Terms	1	$1/n$
In Diffusion Terms	1	$1/n^2$
In Viscous Flow Case	1	1
Frequency in Dynamic Problems	1	n

Table 2.1: **Scaling Relations**

behave. It can be seen in Table 2.1 that consolidation in a model occurs N^2 times faster than for the prototype, thus tests that involve both inertial and consolidation effects must be very carefully performed.

2.4 Princeton University Geotechnical Centrifuge Facility

The Princeton University Geotechnical Centrifuge has been in operation since January 1980. It is located in the basement of the Engineering Quadrangle of the Princeton University (Figure 2.2).

The centrifuge drive and enclosure, a model 1230 – 1 "Genisco", are combined with a special accelerator arm and two swinging platforms (Figure 2.4), designed at Princeton to enable performing of the geotechnical experiments. The "Genisco" drive mechanism is made up of a remote 15 $[Hp]$ electric motor which is coupled to a hydraulic pump and a rotor system capable of spinning the accelerator arm to several hundred RPM. The accelerator arm, made of 5.08 $[cm]$ thick aluminum, has a maximum payload of 10 $[G - tons]$.

Nicolas-Font [12] plots *usable domain* of a centrifuge in the frame of reference (acceleration, platform loading) (Figure 2.3). That indicates the capabilities of the device and an operating range inside which the safety of the equipment and people using it can not be jeopardized. Figure 2.3 shows the change of the usable domain of the Princeton University geotechnical centrifuge due to the shaker installation.

On each end of the 3.05 $[m]$ (10 $[ft]$) (Figure 2.4) accelerator arm is a hinged swinging basket, one for mounting experimental hardware, and another one for balancing the centrifuge. The entire arm is enclosed by a 5/16" $[in]$ thick metal housing whose vibrations are, for safety reasons, monitored with a seismometer. Electric

Figure 2.2: P.U.Geotechnical Centrifuge Laboratory

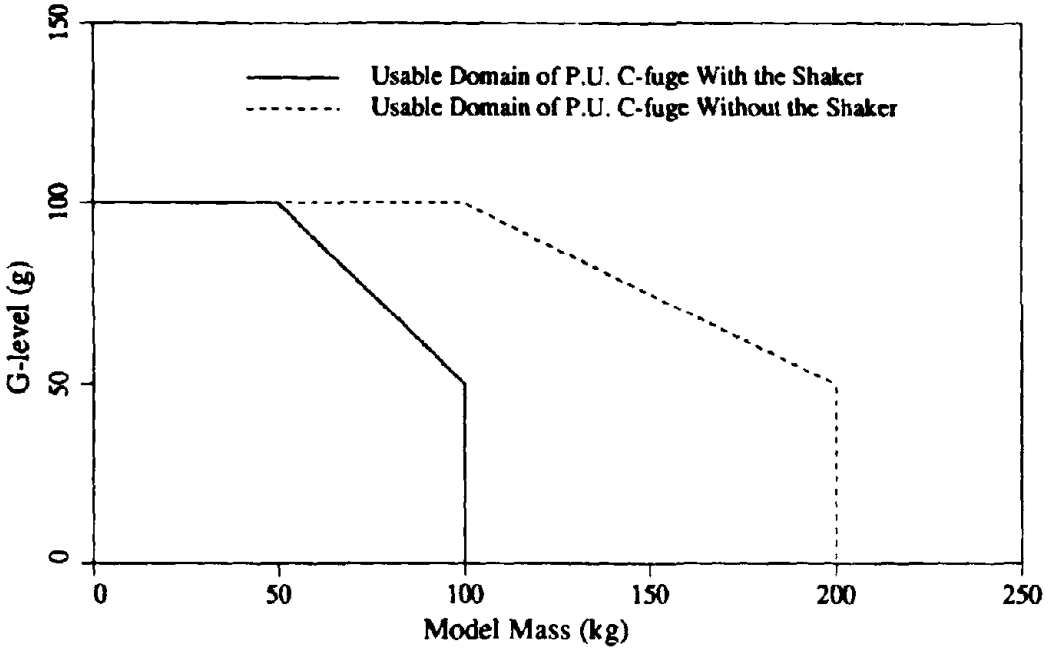

Figure 2.3: **P.U. Geotechnical Centrifuge Operating Range**

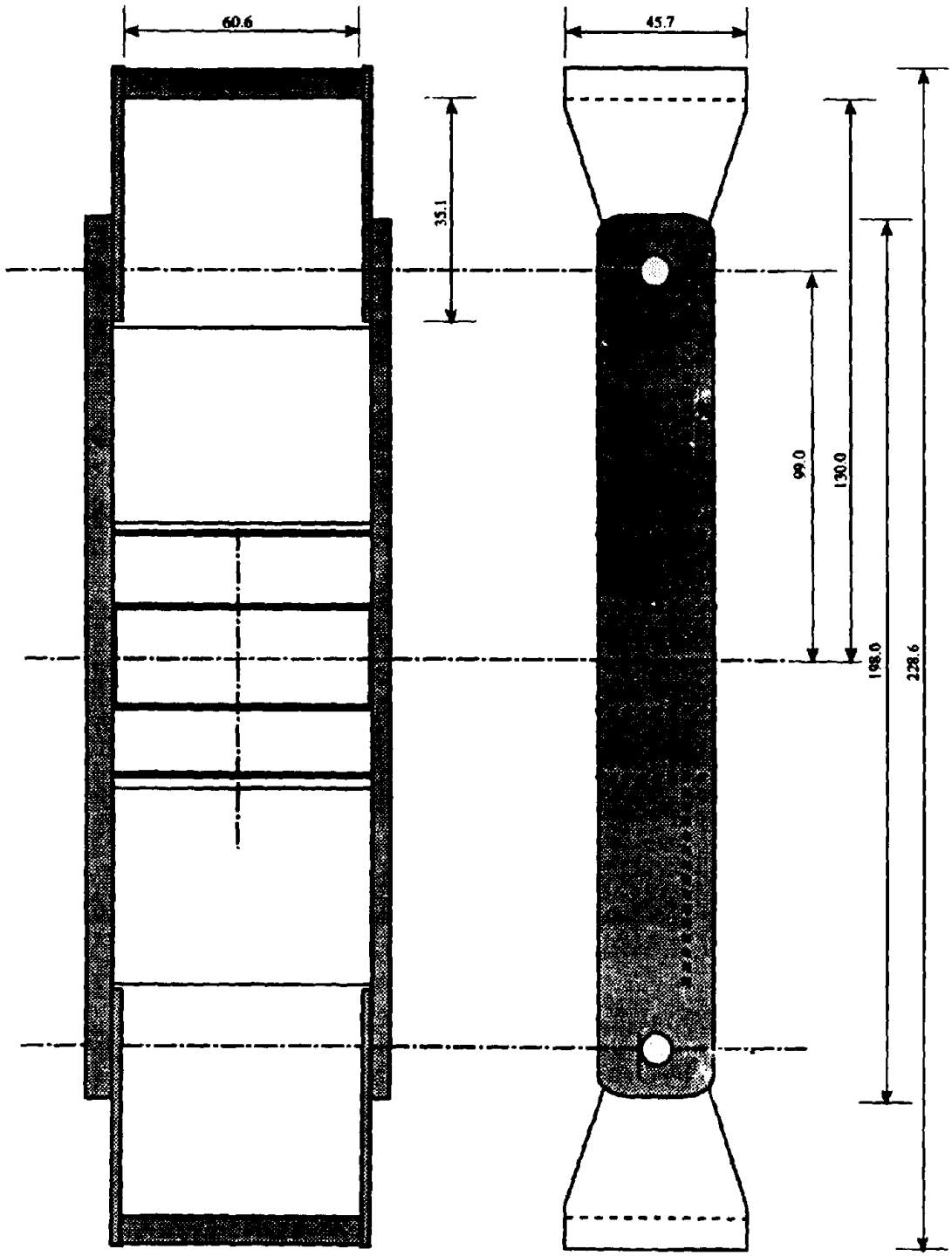

Figure 2.4: P.U. Geotechnical Centrifuge Schematic

Line Type	Available	In Use
High Voltage Power Line	24	12
Low Voltage Data Lines	22	19
Pneumatic Air Lines	2	1

Table 2.2: **Available and Used Connections Through the Centrifuge Axis**

power, pneumatics, and low level voltage data signals are transferred to and from the experiment via high power slip-rings, rotating union, and miniature instrument slip-rings, respectively (Table 2.2).

Section 3

Ground Motion Simulator

3.1 Introduction

As described in Section 1 this study includes the development of a centrifuge ground motion simulator that is used to simulate earthquake motions for small scale geotechnical model testing. It begins with a brief survey of developments in the area of earthquake-like motion simulators, traces some attempts made at Princeton University to design a cheap and simple motion simulator, and ends with a description of the currently operating Princeton University ground motion simulator.

3.2 Types of Ground Motion Simulators

The first experiments with seismic loading in a centrifuge were carried out in 1940 by Pohorsky and Fedorov [23]. A special suspension system was designed which allowed a model to oscillate while the centrifuge was in flight.

A spring actuated shaker able to provide decaying sinusoidal input motion at fixed frequency was part of early dynamic testing at Cambridge University [11], California Institute of Technology [20] and at Princeton University. The 'bumpy road' technique, currently operating at Cambridge University [10], involves a tracks of desired input wave forms mounted over a portion of the centrifuge housing wall.

Shaker Type	Shaker Cost	Simplicity	Adjustability	Freq. Range Low High
Cocked Springs	Very Low	Very Simple	Poor	⊢ ⊣
Piezoelectric	Low	Simple	Good	⊢ ⊣
Explosive	Low	Simple	Moderate	⊢ ⊣
Bumpy Road	High	Complex	Moderate	⊢ ⊣
Hydraulic	Very High[1]	Very Complex	Very Good	⊢ ⊣

Table 3.1: Comparison of Various Methods for Simulating Earthquake Ground Motions on Centrifuge

An earthquake simulator using piezoelectric element has been used in the University of California, Davis [1]. A piezoelectric ceramic element is an artificially polarized wafer whose strain magnitude, when exposed to an electric field, is directly proportional to the magnitude of that field. The motion of the element may be controlled by the electric input.

A simulator system using small explosions as an input was developed at Ecole Politechnique in Paris in the later 1970's [24]. Up to 10 charges of explosive of 1 *to* 5 [g] could be detonated in desired sequence, their explosions modified in an air blast modification chamber, and applied to the vertical face of a soil mass through a rubber membrane.

A hydraulic shaking system was for the first time put into operation on the geotechnical centrifuge at the California Institute of Technology [7]. A flow of oil is directed into one of two opposed pistons to create a motion of the shaking box connected to the actuator device. Comparisons of various methods for simulating earthquake ground motion are given in Table[1] 3.1 [23].

[1] Princeton University ground motion simulator design and construction showed that cost of the hydraulic shakers for small centrifuges does not necessarily have to be very high

3.3 Princeton University Designs

At Princeton University, a hammer-exciter plate device was used to provide internal excitation of a test model [22]. A plate placed near the bottom of a soil mass was activated by an air pressure driven hammer device. The amplitude can be controlled by varying the air pressure in the hammer device, while the frequency content can be varied by changing the plate's dynamic characteristics (Figure 3.1).

The simulated earthquake was similar in amplitude and frequency to some real earthquakes with relatively high frequency contents [22].

The old hammer-exciter plate technique was very simple and cheap, but it was only capable of generating one type of earthquake with high predominant frequencies, and short in duration. In order to achieve better control over the earthquake simulations, it was decided to upgrade the centrifuge with the Acutronic designed spring shaker system.

The idea behind the design was to have a one degree-of-freedom system floating on a powerful 'air hockey table' device (Section 3.4.3). Resulting motion dominant frequencies were too high for the realistic earthquake simulation, and the system was unable to perform in a high g environment.

It seemed reasonable to solve the problem using a device strong enough to induce forced vibrations of the system. The Acutronic springs were replaced with the Ingersoll Rand multi-vane air motor series 4800. The air motor was previously redesigned to maintain needed $5.2\,[kW]$ $(7\,[Hp])$ at $6400\,[RPM]$ from original $2.8[kW](3.7[Hp])at\,560[RPM]$. The constructed system was able to provide sine-like displacement time-histories with reasonable control over the frequency, although the air motor starting and stopping caused some irregularities in the excitation. Due to the imperfect transmission, the whole system generated very high mechanical noise,

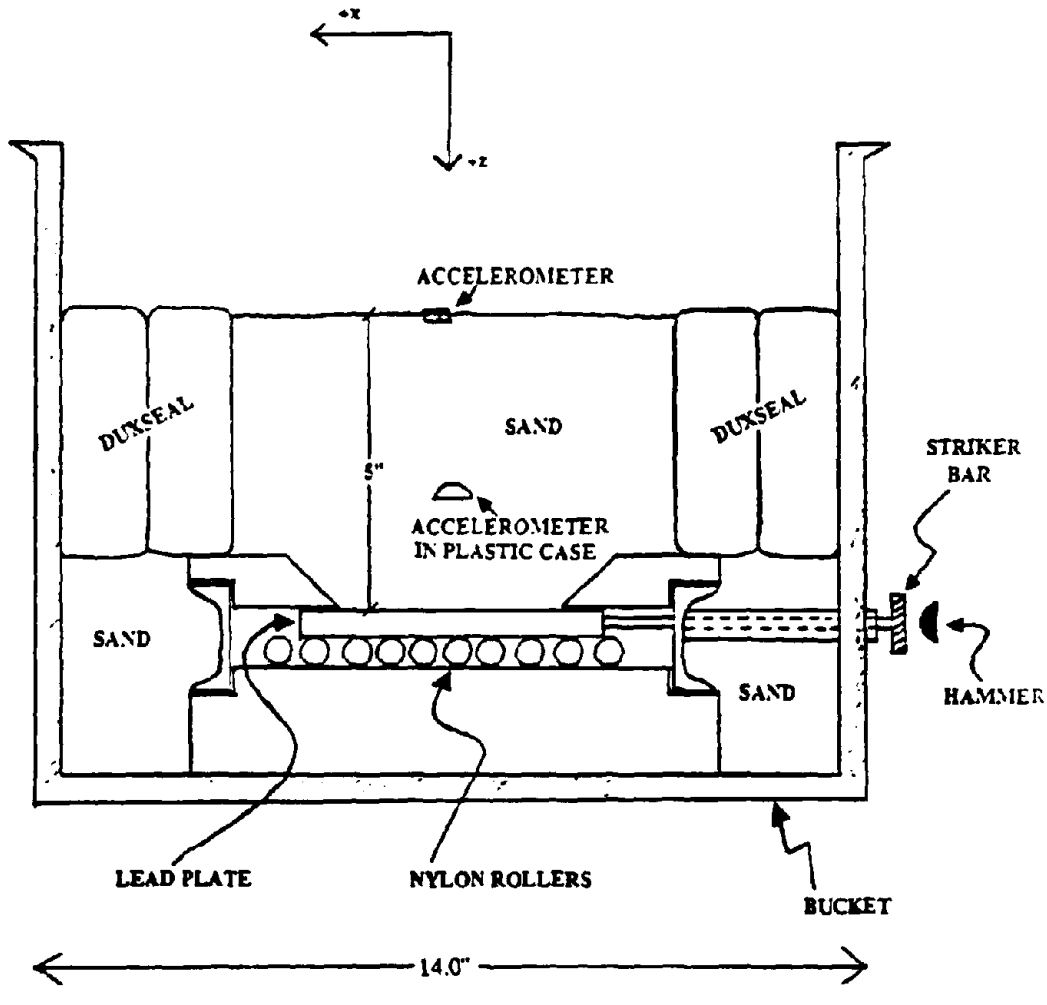

Figure 3.1: Old Hammer-Exciter Shaker on P.U. Geotechnical Centrifuge

and it was impossible to produce the desired number of cycles, which was required to perform VELACS model check test. In spite of the fact that the air motor driven shaker was operational, it was decided to start construction of the electro-hydraulic shaker.

3.4 Electro-Hydraulic Shaker

In 1991, the P.U. centrifuge has been modified to include a one degree of freedom electro-hydraulic shake table, capable of subjecting a test container to various types of dynamic excitation in the direction which lies in a plane of the centrifuge rotation.

An electro-hydraulic shaker is a special hydraulic actuator and a high performance servomechanism, optimized for high frequency operation. A servomechanism is defined as: "an automatic feedback control system in which controlled variable is mechanical position or any of its time derivatives" (ANSI, 1981). The system is capable of vibration testing from DC to 1000 $[Hz]$, and is particularly advantageous for vibration tests requiring high force levels, like those in a high gravitational environment.

An electro-hydraulic vibration test system is made up of three major subsystems:

- Hydraulic Subsystem,
- Electronic Subsystem,
- Slip table.

3.4.1 Hydraulic Subsystem

The whole hydraulic subsystem of the Princeton ground motion simulator is located on the centrifuge arm (Figure 3.2).

The subsystem includes: the hydraulic power supply system, 25 $[l]$ oil tank, manifolds for oil passages, a filtering system, two 1.86 $[l]$ $(1/2\,gallon)$ accumulators, the servovalve and the linear actuator (Figure 3.4). The hydraulic power supply system consists of the Ingersoll Rand air motor and the Airline Hydraulics oil pump. The combination was required to have a full flow capacity of 20.0 $[l/min]$ operating with maximum oil pressure at 20.7 $[MPa]$. The position of the tank, on the centrifuge arm, was chosen such that the oil pump operates in a submerged regime, without suction oil lines, while the centrifuge was in flight.

An additional weight was placed on the centrifuge arm to act as a counterbalast for the oil tank and the power supply units. A filtering system includes a HP010 Moog Filter Assembly rated at 38 $[l/min]$ (10 $gallon/min$) and Beta rating for 3 $microns\ of$ 75, with dirt alarm set to 670 $[kPa]$ (100 $[PSI]$) pressure drop, installed in the high pressure lines before the actuator, and an oil strainer placed on the oil tank outlet.

Beside the main power unit, a system has a supply accumulator as an optional power supply for the actuator when the oil pump is not active, together with a return accumulator used to receive oil on the return side of the actuator. The supply accumulator was precharged with 17.25 $[MPa]$ nitrogen, and the return accumulator was precharged at 1.04 $[MPa]$ nitrogen pressure. The accumulator volume and precharged pressures were chosen in conjunction with the actuator size to provide working volumes and supply duration consistent with the requirements for scaled earthquake-like events, yet without excessive drop in oil pressure. Because the primary power unit can be active while the centrifuge is in flight, accumulators have not yet been used as an alternative power supply.

The linear actuator is a Team Impedance Assembly Head 21/0.5. The full stroke of the piston rod is ± 6.35 $[mm]$ (0.25 $[in]$) and the cylinder diameter is 32 $[mm]$

(1.26 [in]), and the piston rod diameter is 25.4 [mm] (1.0 [in]). Piston working area is 297 [mm^2] (0.46 [in^2]) (Figure 3.3).

A position feedback information for the automatic feedback control is provided by a SCHAEVITZ MHR250 transducer built in the Team actuator. The actuator was sized for stall force at supply pressure, but the device that controls the hydraulics shaker, and connects the hydraulics subsystem with the electronics subsystem is a servovalve.

Servovalve throttles flow from a constant pressure supply to each side of the actuator piston to produce the piston rod motion. A Moog Controls Servovalve model $760 - 912A$ rated at 19 [l/min] (5 [gpm]) was mounted directly on the impedance assembly head to minimize the time for load response. (Figure 3.4). The Moog servovalve together with the SHAEVITZ LVDT make the hydraulic subsystem connection with the electronic subsystem.

3.4.2 Electronic Subsystem

The ground motion simulator electronic subsystem consists of a Moog Controls Model $121 - A132$ servocontroller, a Moog Controls Model $123 - C134$ Exciter-Demodulator, a 'function generator' and an input voltage level regulator (Figure 3.5).

A desired signal generated on 'function generator' (Masscomp computer) is scaled with a simple voltage divider and brought to the servocontroller through a centrifuge slip ring.

The servocontroller processes the signal together with a feedback signal coming from the exciter-demodulator, and sends the *command* to the servovalve. A resulting actuator rod motion is monitored by the LVDT and a new feedback signal is sent to the exciter-demodulator and then back to the servocontroller.

The designed system can provide good control over the actuator piston rod posi-

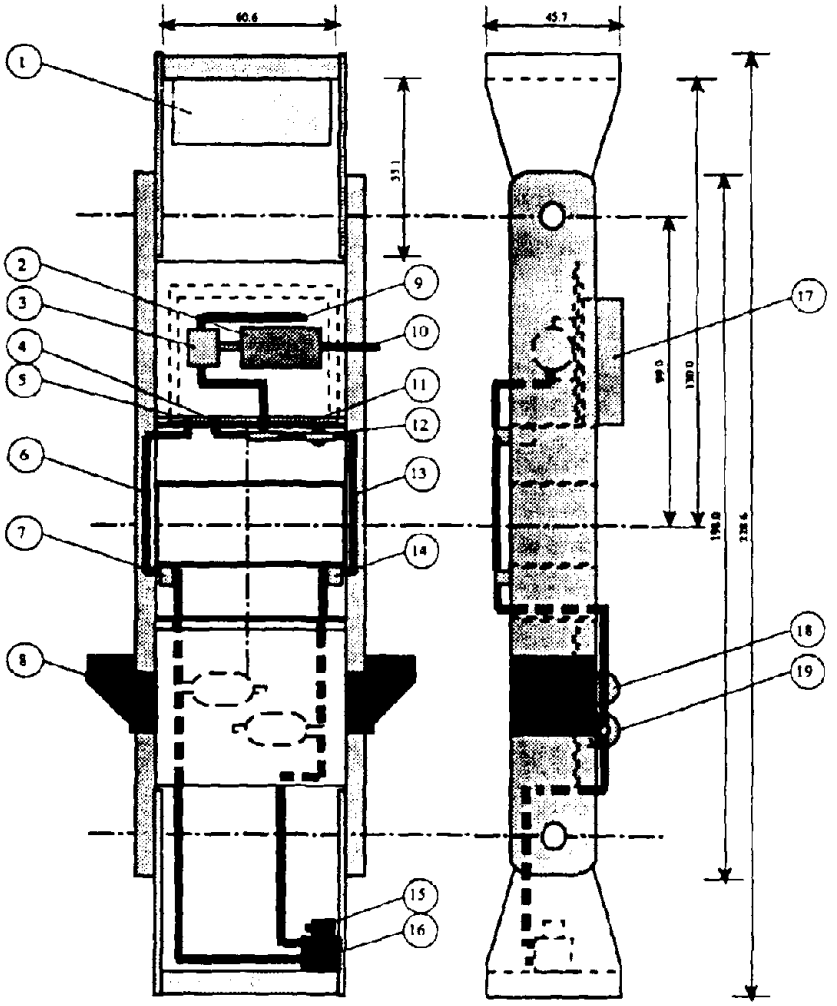

Figure 3.2: Shaker Hydraulic Subsystem on the Princeton Geotechnical Centrifuge

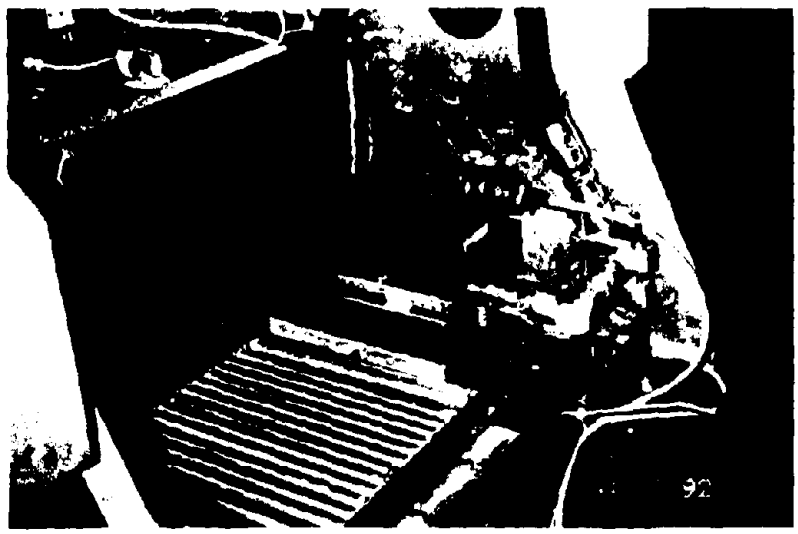

Figure 3.3: Team Assembly Head and Moog Servovalve Mounted on the Swing Platform

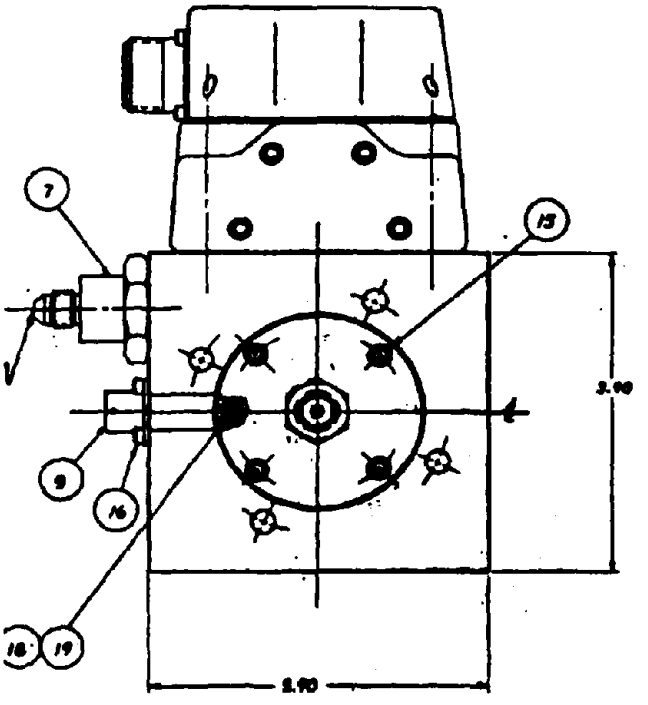

Figure 3.4: **Team Assembly Head and Moog Servovalve**

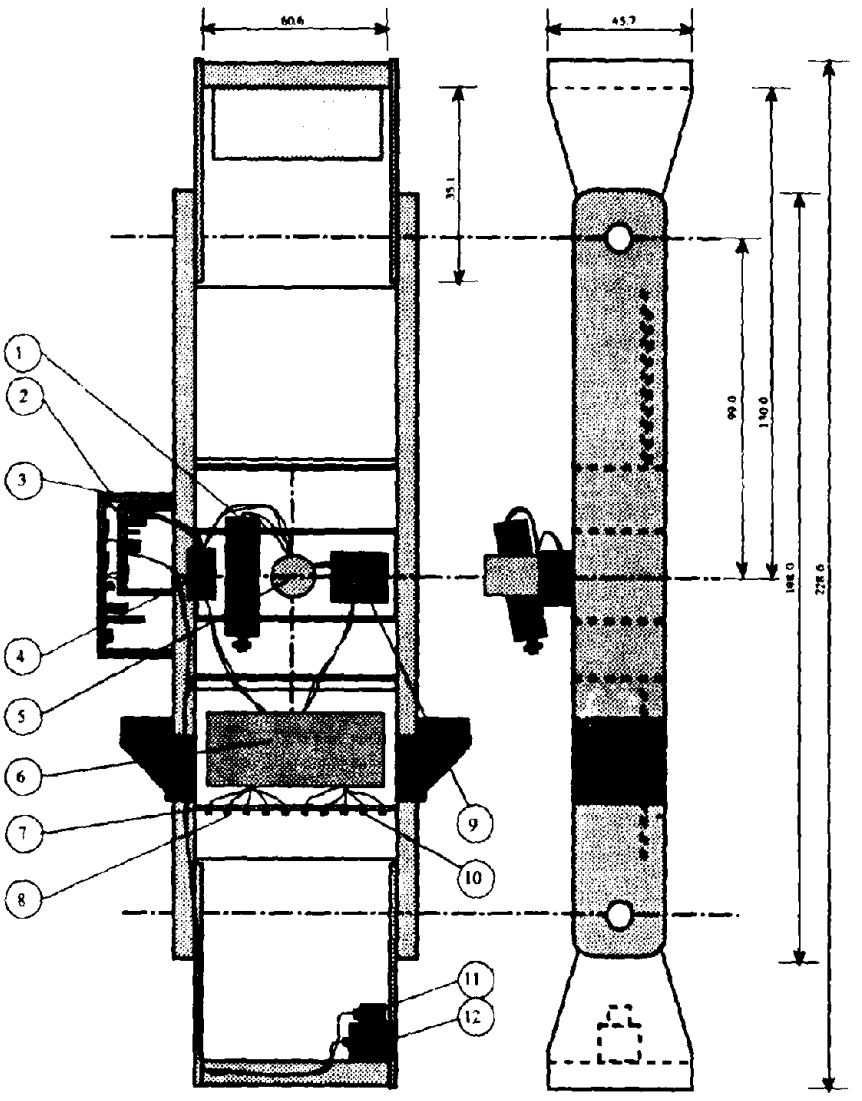

1. Video Camera
2. Moog Exciter-Demodulator
3. Moog Servo Controller
4. High Voltage Power Box
5. Centrifuge Axis
6. Signal Conditioning Box
7. Connector Board
8. BNC Connectors (Acc.)
9. Low Voltage (Data) Box
10. Phone Connectors (PPT & LVDT)
11. Moog Servovalve
12. Team Actuator & Shaevitz LVDT

Figure 3.5: Electronic Subsystem of the Ground Motion Simulator

tion relative to the centrifuge swing container, and eliminate most of the phase lags caused by the hydraulic subsystem components.

3.4.3 Slip Table

The spring shaker system, designed by Acutronic, included a plate floating on air flow attached with four springs. The idea behind that design was to eliminate friction between the oscillating plate and the base of the shaker. To provide 0.57 $[m^3/min]$ (20 $[cfm]$) air flow at 2 $[MPA]$ (300 $[psi]$) needed for the plate to float, a 5.6 $[kW]$ (7.5$[Hp]$) compressor and one cubic meter tank were installed. The plate was initially sitting on the 'air hockey table' with 16 air jets which were supposed to lift the plate once the centrifuge is in flight.

However, due to imperfections in design, and the weight of the sample placed on the plate, once the air was released the plate would tilt and let the air escape without establishing the stable system. Vertical acceleration generated inside the system was impossible to control, and too high for realistic small scale modeling of ground motion.

The slip table currently in use, designed at Princeton University, consists of 12.7 $[mm]$ (1/2 $[in]$) aluminum rollers placed on an aluminum base. The first tests, performed in 100g environment, showed satisfactory performance of the rollers. The only problem, transmission of high frequencies generated in the shaker power supply unit (air motor and oil pump), was eliminated with a 1.6 $[mm]$ (1/16 $[in]$) gasket placed on the interface of the swing platform and the rollers base, and a duct tape on surfaces of a rollers' contact with the base and a test model box. Vertical acceleration generated with the slip table was always below 15% of the horizontal acceleration amplitude with a frequency range similar to one of the input (Figure 3.6).

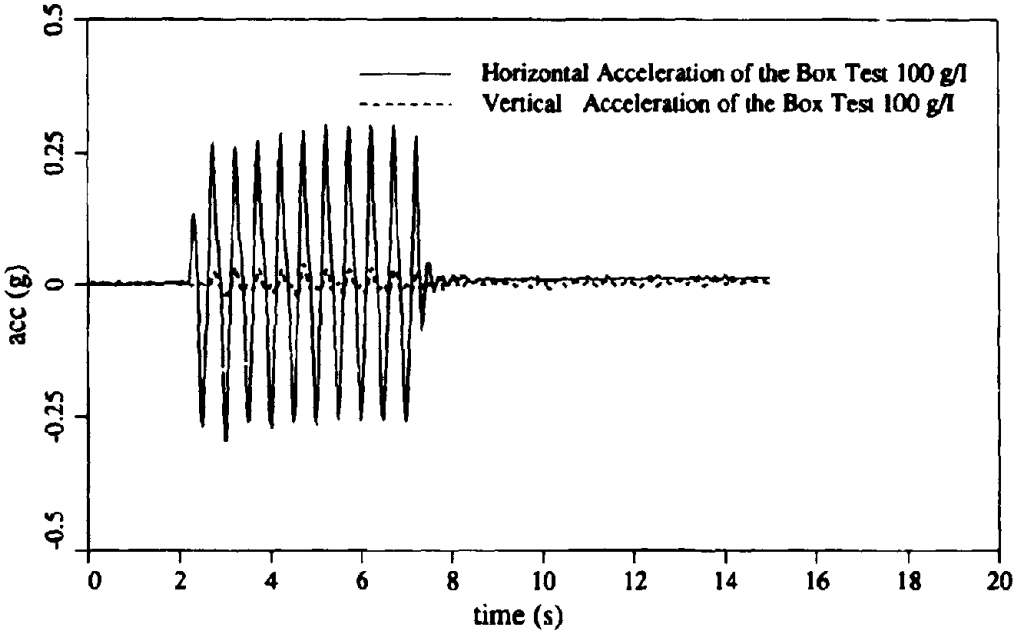

Figure 3.6: Horizontal and Vertical Acceleration Time History Comparison

3.5 Instrumentation and Data Acquisition System

Precise and reliable instrumentation is of major importance for the small-scale modelling. During simulated earthquakes, instrument sensors measured accelerations, pore pressures and displacements.

Accelerations are measured by miniature piezoelectric accelerometers that have to be placed at desired locations of the model. The accelerometers used at Princeton University are Kistler PICOTRON series 8616A. When used in a saturated environment, transducers were protected with a silicone case.

Pore pressure transducers used in tests described in Sections 4 and 5 were Druck PDCR81 with pressure range of $\sim 200\ [kPa]$.

Displacements are measured with *contact* and *non-contact* LVDTs. The non-contact position measuring system used in centrifuge tests is Kaman $KD-2300-8CM$ differential impedance transducer with linear range of 12.7 $[mm]$.

The instrument sensors were plugged into a board supporting BNC connectors for the accelerometers and phone connectors for the pore pressure transducers and the LVDTs. The board is connected with a signal conditioning box which includes amplifying, filtering and voltage to current converting devices. Conditioned signals are then transmitted through slip rings into an instrument room.

The signals generated during a simulated earthquake are, at the same time, recorded on a 9 channel Aiwa tape recorder, and a 16 channel data acquisition oriented Masscomp computer. Short term measured traces are momentarily portrayed on the Masscomp color screen. Long term time histories can be recovered from the tape recorder and plotted on the screen after a sampling rate has been changed.

Section 4

VELACS project

4.1 Introduction

VELACS - Verification of Liquefaction Analysis by Centrifuge Studies, is a geotechnical centrifuge study which includes the following collaborating universities: University of California, Davis; University of California, Berkeley; University of Colorado at Boulder; Rensselaer Polytechnic Institute; Massachusetts Institute of Technology; Cambridge University, U.K.; and Princeton University.

A primary objective of the VELACS project is to undertake a program of dynamic centrifuge tests on a variety of different models in order to study different mechanisms of failure and to verify various numerical procedures in liquefaction analysis.

A secondary objective of the program is to evaluate the test results' dependence on used testing devices and procedures. This would be achieved by performing a series of *standard model check tests* on all available centrifuges, and by repeating some selected tests on different centrifuges.

The significance of the results of this study is that it would provide verification of available numerical procedures for analyzing liquefaction problems. The validation of these procedures would be of great importance for engineering practice.

4.2 Standard Model Check Test

The first consideration of the VELACS project was the standard model check test, in order to estimate the variation of results from tests performed by the different participating experimental groups. Each group was supposed to use its own ground motion simulator, and to the best extent possible the same test box, soil type, preparation technique, and test procedure.

The standard model consists of Nevada sand (#120) and Silica silt provided by Earth Technology, INC. (ETI). The pore liquid was water, and a test was performed on a sand prepared to a relative density of 60% with a dry pluviation technique. A test was supposed to be performed on a 3.0 $[m]$ (prototype) thick layer of saturated sand, overlaid by a 3.0 $[m]$ thick layer of saturated silt.

It was decided to apply vacuum to ensure full saturation of sand, and to pour silt in a form of the slurry after the sand layer was prepared. The sample preparation procedure had to be carried out 24 hours before the centrifuge test. The free water surface had to be above the silt surface to ensure that the silt layer is completely submerged.

The centrifuge had to be brought up to a centrifugal acceleration of $50g$, and the test container maintained at this level for 20 minutes before the application of the earthquake-like event. The event had to consist of approximately 10 cycles of sinusoidal motion at a peak acceleration of $0.25g$ (prototype) [21].

There have been two major groups of the tests performed at Princeton University (Table 4.1), each of them performed at a different centrifugal acceleration level.

The first group of tests were performed during the summer '91 [9]. Due to the size of the centrifuge swing platform, the test box was half the size of the standard VELACS box, and the tests have therefore been performed at $100g$ centrifugal ac-

Test	G's	Date	Ref.	Acc.	P.P.T.	LVDT
VELACS Check Silica Silt	100	20-Jun-91	100 g/I	3	2	1
VELACS Check Silica Silt	100	30-Jul-91	100 g/II	5	3	0
VELACS Check Silica Silt	75	06-Oct-91	75 g/I	6	4	0
VELACS Check Silica Silt	75	01-Nov-91	75 g/II	6	4	0
VELACS Check Bonnie Silt	75	20-Apr-92	Bonnie/I	3	2	2
VELACS Check Bonnie Silt	75	10-Jun-92	Bonnie/II	3	3	2

Table 4.1: Standard VELACS Model Tests Performed on Princeton Geotechnical Centrifuge

celeration. The old Princeton box had an inside plan area of 216 $\times$ 97 $[mm]$, and a height of 114 $[mm]$.

The second group of tests was performed in a $75g$ environment after the ground motion simulator, and the slip table was redesigned to accept a larger testing box.

4.3 $100g$ Tests

The samples were constructed in two layers. The lower layer consists of approximately 3.0 $[cm]$ (3.0 $[m]$ prototype) of Nevada sand (#120) and the top one consists of 3.0 $[cm]$ of silt. Since the box was fairly small, the bottom of the sample , and the surface of the sand layer were not shaped. The surface of the silt was formed by the centrifuge force, while the centrifuge was in flight. The box was able to sustain 50 $[cm]$ of mercury vacuum used during the saturation process. A drainage hose 2 $[mm]$ in diameter was placed on the bottom of the sample to obtain slow and uniform watering of the sample, and to prevent sand particle flow after the valve

was open. The volume of the hose together with the pressure transducers and the accelerometers was measured ($\sim 5\%$) and subtracted from the sample volume.

The pressure transducers were first de-aired in a vacuum and stored in water until placed in the sample. Approximately 950 $[g]$ of dry sand was pluviated through a raining device . Pluviation was stopped once (for the first test and twice for the second test) in order to place accelerometer(s) and pressure transducers in the middle (and at the bottom for the second test) of the sand layer. The bucket was then sealed and the vacuum introduced to the sample. Water was subjected to the vacuum and was de-aired with a magnetic stirrer. De-aired water was then slowly drawn (sucked from the container with a lower vacuum level to the box with a higher vacuum level) to cover the sand surface.

The silt was first mixed with water to form a slurry, and then poured slowly over the sand. Pouring was halted once to place accelerometers in the middle of the silt layer.

After the samples were allowed to sit for 12 hours, some additional silt was added in order to reach the required depth for the silt layer, and the centrifuge was brought up to $100g$ level. The samples were left in flight at $100g$ for approximately ten minutes before it was stopped, and visually checked. An LVDT core with a supporting footing was placed on the surface of the sample in the first test.

A high level of the core footing sinking was noticed after the first test. Since this problem has not been solved, the vertical displacement during the second test was not measured. The centrifuge was then spun back up to the $100g$, and the tests were performed after the pressure transducers' readings had stabilized.

4.3.1 $100g$ Tests Comparison

Since the first test was performed with the old data acquisition system, with limited capabilities, only few comparisons were made. Due to the different forms of the shaker input files (number of zero points preceding the earthquake-like event) time history recordings of tests *I* and *II* do not coincide in a displayed interval of 20 seconds. To insure a same (close) beginning time for the both events, the event *I* was moved forward in time for approximately 0.5 [*s*].

Locations of the instruments in both tests are given on Figures B.1 and B.9 in Appendix B. Comparisons of the recorded acceleration time histories are given on Figure 4.1. The input acceleration (vertical and horizontal) time history comparisons demonstrate the ground motion simulator ability to produce consistent output. The silt layer horizontal acceleration time histories coincide during the first two cycles, and show a similar trend for the rest of the event, both signals were significantly damped, after the liquefaction had occured in the sand layer.

Short and long pore pressure time histories are shown on Figures 4.2 and 4.3, respectively. Both transducers placed on the interface of the two materials recorded relatively high noise, which might be due to the boundary conditions (Section 4.7). However, the resulting maximum level of excessive pore pressure is in good agreement both for the interface and for the sand layer. Looking at the end of the interval of 1000 [*s*] one can see that excessive pore pressures coincide, but the rate of pore pressure change is not consistent for both tests. The reason for that difference might be the fairly small testing box which does not allow precision during the sample preparation, so one has to be extremely careful during the modelling of dissipation problems.

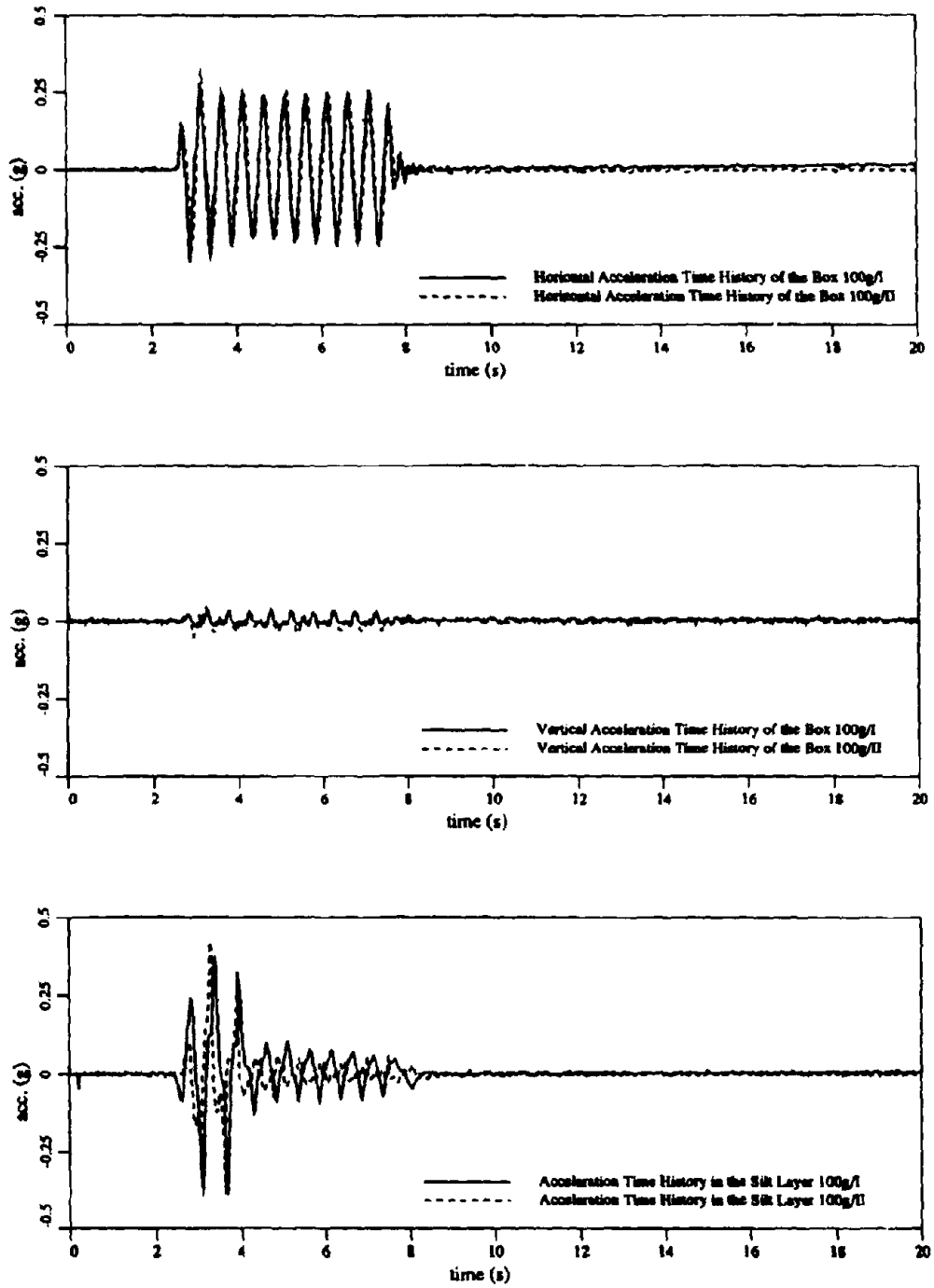

Figure 4.1: Comparison of the Measured Acceleration Time Histories of the 100*g* Tests

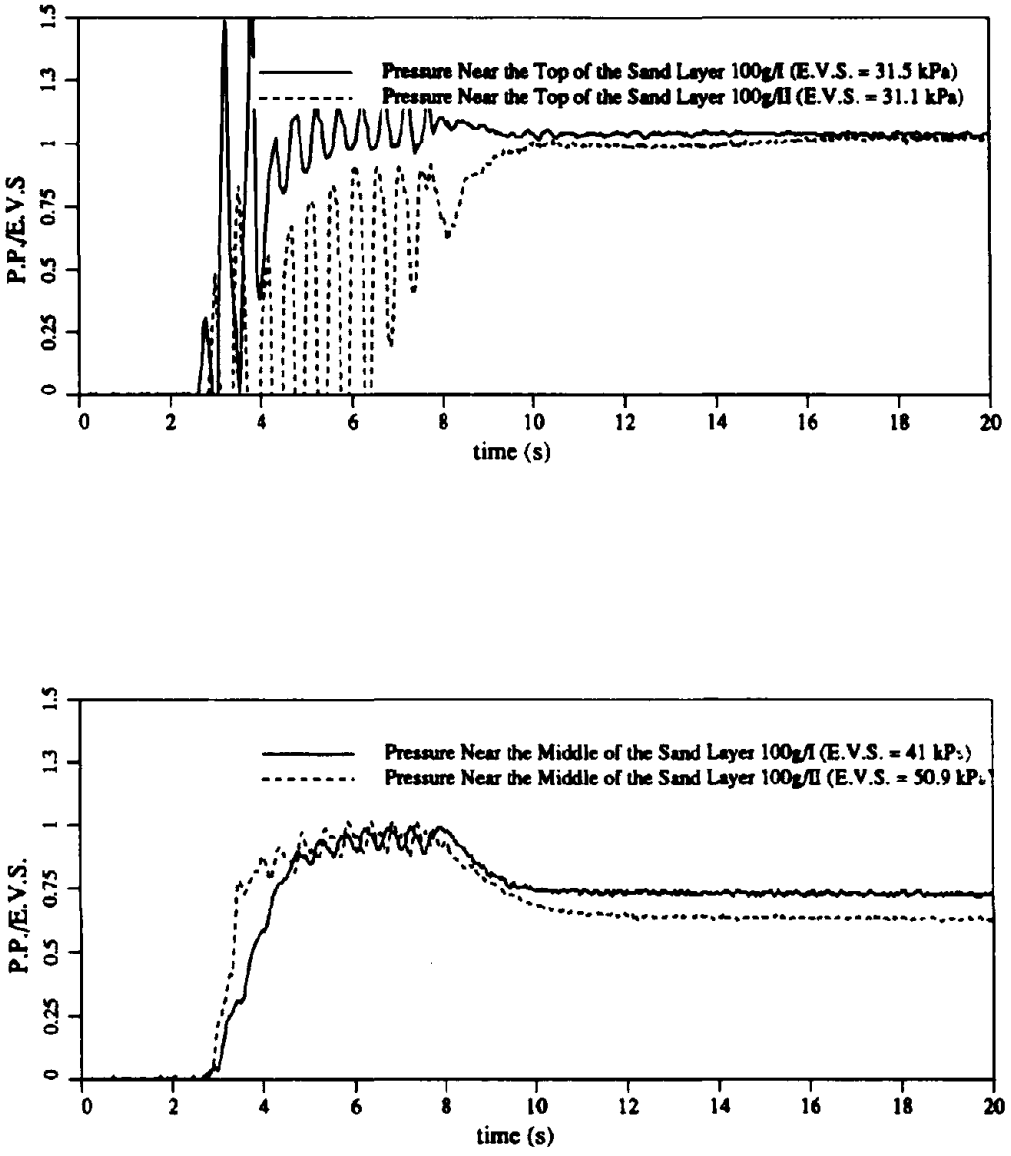

Figure 4.2: Comparison of the Measured Pore Water Pressure Time Histories of the 100*g* Tests

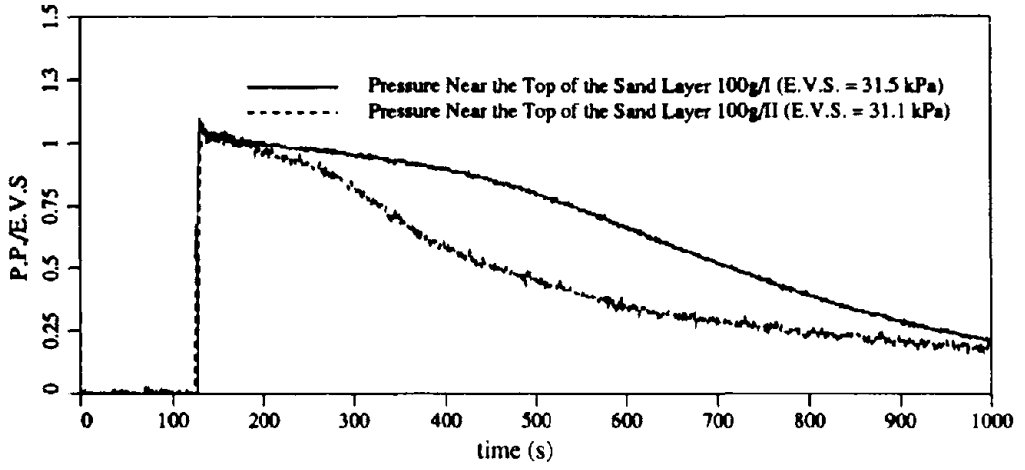

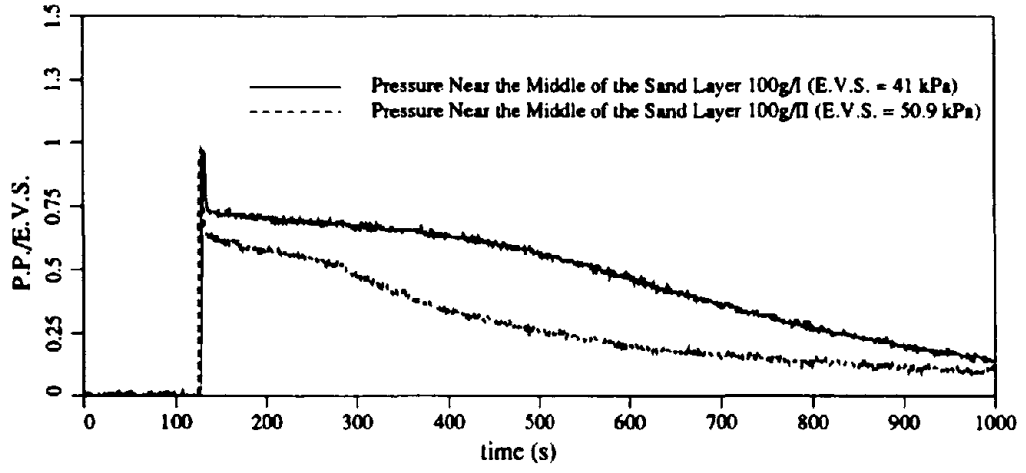

Figure 4.3: Comparison of the Measured Pore Water Pressure Time Histories (Long-Term) of the 100g Tests

4.4 $75g$ Tests

In September 1991 the shaker system was modified, and the old slip table was replaced with a new one with dimensions 310 $\times$ 210 $[mm]$. The performed changes now allow the centrifuge bucket to accept a larger testing box. The old standard VELACS box was then replaced with a new one, which is 2/3 the size of the box used by the other VELACS participants.

The new model box, when tested at $75g$ centrifuge acceleration, has the same prototype dimensions as the old model box for the $100g$ tests. The new system was extensively tested to determine a voltage input level for the servocontroller required to achieve $0.25g$ acceleration amplitude, and to test whether the new slip table and the test box have any impact on the shaker performance. The shaker performed well, and the new slip table had a vertical acceleration level less than 12% of the horizontal acceleration level (Figure C.3).

The second group of tests was performed on the modified system, at $75g$ centrifugal acceleration. All results and detailed description of the tests can be found in Appendix C.

4.4.1 $75g$ Tests Comparison

Figure 4.4 shows horizontal acceleration time history comparisons, and Figures 4.5 and 4.6 show excessive water pressure comparisons. All results have good agreement, even long term pore pressure time histories show reasonably consistent dissipation. Difference in excessive pore water pressure levels on Figure 4.5 are due to the different positions (depth) of the pressure transducers.

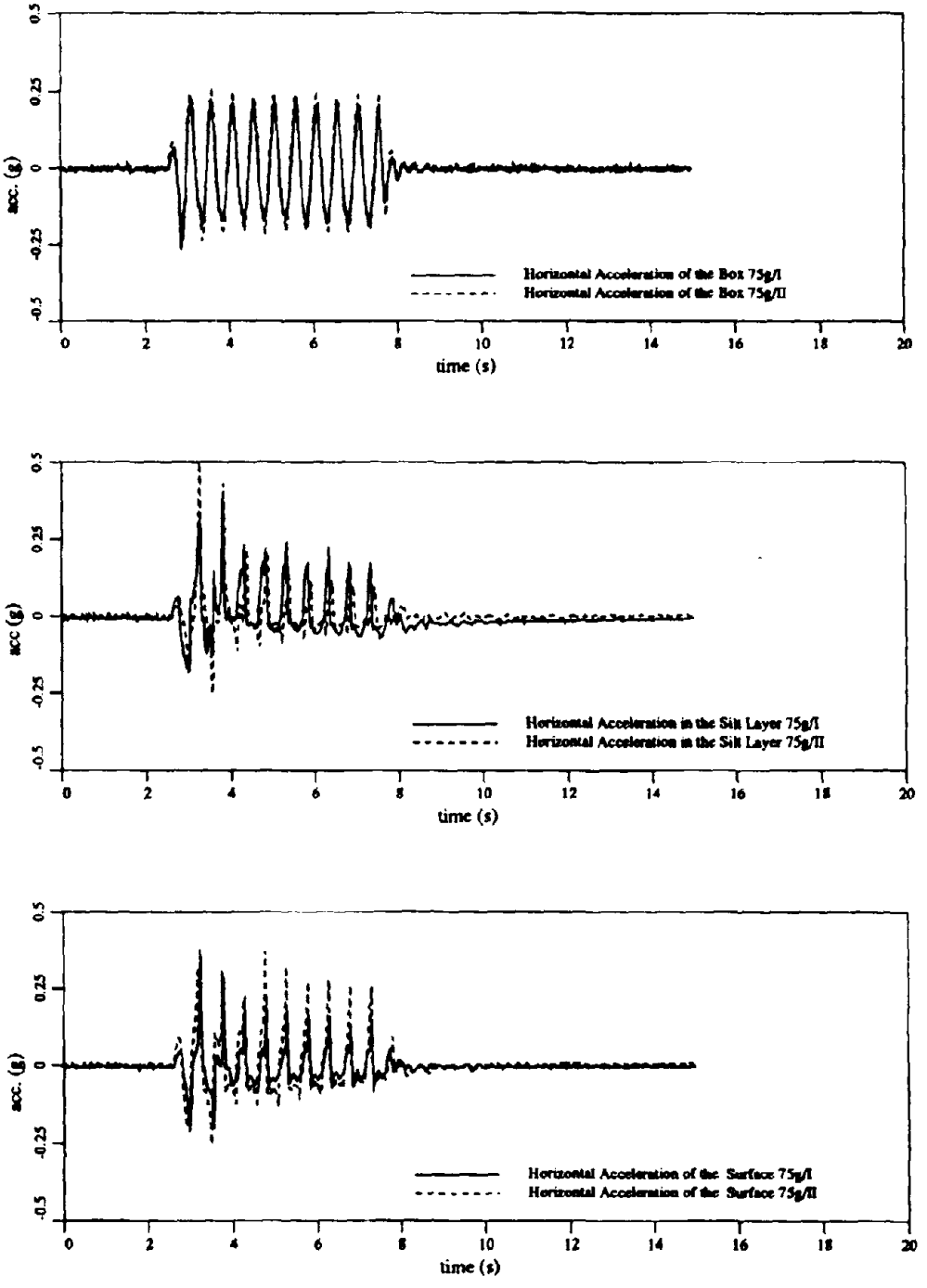

Figure 4.4: Comparison of the Measured Horizontal Acceleration Time Histories of the 75*g* Tests

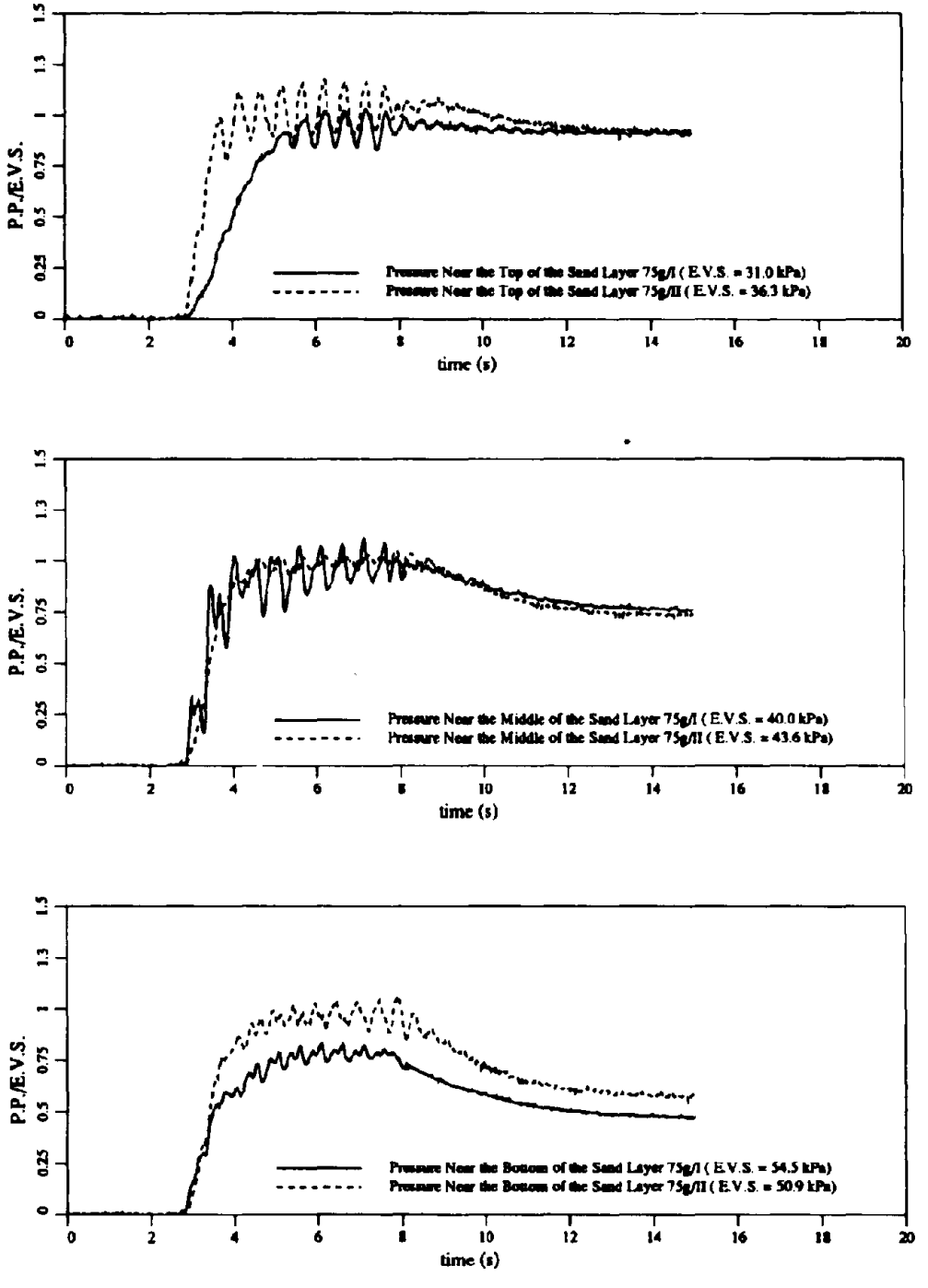

Figure 4.5: Comparison of the Measured Pore Water Pressure Time Histories of the 75*g* Tests

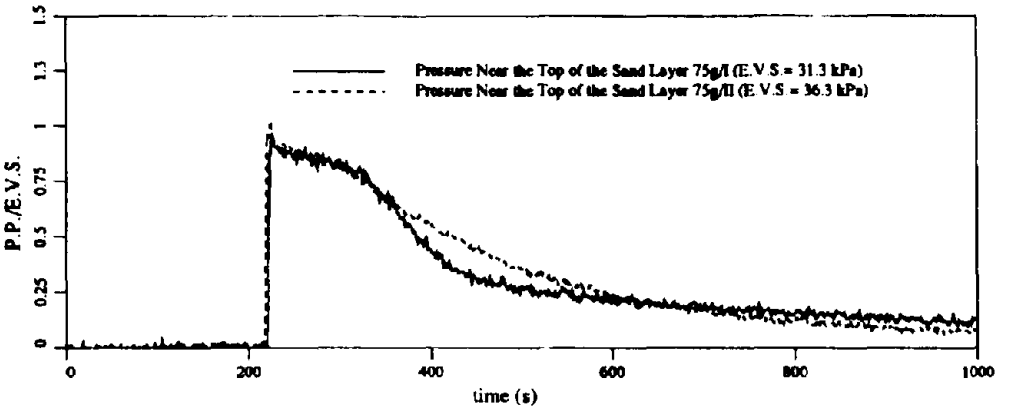

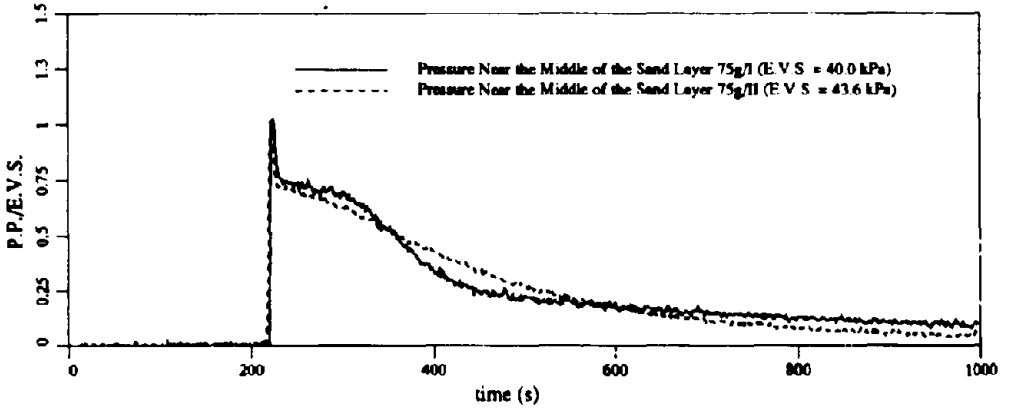

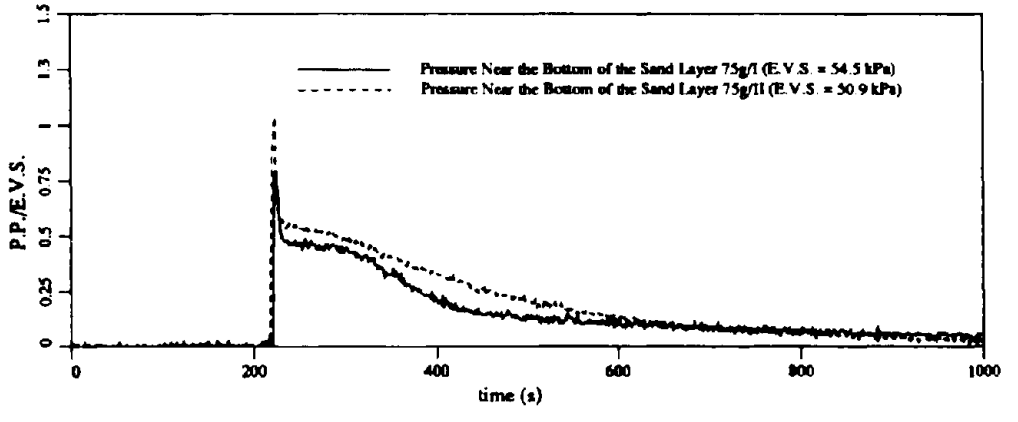

Figure 4.6: Comparison of the Measured Pore Water Pressure Time Histories (Long-Term) of the 75*g* Tests

4.5 Comparison Between the $100g$ and the $75g$ Tests (Modelling of Models Concept)

Centrifuge modelling principles used to interpret model tests in terms of prototype behavior can not often be verified with the prototype results. Prototype monitoring is always expensive and not always possible. The modelling of models concept evolved as an alternative to provide a good check of centrifuge modelling procedures.

In the absence of the prototype, comparison was made between the first and the second group of tests, performed with models of different sizes at different centrifugal accelerations. Model dimensions, of both groups, scaled with a g level, corresponding to each test, give the same prototype geometry.

Figure 4.7 provides acceleration time history comparisons. Since few data were recorded in the first $100g/I$ test, most of the comparisons were made with the second $100g/II$ test and the two $75g$ tests. Time histories of the $100g$ tests were given a very small offset in order to make the comparison easier, otherwise it would be hard to distinguish the two diagrams. The first two peaks of the acceleration time histories have about 30% higher level than input acceleration both in the silt layer and at the top of the silt. But after the sand close to the silt layer liquefies, the acceleration level decreases, which can be explained by the inability of the shear waves to propagate through liquefied sand.

Figures 4.8 and 4.9 show a short and a long term pore pressure time history comparisons. For both tests, the peak residual pressure may be observed when the excitation has ceased at about 8 seconds, and before significant drainage has time to occur. It can be seen that fluctuations in the pore pressure time histories, recorded during the $100g$ tests, were significantly reduced during the $75g$ tests due to new orientation of the transducers (perpendicular to the shaking direction).

Due to the different time scaling of the dissipation effects, one would expect faster pore pressure dissipation in $100g$ tests, which is not the case, but significant difference in pore pressure dissipation has been noticed between the two $100g$ tests as well.

Similar behavior of both models extrapolated to the projected prototype is a good verification of the scaling relations used, as well as of the consistency of the centrifuge model testing scheme [8].

4.6 Vertical Displacements

The old Linear Voltage Displacement Transducer which was used in the first test ($100g/I$) did not allow careful measurements of the vertical displacements of the silt surface. The reason was the sinking of the LVDT core support plate in the silt layer. It was impossible to distinguish which part of the recorded displacements was due to the sinking of LVDT core, and which part were actual settlements of the silt surface.

In order to eliminate the problem with the LVDT, it was necessary to use a device capable of measuring displacements of a remote object without physical contact with that object. The non-contact position measuring instrument used in $75g$ tests (Bonnie I and Bonnie II) was KAMAN KD-2300-8CM differential impedance transducer with linear range of 12 $[mm]$.

The device uses a metal object (surface) as a target, and gives voltage (current) output proportional to the distance between the transducer's head and the metal target. The impedance head was placed above the soil sample (Figure C.27), and a piece of a very light aluminum foil placed on the silt surface was used as a target.

Figures 4.10 and 4.11 show good repeatability of the short and the long-term vertical displacements recorded in the two tests. It can be observed that contact LVDT has larger final displacements, with most of the displacements occuring during

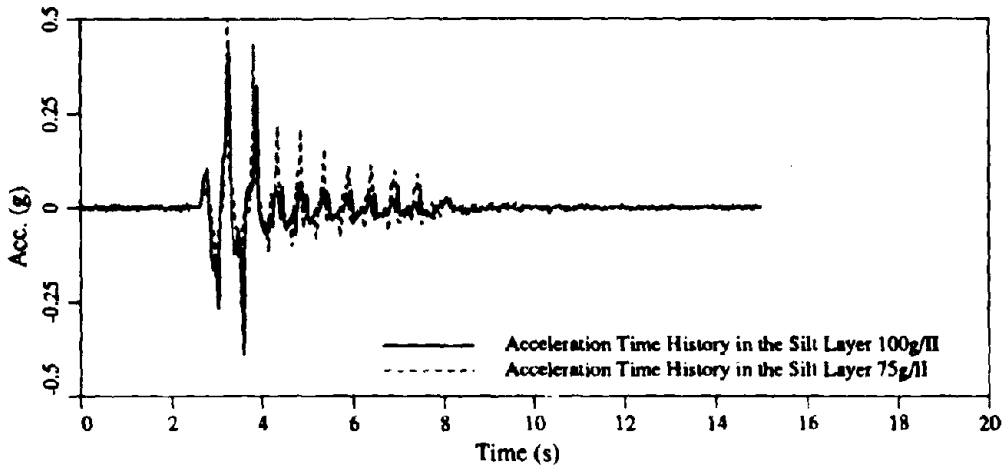

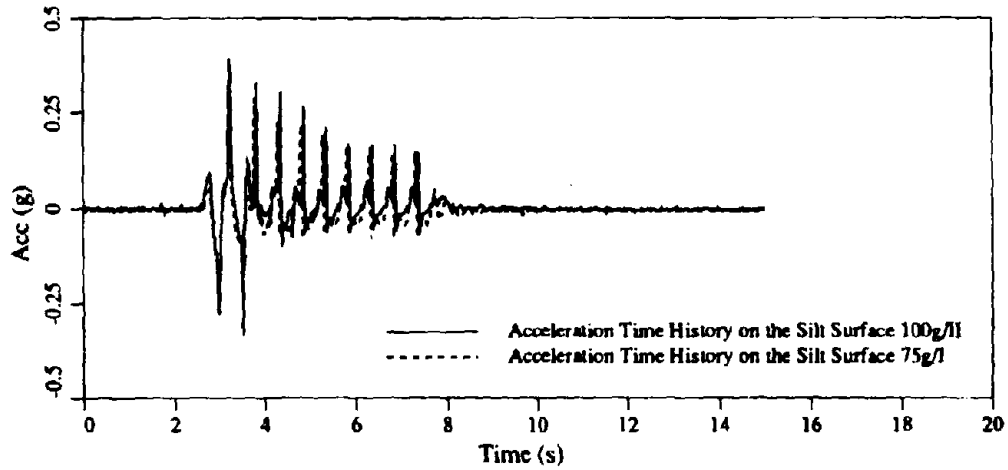

Figure 4.7: Standard VELACS Model Test Acceleration Time Histories Comparison Between 100*g* and 75*g* Tests

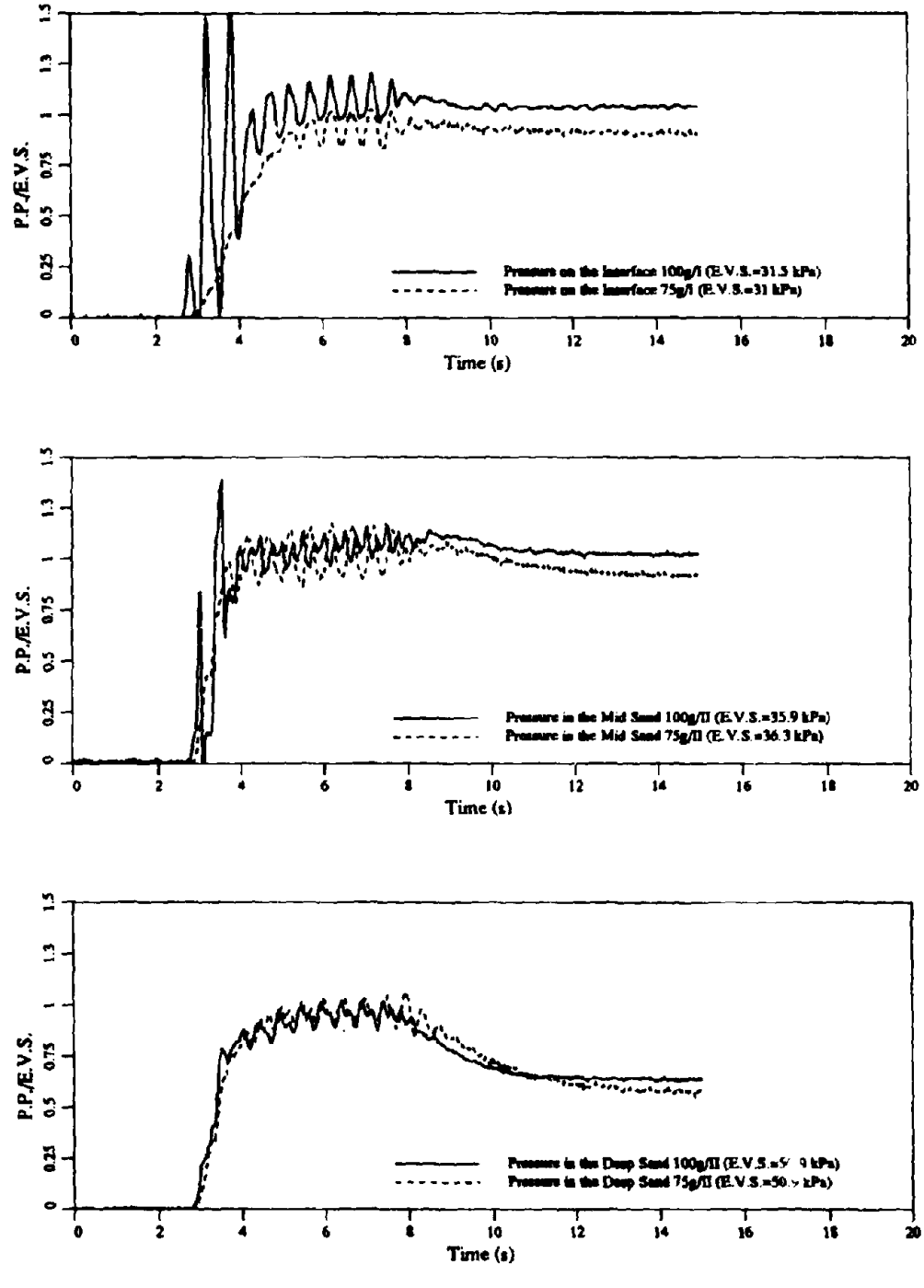

Figure 4.8: Standard VELACS Model Test Short Term Pore Pressure Ratio Time Histories Comparison Between 100*g* and 75*g* Tests

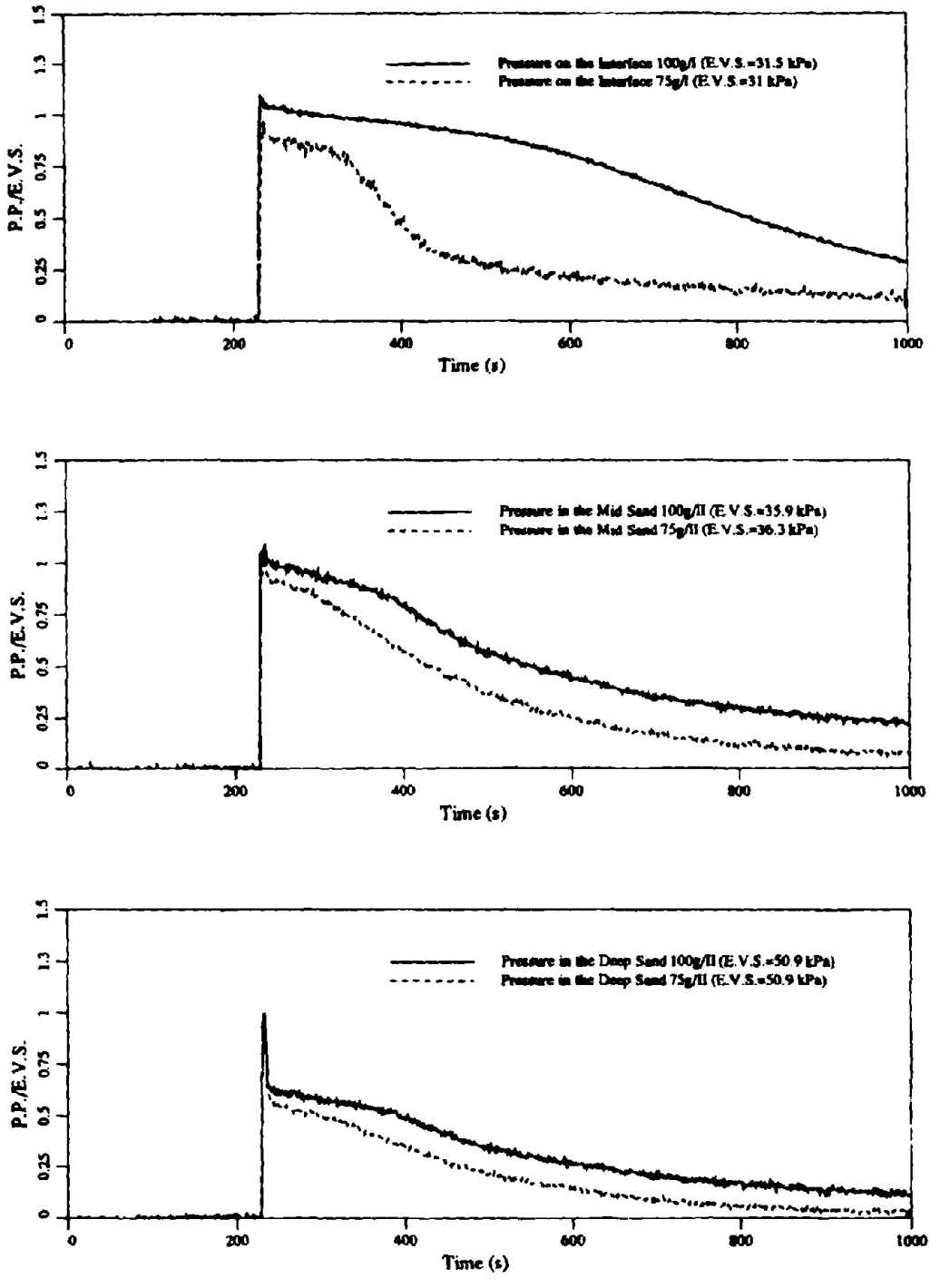

Figure 4.9: Standard VELACS Model Test Long Term Pore Pressure Ratio Time Histories Comparison Between 100g and 75g Tests

the shaking. On the other hand, the KAMAN (non-contact device) has recorded less deformations with all displacements taking place after the event.

From Figure 4.12 one can observe that the time interval needed for most of the displacements to occur corresponds in length to the time interval during which most of the excessive pore water pressure is dissipated. The displacement time histories recorded with LVDT show some post-event settlements as well.

The second test sample was left until the Bonnie silt was completely dry. The LVDT core support plate and the aluminum target were then removed. While the aluminum foil stayed on the surface of the silt, the LVDT core support plate sank in the silt producing a crater close to 1 [mm] deep. Since the test was performed in a $75g$ environment, corresponding prototype crater depth is close to 7.5 [cm].

All these results are suggesting that the vertical displacements recorded with a contact device whose footing is sitting on the silt surface, during the short earthquake-like event, are most likely caused by the footing sinking in the silt. However, post-shaking measurements are fairly accurate, although one can never be completely confident in obtained results, because the footing can sink even deeper.

Measurements obtained by KAMAN (non-contact) apparatus support thinking that a vertical displacement of a fully saturated porous material layer is possible only if water is allowed to evacuate from the porous material.

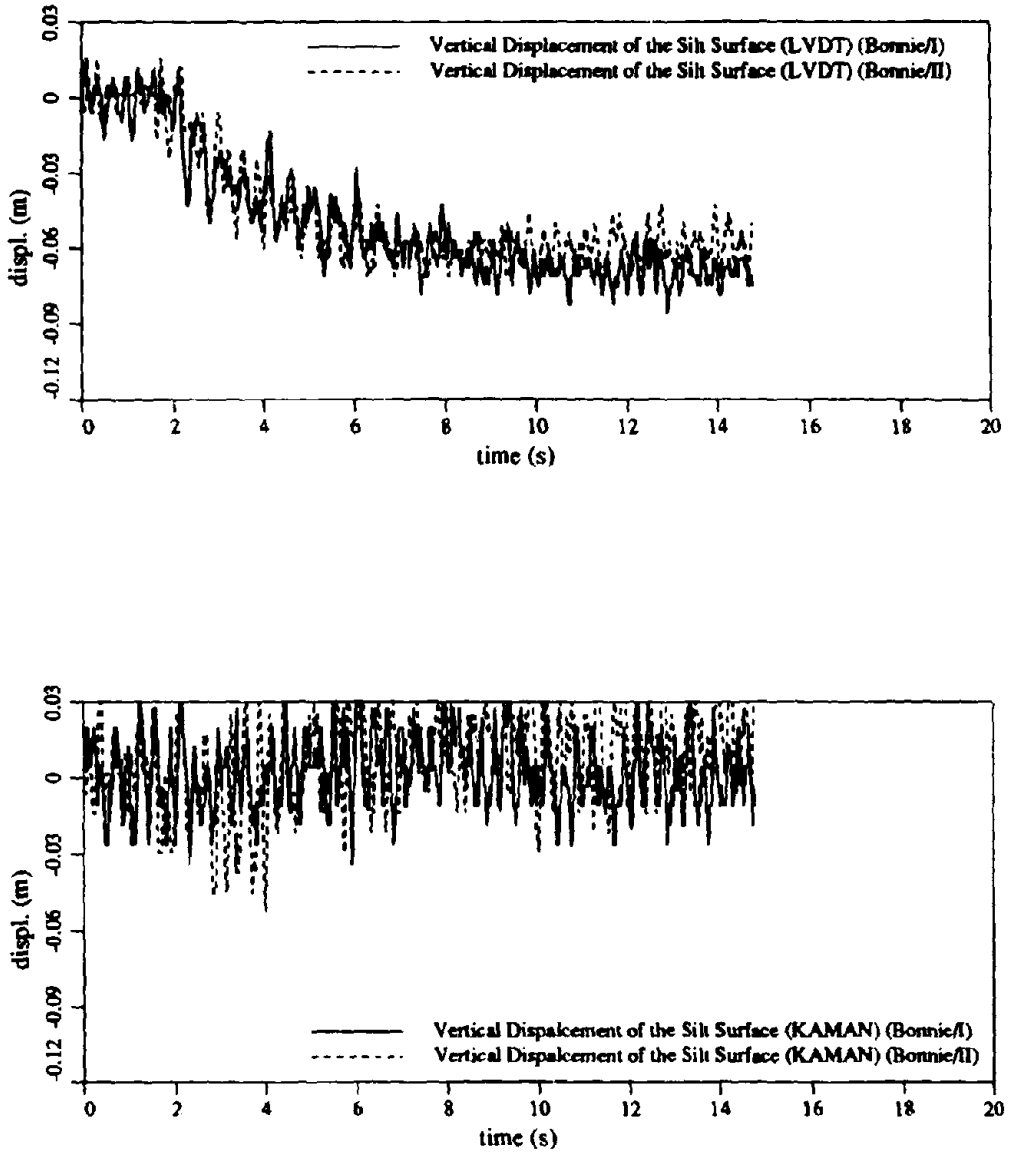

Figure 4.10: Short Term Vertical Displacement Comparisons of the Two 75*g* Tests With the Bonnie Silt

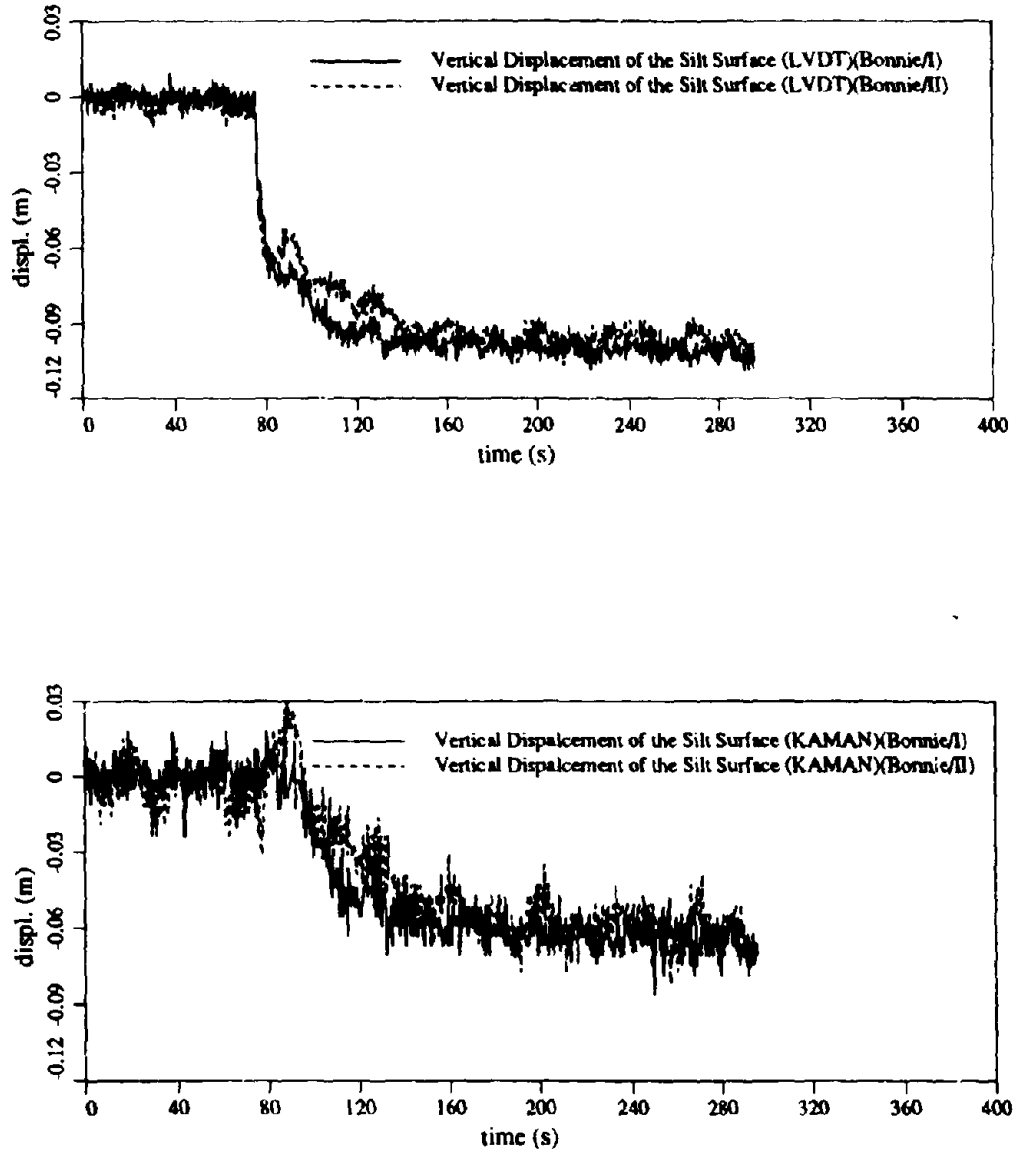

Figure 4.11: Long Term Vertical Displacement Comparisons of the Two 75*g* Tests With the Bonnie Silt

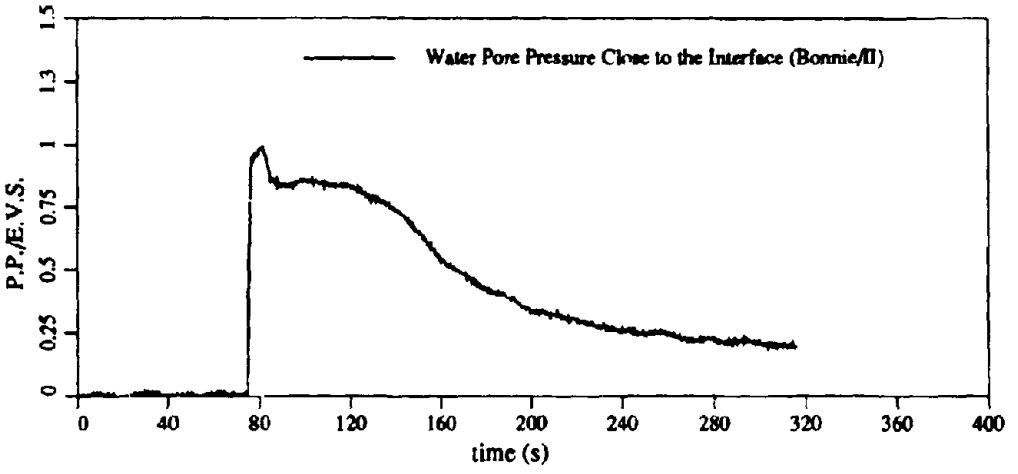

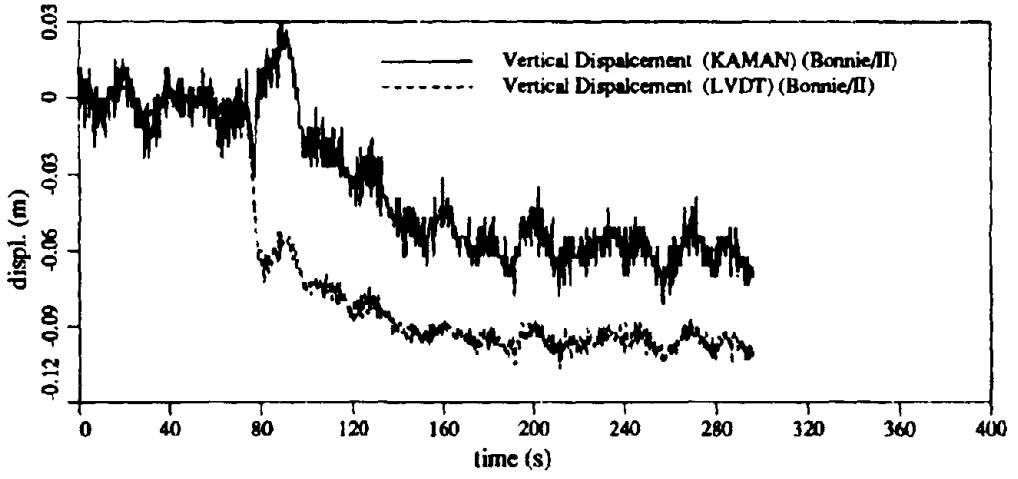

Figure 4.12: Long Term Vertical Displacements and Long Term Pore Water Pressure Time History of the Test Bonnie/I

4.7 Numerical Simulation

4.7.1 Introduction and Background

Several numerical analyses were performed in an effort to accurately simulate the performed centrifuge tests. In the first group of analyses, the Standard VELACS check test was idealized assuming a one-dimensional geometry: deformations and stresses are assumed to be uniformly distributed over the horizontal layers. The second group of analyses involved 2D geometry which can introduce various types of boundary conditions.

Numerical simulations were performed using the computer codes DYNA1D [16], and DYNAFLOW [18] Both DYNA1D and DYNAFLOW analyses involve evaluation of the spatial and temporal variation of ground motions together with the determination of the effects of seismic waves (potential liquefaction).

The assumptions used in one-dimensional analysis are that the site consists of horizontal layers, and excitation consists of vertically propagating dilatational and shear waves. Some authors [3] take in consideration only horizontal motions generated by shear waves' vertical propagation through the system. Such an assumption is valid for saturated soil media if no drainage of the pore water can take place during the seismic event [16]. However, for the soil deposits with moderate permeabilities, in the case of the VELACS check test, drainage can take place and vertical motions should be included in the analysis. Further, a complete effective stress analysis that models nonlinear stress-strain response should be conducted in cases where liquefaction is possible. DYNA1D is a finite element analysis program designed to perform nonlinear seismic site response calculations, taking into account:

- the nonlinear, anisotropic and hysteretic stress-strain behavior of the soil materials;

- the effects of the transient flow of the pore water through the soil strata.

Procedures used in DYNA1D are general and can be applied in multidimensional analysis (DYNAFLOW). The appendix to this section provides some results of the 1D and 2D analysis performed with the same procedures (field and constitutive equations), and the same material properties.

Although very reliable and simple to use, one-dimensional analysis does not consider boundary conditions inside the centrifuge. In order to include the effects of the testing box, it was necessary to perform a two-dimensional analysis with DYNAFLOW.

4.7.2 One-Dimensional Finite Element Discretization

Each of the two horizontal layers was modeled with six two-node one-dimensional elements (Figure 4.13), with the following analysis options:

- hyperbolic type analysis for two phase porous continuum;
- 4 d.o.f. per node;
- 2000 time steps of 0.01 $[s]$;
- water table at the silt surface;
- compressible fluid;
- implicit-explicit treatment for the solid effective stress contribution to the equations of motion;
- select integration scheme parameters $g = 0.65$ and $b = 0.33$ for the introduction of the high frequency numerical dissipation;
- 12 elements, 13 nodes resulting in 49 equations;

- prescribed acceleration for the solid phase horizontal d.o.f. at the base node;
- no vertical displacement allowed for both phases at the base node.

Since 1D analysis requires a considerably smaller amount of computer time than 2D analysis, parametric study involving change of material permeabilities was performed with DYNA1D. 2D analysis was then performed with material properties obtained with 1D parametric study.

4.7.3 Two-Dimensional Finite Element Discretization

The finite element model for 2D analysis consists of the 132 equally sized rectangular elements (Figure 4.14). The following options were employed in 2D analysis:

- hyperbolic type analysis for two phase porous continuum;
- 4 d.o.f. per node;
- 2000 time steps of 0.01 [s];
- water table at the silt surface;
- compressible fluid;
- modified Newton-Raphson iteration procedure;
- implicit-explicit treatment for the solid effective stress contribution to the equations of motion;
- select integration scheme parameters $g = 0.65$ and $b = 0.33$ for the introduction of the high frequency numerical dissipation;
- 132 elements, 156 nodes resulting in 539 equations;

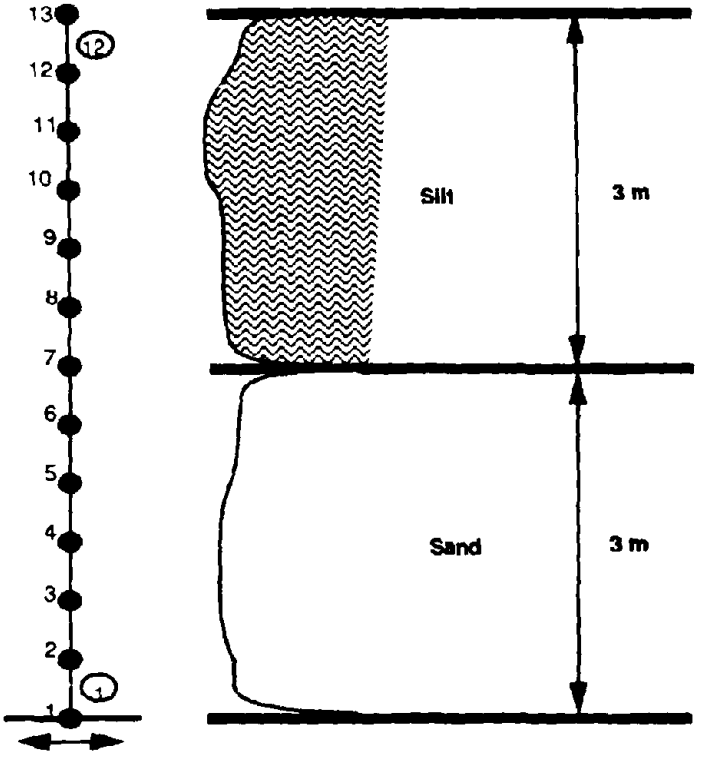

Figure 4.13: 1D Numerical Model for the VELACS Standard Test

- prescribed acceleration for the solid phase horizontal d.o.f. for the base nodes and for the nodes on both sides to simulate *the box effect*;
- no vertical displacement allowed for both phases for the base nodes;
- slaved horizontal d.o.f. for the water phase for all nodes at the base;
- slaved vertical d.o.f. for the water and the solid phase on the both sides of the mesh;

4.7.4 Material Properties

The elasto-plastic purely kinematic hardening constitutive model for pressure sensitive materials was adopted to simulate the soil behavior [15]. The material properties used for the analysis are shown in Table 4.2.

Where available, the material parameters were evaluated from the soil laboratory test results reported by Earth Technology Corporation [4], otherwise, they were assumed. A parametric study was performed with different values for the material permeabilities.

Material properties for the Ottawa silt were assumed to be the same as those reported for the Bonnie silt [4] .

$$Specific\ Gravity = 2.67 \tag{4.1}$$

$$Void\ Ratio = 0.687 \tag{4.2}$$

$$Permeability = 1.0E-08\ [m/sec] \tag{4.3}$$

The initial shear modulus value is the mean of the resonant column tests data obtained for the effective confining pressure of $80kPa$ [4].

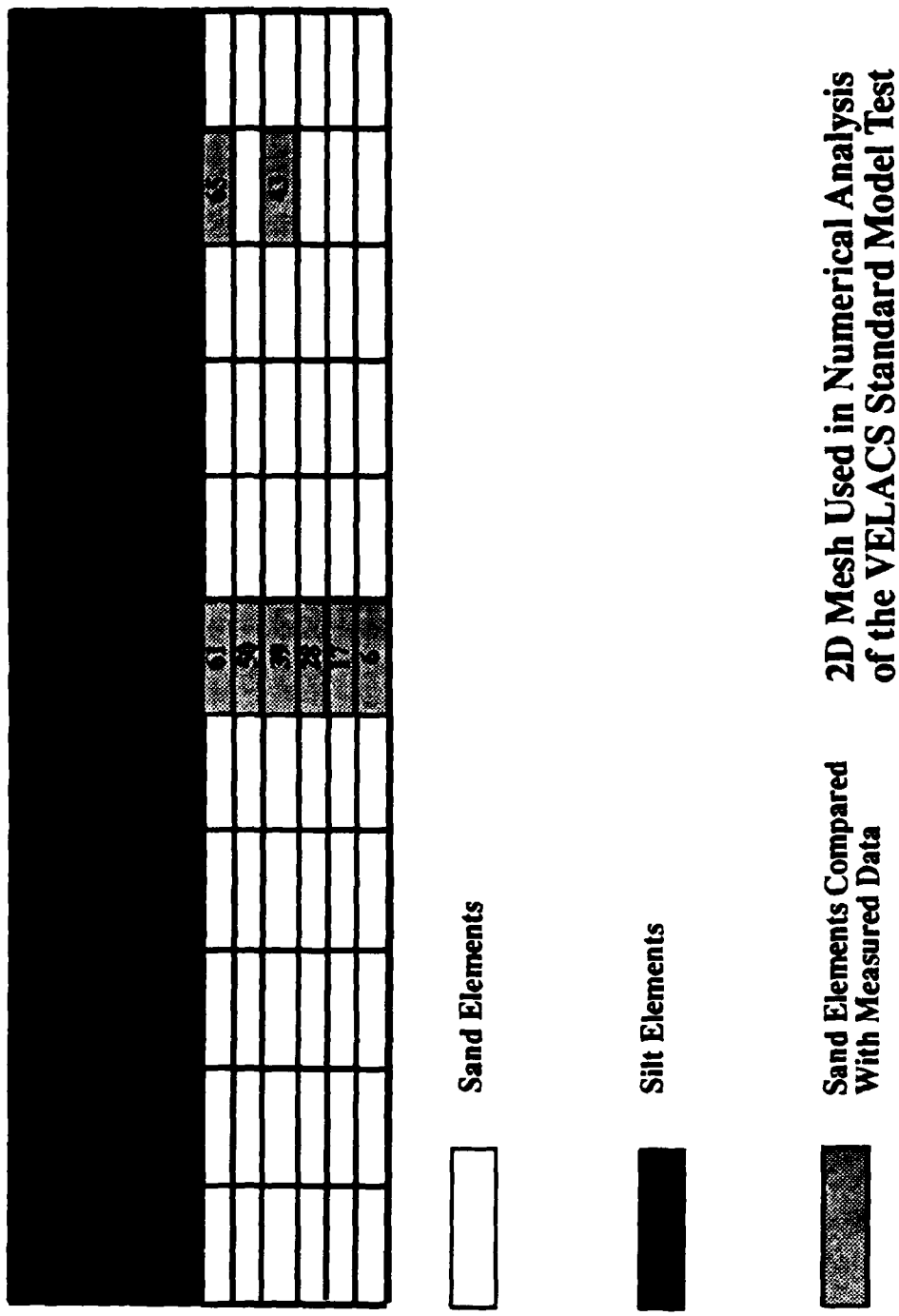

Figure 4.14: **2D Numerical Model for the VELACS Standard Test**

Property	Nevada Sand	Ref.	Silica Silt	Ref.
Mass density (Kg/m^3)	2680	[4]	2670	[4]
Porosity	0.4	R.D. 60 %	0.42	
Permeability	5.6×10^{-5}	[4]	1.0×10^{-8}	[4]
Low Strain Shear Modulus (MPa)	68.9	[4] Eq. 4.6	2.7	Assumed, see text
Poisson's Ratio	0.3	[13]	0.4	[13]
Bulk Modulus (MPa)	149.3		12.7	
Fluid Bulk Modulus (MPa)	2000		2000	
Cohesion (kPa)	0		10	[13]
Reference Mean Normal Stress (kPa)	60		23.3	
Dilatation Angle (compress. and ext.)	25°	[4] see text	15°	Assumed, see text
Dilatation Parameter	0.05		0.02	
Friction Angle (compress. and ext.)	30°	Assumed, see text	20°	Assumed, see text
Coefficient of Lateral Stress	0.5	[13]	0.67	[13]
Slope of the Stress Path	0.33		0.33	
Max. Shear Strain in Compression	0.05		0.05	
Max. Shear strain in Extension	0.03		0.03	

Table 4.2: **Material Properties Used in Numerical Analysis**

$$Test\,60-41 \quad G_0 = 85.71 MPa \tag{4.4}$$

$$Test\,60-43 \quad G_0 = 73.45 MPa \tag{4.5}$$

The dependence of the moduli on the mean effective stress was taken into account by referring the initial moduli G_0 to the reference mean stress p_1 as:

$$G_1 = G_0 \left(\frac{p_1}{p_0}\right)^n \tag{4.6}$$

Where p_1 is a reference mean stress for the model, p_0 is confining pressure in a resonant column test, and the parameter $n = 0.5$ for the sand, and $n = 0.8$ for the silt. The shear modulus for the silt was assumed to be 10% of the sand shear modulus. Values for Poisson ratios and the coefficients of lateral stress were assumed within the range proposed by Nonveiller [13] as:

$$Sand\ k_0 = 0.43 - 0.54\ \nu = 0.30 - 0.35 \tag{4.7}$$

$$Silt\ k_0 = 0.67 - 0.69\ \nu = 0.40 - 0.45 \tag{4.8}$$

Sand friction angle was obtained from monotonic 'triaxial' soil test data [4]. Diagrams on Figure 4.16 show mobilized friction angle in relation to shear and volumetric strains. The friction angle mobilized at 5 % shear strain is close to 38°, with dilation angle of 25°. From the extension 'triaxial' tests (Figure 4.17) one can obtain friction angle of − 30°, mobilized at 3 % shear strain, and dilation angle 25°.

For the purpose of this analysis it was decided to use 30° friction angle in compression, which was obtained by matching plain-strain assumption with Mohr-Coulomb yield criterion.

The yield criterion used in numerical modelling of the Nevada sand was proposed by Drucker and Prager as a simple generalization of Mohr-Coulomb as follows [17]:

$$f = -\alpha \left[\frac{I_1}{3} + \frac{c}{tan\,\varphi} \right] + \sqrt{J_2} - k = 0 \tag{4.9}$$

where α and k are positive material parameters which can be expressed in terms of the cohesion c and friction angle φ. For axial compression ($\sigma_2 = \sigma_3$ *and* $\theta = -\frac{\pi}{6}$) one finds:

$$\alpha = \frac{2\sqrt{3} sin\varphi}{(3 - sin\varphi)} \quad ; \quad k = \frac{2\sqrt{3}\, c\, cos\varphi}{(3 - sin\varphi)} \tag{4.10}$$

and for noncohesive materials:

$$\alpha = \frac{2\sqrt{3} sin\varphi}{(3 - sin\varphi)} \quad ; \quad k = 0 \tag{4.11}$$

Figure 4.15 shows trace of both Mohr-Coulomb and Drucer-Prager surfaces onto the deviatoric stress plane Π. The distance from the origin of any deviatoric plane to the trace of the yield surfaces is given by:

$$\left(\frac{R}{p_a}\right)_{M.C.} = \left(\frac{\sqrt{2}\, sin\varphi}{cos\theta + \frac{1}{\sqrt{3}}\, sin\theta\, sin\varphi} \right) \tag{4.12}$$

$$\left(\frac{R}{p_a}\right)_{D.P.} = \alpha\sqrt{2} \tag{4.13}$$

$$R = \sqrt{2\, J_2} \quad ; \quad p_a = \frac{I_1}{3} \tag{4.14}$$

Using the plain-strain and associative flow assumptions one can obtain the following [17]:

$$sin\,\theta = \frac{\alpha}{\sqrt{3}} \tag{4.15}$$

Equivalent friction angle can be obtained by matching distances from the origin of any deviatoric plane to the trace of the yield surfaces of both criteria:

$$\left(\frac{R}{p_a}\right)_{M.C.} = \left(\frac{R}{p_a}\right)_{D.P.} \tag{4.16}$$

which upon substitution of Eqs. 4.12 and 4.13 leads to:

$$\frac{\sqrt{2}\ sin\varphi_e}{cos\theta + \frac{1}{\sqrt{3}}\ sin\theta\ sin\varphi_e} = \frac{2\sqrt{6}sin\varphi}{(3 - sin\varphi)} \tag{4.17}$$

where φ_e is equivalent friction angle.

Diagram 4.18 shows correlation between friction angle in axial compression and equivalent friction angle in plain strain. Equivalent friction angle that corresponds to the axial compression friction angle of 38° is 26°. Therefore, assumed angle of 30 degrees is on the conservative side.

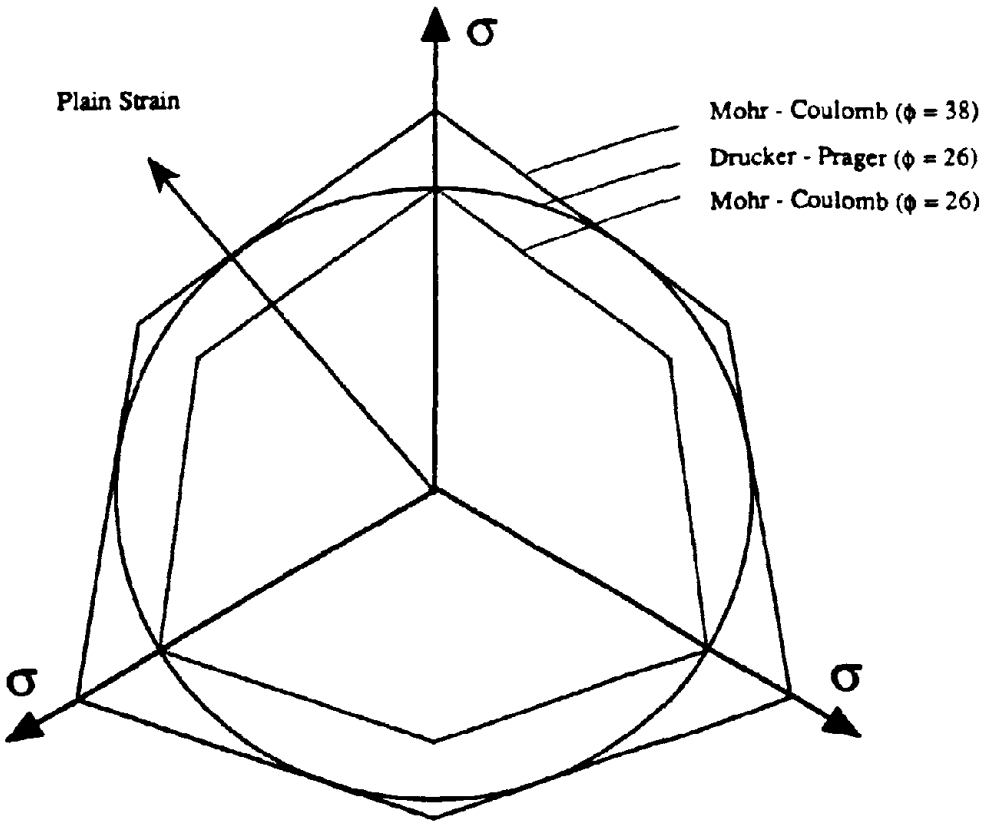

Figure 4.15: Drucker-Prager and Mohr-Coulomb Criteria

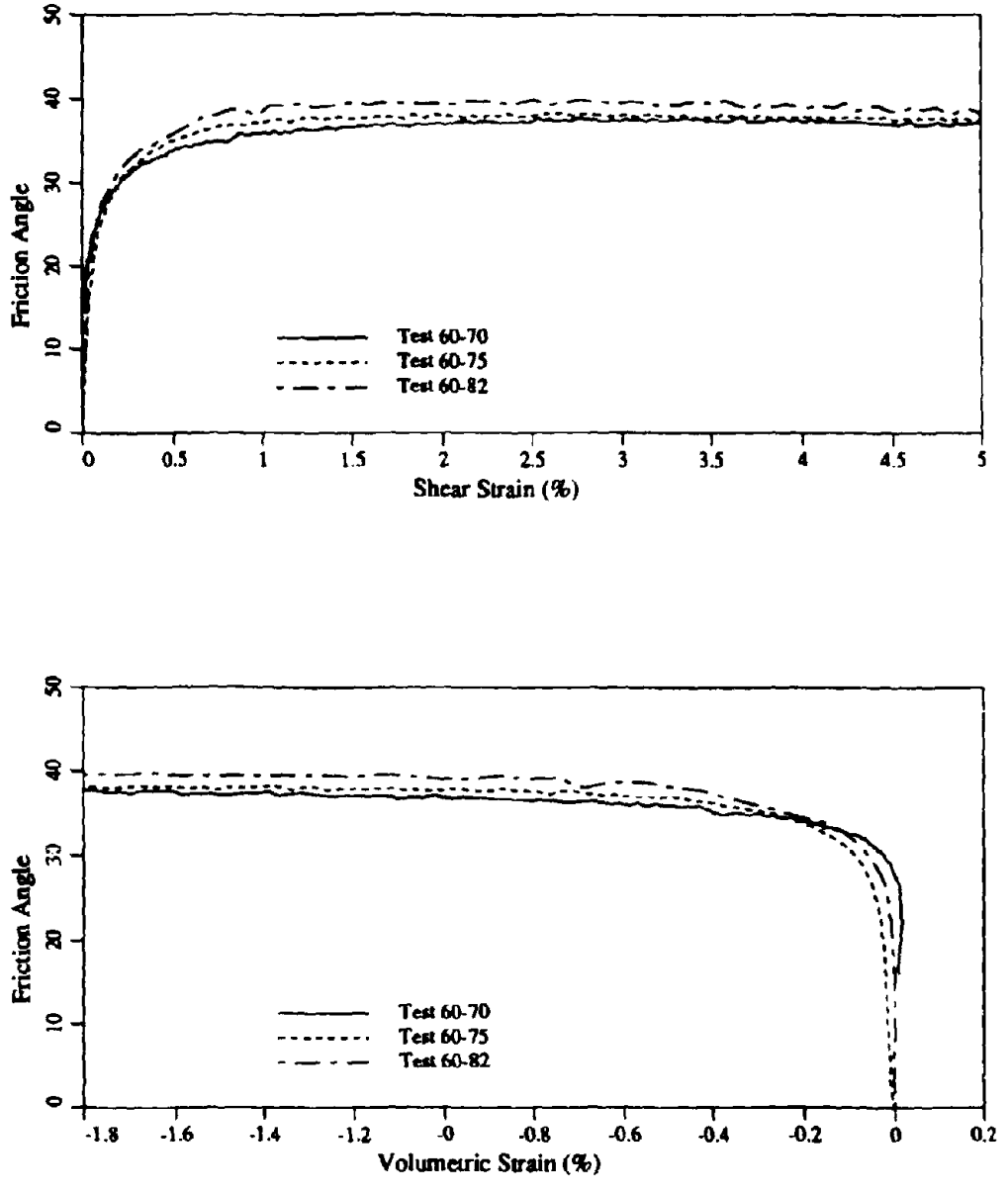

Figure 4.16: Mobilized Friction Angle From the 'Triaxial' Compression Tests

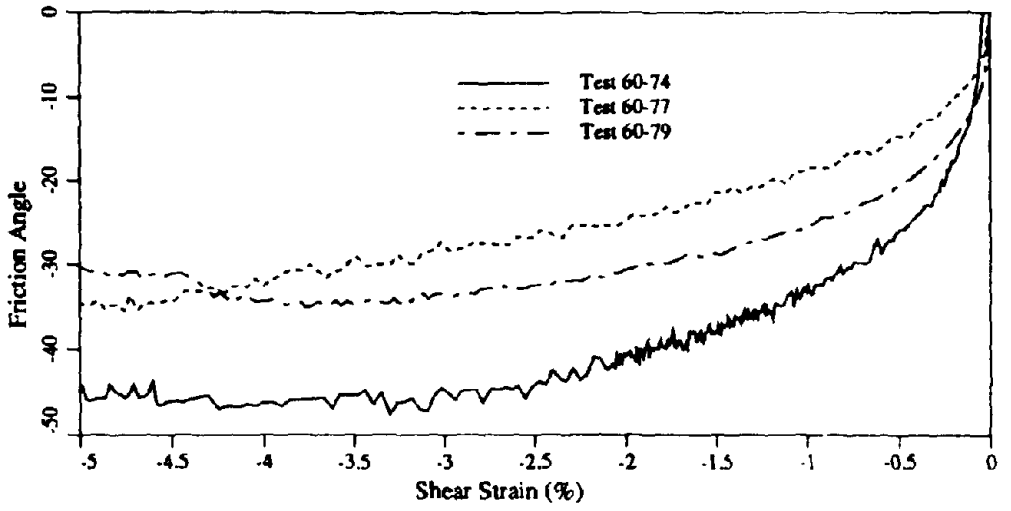

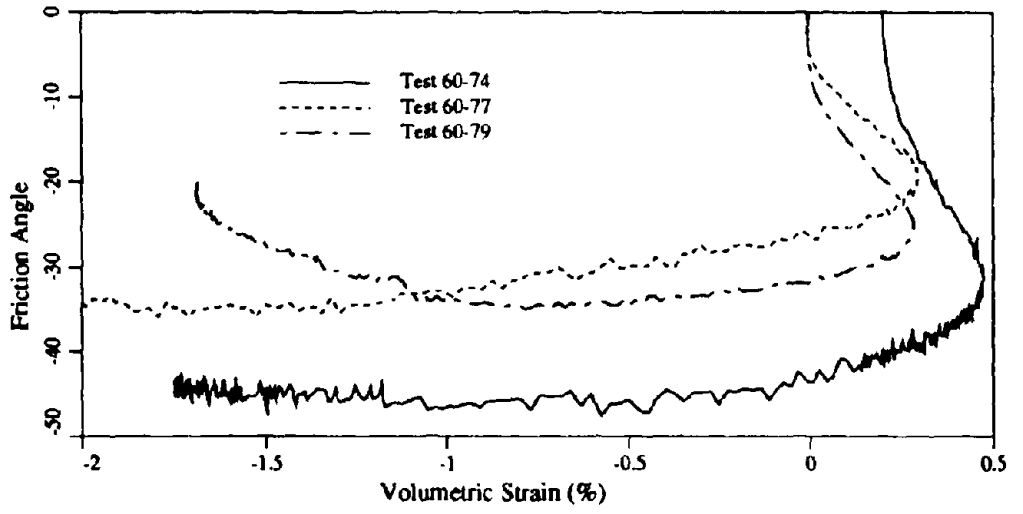

Figure 4.17: Mobilized Friction Angle From the 'Triaxial' Extension Tests

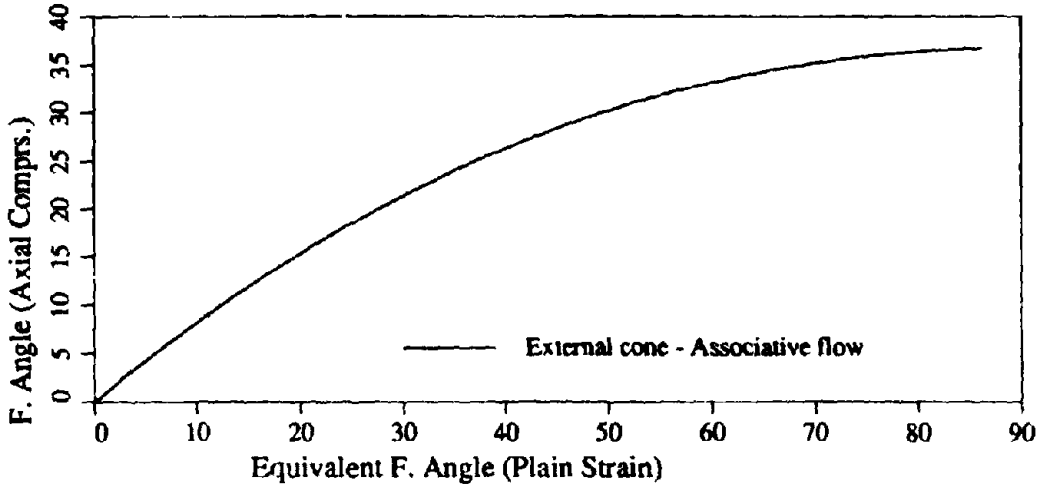

Figure 4.18: **Equivalent Friction Angle (Plain Strain) Versus Friction Angle (Axial Compression)**

4.7.5 Test Results

The first 1D numerical simulation was performed using permeabilities obtained from soil laboratory test results. The horizontal acceleration time history at the base recorded during the first 75g centrifuge test was used as an input motion.

Figures 4.19 and 4.20 show a comparison between computed and measured acceleration time histories for the centrifuge model tests with the different centrifugal acceleration levels. One can notice that, in general, the computed acceleration time histories are in better agreement with the recorded time histories at the silt surface than in the middle of the silt layer. It can be observed that the computed motions are damped faster than the recorded ones.

Figures 4.21 and 4.22 show pore pressure time histories comparisons of computed (DYNA1D) results with the 100g and the 75g tests, respectively. One can detect good coincidence of a pore pressure rise at the sand-silt interface and in the middle of the sand layer, but the level of the computed excessive pore pressure time history

in the deep sand is higher than the measured value.

It can also be seen that computed pore pressure does not dissipate as fast as measured. If the linear scale factor between model and prototype is n then excess pore water pressures dissipate approximately n^2 times faster in the model than in the prototype [2].

Attempts were made by some investigators to increase the model pore fluid viscosity in order to accurately model pore pressure dissipation in the prototype. In this case, when an attempt was made to simulate the behavior of the centrifuge model, it seemed reasonable to expect the residual pore pressure to dissipate faster, and a lower level of excessive pore pressure with increased permeability. Permeabilities of sand and silt were increased 75 times in the second numerical simulation, and results were compared with second group of experimental tests ($75g$ tests). Change in permeability did not affect the acceleration time histories in the silt layer. In a case of pore water pressures, except for the interface pore water pressure, where agreement was satisfactory, increased permeability did not allow pressure to build up in the sand layer (Figure 4.23).

Among the group of tests performed with the different permeabilities (all results are available at Princeton University) congruity of the measured and the calculated time histories (Figure 4.24) was observed with the initial permeability increased 10 times.

In general, it takes more time for the numerical model to build up the pore pressure in the sand layer, but on the other hand the pore pressure is dissipated faster in the centrifuge model.

If one compares the measured pore pressure time history close to the side of the testing box (Figure 4.26) with results obtained with 1D (infinite layers) analysis it becomes clear that some effects of the rigid box boundaries can not be included in

1D analysis. For precise evaluation of the performed centrifuge test it was necessary to introduce the boundary conditions.

2D analysis was performed with permeabilities 10 times larger than ones obtained in the soils laboratory tests. From Figure 4.25 it can be noted that the computed time history curves in the center of the sample are closer to the recorded ones than the 1D time histories. It seems that the rigid box effect decreases the time interval needed for the full pore pressure rise in the numerical model; the time histories obtained with 2D analysis have steepest positive slope. Correlation is even better if comparison is made at points close to the boundary of the sample 4.28. High fluctuations of the water pressure close to the boundaries, in the physical model, can be captured with the numerical model only if input acceleration is introduced to the side nodes, and if both sides are made impervious.

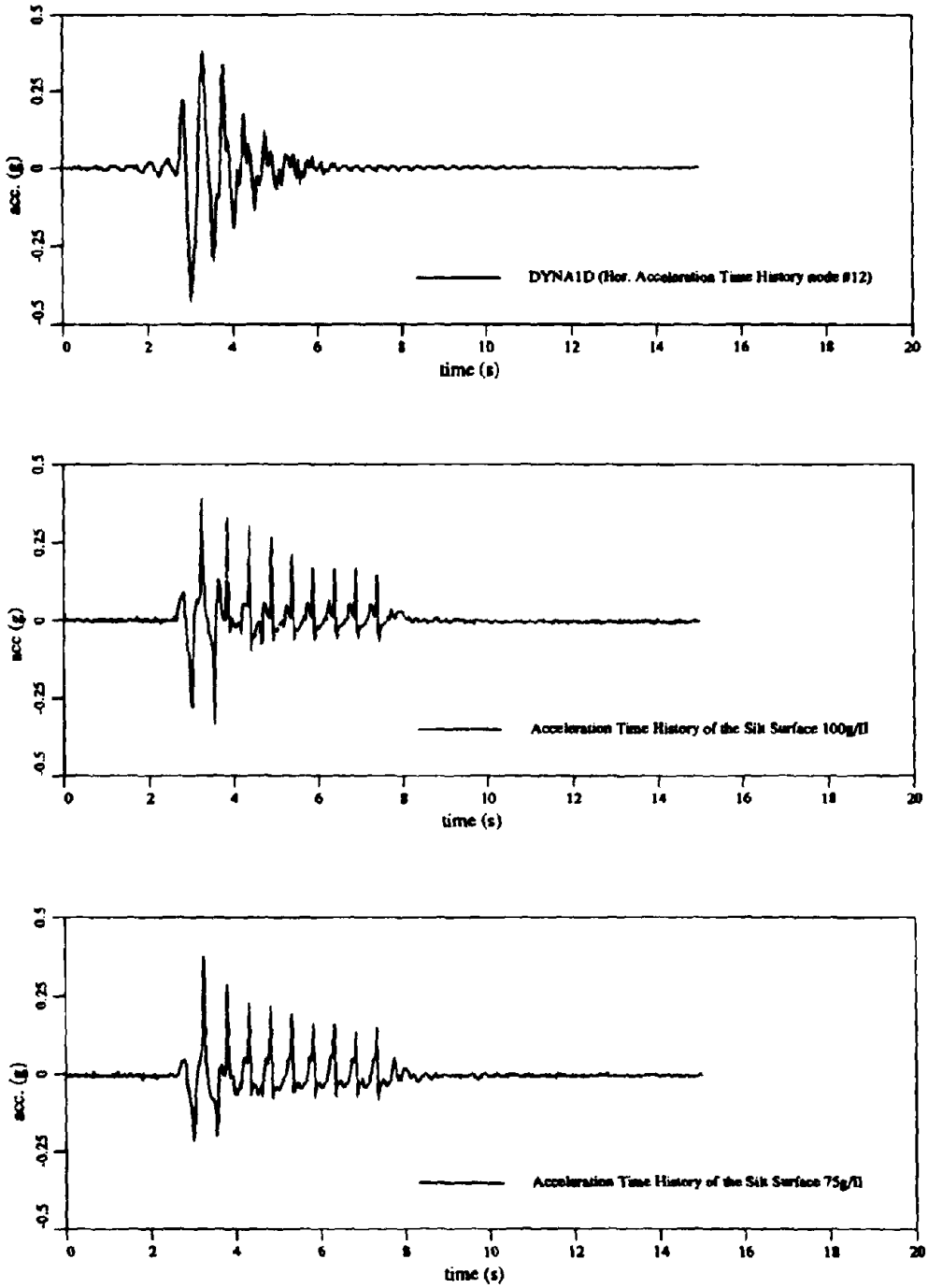

Figure 4.19: Comparison of the Measured and Computed Acceleration Time Histories on the Silt Surface

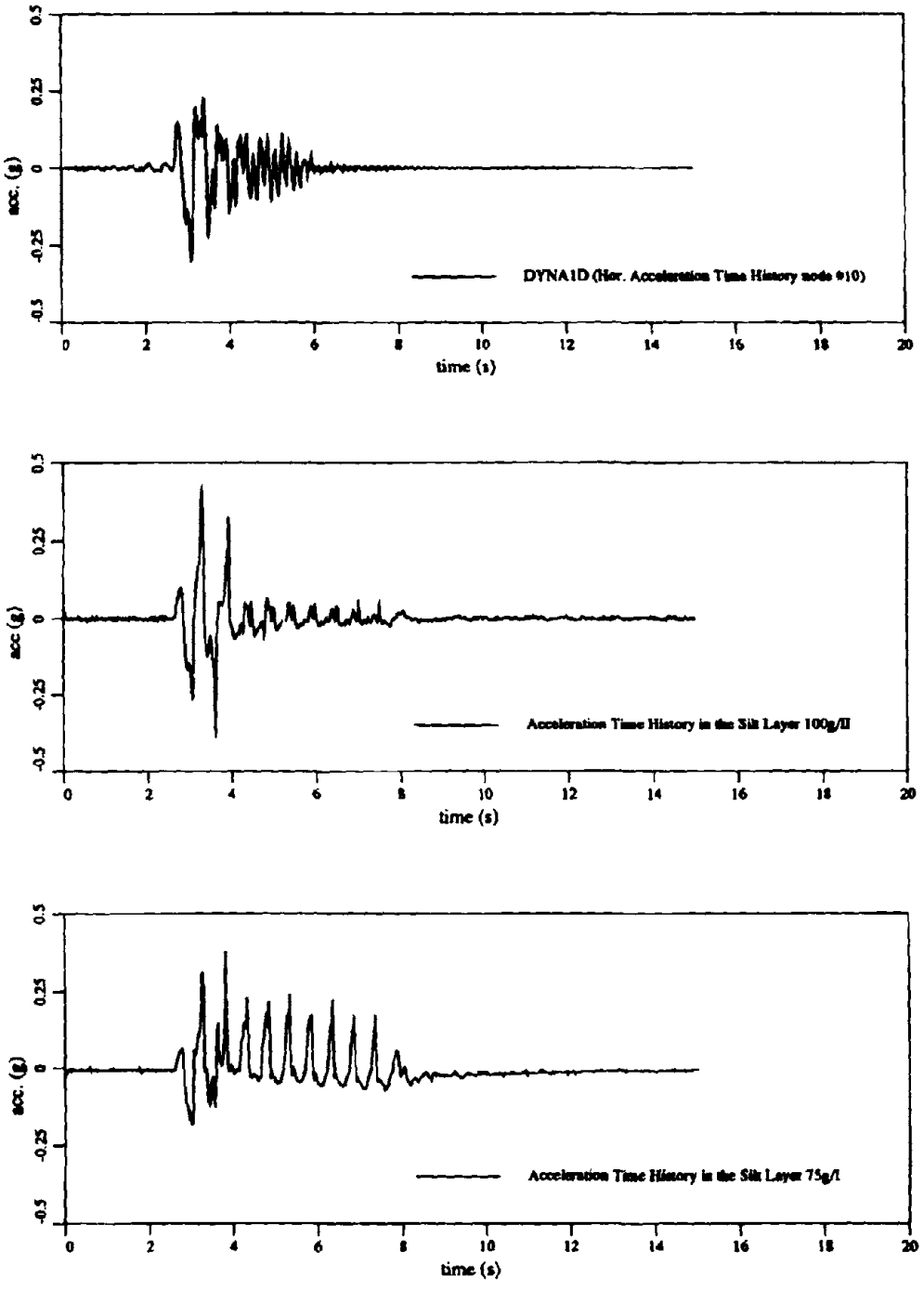

Figure 4.20: Comparison of the Measured and Computed Acceleration Time Histories in the Silt Layer

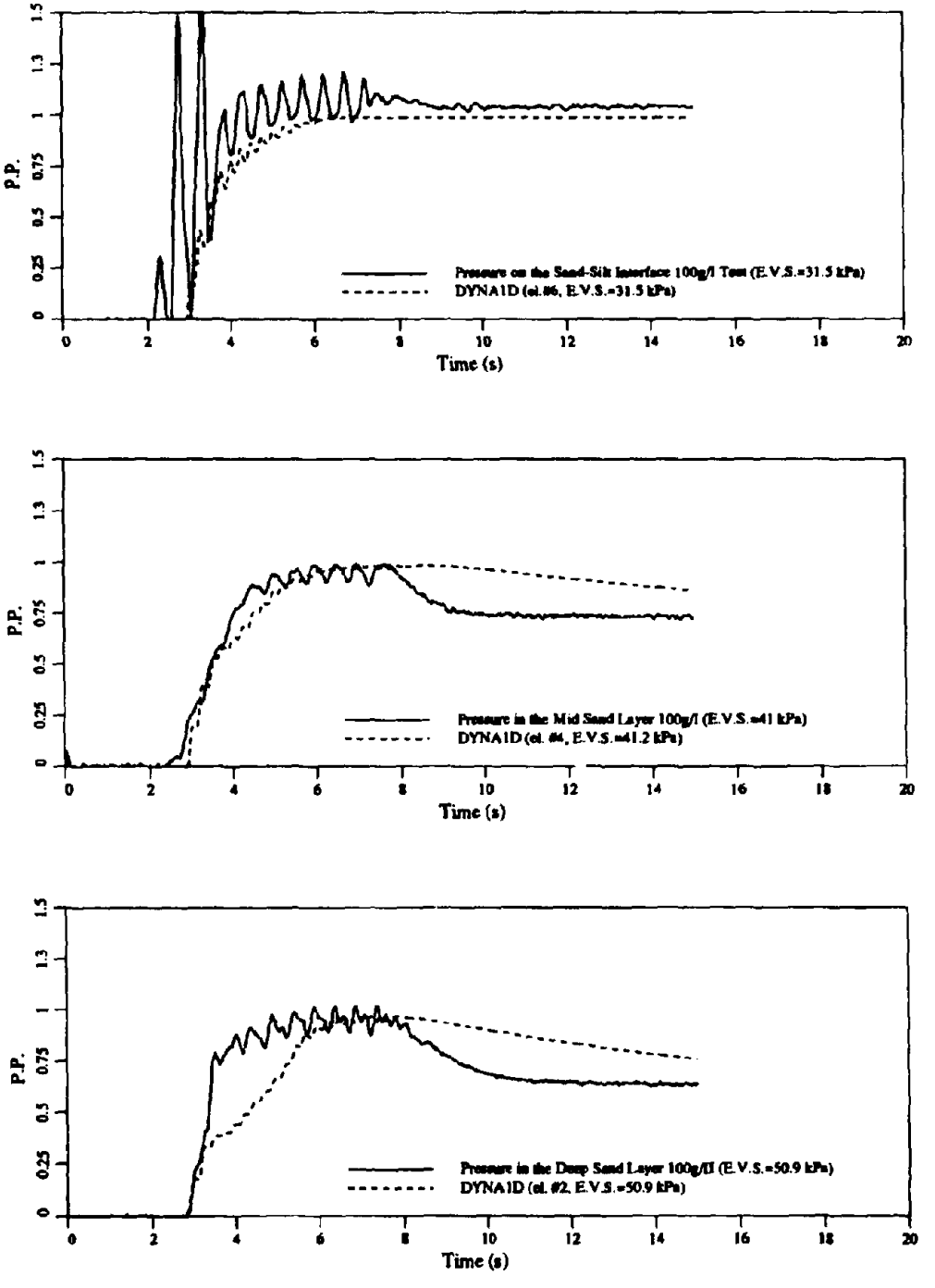

Figure 4.21: Comparison of the Measured and Computed Pore Pressure Time Histories in the Sand Layer

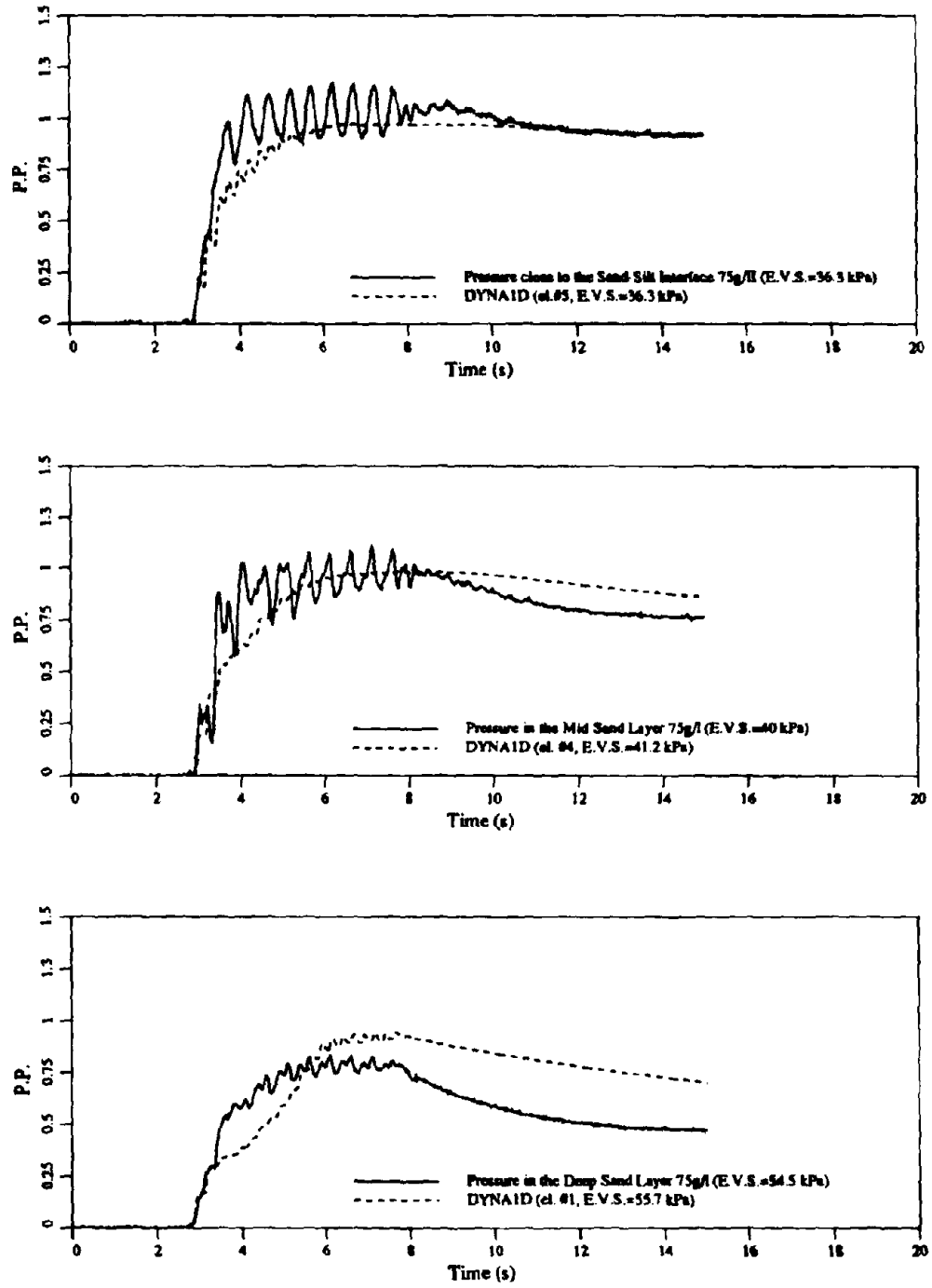

Figure 4.22: Comparison of the Measured and Computed Pore Pressure Time Histories in the Sand Layer

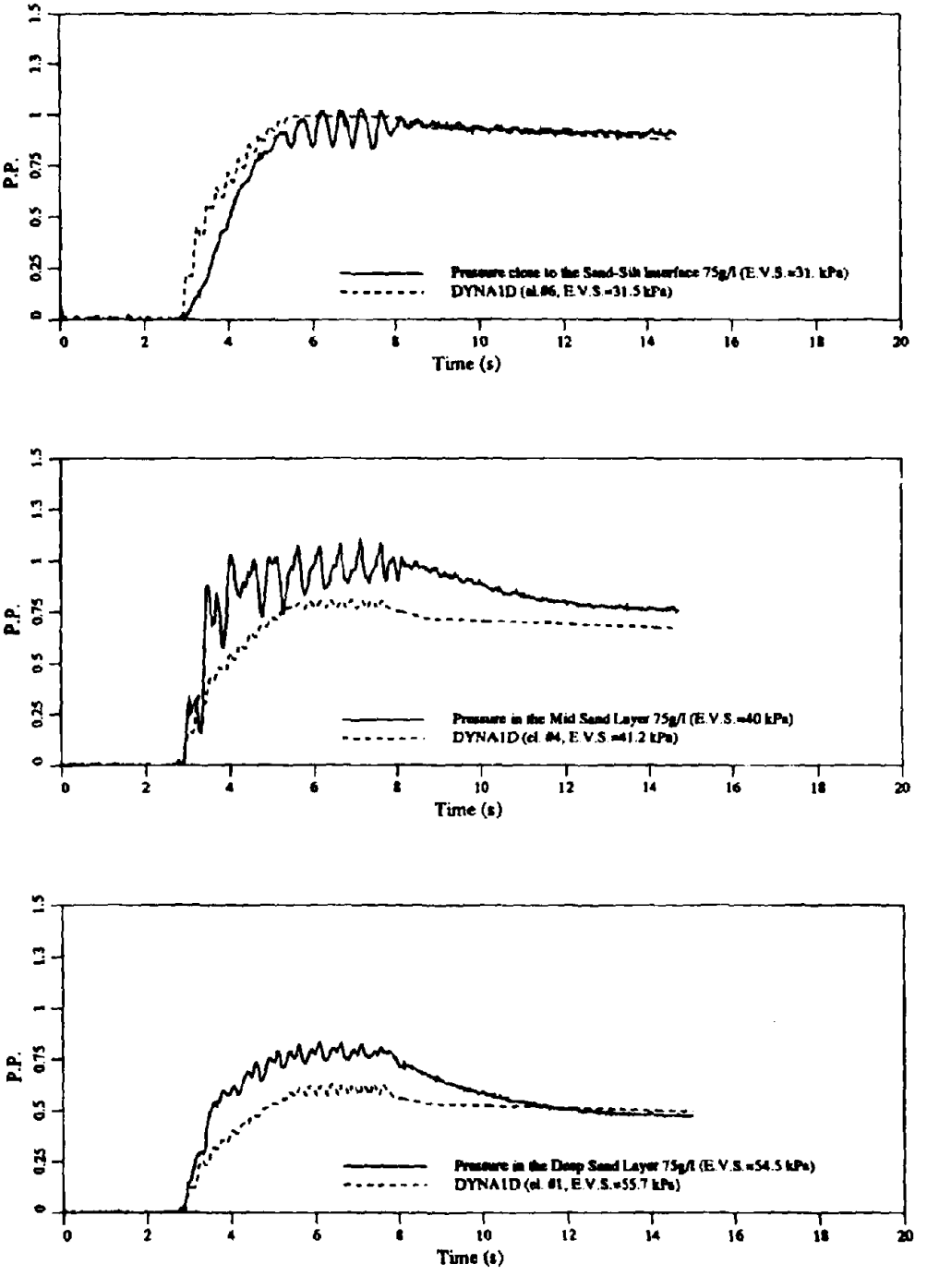

Figure 4.23: Comparison of the Measured and Computed Pore Pressure Time Histories in the Sand Layer With Permeabilities Increased 75 Times

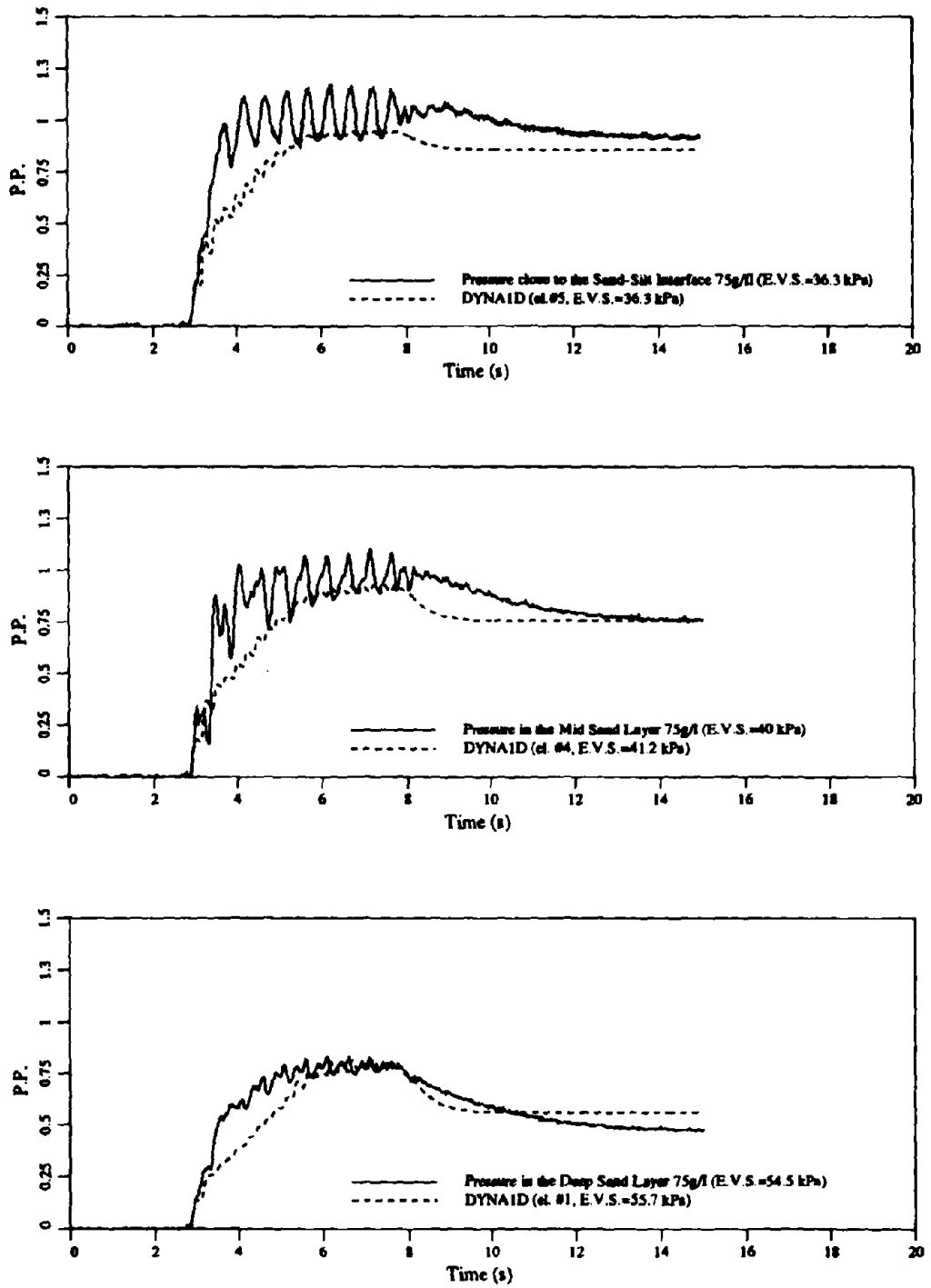

Figure 4.24: Comparison of the Measured and Computed Pore Pressure Time Histories in the Sand Layer With Permeabilities Increased 10 Times

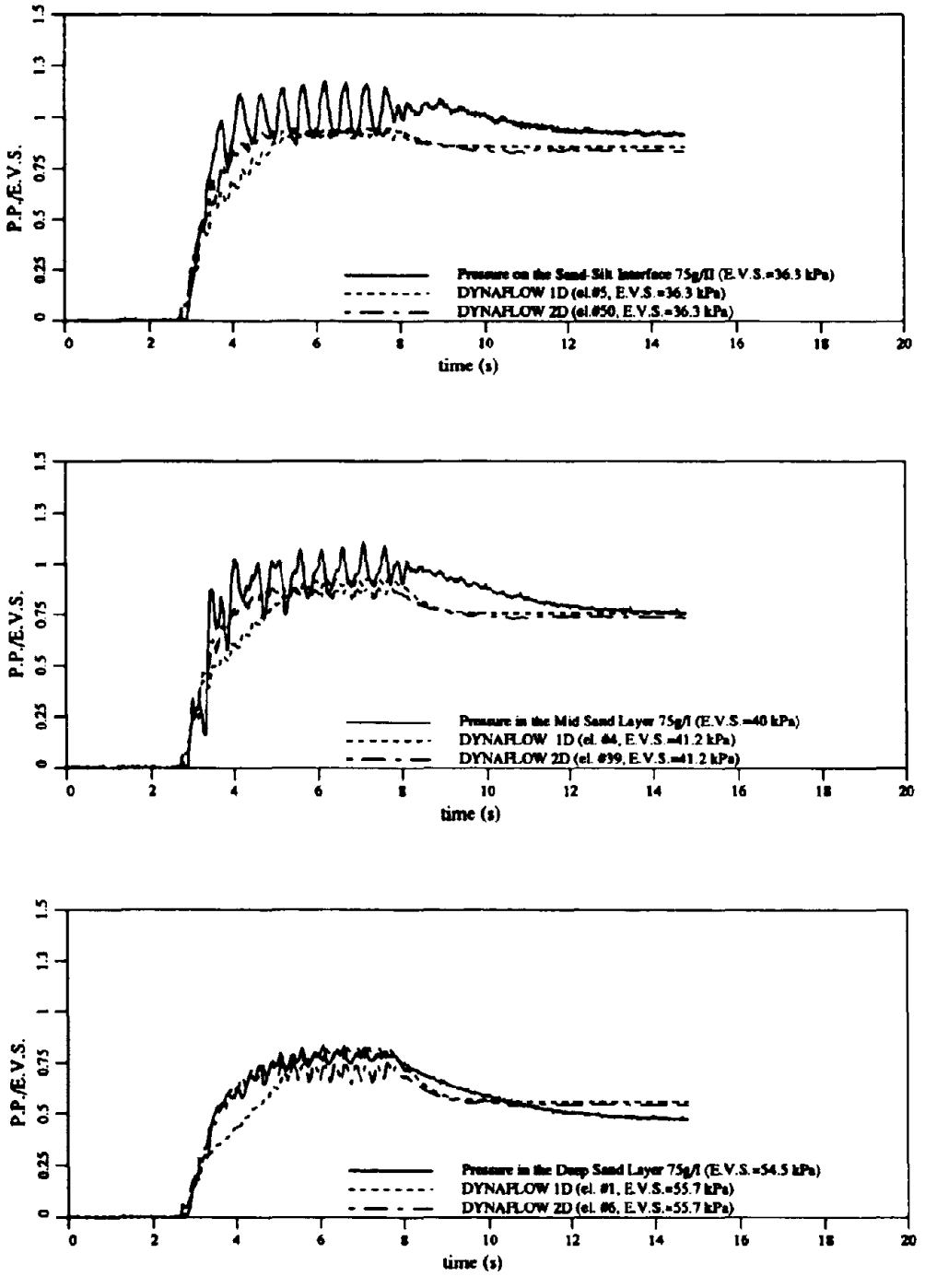

Figure 4.25: Comparison of the Measured and Computed Pore Pressure Time Histories in the Sand Layer With 1D and 2D Analysis

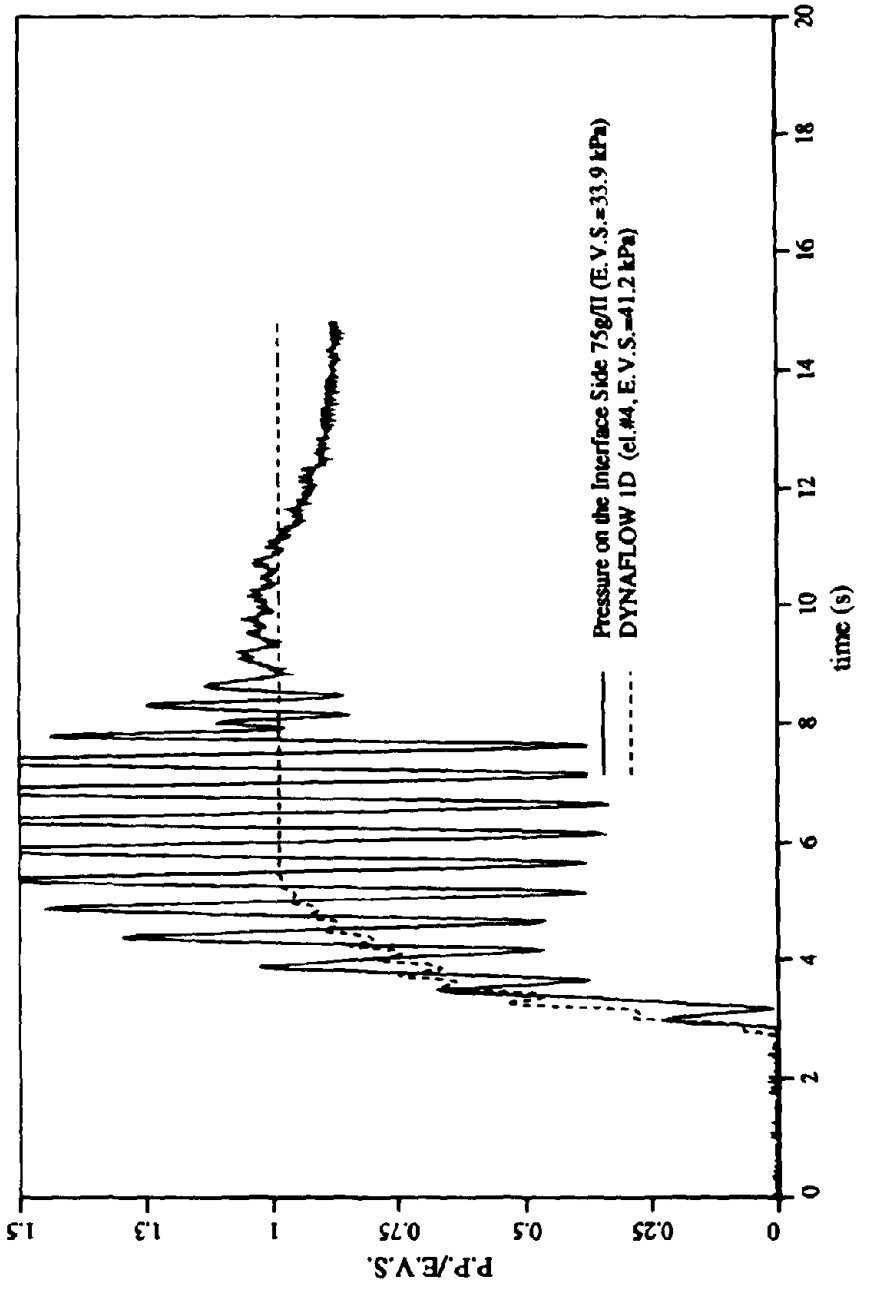

Figure 4.26: Comparison of the Measured Pore Pressure Time Histories in the Sand Layer on the Side of the Box With Corresponding Results of the 1D Analysis

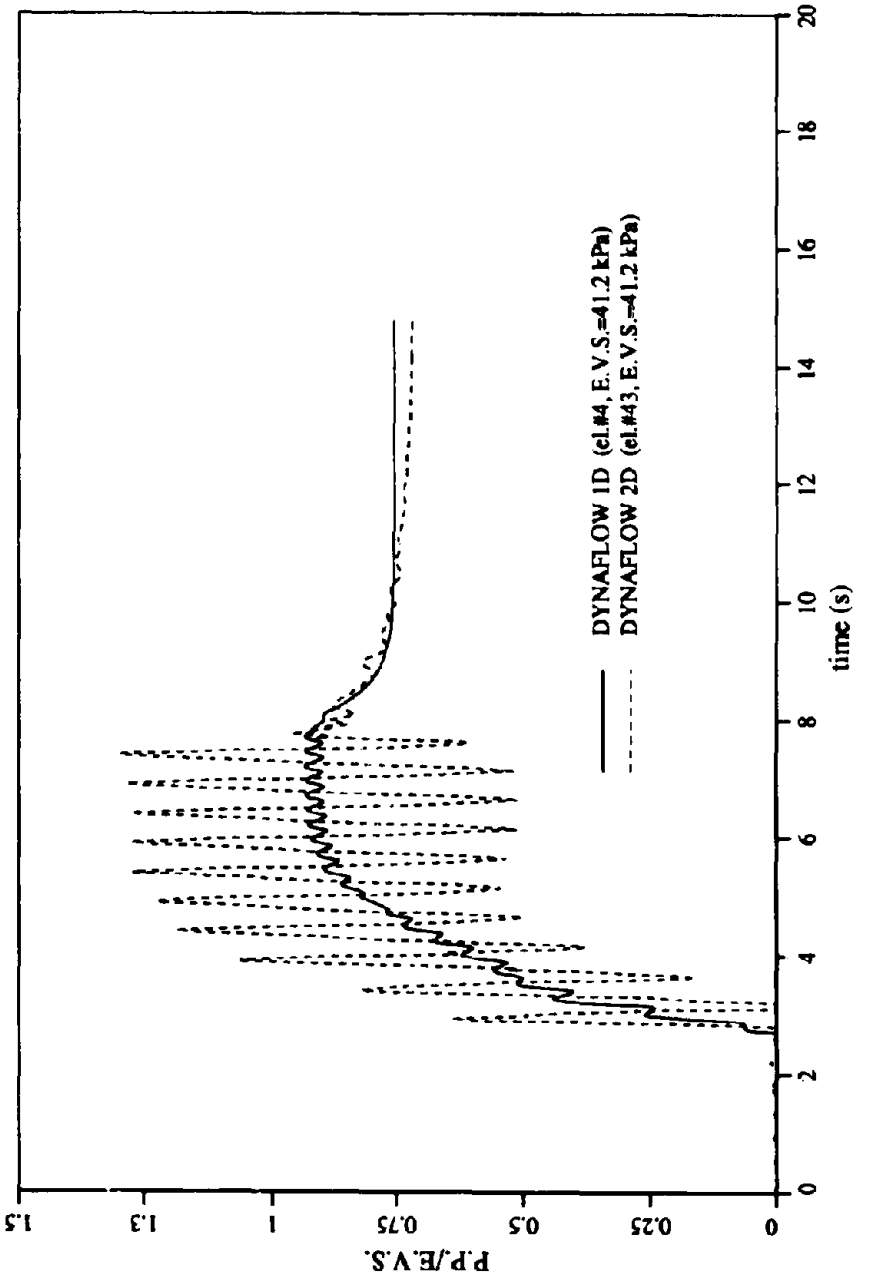

Figure 4.27: Comparison of the Computed Pore Pressure Time Histories in the Sand Layer With 1D and 2D Analysis on the Side of the Box

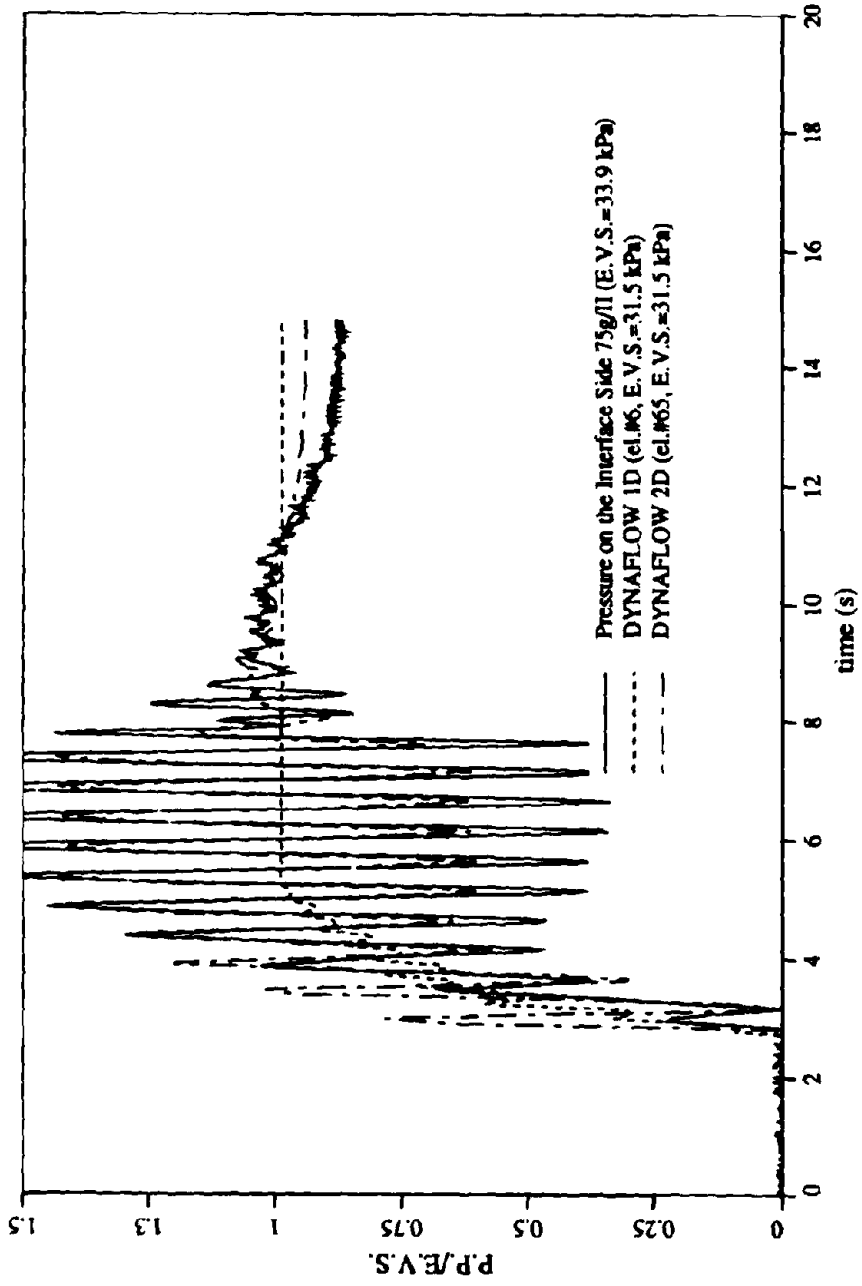

Figure 4.28: Comparison of the Measured and Computed Pore Pressure Time Histories in the Sand Layer With 1D and 2D Analysis on the Side of the Box

4.8 Appendix

In an effort to validate performed analysis, and to show that differences in results are not due to the inconsistency of used codes (and procedures), but to the difference in the physics of the numerical models, some additional analyses were done with computer code DYNAFLOW. This finite element analysis program should enable computation of one-, two- and three-dimensional system, and despite large system capacity, no loss of accuracy and efficiency should be encountered in solving small problems.

Figure 4.29 shows comparison of the performed DYNA1D analysis and results of the one-dimensional numerical model computed with DYNAFLOW. It is obvious that both codes obtained the same level of the pore pressure rise. DYNAFLOW enables 2D analysis of a one-dimensional element. Results of that analysis compared with 1D DYNAFLOW analysis are shown on Figure 4.30.

2D (DYNAFLOW) analysis of infinite, horizontal layers, which was the main assumption used in 1D analysis, gives exactly the same answer as 1D analysis (Figure 4.31). However, 1D analysis needs 20 times less computation time than 2D analysis.

Finally, to establish the connection between DYNA1D and DYNAFLOW 2D analysis that includes the *rigid box* boundary conditions, DYNAFLOW 1D results were compared with DYNAFLOW 2D results in Figure 4.32, which is almost identical to Figure 4.25

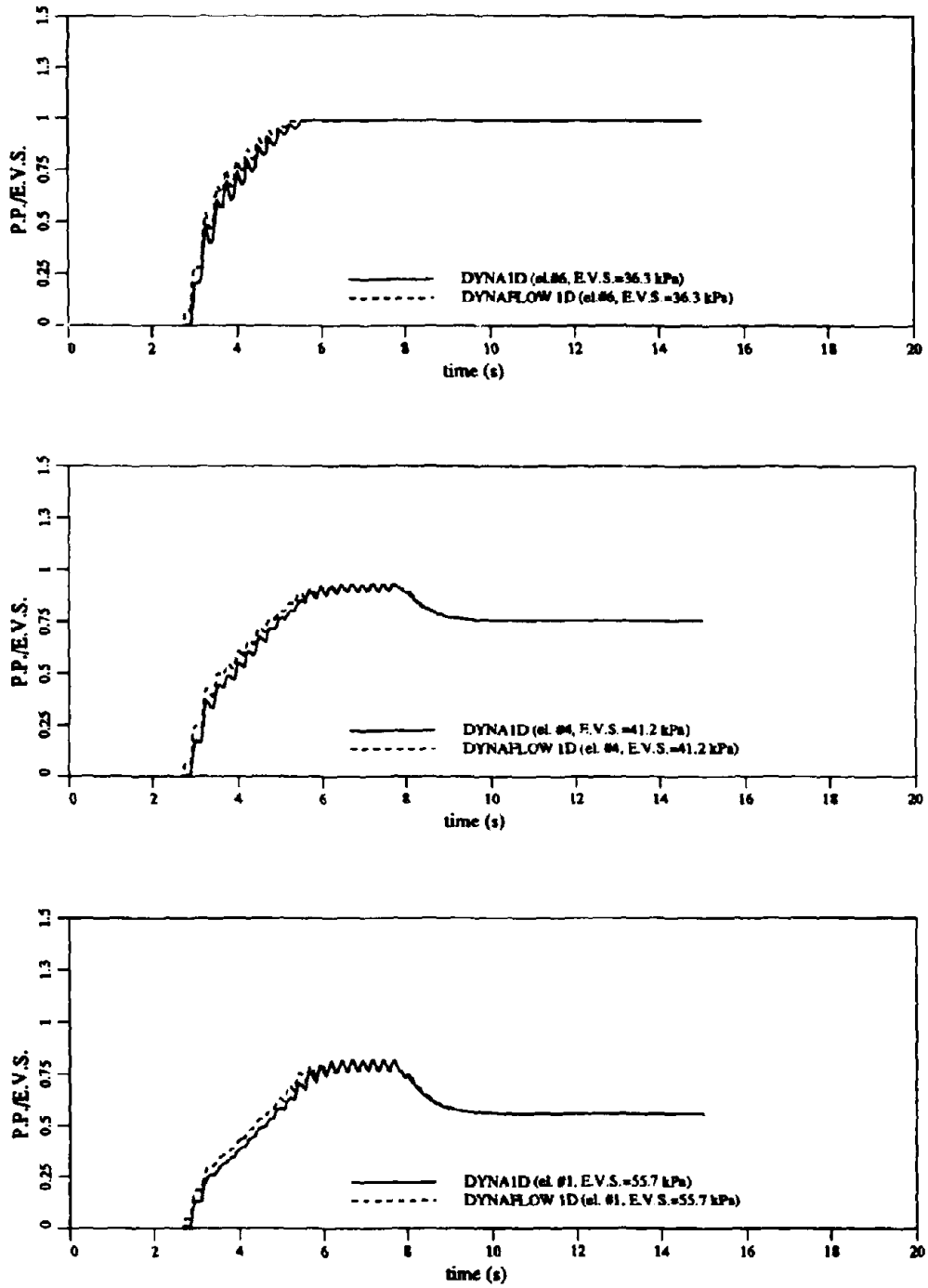

Figure 4.29: Comparison of the Pore Pressure Time Histories in the Sand Layer Obtained With DYNA1D and DYNAFLOW 1D Analysis

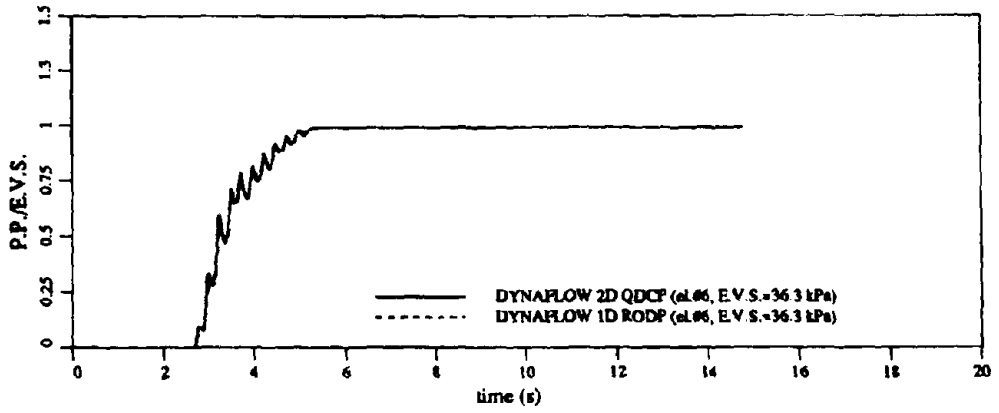

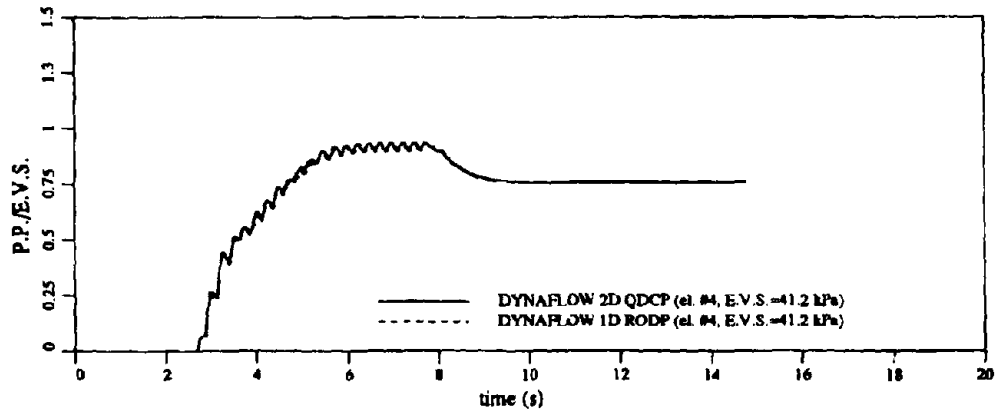

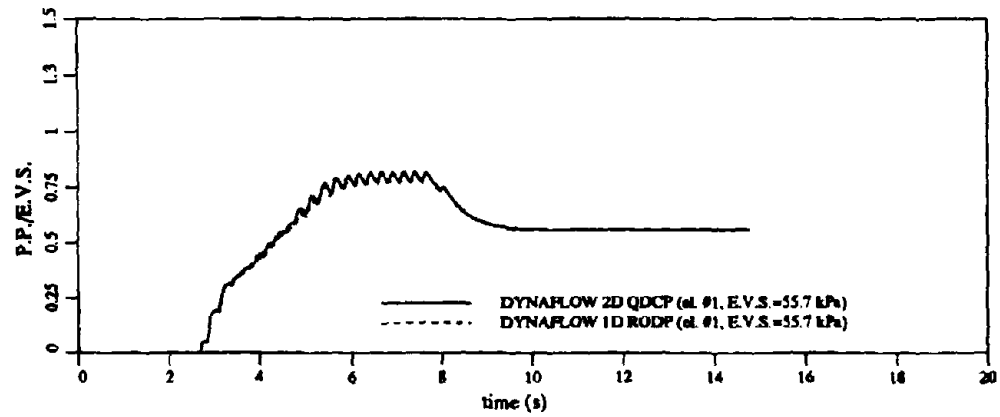

Figure 4.30: Comparison of the Pore Pressure Time Histories in the Sand Layer Obtained With DYNAFLOW 1D Analysis and 2D Analysis of 1D Elements

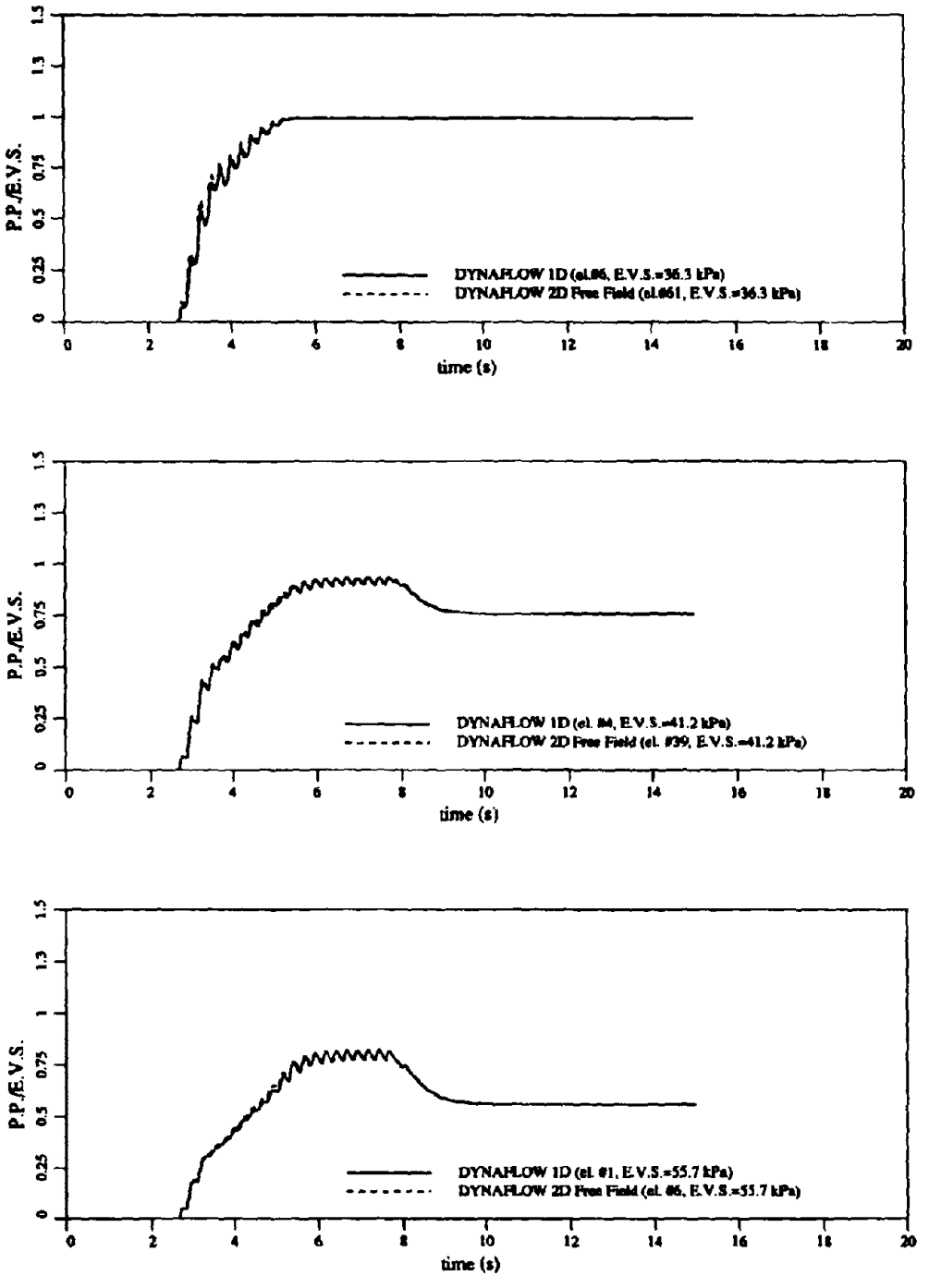

Figure 4.31: Comparison of the Pore Pressure Time Histories in the Sand Layer Obtained With DYNAFLOW 1D and DYNAFLOW 2D With Free Field B.C. Analysis

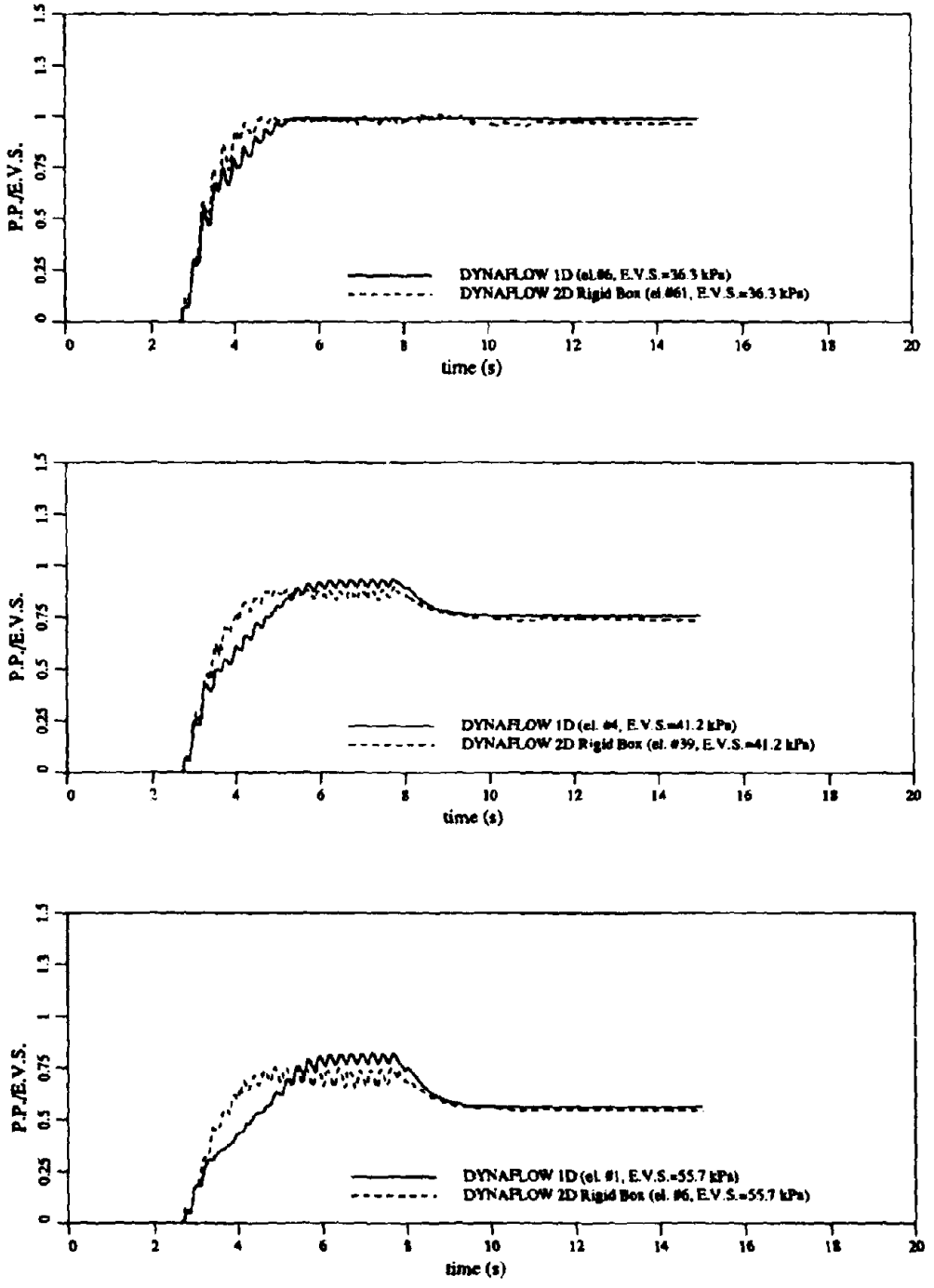

Figure 4.32: Comparison of the Pore Pressure Time Histories in the Sand Layer Obtained With DYNAFLOW 1D and DYNAFLOW 2D With Rigid Box B.C. Analysis

Section 5

Soil-Structure Interaction

5.1 Introduction

One of the most important tasks in civil engineering is to design a structure that will resist the effects of strong earthquakes. These effects can be evaluated only by considering the interaction between the structure and the soil or rock foundations.

Interest in soil-structure interaction is rapidly growing in the field of earthquake engineering. For complete evaluation of a soil-structure interaction problem it is necessary to determine the properties and the motions of both the structure and the foundation. Unfortunately, current ability to solve the soil-structure interaction problem is limited due to the lack of knowledge about soil behavior during seismic events. In addition, there is a lack of physical data for verification of existing techniques, so experimental modelling and simulations are vital for a further understanding of the fundamentals of the soil-structure interaction problem. In this section, a centrifuge model is presented which is capable of realistically representing a soil-structure system subjected to an earthquake-like event.

5.2 Soil Structure Interaction Centrifuge Tests

A geometry of the model (Figure D.1) corresponds to the geometry of the Niigata apartments collapsed because of the liquefaction induced by 1964 Niigata Earthquake (Figure 1.1).

A lexan box $7 \times 10 \times 14\,[cm]$ (Figure 5.1) has been designed and filled with lead shot to simulate the apartment building with a center of gravity six meters above the ground. The model weight of the box filled with the lead shot was computed to simulate bearing pressure of 200 $[kN/m^2]$. The test box used for this test was the same as the one used for the VELACS Standard Model Test performed in a $75g$ environment. The 0^{th} tests are always performed to calibrate shaker input voltage level which can produce an event with desired acceleration amplitude. In this case, it was not certain if the shaker could provide desired acceleration level for the large box filled with sand at the $100g$ centrifuge acceleration level.

Input was similar to the VELACS Standard Model tests, ten cycles of sine function with an objective amplitude of $0.30g$. Ten channels were recorded directly on the Masscomp data acquisition system with a sampling rate of $10000[Hz]$. Nine channels were at the same time recorded on the tape recorder. Due to the limited capacity of the tape recorder (nine channels), input vertical acceleration was recorded only on the Masscomp computer.

5.2.1 Sample Preparation

It was decided to use the Nevada sand with relative density of 60 %. A 14 $[cm]$ thick sand layer was pluviated through the same device used for preparation of Standard VELACS Test samples. The pluviation was stopped when the pressure transducers were installed in the sample. Three pressure transducers were placed under the structure and one in the field. It was assumed that 14 $[cm]$ change of pluviation

height does not effect relative density of the sand. Because of the structure height, it was impossible to seal the box with the structure placed on the sand.

A shallow rectangular frame the size of the structure was placed in the sand after the pluviated sand reached a depth of 13 $[cm]$. Following the pluviation process, the sand inside the frame was removed with a vacuum cleaner, the model was sealed and a vacuum was introduced to the sample. Even though the sample was slightly disturbed due to the large distortion of the front side of the box (the lexan plate deformed close to 5 $[mm]$ in the center) under the vacuum, it was decided to perform the test.

De-aired water was slowly drawn into the sand sample through the drainage hose on the bottom of the model box. A water level was planed to be one meter below the sand surface, but during the sample preparation it was decided to rise it one meter above the sand surface. It was difficult to estimate water level while the water was below the sand surface.

After the sand was saturated, the structure was placed in the frame and its standing was checked with bubble levels. The sample was placed in the centrifuge and the centrifuge was brought up to $100g$ level.

5.2.2 Test Procedure

The sample was left in flight at $100g$ for approximately ten minutes before it was stopped, and an LVDT core with a supporting footing was placed on the surface of the sample and the structure was checked for vertical deformations and tilting.

The sample was shaken four times with increasing acceleration level of the shaker before the centrifuge was stopped. The first event had an acceleration level below $0.15g$ and the last one above $0.28g$. The Team electro-hydraulic shaker performed well, it induced $0.25g$ level with voltage input of 0.95 $[V]$ (maximum input is 10 $[V]$)

while the pressure in the oil lines was 50% of the maximum allowed oil pressure.

Large vertical and horizontal deformations of the structure were noticed after the tests. The structure leaned on the displacement transducer on the left hand side and its front side tipped. Surface cracks in the sand surface were noticed together with a distortion of the lexan plate. From recorded time histories, it was not possible to determine after which event the structure collapsed.

Two more tests were performed after the sample box was redesigned to prevent large deformations of the lexan plate due to the high pressure induced by vacuum during the sample preparation process. Results and schematics of both tests can be found in Appendices D.1 and D.2.

Figures 5.2 to 5.4 show comparisons of the results of the two performed soil-structure tests. All results are in good agreement, and even the visually observed vertical displacements show similarity of model structure behavior in both tests.

5.3 Numerical Analysis

Once again, performed centrifuge model tests were utilized to investigate the validity of DYNAFLOW [18] in solving liquefaction and soil-structure problems.

The following discussion is a comparison of the experimental and computed results with a brief description of the numerical analysis performed.

5.3.1 Simulation Procedure

Simulation of the test case was performed using the 2D solver of DYNAFLOW code. The finite element model of the ground and the structure is shown in Figure 5.5. The mesh consists of 119 elements, and 154 nodes. Input for the model consists of the acceleration time history recorded during the centrifuge model test at the base of the testing box. The required material constitutive parameters are given in Table 5.1.

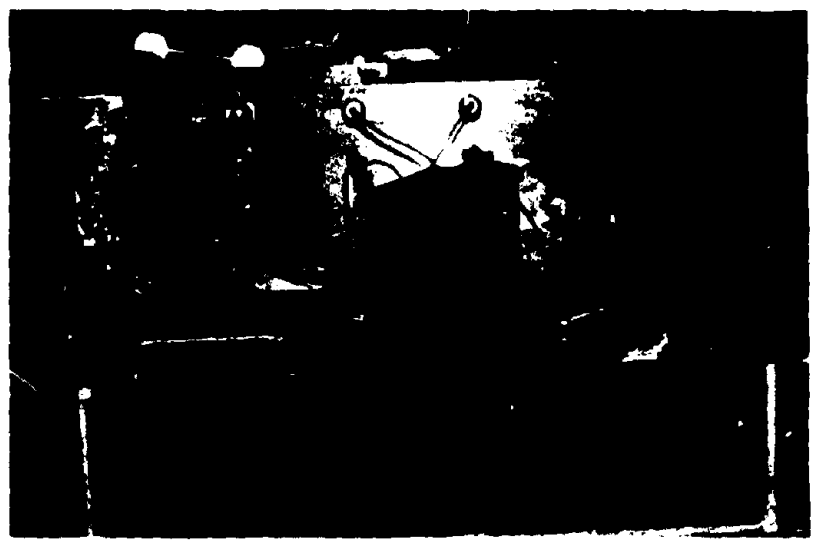

Figure 5.1: Soil-Structure Interaction Model Test # I, Before and After the Event

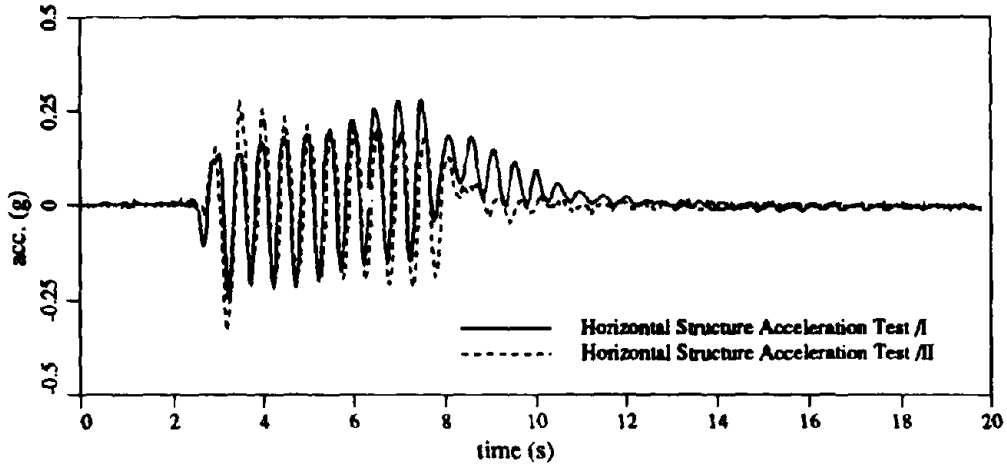

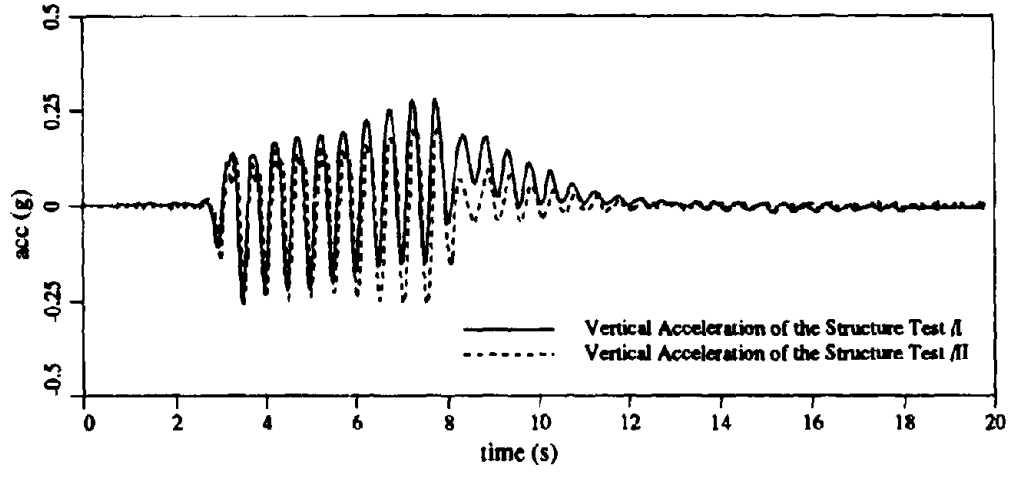

Figure 5.2: Acceleration Time Histories Comparisons

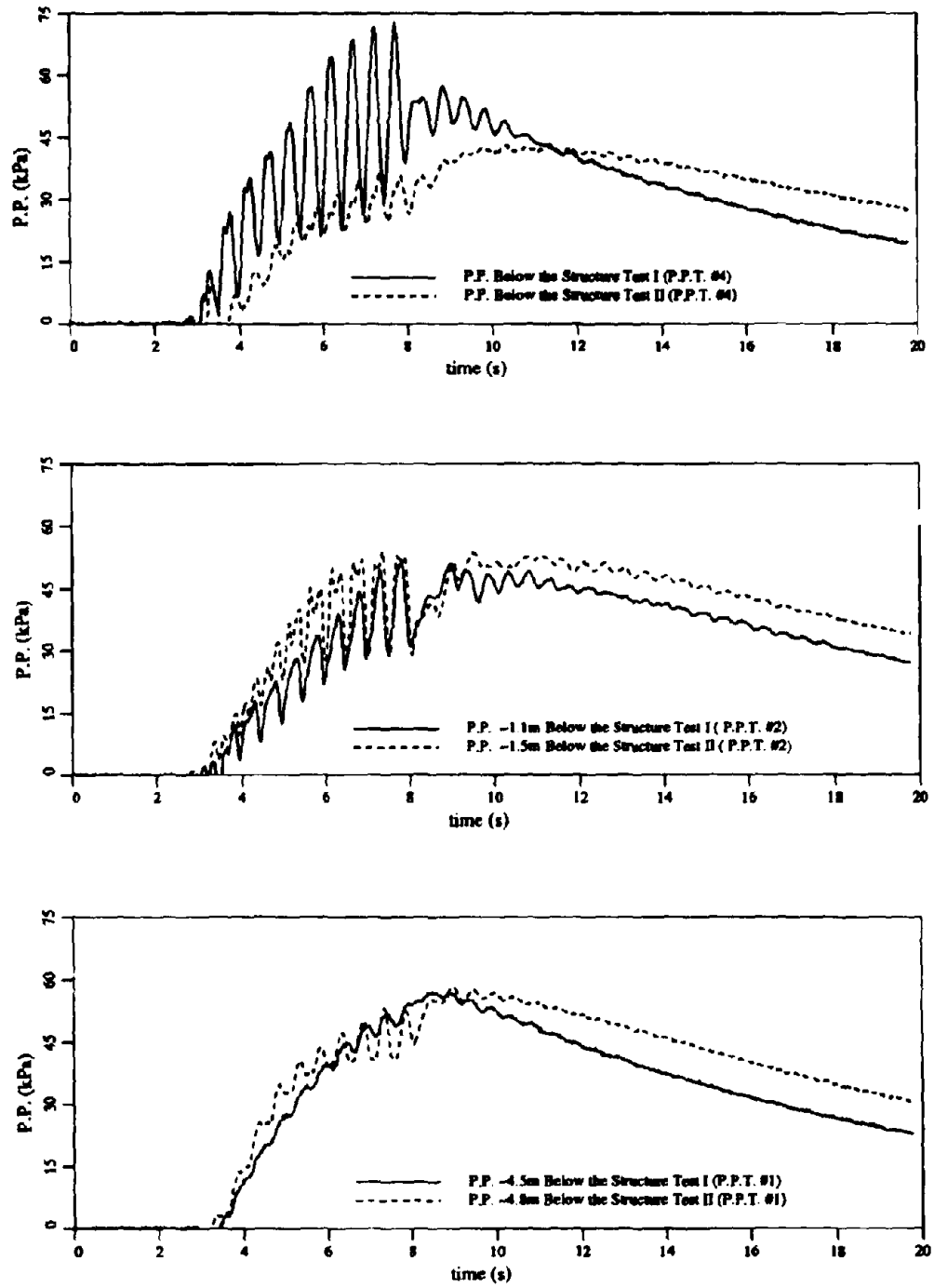

Figure 5.3: Comparisons of the Excessive Pore Pressure Time Histories Below the Structure

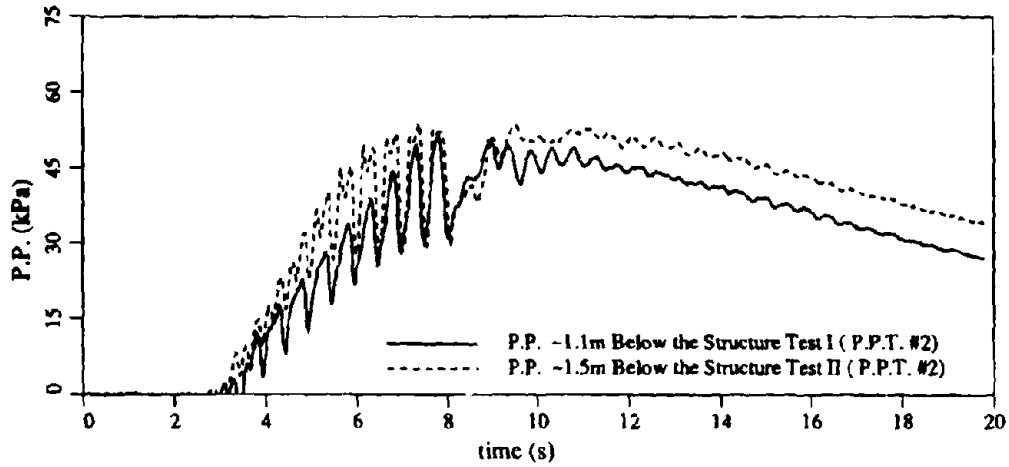

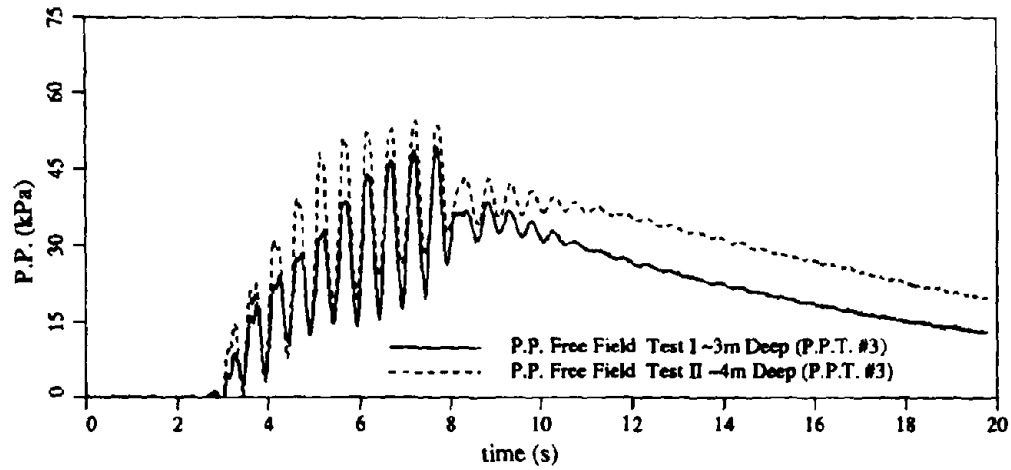

Figure 5.4: Comparisons of the Excessive Pore Pressure Time Histories, Free Field Versus Below the Structure

The following analysis options were used in the simulation:

- hyperbolic type analysis for two phase porous continuum;
- total number of yield surfaces was set equal to 20;
- 4 d.o.f. per node;
- 2000 time steps of 0.01 [s];
- water table at the sand surface;
- compressible fluid;
- implicit-explicit treatment for the solid effective stress contribution to the equations of motion;
- select integration scheme parameters $g = 0.65$ and $b = 0.33$ for the introduction of the high frequency numerical dissipation;
- prescribed acceleration for the solid phase horizontal d.o.f. for the base nodes and for the nodes on both sides to simulate *the box effect*;
- slaved horizontal d.o.f. for the water phase for all nodes at the base;
- slaved vertical d.o.f. for the water and the solid phase on the both sides of the mesh;
- three element groups, one for the structure and two for the sand (free field, and under the structure);
- structure simulated as a rigid body

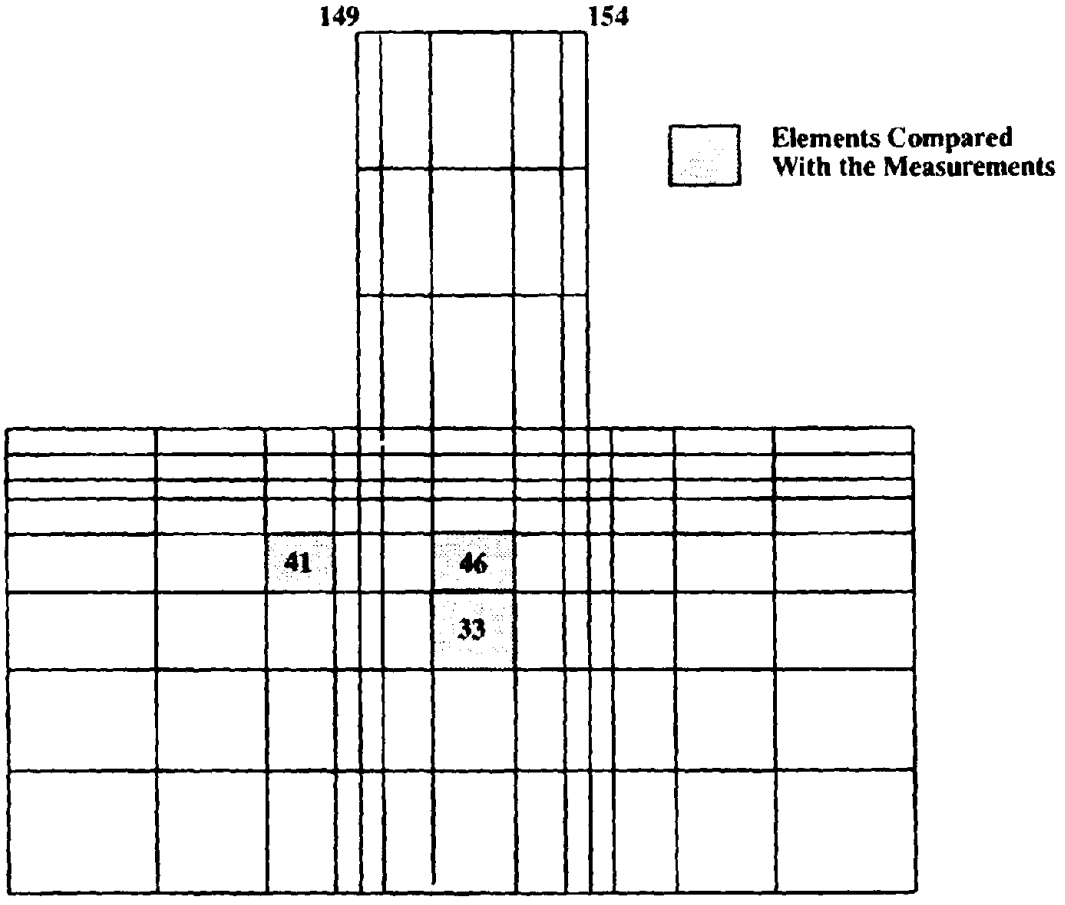

Figure 5.5: **Soil-Structure Finite Element Mesh**

5.3.2 Material Properties

The elasto-plastic purely kinematic hardening constitutive model for pressure sensitive materials was adopted to simulate the soil behavior [15].

The sample was divided in two zones with different material properties [14]. One zone was below the structure and one in the free field. Material properties of the zone # 1 (free field) are the same as the properties of the sand used in the VELACS standard test, with permeability 10 times larger than one obtained in laboratory results [4].

Vertical settlements of the model structure during the centrifuge tests probably caused densification of the sand below the structure. It seemed reasonable to model the sand below the structure with different material. Material parameters of the zone # 2 material were evaluated by Popescu [14].

Property	Nevada Sand Free Field	Ref.	Nevada Sand Bellow Struct.	Ref.
Mass density (Kg/m^3)	2680	[4]	2680	[4]
Porosity	0.4	R.D. 60 %	0.4	
Permeability	5.6×10^{-4}	Chap. 4	5.6×10^{-4}	Chap. 4
Low Strain Shear Modulus (MPa)	68.9	[4] Eq. 4.6	21	[14]
Poisson's Ratio	0.3	[13]	0.3	[13]
Bulk Modulus (MPa)	149.3		45.5	
Fluid Bulk Mod. (MPa)	2000		2000	
Cohesion (kPa)	0		0	
Reference Mean Normal Stress (kPa)	100		100	
Dilatation Angle (compress. and ext.)	25°	Chap. 4	34°	[14]
Dilatation Parameter	0.05		0.10	
Friction Angle (compress. and ext.)	30°	Chap. 4	36°	[14]
Coefficient of Lateral Stress	0.5	[13]	0.5	[13]
Slope of the Stress Path	0.33		0.0	[14]
Max. Shear Strain in Compression	0.05		0.10	
Max. Shear strain in Extension	0.03		0.10	

Table 5.1: **Material Properties Used in Numerical Analysis**

5.4 Test Results and Comparisons

Figure 5.6 shows the comparison of the structure acceleration time histories. The time histories are in good agreement, except for the last five cycles of the right structure corner vertical acceleration. This difference might be due to the disturbed structure standing noticed in the centrifuge model (Figure 5.1) which can not be modelled as an axisymmetric problem.

The excess pore-water pressure time histories are shown in Figure 5.7. The experimental and numerical models accede in the rise of the pore-water pressure, and the fluctuations of the pressure in the free field, while the numerical results have higher frequency of the fluctuations under the structure.

Due to the technical problems, only rough measurements of the vertical displacement were available for the comparison with the computed results. It was observed that on average, the right side of the structure had vertical displacement between 30 and 40 [cm], while the left side had displacement between 50 and 60 [cm]. The deformed mesh on Figure 5.8 shows displacement after the event. Although the structure standing in the numerical model was not disturbed as much as in the physical model, the vertical displacements (Figure 5.9) match the observations made during the experiments.

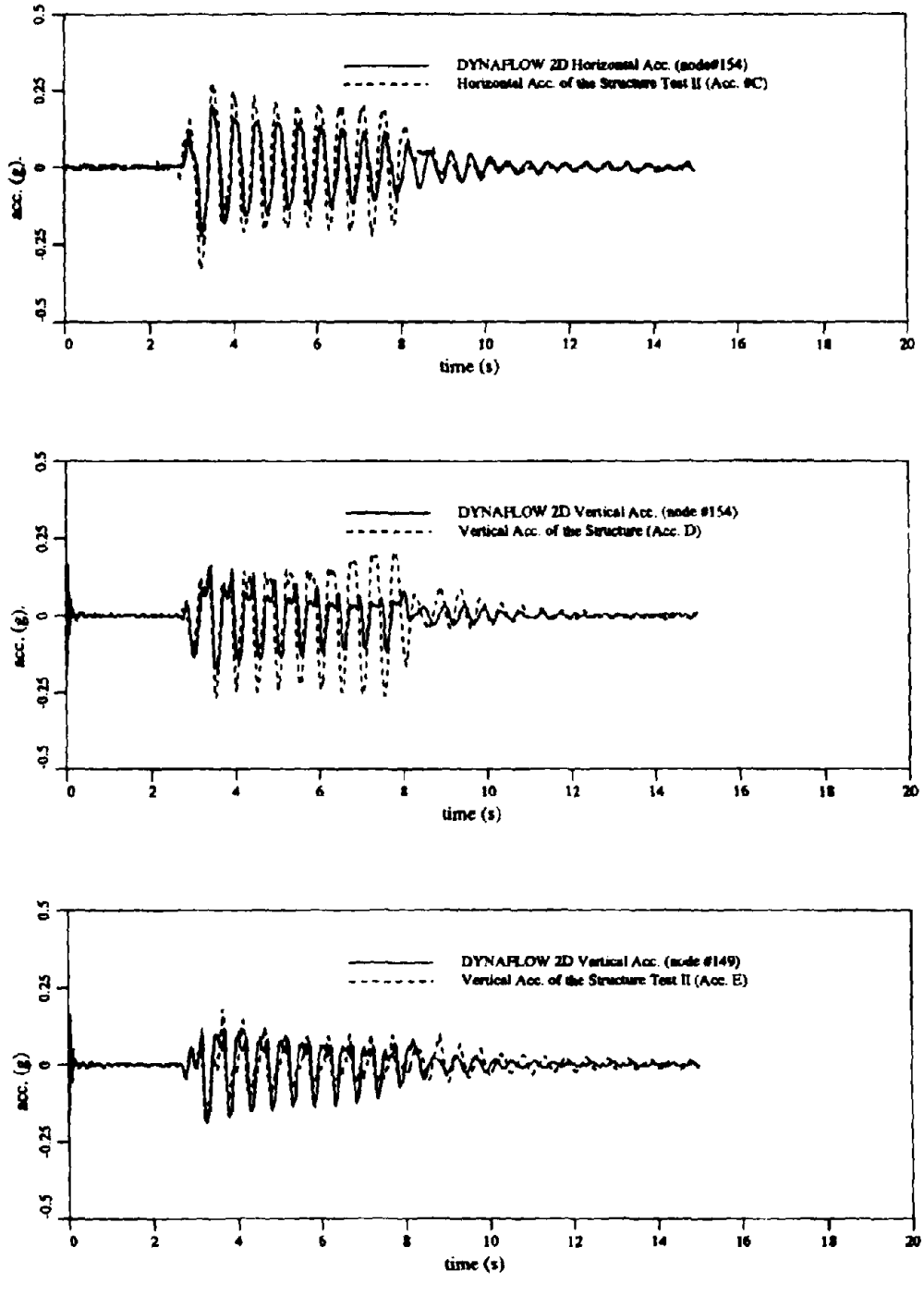

Figure 5.6: Comparison Between the Computed With DYNAFLOW and the Recorded Acceleration Time Histories of the Structure (Test II)

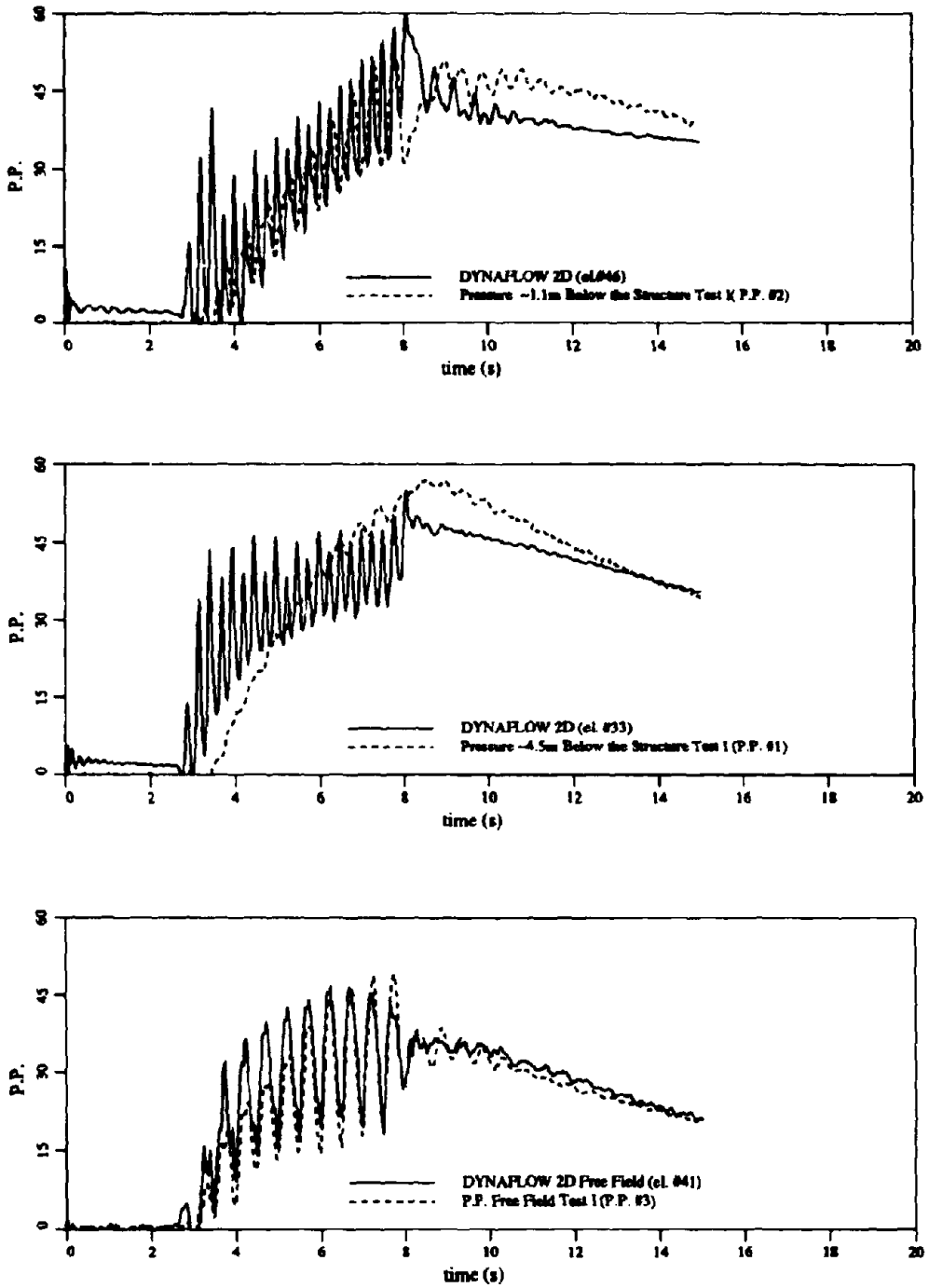

Figure 5.7: Comparison Between the Computed With DYNAFLOW and the Recorded Excessive Pore Pressure Time Histories

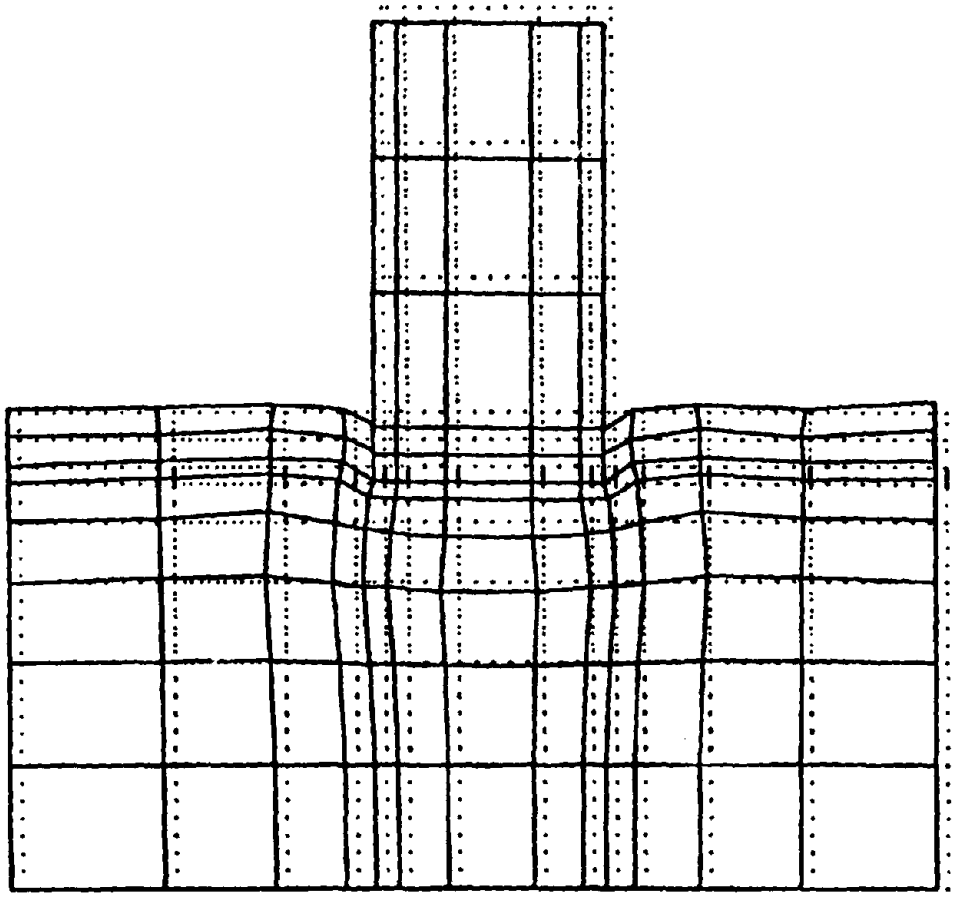

Figure 5.8: Deformed Finite Element Mesh

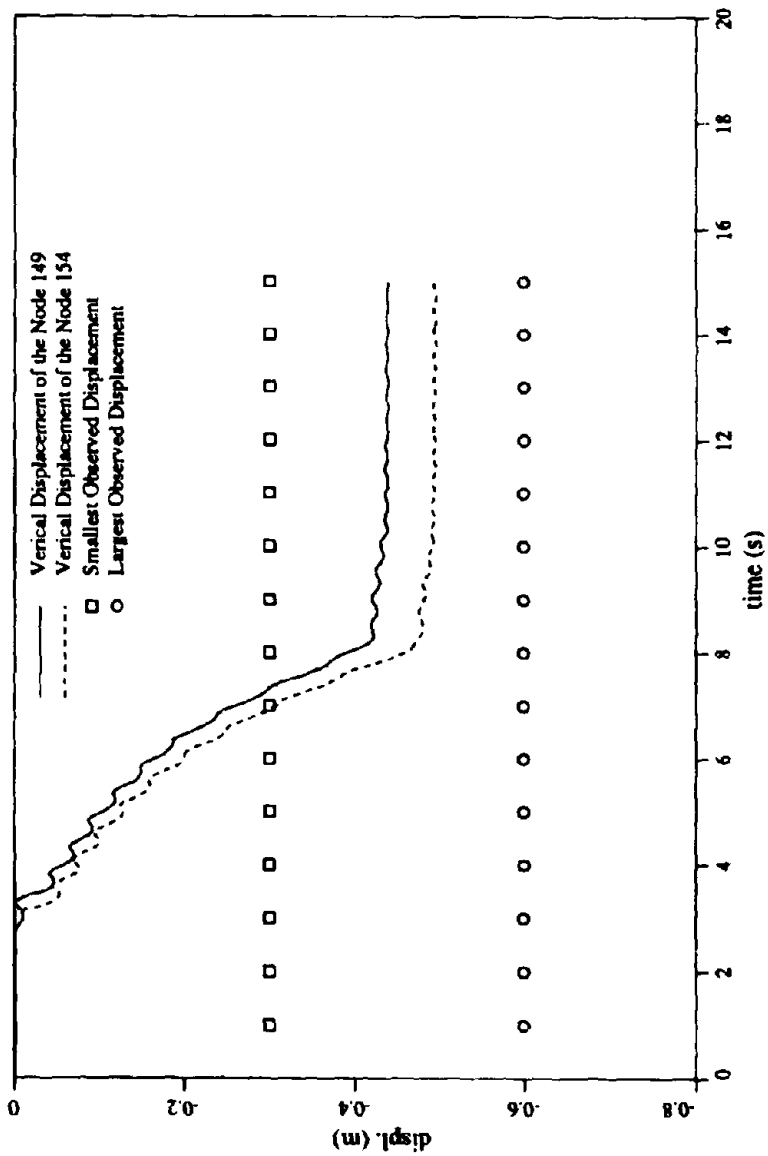

Figure 5.9: Computed Structure Vertical Displacement Time Histories

Section 6

Conclusions

This report has described the development of an earthquake motion simulator for centrifuge testing, and its use for studying the dynamic response of saturated soil deposits.

The development of the Princeton University ground motion simulator represents a successful application of electro-hydraulic system technology for dynamic centrifuge modelling, without large investments in the testing equipment.

Although tested only with a sine like input, the electro-hydraulic shaker proved to be capable of subjecting testing containers of various sizes to a strong motion in a high g environment. The performance tests, and estimation of the system frequency response with a careful study of the shaker capabilities, and possible application of the 'real' earthquake motions should be a part of future research.

Results of the first group of experiments, performed as a part of the VELACS project, were used to study validity of the liquefaction analysis programs DYNA1D and DYNAFLOW.

As a result, it was confirmed that both DYNA1D and DYNAFLOW programs are suitable for closely simulating the details of the experimental centrifuge liquefaction test, such as: the time history response of excess pore pressures in the center of the model, and acceleration time histories of the silt layer. DYNA1D proved to be

inadequate for evaluation of the boundary condition effects. However, one should still consider using it to evaluate *free field* problems, because of the considerable savings in computer time. On the other hand, DYNAFLOW 2D analysis has been found to be in good agreement with all the experimental data.

VELACS check tests were performed at different levels of centrifugal acceleration following the modelling of models concept. Similar behavior of both models extrapolated to the projected prototype proved to be a good verification of the scaling relations, as well as of the consistency of the centrifuge model testing scheme.

The second group of centrifuge tests involved a study of the soil-structure interaction effects. A scaled structure model of the collapsed Niigata apartments lost its standing during the event, which was exactly the effect observed on the prototype structures.

Simulation of the test was performed using the program DYNAFLOW. Comparisons of computed versus recorded structure accelerations and pore-water pressure variations have been discussed and found in a good agreement. The computed vertical displacement magnitude was within the range of observations made after the centrifuge model tests.

Finally, phenomenological aspects of soil-structure interaction, and soil liquefaction demonstrated in centrifuge tests can be fully represented with numerical procedures encompassed in code DYNAFLOW.

Future work might include, besides the complete study of the shaker capabilities, some improvements of the current facility which would allow earthquake-like motion excitations in two perpendicular directions. This improvement would allow results of the three dimensional numerical analysis to be verified.

References

[1] K. Arulanandan at al. Simulation of eartquake motion in the c-fuge. *Proc. ASCE*, 108, 1982.

[2] W.D.L. Finn at. al. Analysis of porewater pressures in seismic centrifuge tests. In A. Cakmak, editor, *Soil Dynamics and Liquefaction*. Elsevier, 1987.

[3] H.B. Seed B. Schnabel, J. Lysmer. SHAKE a computer program for earthquake response analysis of horizontally layered sites. Technical report, U.C. Berkeley, 1972.

[4] THE EARTH TECHNOLOGY CORPORATION. Velacs laboratory testing program preliminary data report. Technical report, Earth Technology Project No. 90-0562, 1991.

[5] National Research Council. Liquefaction of soils during earthquakes. Technical report, NRC, CETS-EE-001, 1985.

[6] W.H. Craig. Edouard Phillips and the idea of centrifugal modeling. *Geotechnique*, 39, 1989.

[7] R.F. Scott et al. C-fuge earth dam studies: Earthquake tests and analysis. Technical report, Report to National Science Foundation, 1985.

[8] H.Y. Ko. Summary of the state-of-the-art in the c-fuge model testing. In W. Craig and A.N. Schofield, editors, *Centrifuges in Soil Mechanics*. Balkema, Rotterdam, 1988.

[9] I. Krstelj and J.H. Prevost. P.U. standard VELACS test report. Technical report, Princeton University, 1991.

[10] B.L. Kutter. Geotechnical centrifuges and earthquake simulator, 1983. Proc. 4th Eng.Mech.Div. Spec. Conference, ASCE, Perdue U.

[11] D.V. Morris. Dynamic soil-struct. inter. modeled exp. on gtch. c-fuge. *Canadian Geotechnical Journal*, 20, 1981.

[12] J. Nicolas-Font. Design of geotechnical centrifuges. In Corte, editor, *Centrifuge 88*. Balkema, Rotterdam, 1988.

[13] E. NONVEILLER. *Mehanika Tla i Temeljenje Gradjevina (Soil Mechanics and Foundations)*. Š kolska Knjiga Zagreb, Hrvatska, 1981.

[14] R. Popescu. Personal comunications and unpublished internal papers, 1992.

[15] J.H. PREVOST. A simple plasticity theory for frictional cohesionless soils. *Soil Dynamics and Earth. Engin.*, 4, 1985.

[16] J.H. PREVOST. Dynald a computer program for nonlinear seismic site response analysis technical documentation. Technical report, NCEER-89-0025, 1989.

[17] J.H. PREVOST. Modelling the behavior of geomaterials. Unpublished Internal Papers, 1992.

[18] J.H. PREVOST. Dynaflow manual, March 1992.

[19] A.N. Schofield. Cambridge geotechnical centrifuge operations. *Geotechnique*, 30, 1980.

[20] L.A.Ortiz R.F. Scott and J. Lee. Dynamic C-fuge testing of cantilever retaining wall. *Earthquake Engineering and Structural Dynamics*, 11, 1983.

[21] R.F. Scott. NSF VELACS project. Technical report, Caltech, 1989. Experimenters Committee, Minutes of Nov. 20,1989 Meeting.

[22] Karen Weissman. *C-fuge Modelling of Dynamic Soil-Structure Interaction*. PhD thesis, Princeton University, 1989.

[23] R.V. Whitman. Experiments with earthquake ground motion simulator. In W. Craig and A.N. Schofield, editors, *Centrifuges in Soil Mechanics*. Balkema, Rotterdam, 1988.

[24] A. Zelikson. Scale modelling of a soil structure interaction during earthquakes using a programmed series of explosionr during centrifugation. *Proc. Conf. on Recent Advanced in Geotech. Erthq. Eng. and Soil Dynamics*, 1, 1981.

Appendix A

Summary of the Model Tests

Test	G's	Date	Ref.	Comments
VELACS Check Silica Silt	100	20-Jun-91	100 g/I	Appendix B.1
VELACS Check Silica Silt	100	30-Jul-91	100 g/II	Appendix B.2
VELACS Check Silica Silt	75	06-Oct-91	75 g/I	Appendix C.1
VELACS Check Silica Silt	75	01-Nov-91	75 g/II	Appendix C.2
VELACS Check Silica-Glycerin	75	18-Dec-91	Glycerin/I	Appendix C.3 Pore Fluid Water + Glycerin
VELACS Check Silica Silt	75	08-Mar-92	Noncontact Device Test	Device Malfunctioned, Test Disregarded
Soil-Structure Interaction	100	20-Mar-92	S-S/0	Initial Test (Dummy), Deformed Lexan, Disregarded
Soil-Structure Interaction	100	26-Mar-92	S-S/I	Appendix D.1
Soil-Structure Interaction	100	09-Apr-92	S-S/II	Appendix D.2
VELACS Check Bonnie Silt	75	20-Apr-92	Bonnie/I	Appendix C.4
VELACS Check Bonnie Silt	75	10-Jun-92	Bonnie/II	Appendix C.4
VELACS Check Bonnie Silt	75	20-Jun-92	Bonnie/III	Curved Sand Surface, Not Satisfactory, Disregarded

Appendix B

VELACS $100g$ Tests

B.1 Test $100g/I$

Test $100g/I$ was performed on June, 20, 1991 (Figure B.1). Due to the limited capacity of the old data acquisition system, data could only be recorded on 6 channels. Four channels were recorded directly on the Norland four channel oscilloscope, and two had to be played back from the tape recorder (accelerometers A and B).

Figure B.2 shows the measured horizontal acceleration time history of the box, later referred to as the base, (accelerometer C), with a normalized frequency content and a response spectra. Fast Fourier Transform of the acceleration time history, with the 5000 $[Hz]$ sampling rate, was scaled with its maximum value, after changing to polar coordinates.

The Response Spectrum with 5% damping was calculated in 500 steps applying the Newmark method. A vertical acceleration trace (Figure B.3) had been recorded previously during a dummy test performed previous to Test I. The dummy test had been performed to determine a voltage input level for the servocontroller required to achieve $0.25g$ acceleration amplitude of the event.

Good repeatability can be observed after comparing with the vertical acceleration recorded during Test II (Figure B.11). Figure B.4 shows the horizontal acceleration

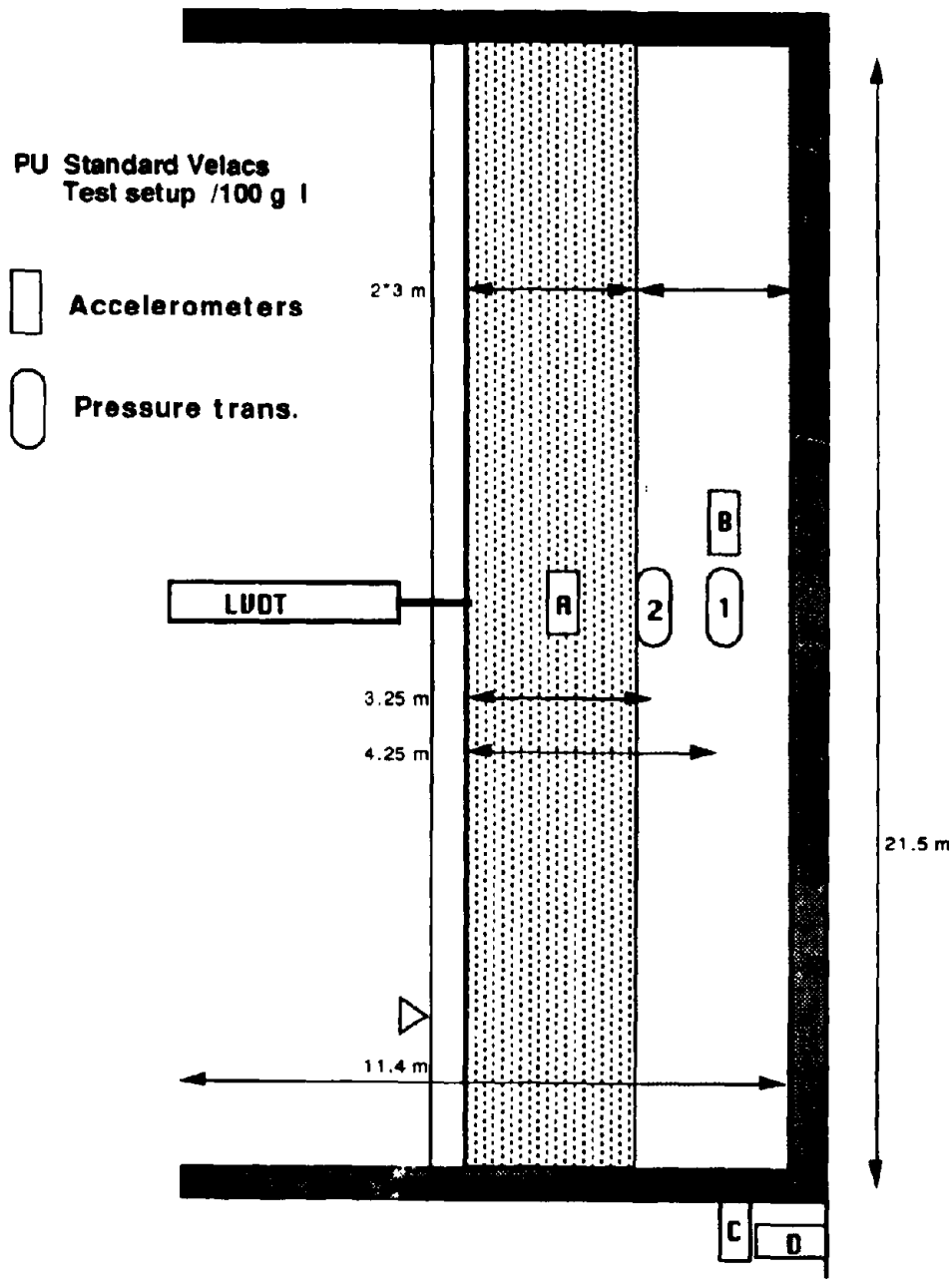

Figure B.1: **Standard Velacs Model Test 100 g/I**

time history, its normalized frequency content, and a response spectra, recorded in the silt layer (accelerometer A). The normalized frequency content was obtained by scaling the FFT results with maximum of the FFT result of the horizontal acceleration of the base, same for the acceleration time history of the silt layer as for the vertical acceleration of the base.

Pore pressure transducers had been placed horizontally with a porous stone facing in the shaking direction. Due to the small test box it was hard to form relatively stiff transducer cables without disturbing the sample under the transducer.

As was mentioned before, a sample rate has been changed from 10000 $[Hz]$ to 5000 $[Hz]$, and all data records have been zeroed with subtracting average value of the first 50 points. Positions of the pore pressure transducers were measured with a ruler after the test. All the dimensions in Figure B.1 show the distances measured from the surface to the center of the transducers. Effective vertical stresses were calculated with these values and the assumed densities of 1950 $[kg/m^3]$ for the sand and silt (no soil data were available).

Pore pressure ratios were shown in Figure B.5 as short-term time histories and Figure B.6 as long-term time histories. While the short-term pore pressure time histories were available directly from the oscilloscope, the long-term time histories were obtained from the tape recorder with a sampling rate of 100 $[Hz]$. Figure B.7 shows stress and pore pressure variations with depth. Values of the excessive water pressures were obtained by inspection from the Figure B.5.

A vertical displacement was measured only on the surface of the sample (Figure B.8). A $25 \times 25\,[mm]$ plastic footing was used to support a LVDT core. Heavy sinking of the LVDT footing was noticed while the centrifuge was in flight, as well as after the test, so the reported measurement of the vertical displacement must be considered with caution.

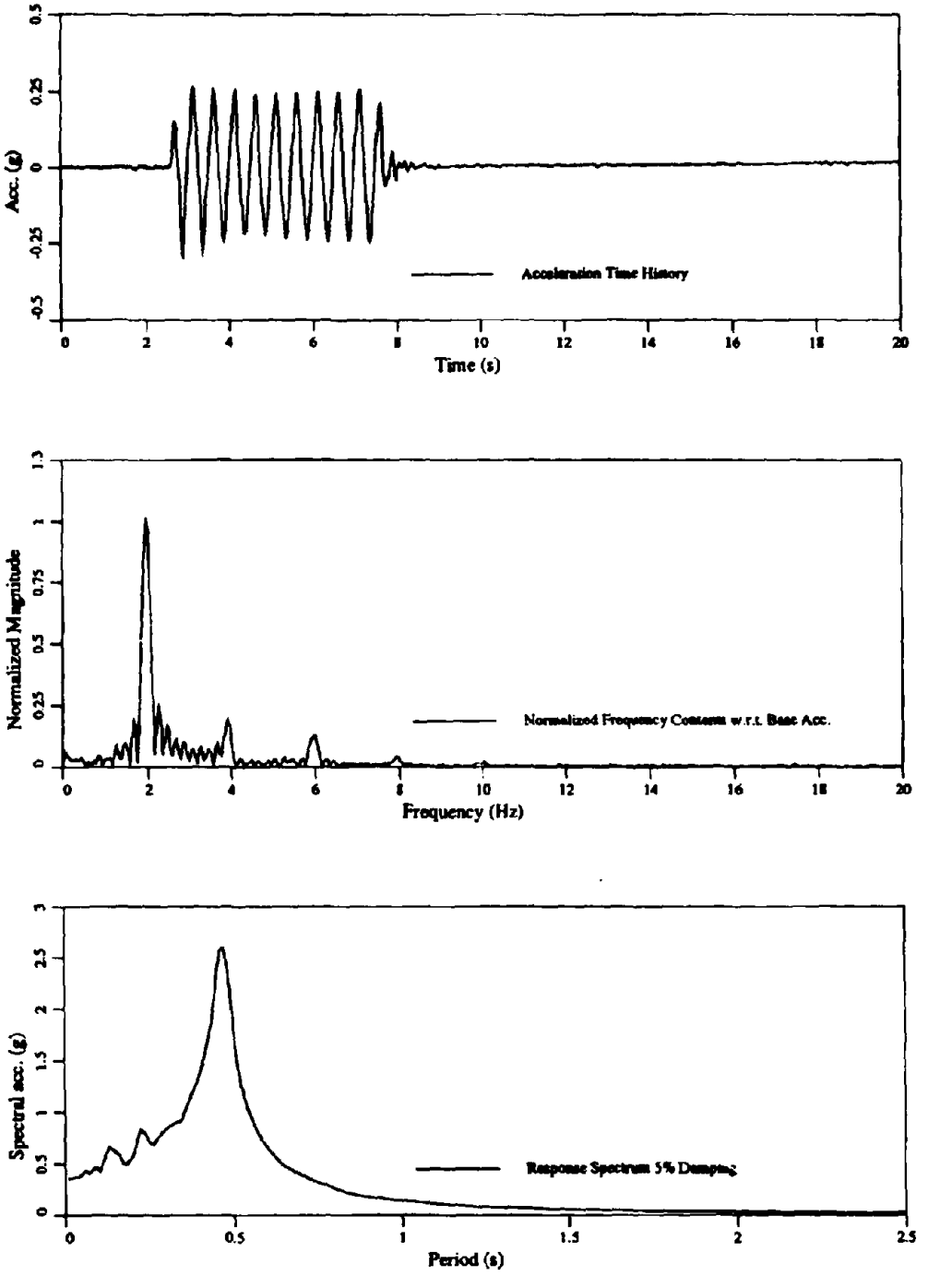

Figure B.2: Standard VELACS Model Test $100g/1$ Horizontal Acceleration of the Base

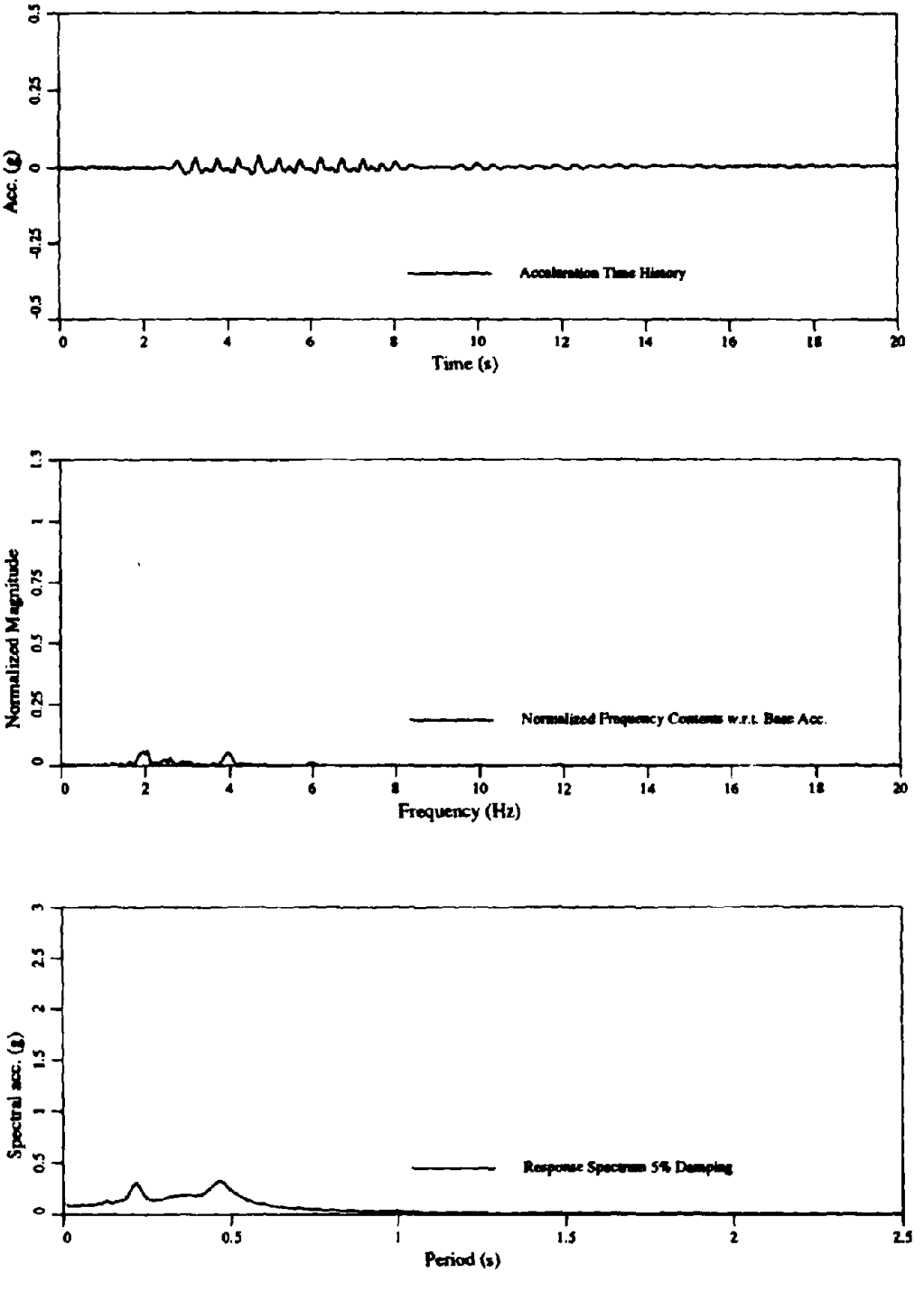

Figure B.3: Standard VELACS Model Test $100g/1$ Vertical Acceleration of the Base

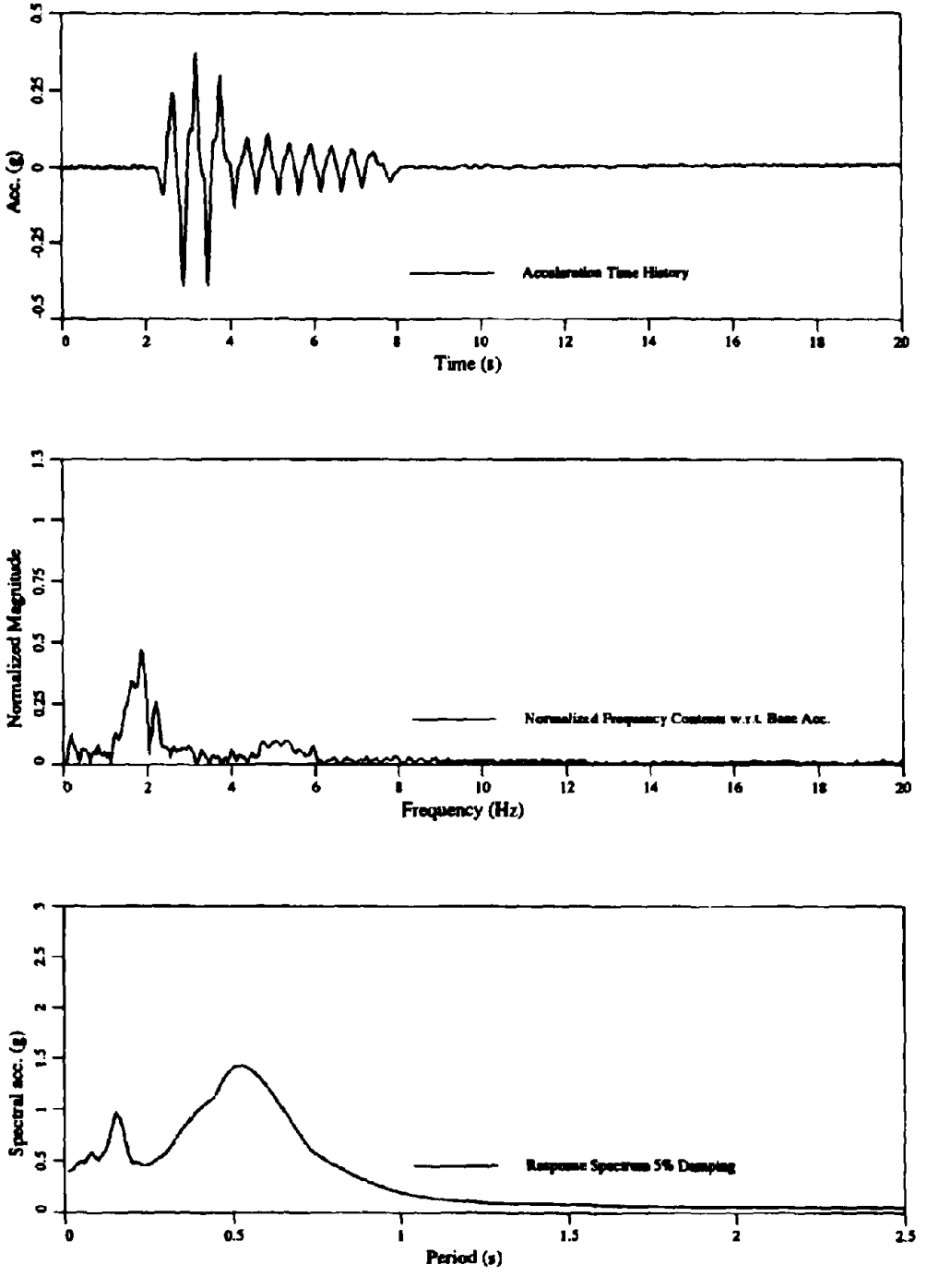

Figure B.4: Standard VELACS Model Test $100g/1$ Horizontal Acceleration in the Silt Layer

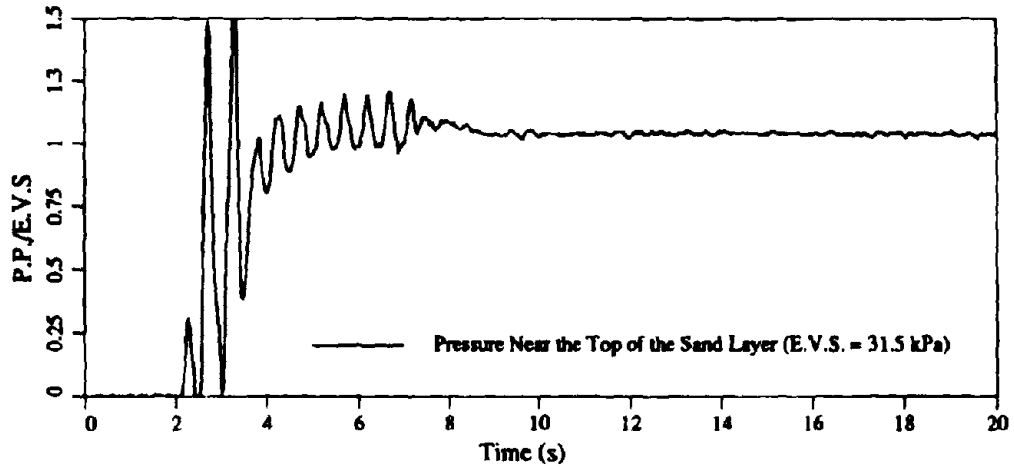

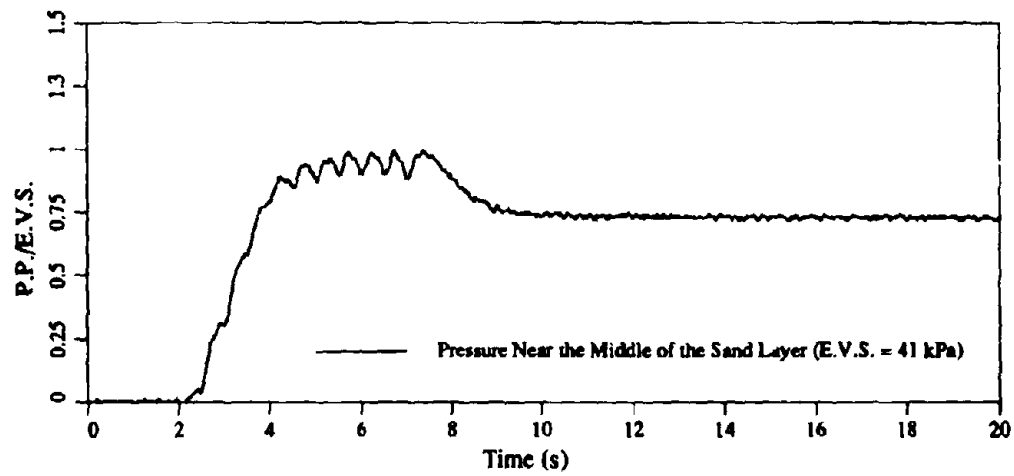

Figure B.5: Standard VELACS Model Test 100g/l Short Term Pore Pressure Ratio Time Histories

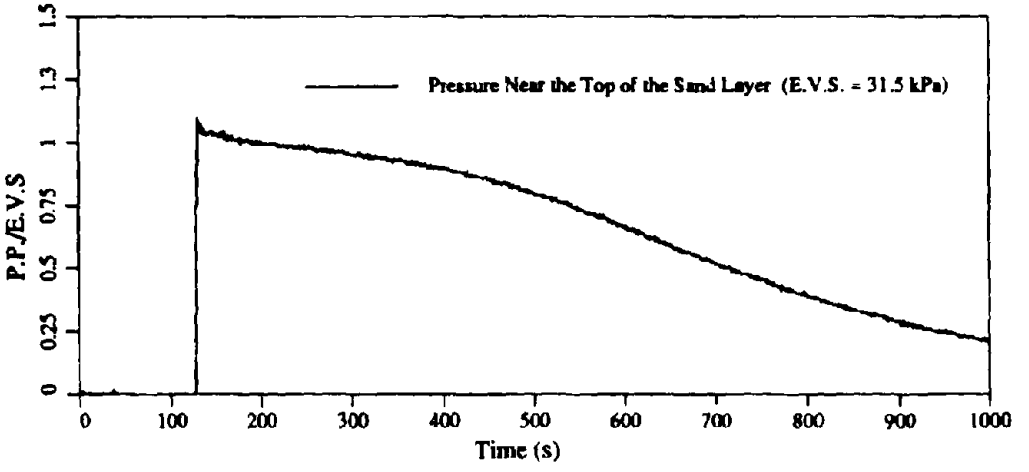

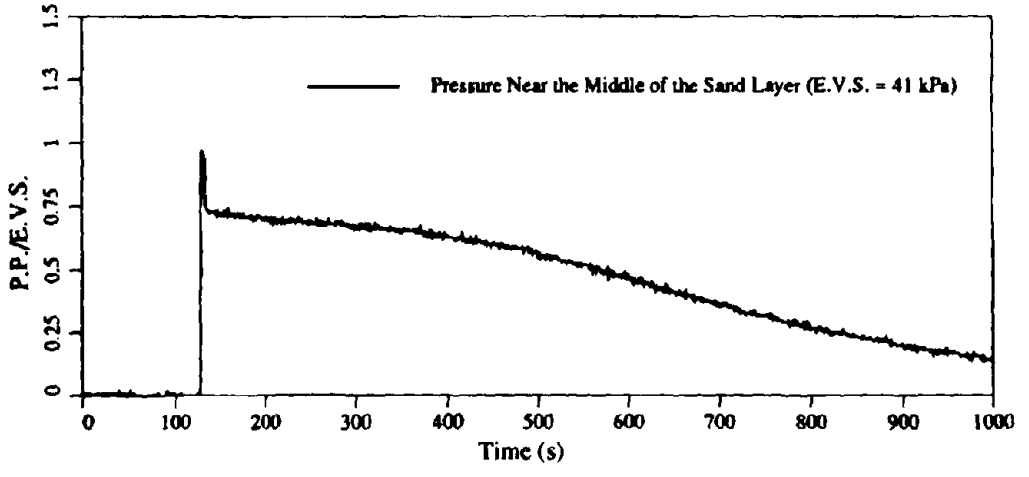

Figure B.6: Standard VELACS Model Test 100g/l Long Term Pore Pressure Ratio Time Histories

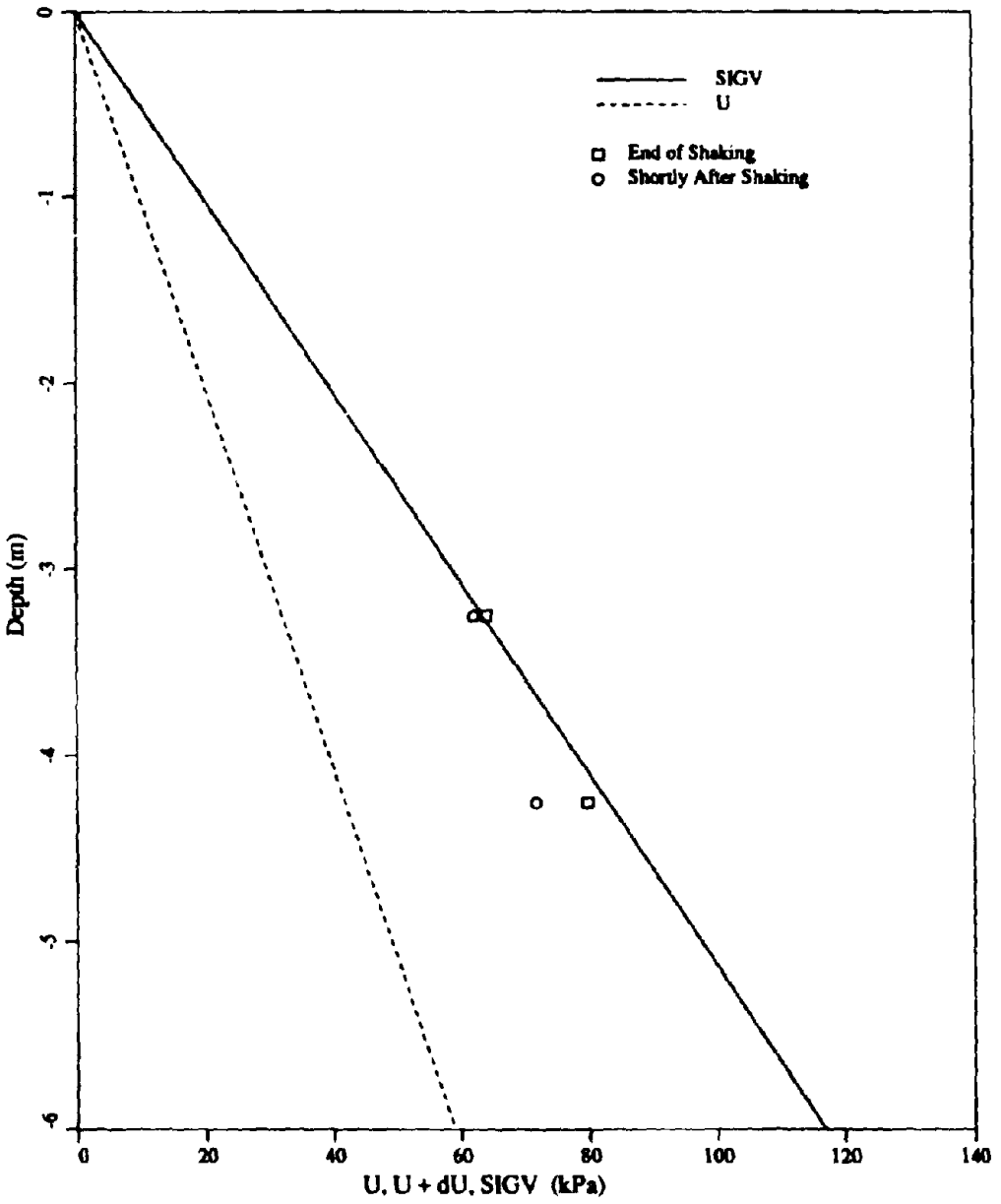

Figure B.7: Standard VELACS Model Test $100g/1$ Stress and Pore Pressure Variations With Depth

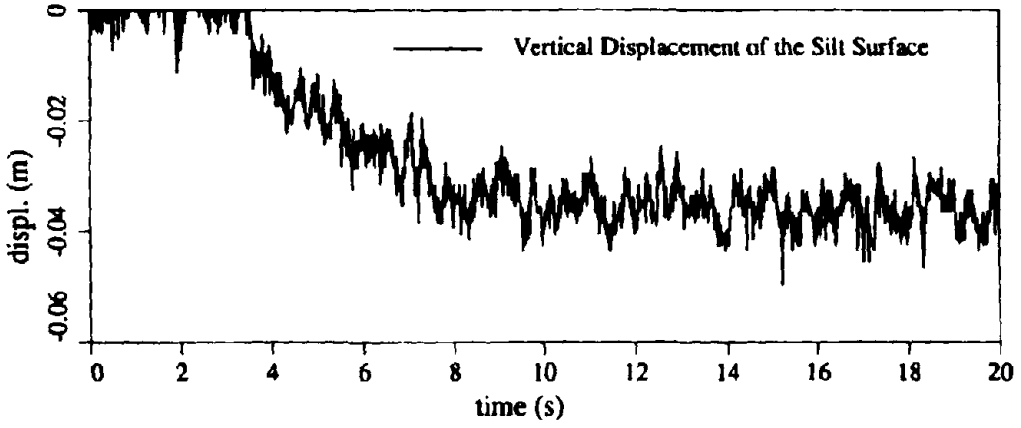

Figure B.8: Standard VELACS Model Test $100g/I$ Vertical Displacement of the Silt Surface

B.2 Test $100g/II$

Test II was performed on July, 30, 1991 (Figure B.9), after the data acquisition system had been upgraded. A new signal conditioning system was built and mounted on the centrifuge arm. The system was designed to support the Masscomp computer with a 16 channels capacity, which was used during Test II.

Increased volume of the transducers B.9 was neglected during the sample preparation, and it was assumed that volume of the all objects in sample was 5% of the sand layer volume. The sample preparation process had not been changed except during the pluviation which was stopped twice in order to place the transducers in the sand layer. During the test accelerometer E came off, so acceleration time history, reported here, was recorded in a dummy test, which had been performed before Test II. Numerous tests had been performed on the P.U. shaker with the same input (2 $[Hz]$, 10 cycles), (all records available on P.U.), and all had similar output acceleration time histories.

Figure B.11 shows a vertical acceleration time history of the test box with its normalized frequency contest and response spectra. Horizontal accelerations of the mid silt layer and the silt surface are shown in Figures B.12 and B.13 , respectively.

Effective vertical stresses were calculated the same as in Test I. The short-term pore pressure time histories were available from Masscomp computer, and the long-term time histories were played back from the tape recorder (Figures B.14, B.15). Figure B.16 shows stress and pore pressure variations with depth, with the values of the excessive water pressures obtained by the inspection of Figure B.14. Since the problem with the sinking footing of the LVDT core had not been solved at the time Test II was performed, vertical displacement of the silt surface was not measured.

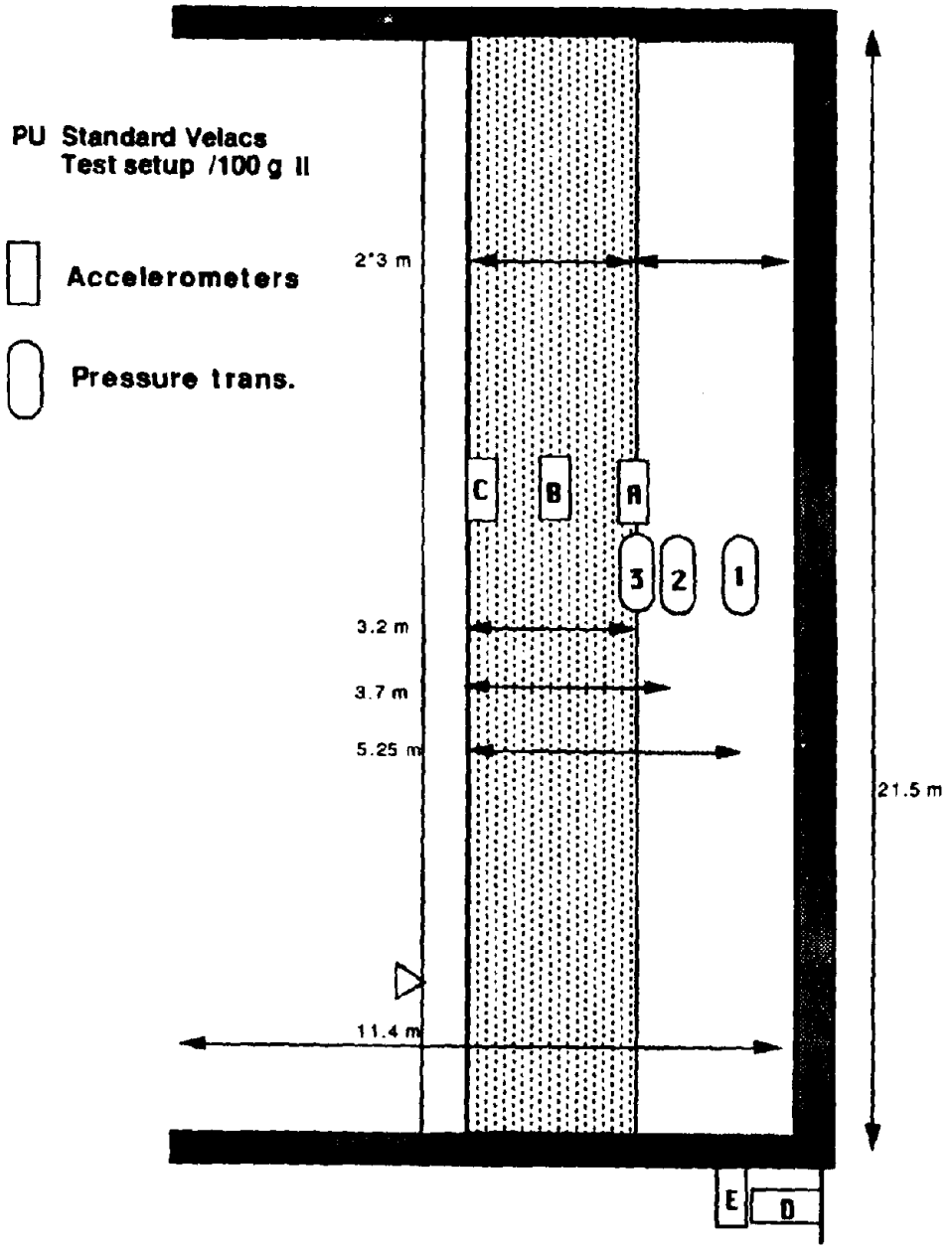

Figure B.9: Standard Velacs Model Test 100 g/II

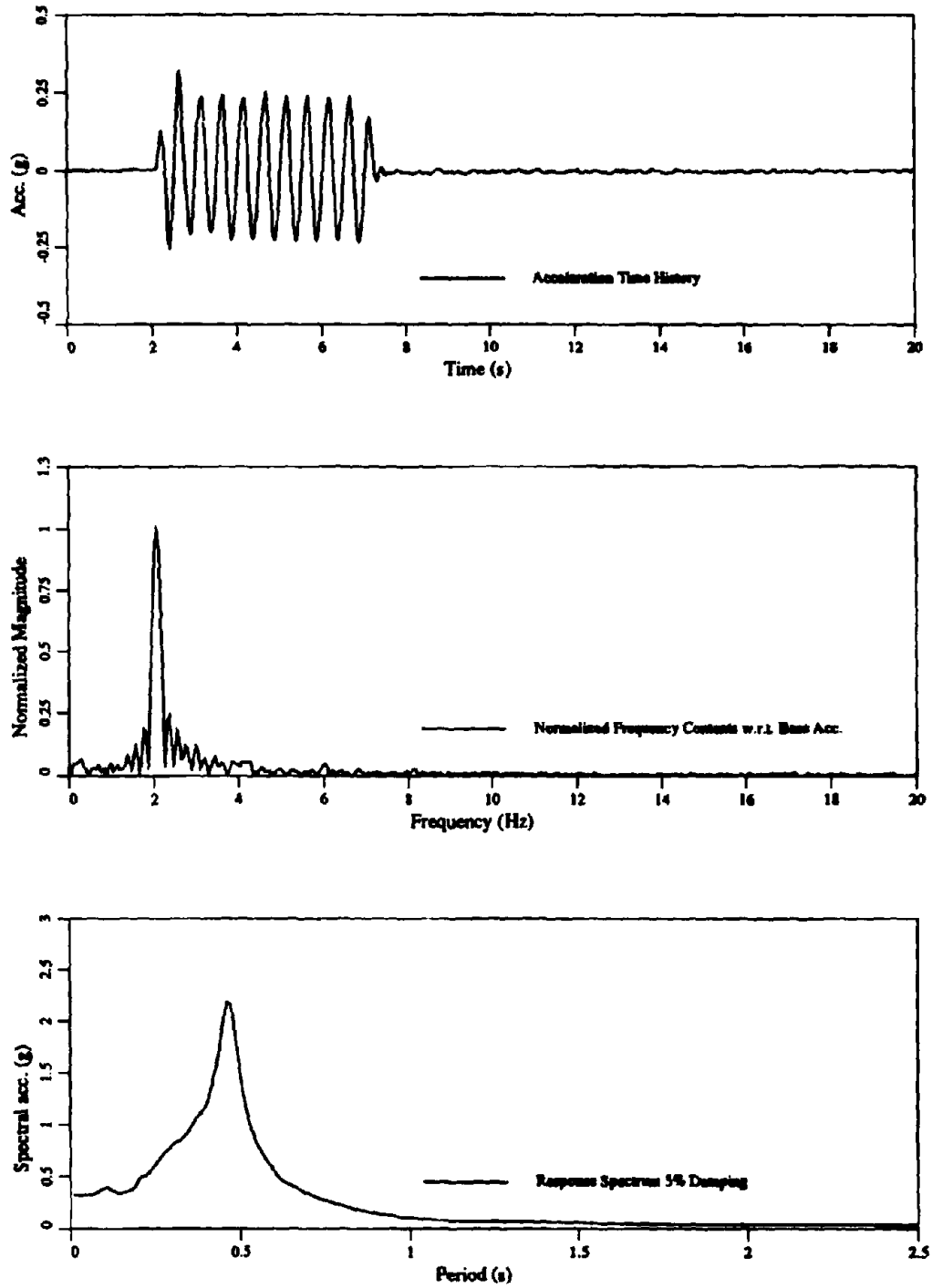

Figure B.10: Standard VELACS Model Test $100g/11$ Horizontal Acceleration of the Base

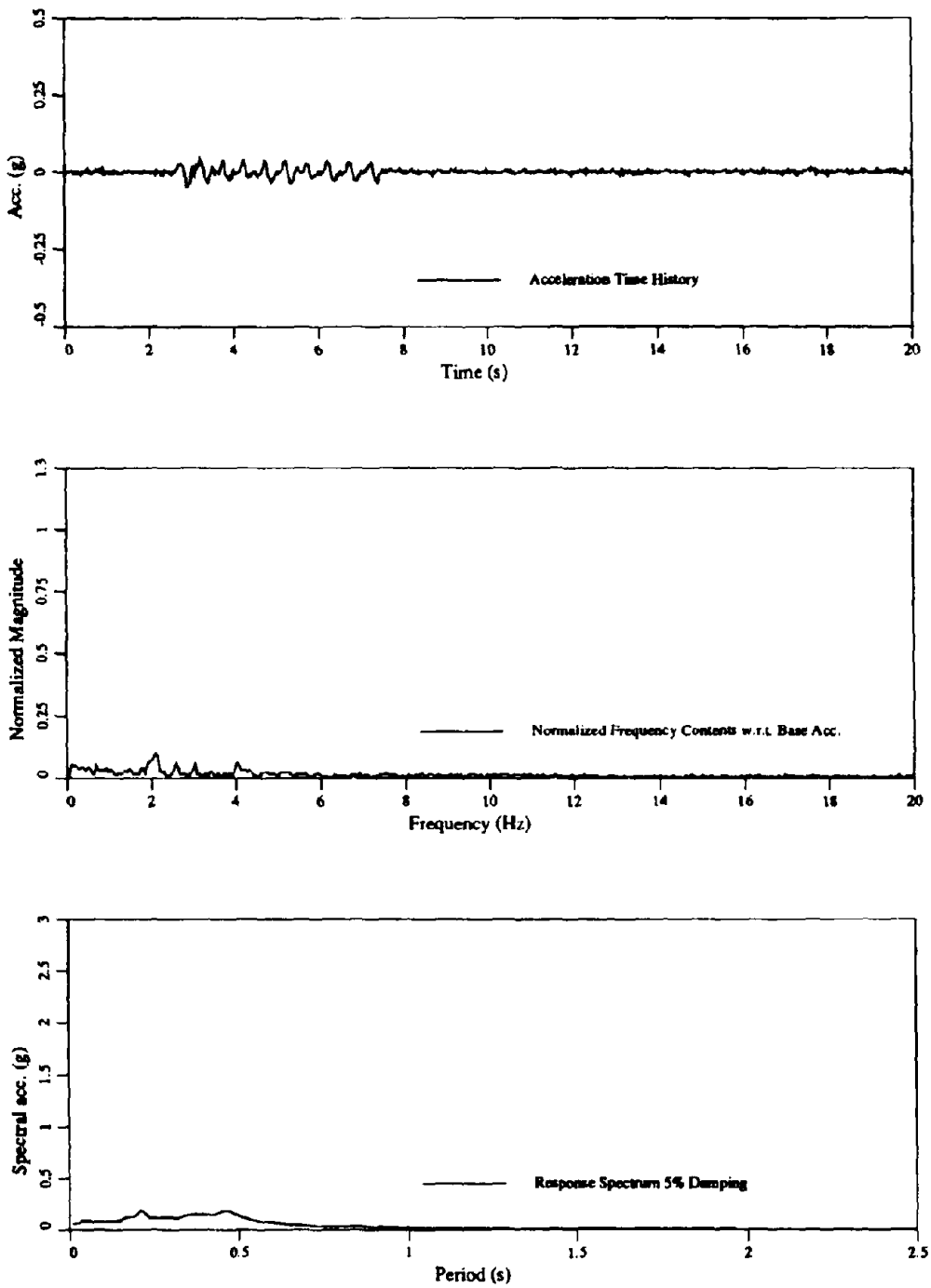

Figure B.11: Standard VELACS Model Test $100g/II$ Vertical Acceleration of the Base

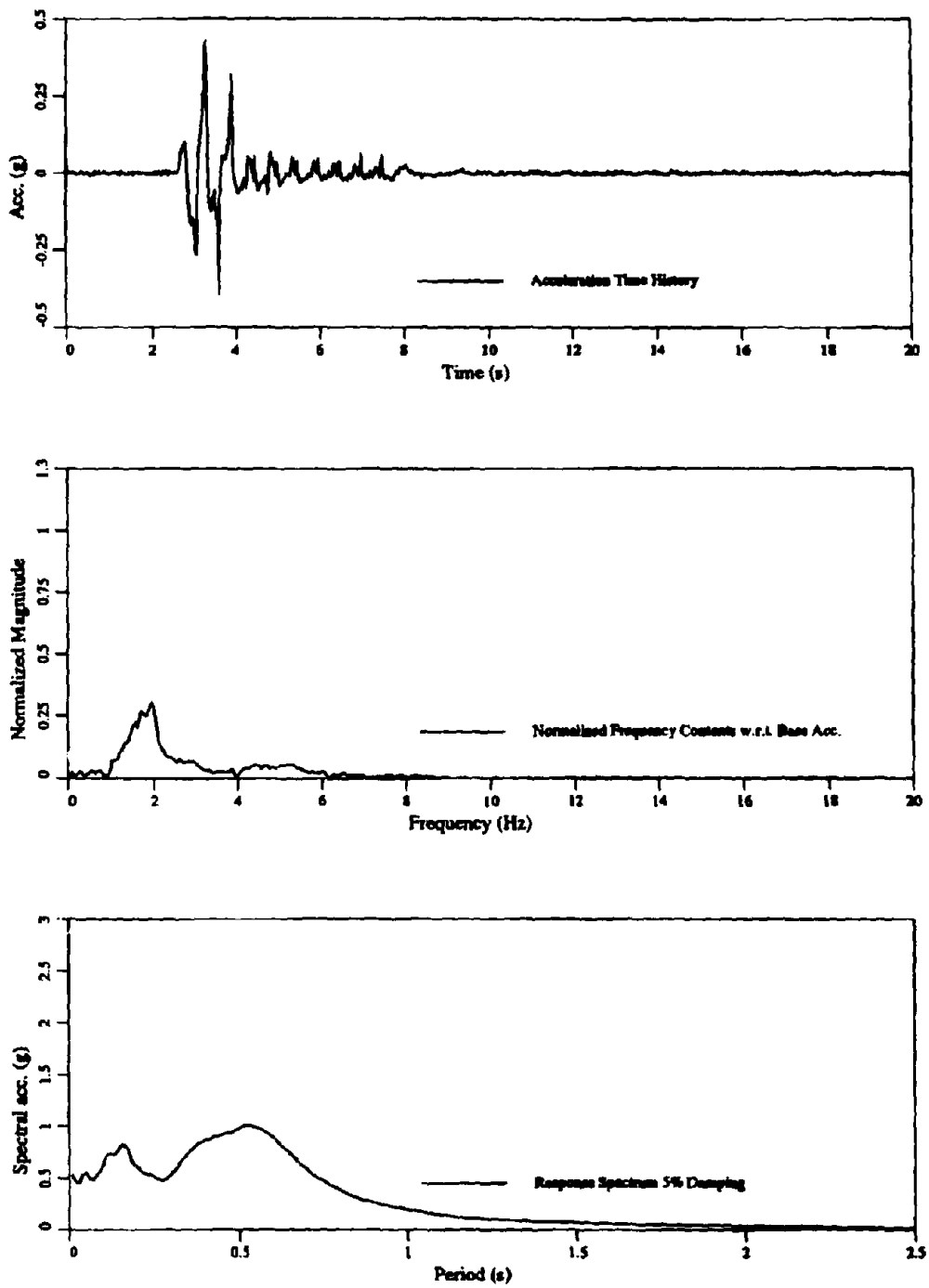

Figure B.12: Standard VELACS Model Test $100g/II$ Horizontal Acceleration in the Silt Layer

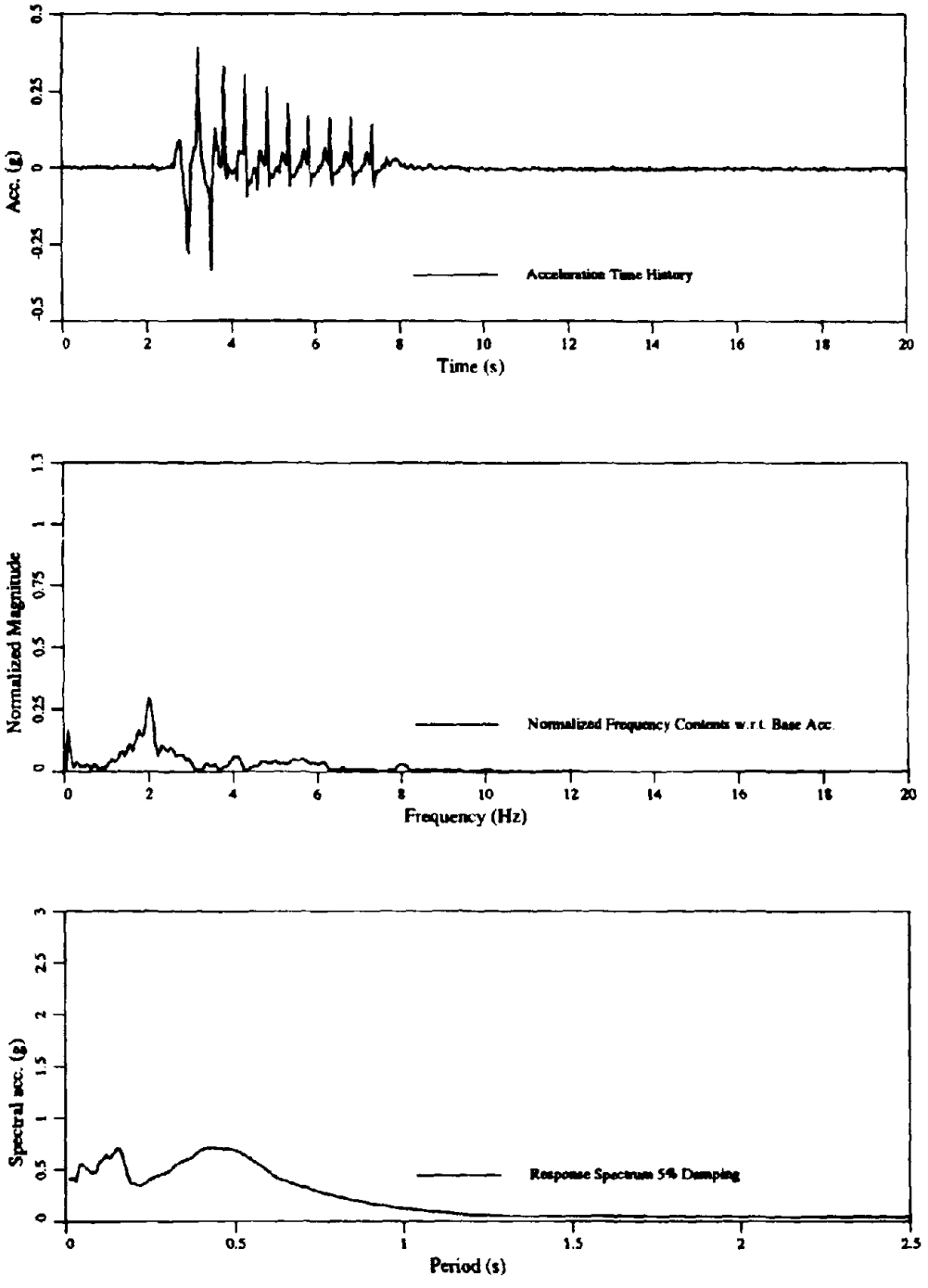

Figure B.13: Standard VELACS Model Test $100g/11$ Horizontal Acceleration on the Silt Surface

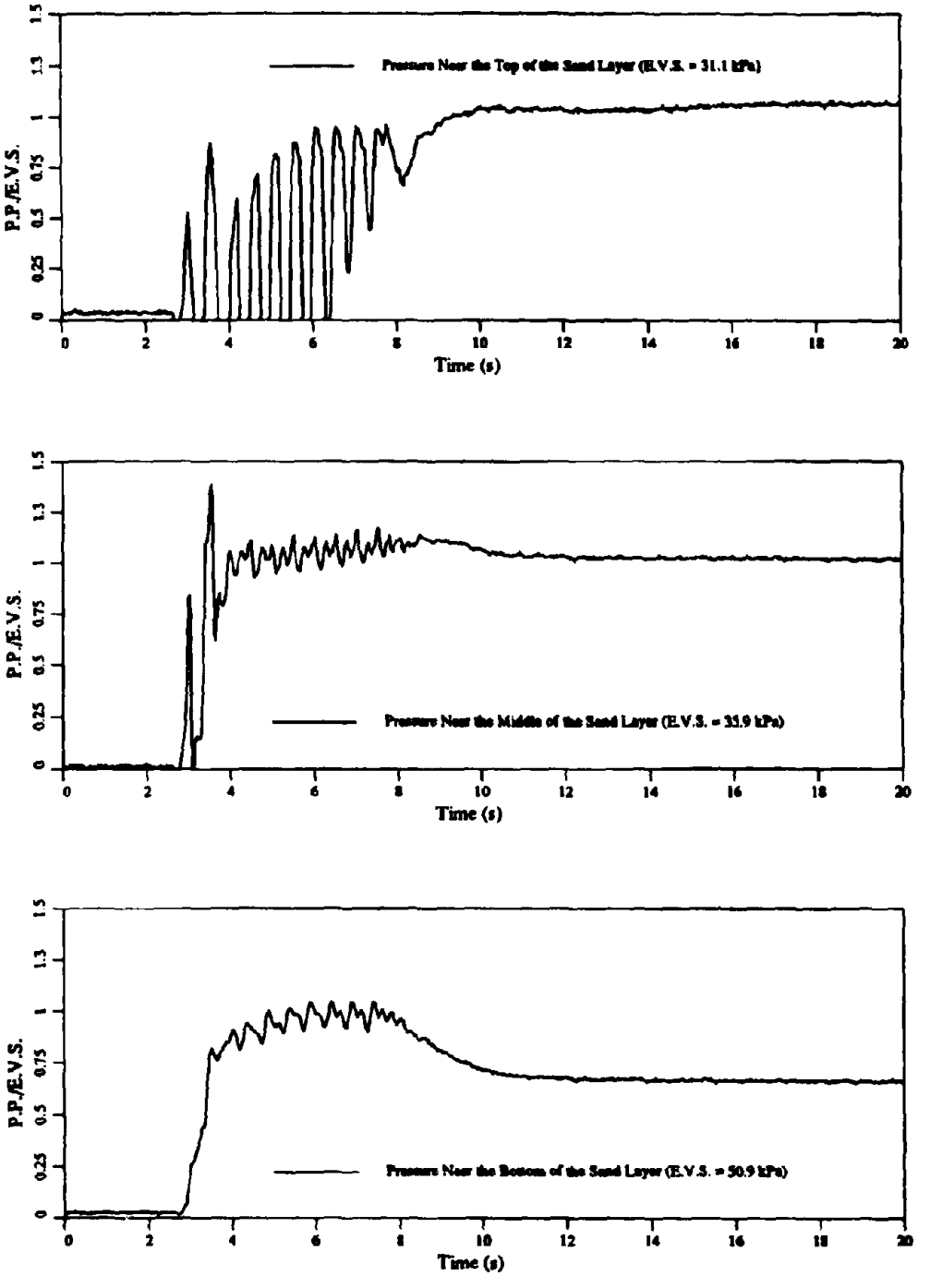

Figure B.14: Standard VELACS Model Test $100g/II$ Short Term Pore Pressure Ratio Time Histories

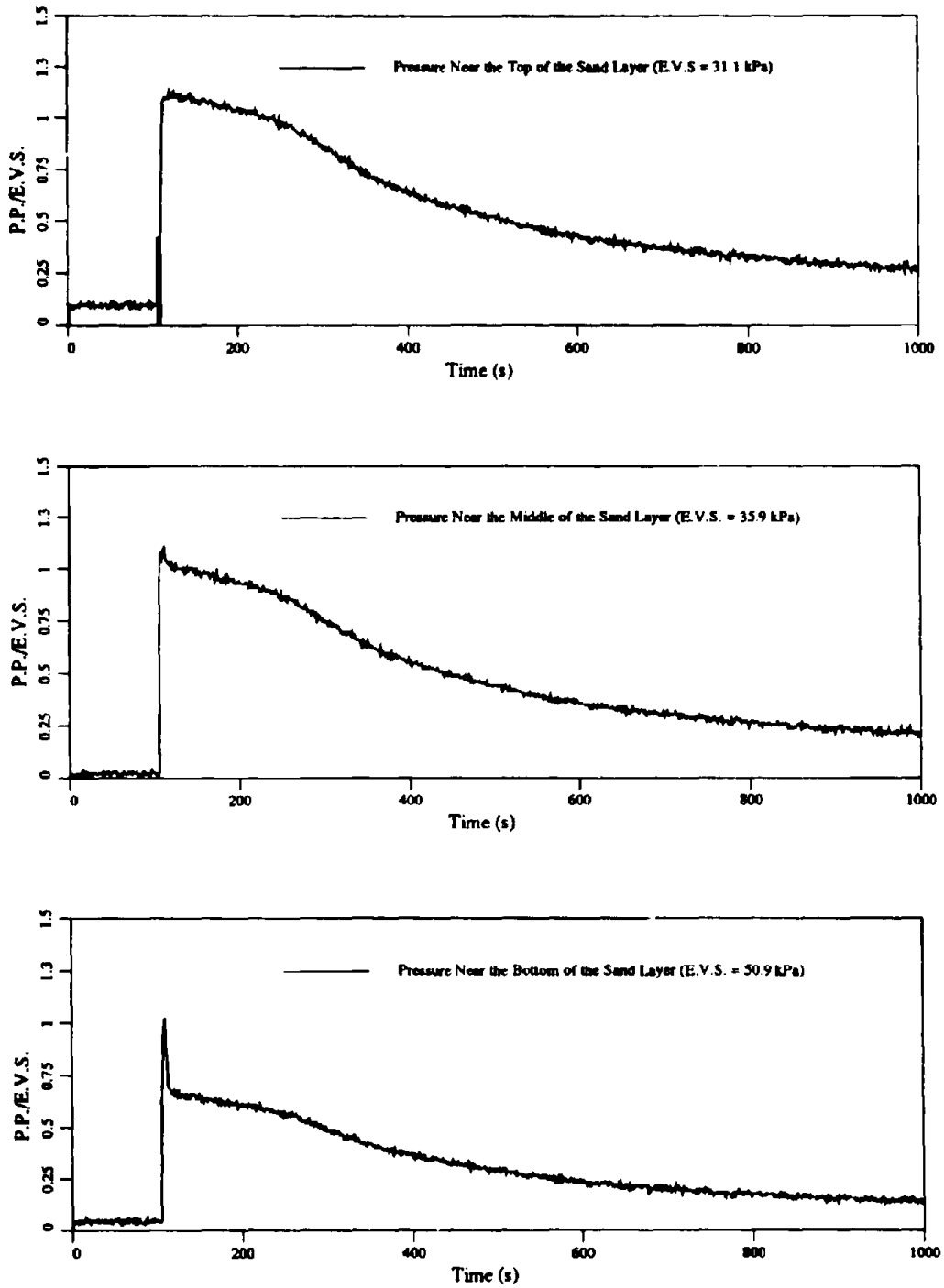

Figure B.15: Standard VELACS Model Test $100g/II$ Long Term Pore Pressure Ratio Time Histories

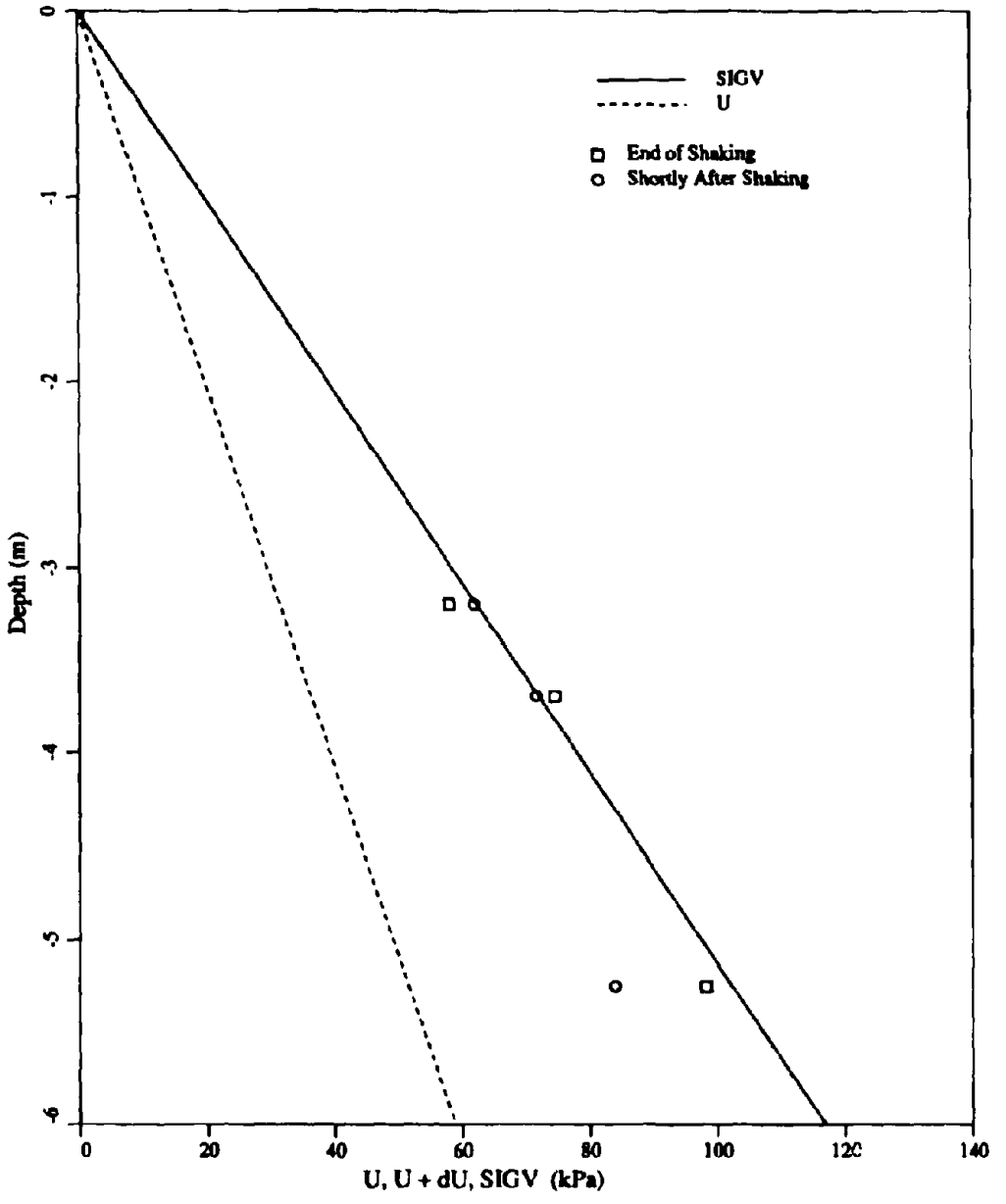

Figure B.16: Standard VELACS Model Test $100g/II$ Stress and Pore Pressure Variations With Depth

Appendix C

VELACS $75g$ Tests

C.1 Test $75g/I$

Test $75g/I$ was performed on October, 6, 1991 with an upgraded data acquisition system (Figure C.1). The centrifuge bucket had been redesigned to accommodate larger models, such that the model box for the $75g$ test has the same prototype dimensions as the model box for the $100g$ tests.

Ten channels were recorded directly on the Masscomp data acquisition system with a sampling rate of 7500 $[Hz]$, in order to have the same prototype time step as the one in $100g$ tests. Eight channels were backed up with the tape recorder; due to the limited capacity of the tape recorder (eight channels), accelerometers A and C were recorded only on the Masscomp. During the sample preparation process accelerometer A changed its orientation, so data recorded from acc. A is not valid.

Because of the larger box it was possible to place all pressure transducers except PT # 2, perpendicular to the shaking direction. Unfortunately, PT # 2 did not function during the test, so it was impossible to make a comparison between them. But when comparing a pore pressure time history of the PT # 1 with a corresponding time history of the $100g$ test, it is obvious that the level of noise in pore pressure time history has been decreased.

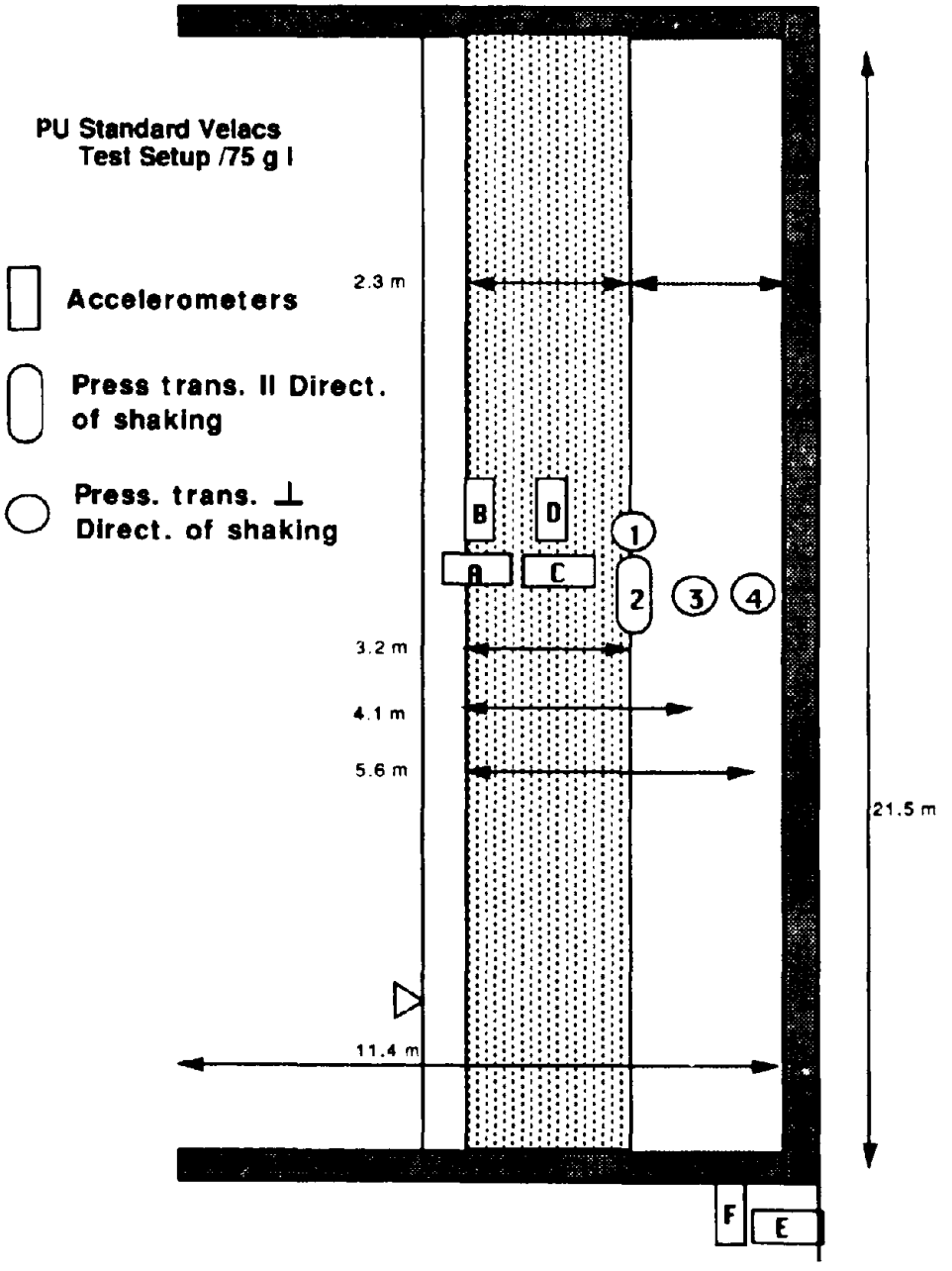

Figure C.1: **Standard Velacs Model Test 75 g/l**

A sample rate was changed from 7500 $[Hz]$ to 3750 $[Hz]$, and all data records were zeroed with subtracting average value of the first 50 points. Positions of the pore pressure transducers were measured with a ruler after the test. All the dimensions in Figure C.1 show the distances measured from the surface to the center of the transducers. Effective vertical stresses were calculated with these values and the assumed densities of 1950 $[kg/m^3]$ for the sand and silt (no soil data were available).

Input time histories were shown on Figures C.2and C.3. Horizontal and vertical acceleration time histories of the silt layer and the silt surface are presented in Figures C.4 to C.7. Short and long term pore pressure ratios were shown in Figures C.8 and C.9.

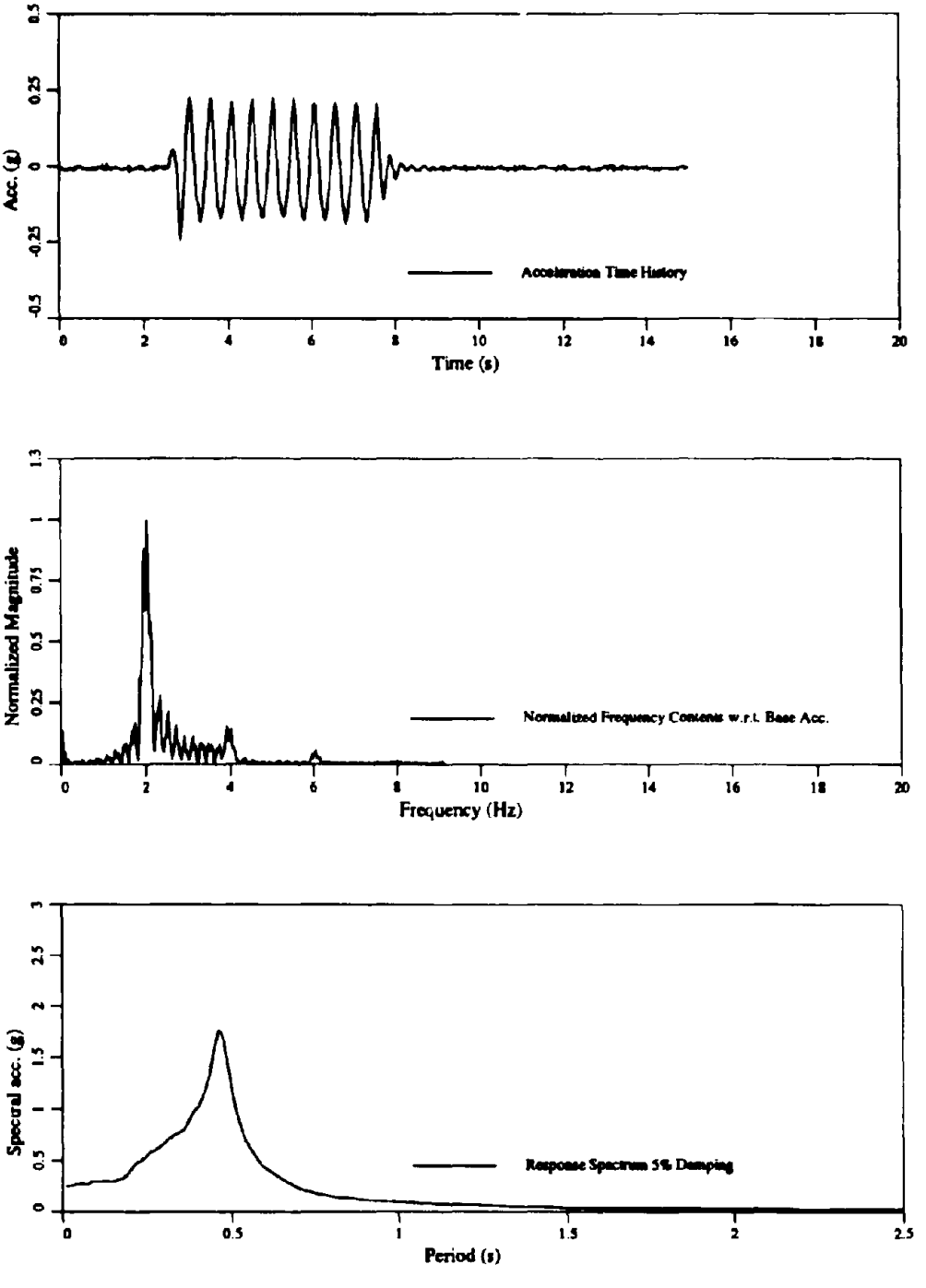

Figure C.2: Standard VELACS Model Test $75g/l$ Horizontal Acceleration of the Base

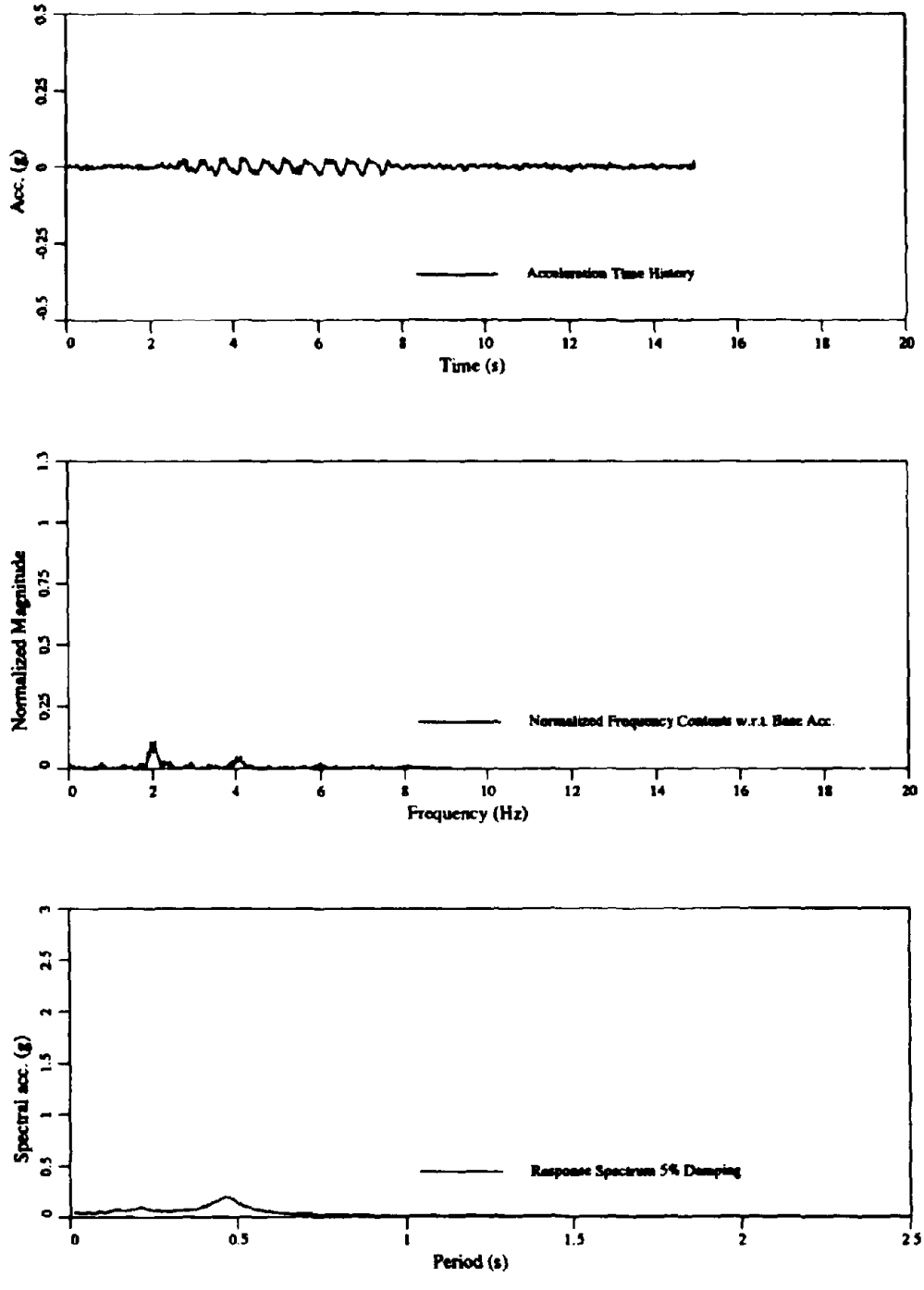

Figure C.3: Standard VELACS Model Test $75g/1$ Vertical Acceleration of the Base

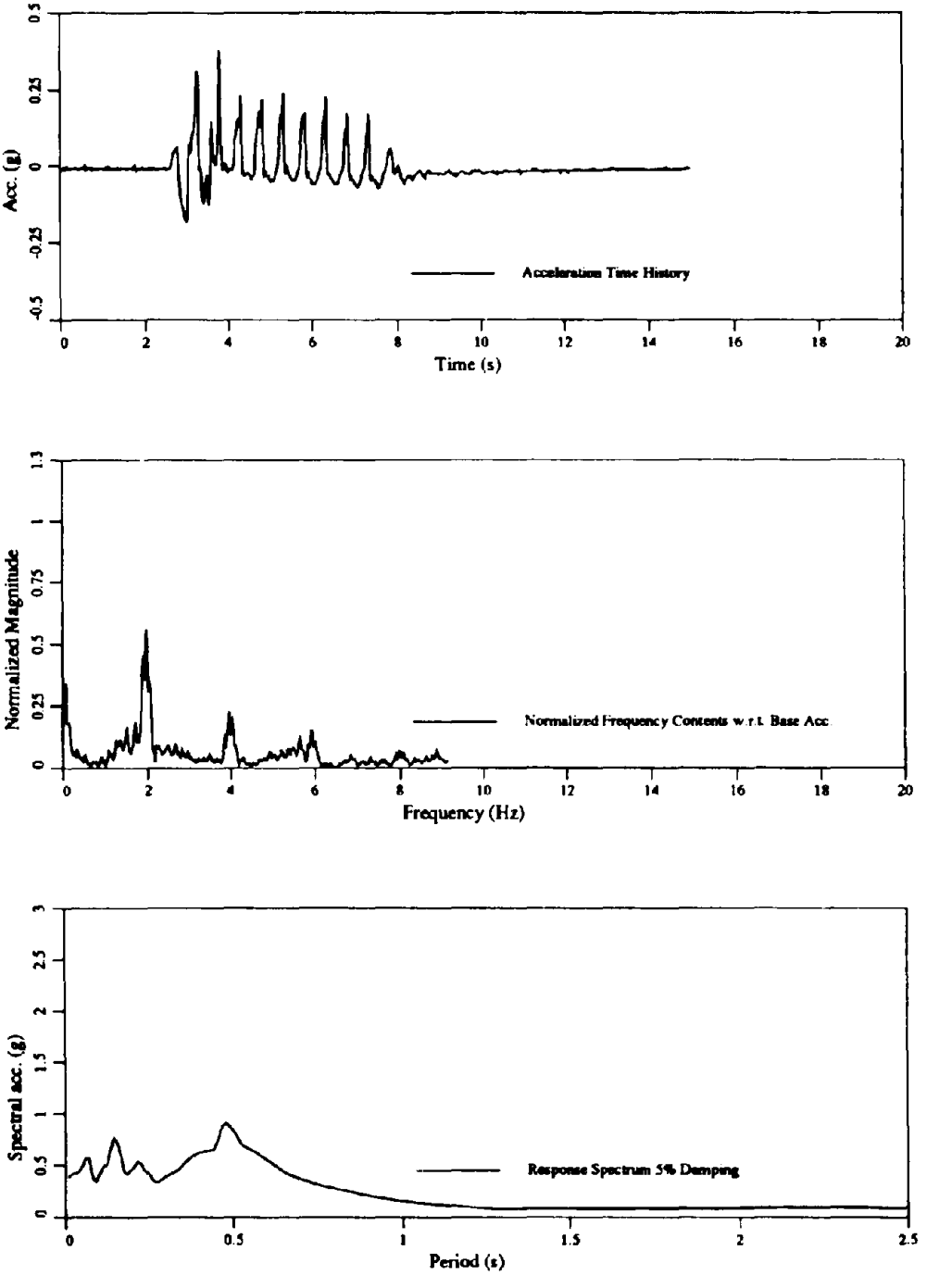

Figure C.4: Standard VELACS Model Test 75g/l Horizontal Acceleration in the Silt Layer

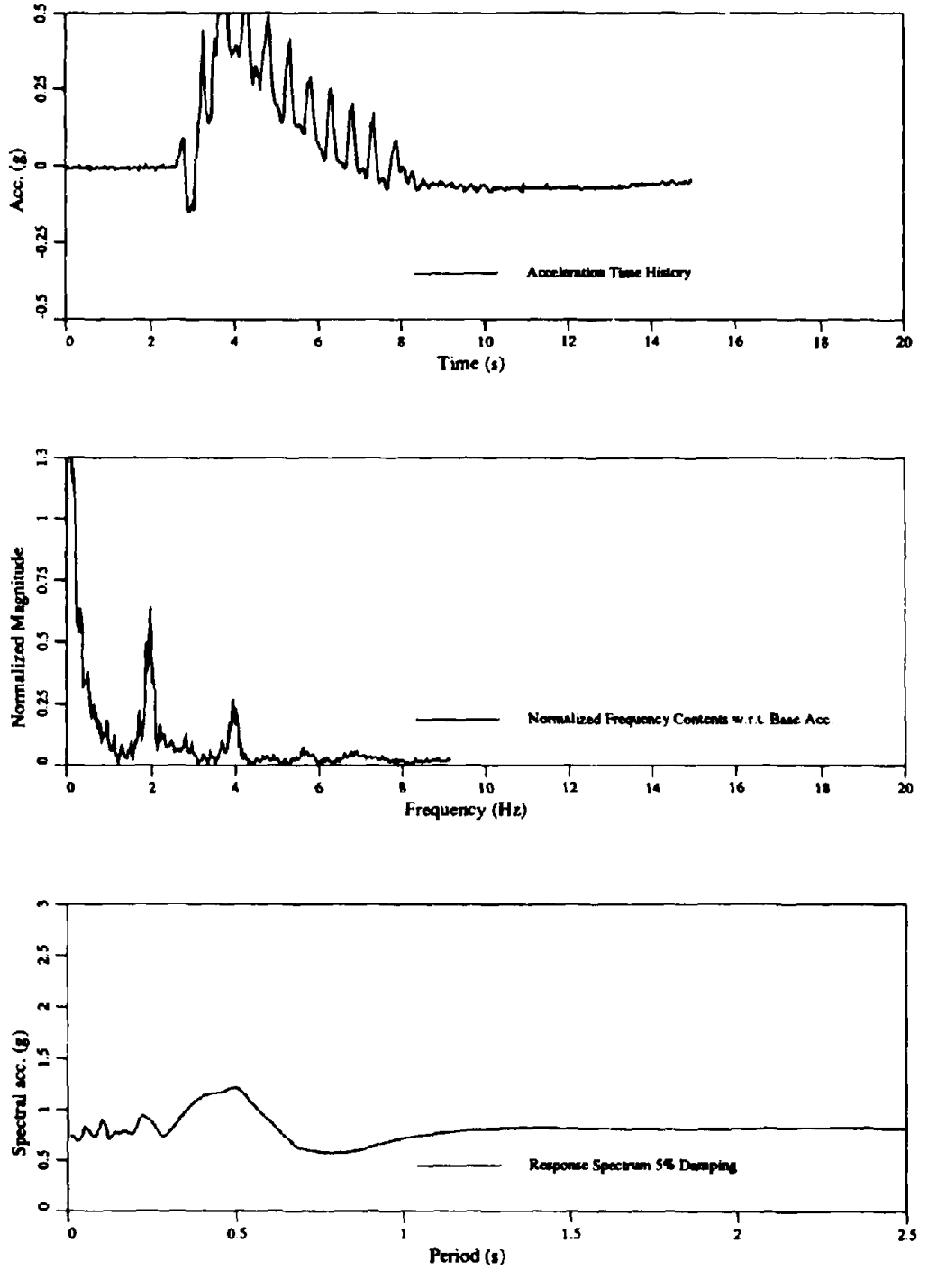

Figure C.5: Standard VELACS Model Test $75g/1$ Vertical Acceleration in the Silt Layer

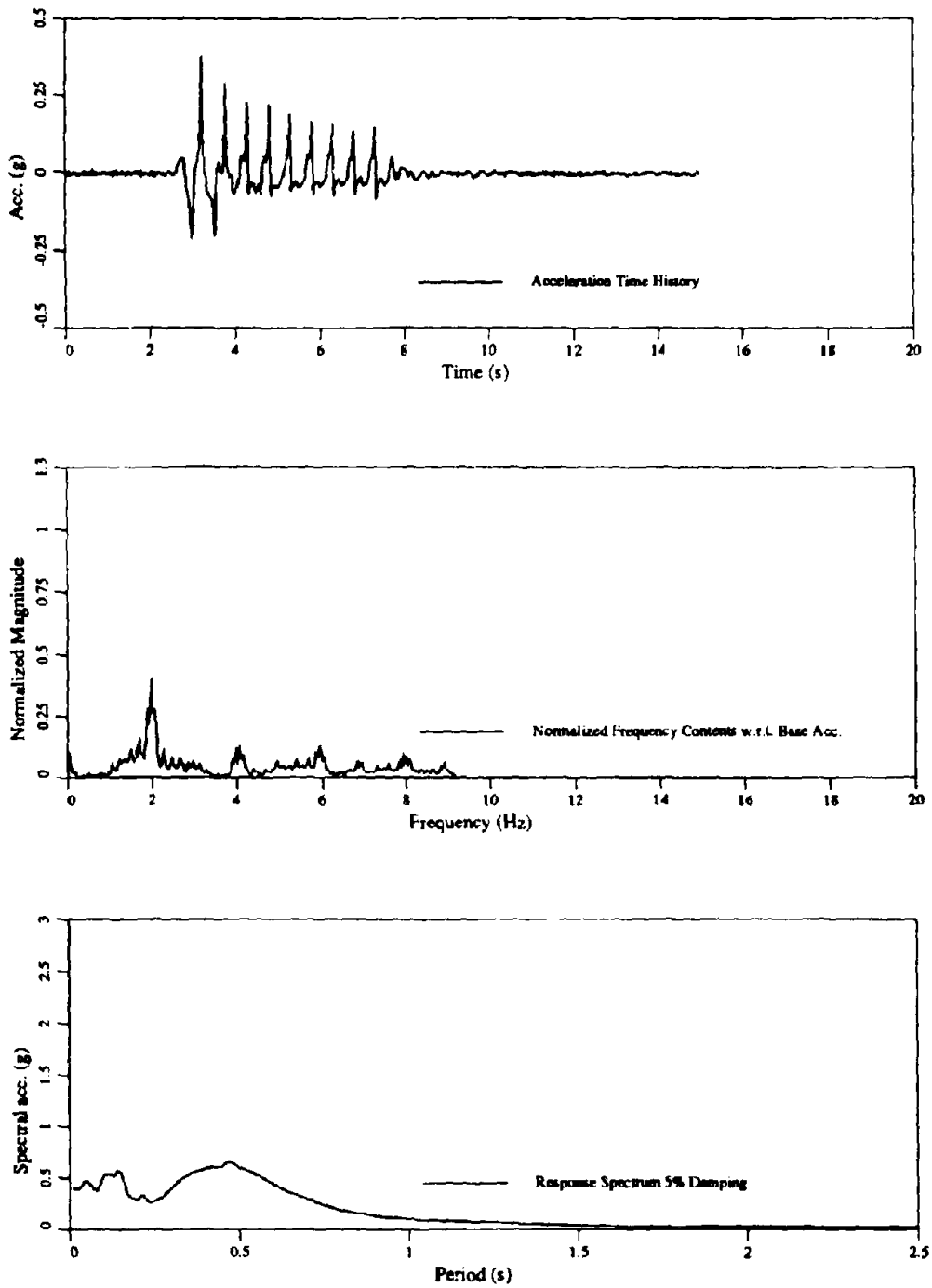

Figure C.6: Standard VELACS Model Test $75g/1$ Horizontal Acceleration on the Silt Surface

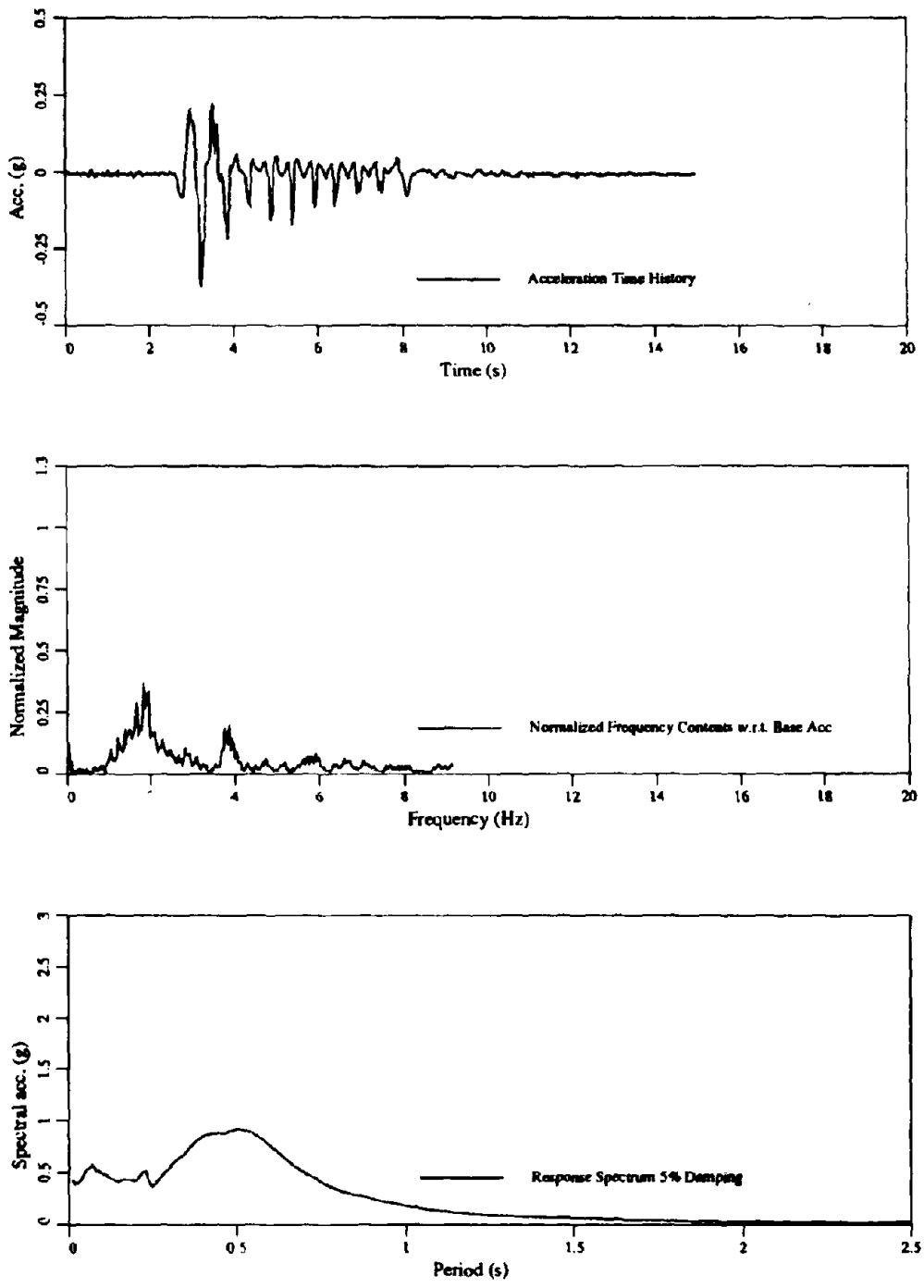

Figure C.7: Standard VELACS Model Test $75g/1$ Vertical Acceleration on the Silt Surface

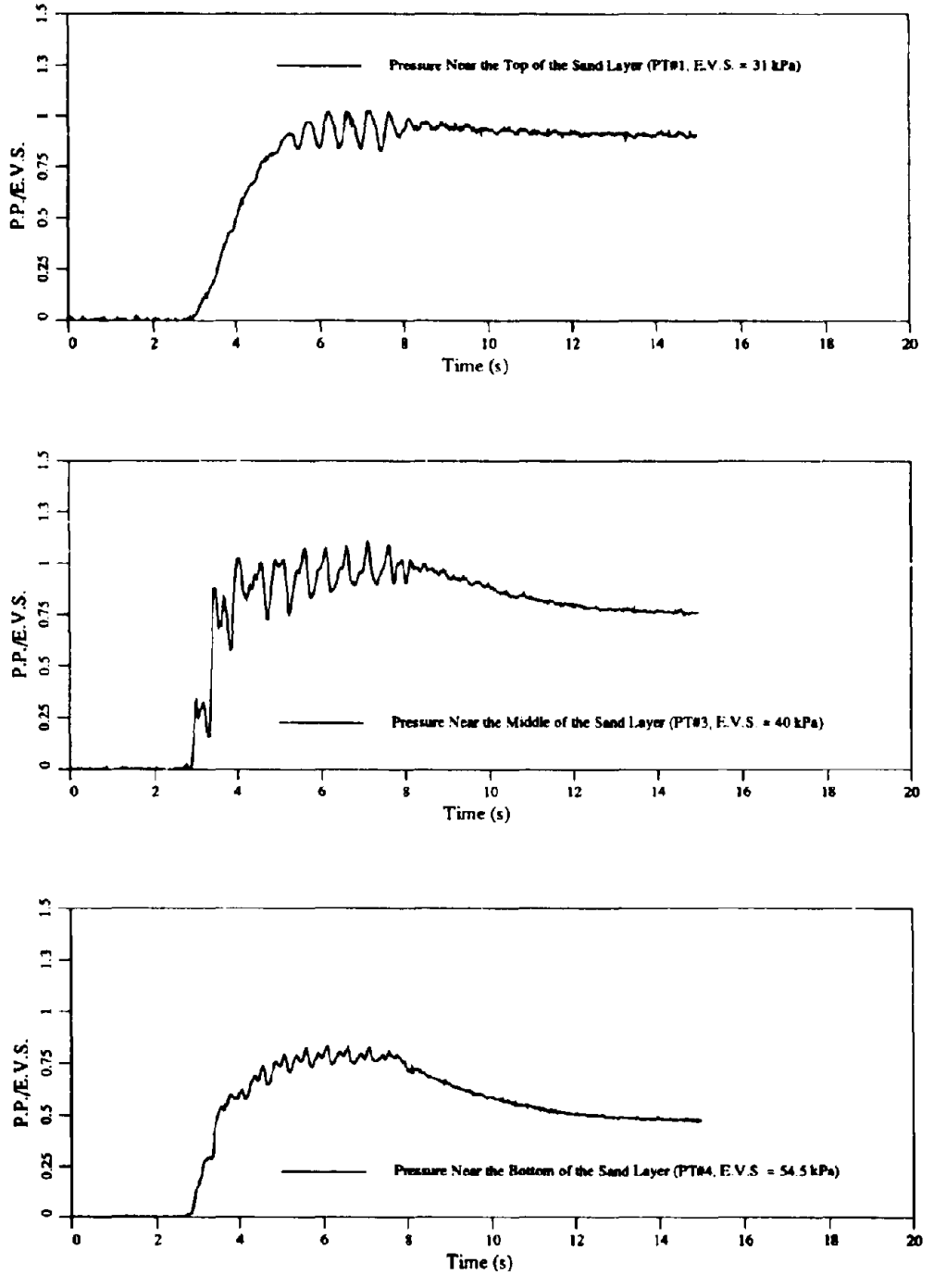

Figure C.8: Standard VELACS Model Test $75g/1$ Short Term Pore Pressure Ratio Time Histories

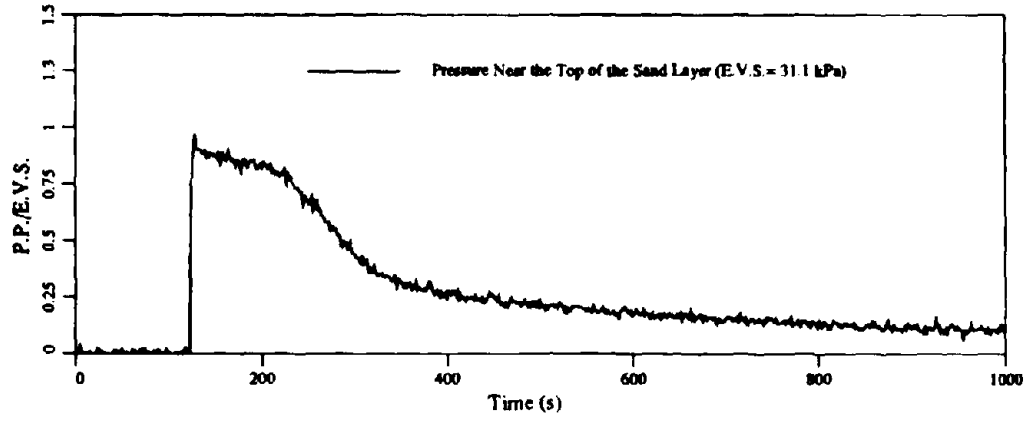

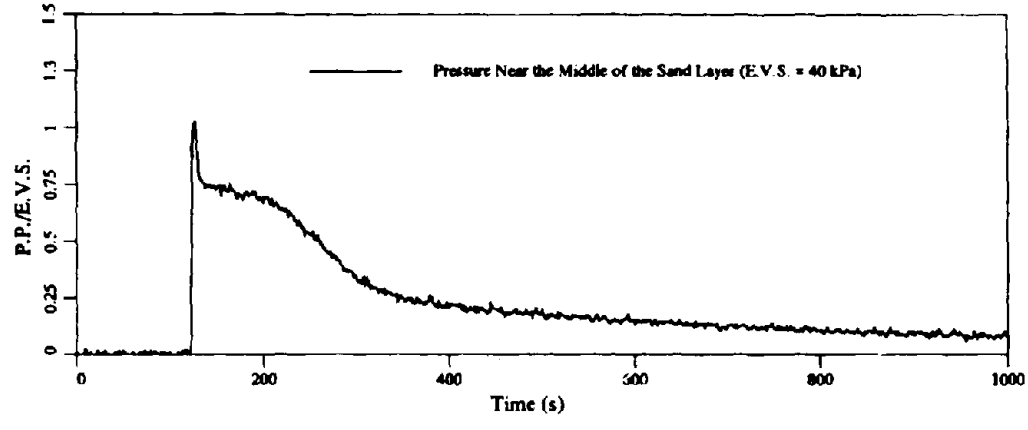

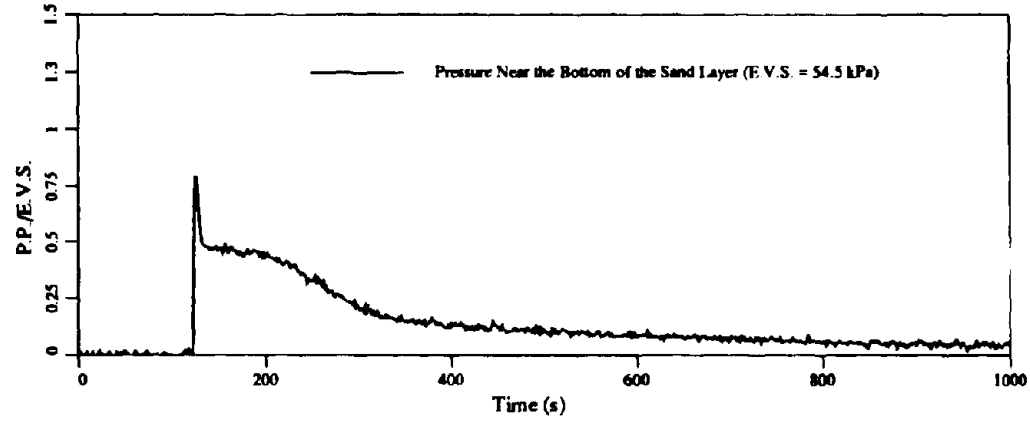

Figure C.9: Standard VELACS Model Test $75g/1$ Long Term Pore Pressure Ratio Time Histories

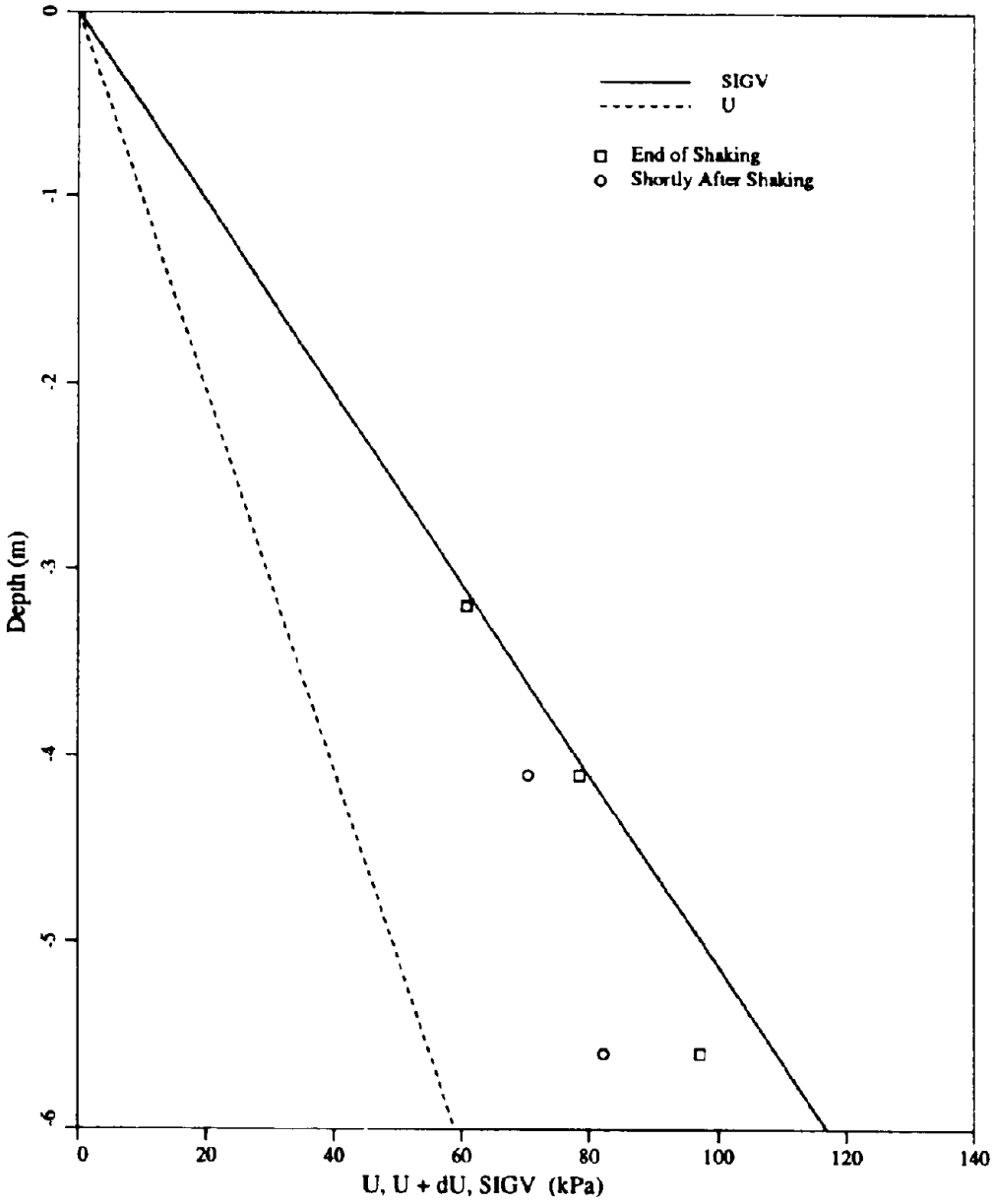

Figure C.10: Standard VELACS Model Test $75g/1$ Stress and Pore Pressure Variations With Depth

C.2 Test $75g/II$

Test $75g/II$ was performed on November, 1, 1991 (Figure C.11) to verify the results of Test I. Ten channels were recorded directly on the Masscomp data acquisition system with a sampling rate of 7500 $[Hz]$. Eight channels were at the same time recorded on the tape recorder. Due to the limited capacity of the tape recorder (eight channels), accelerometers A and C were recorded only on the Masscomp.

All pressure transducers were placed with porous stone facing a direction perpendicular to the shaking direction. PT# 2 was placed close to the box side in order to monitor boundary effects on a pore pressure time history.

Input time histories were shown on Figures C.12 and C.13. Horizontal and vertical acceleration time histories of the silt layer and the silt surface are presented in Figures C.14 to C.17. Short and long term pore pressure ratios are shown in Figures C.18 and C.20. Figure C.19 shows comparison of the pore-water pressure time histories of the side and the center of the testing box. It seems reasonable to explain the higher pore-water pressure fluctuations recorded with PT # 2 with the boundary effects of the box.

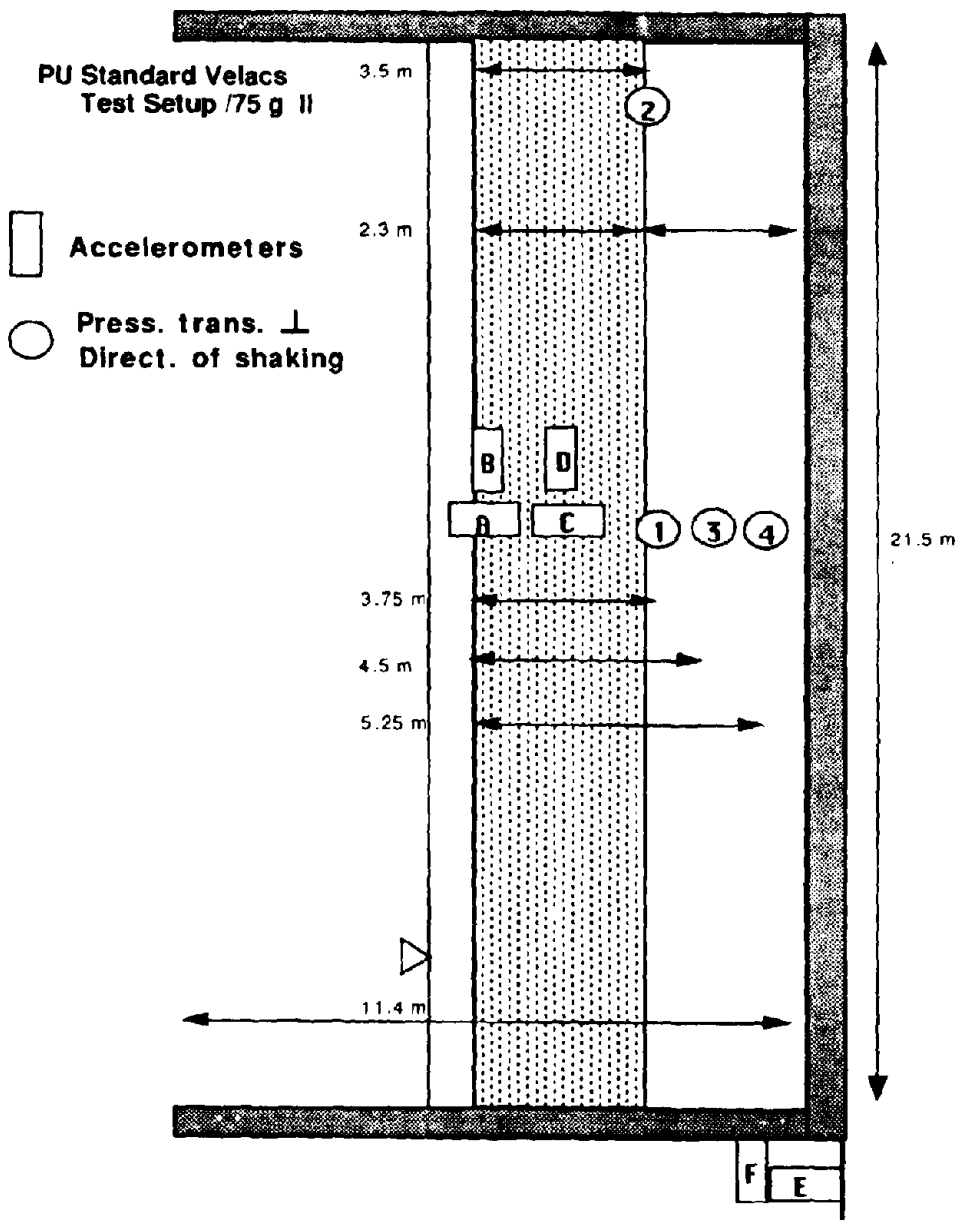

Figure C.11: **Standard Velacs Model Test 75 g/II**

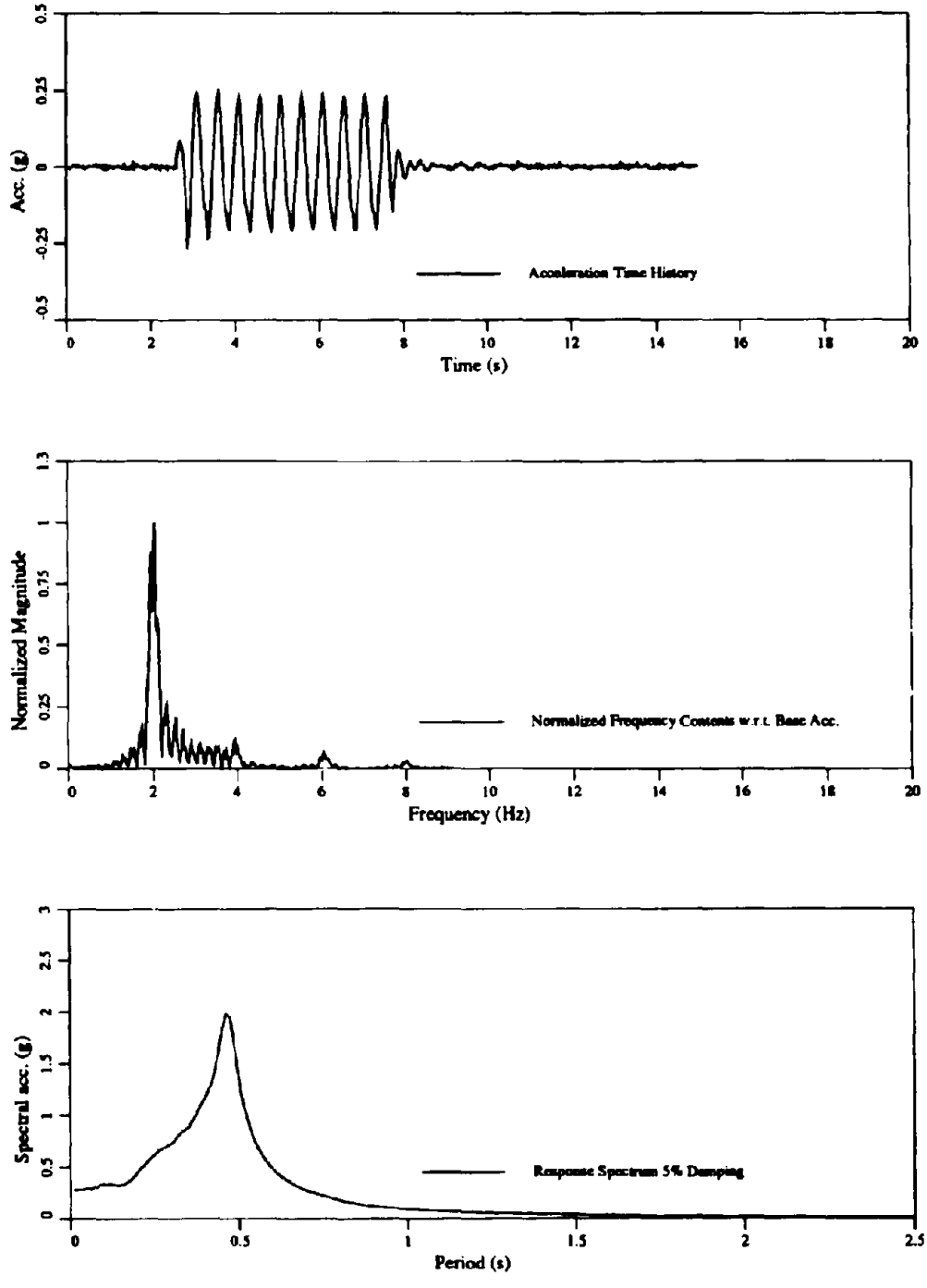

Figure C.12: Standard VELACS Model Test $75g/II$ Horizontal Acceleration of the Base

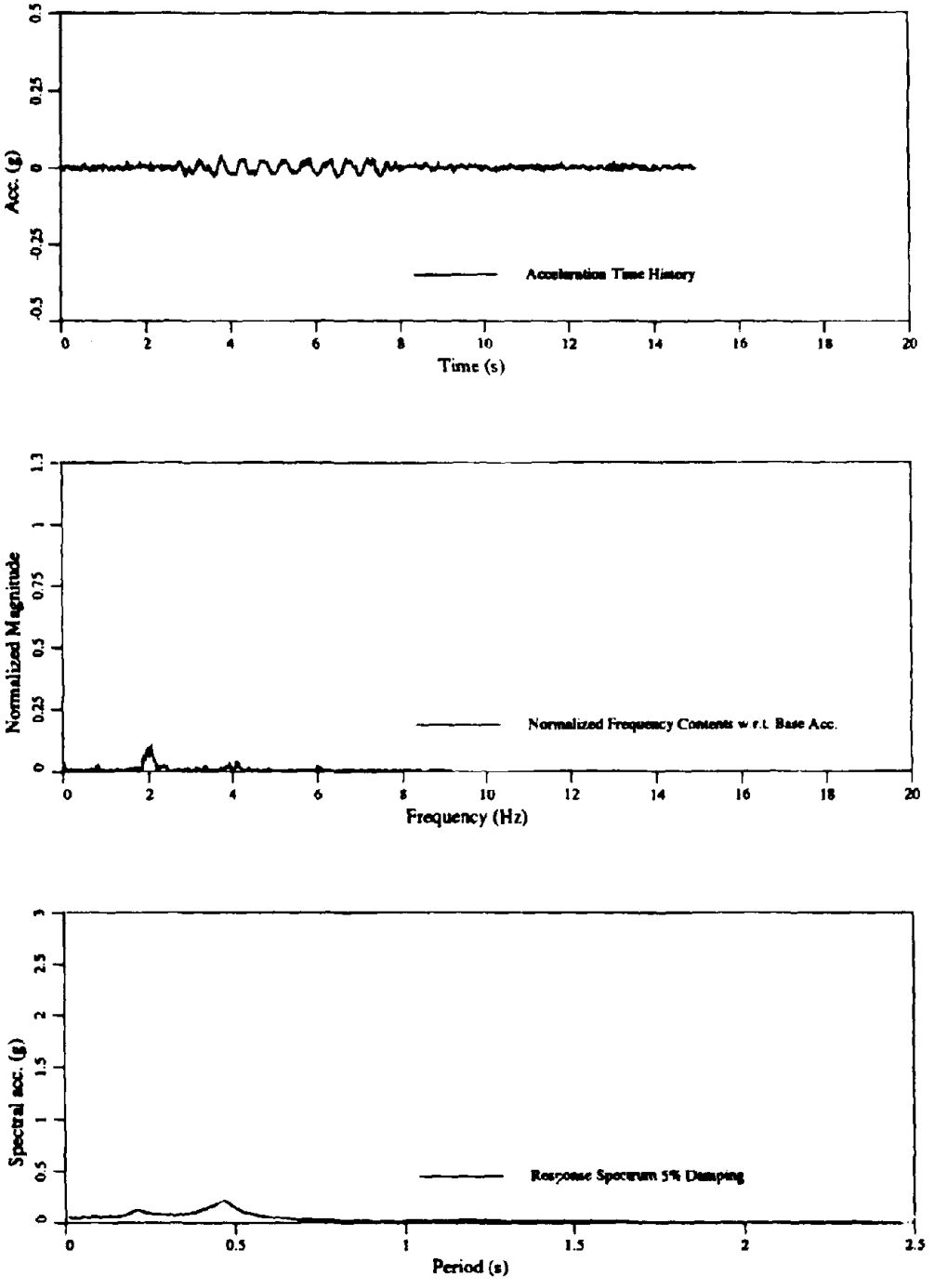

Figure C.13: Standard VELACS Model Test $75g/II$ Vertical Acceleration of the Base

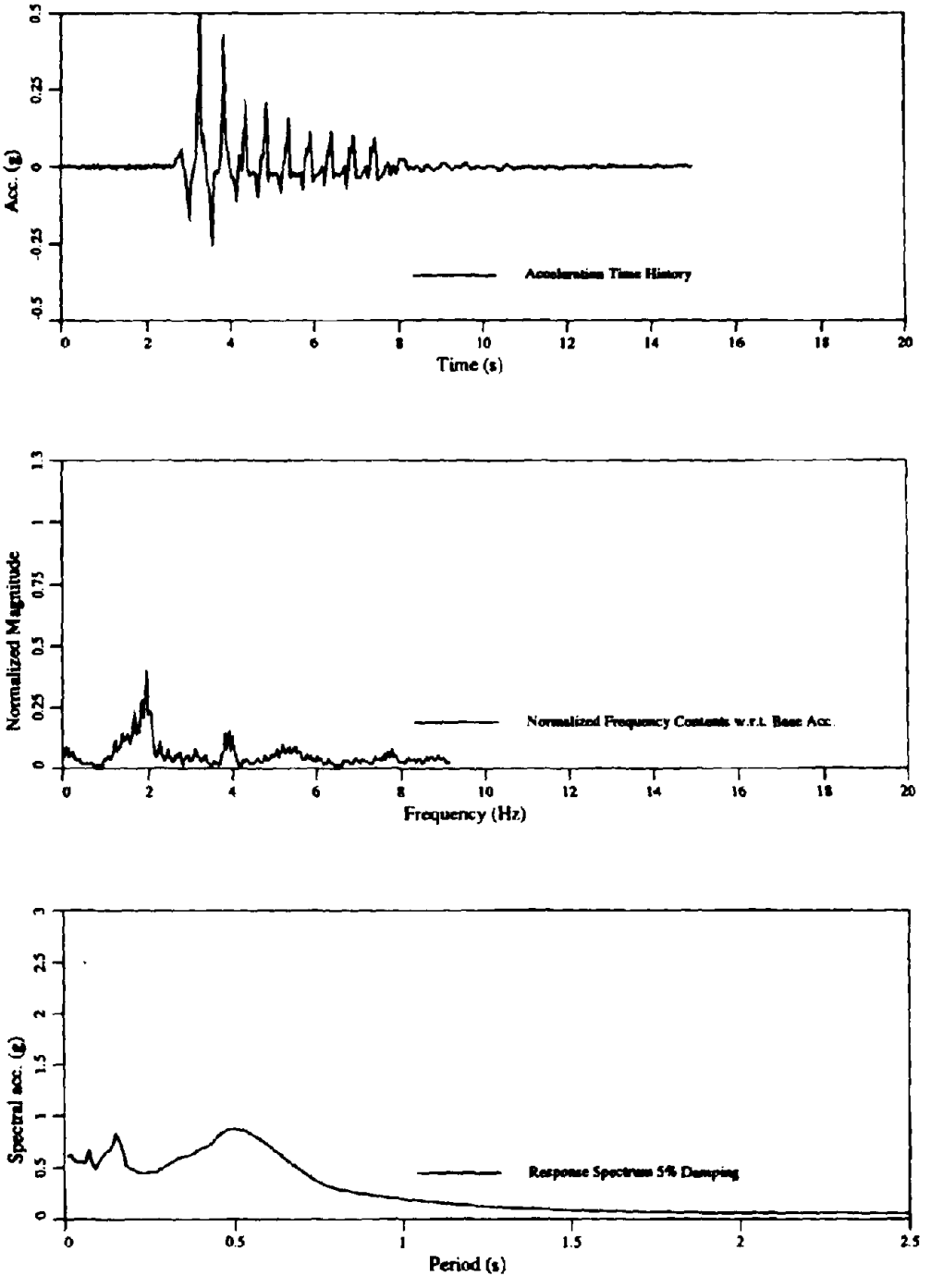

Figure C.14: Standard VELACS Model Test $75g/II$ Horizontal Acceleration in the Silt Layer

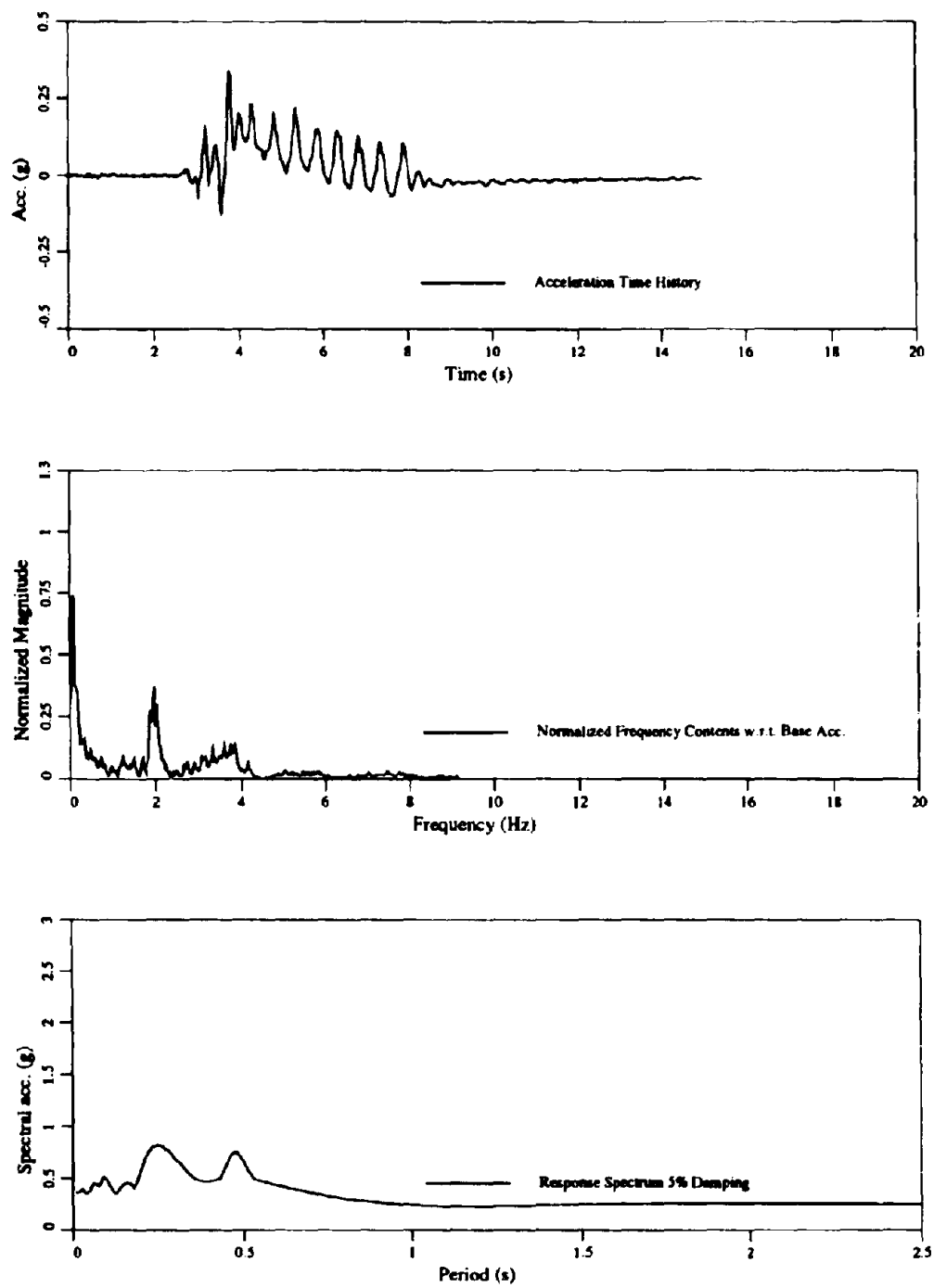

Figure C.15: Standard VELACS Model Test $75g/II$ Vertical Acceleration in the Silt Layer

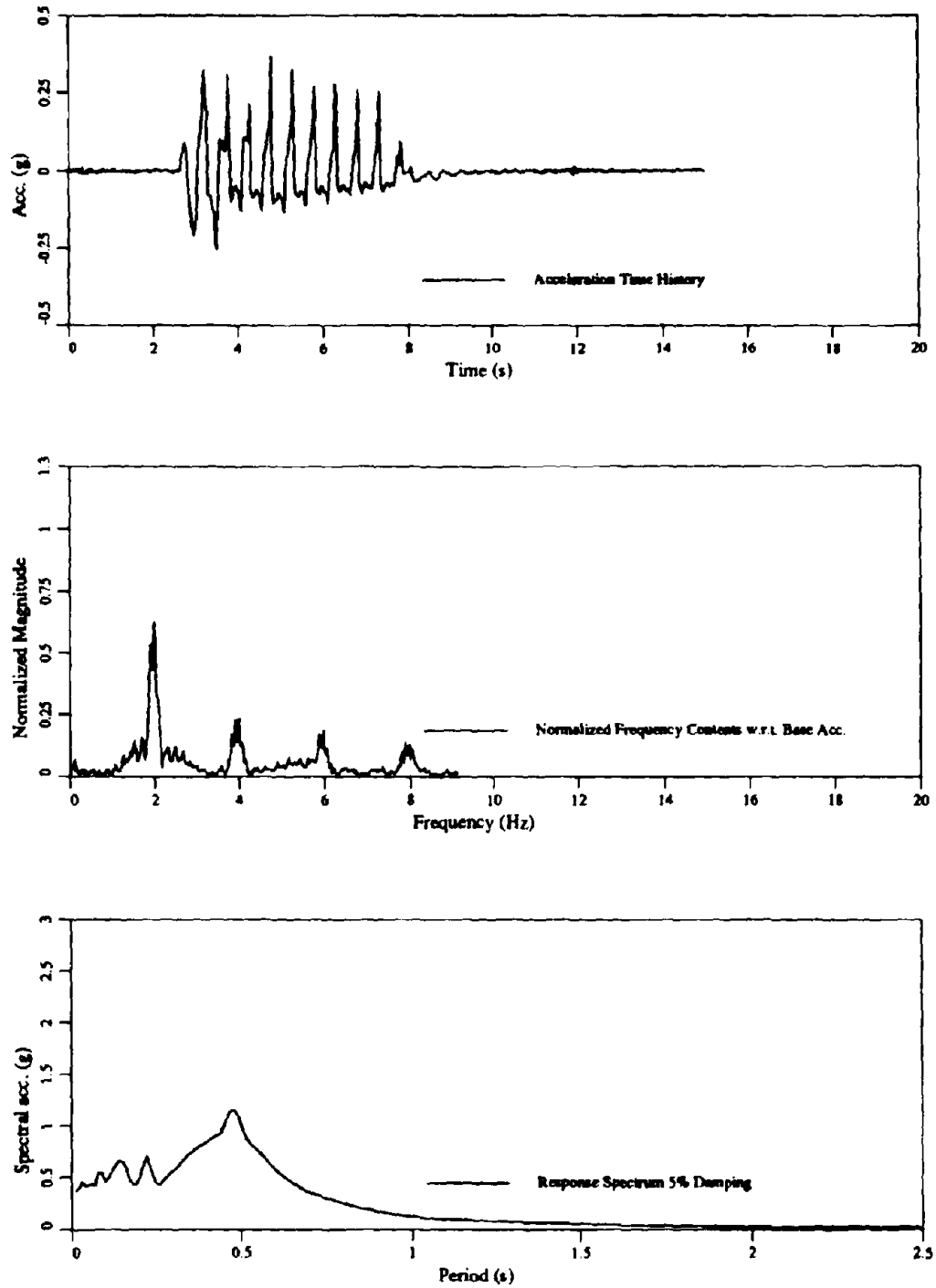

Figure C.16: Standard VELACS Model Test 75*g*/*11* Horizontal Acceleration on the Silt Surface

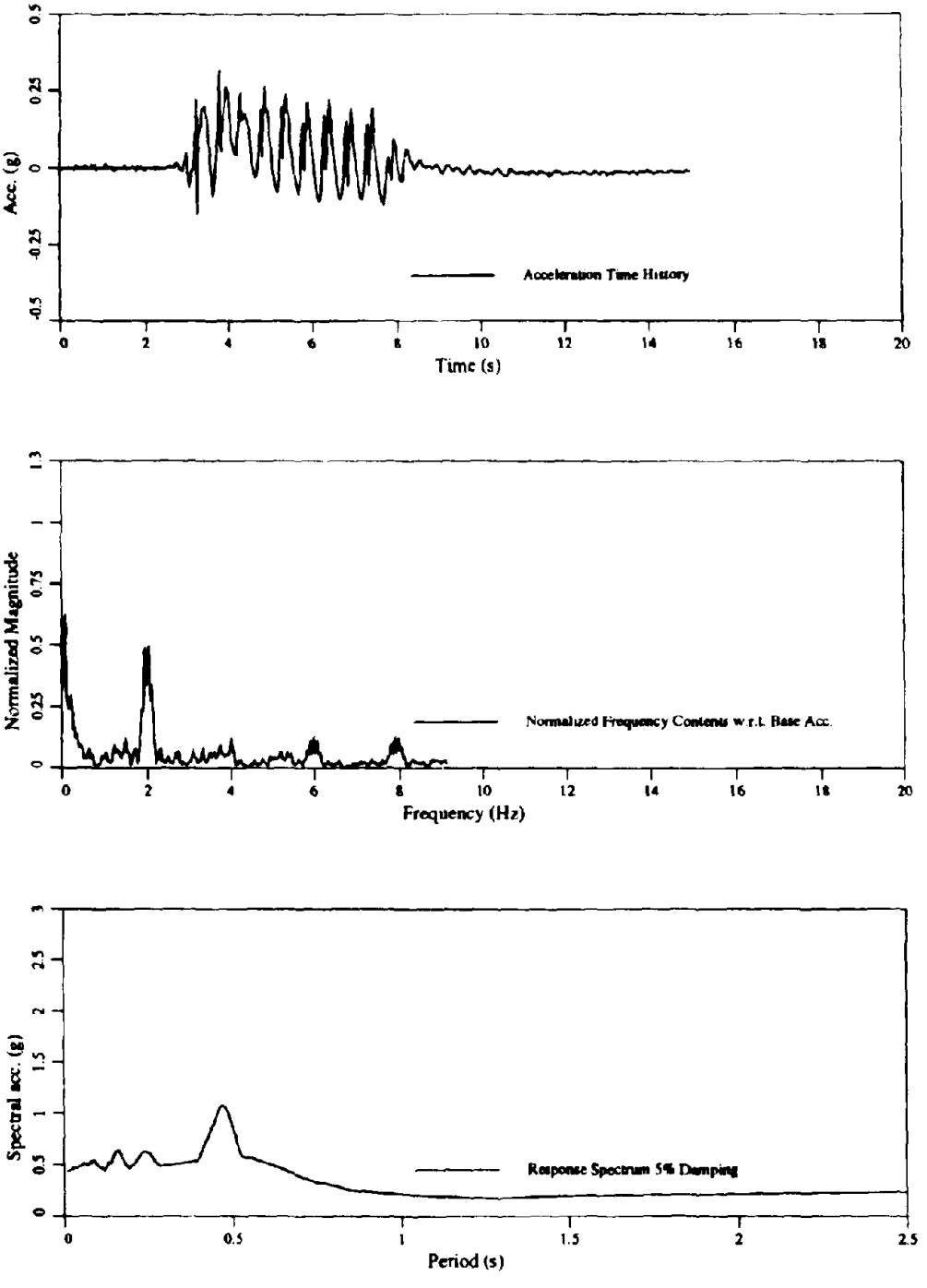

Figure C.17: Standard VELACS Model Test $75g/11$ Vertical Acceleration on the Silt Surface

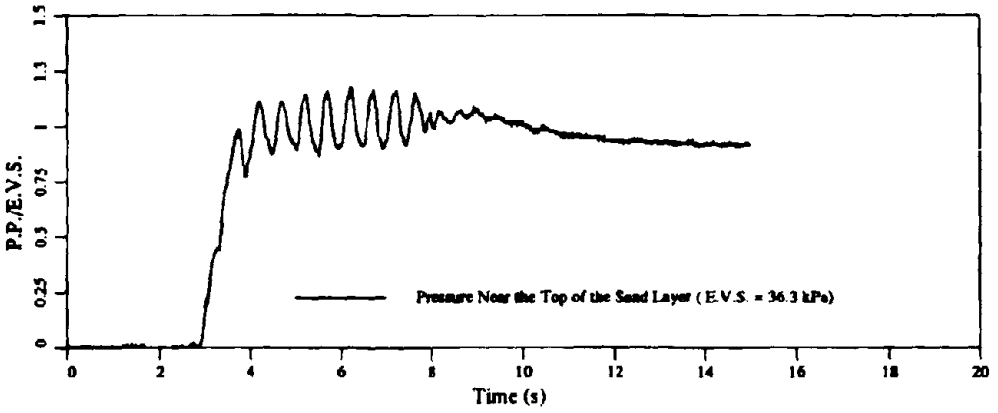

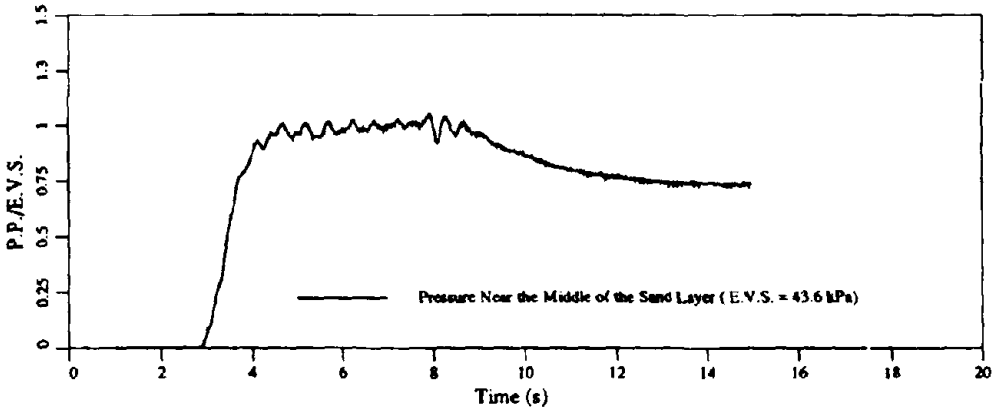

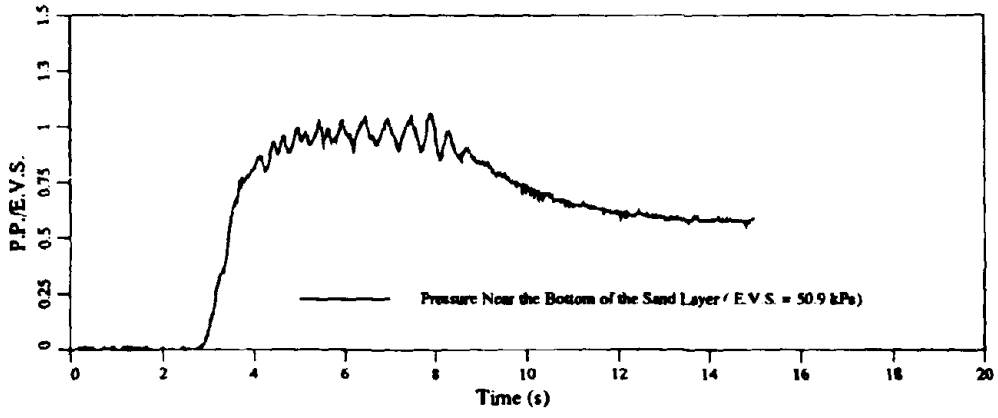

Figure C.18: Standard VELACS Model Test $75g/II$ Short Term Pore Pressure Ratio Time Histories

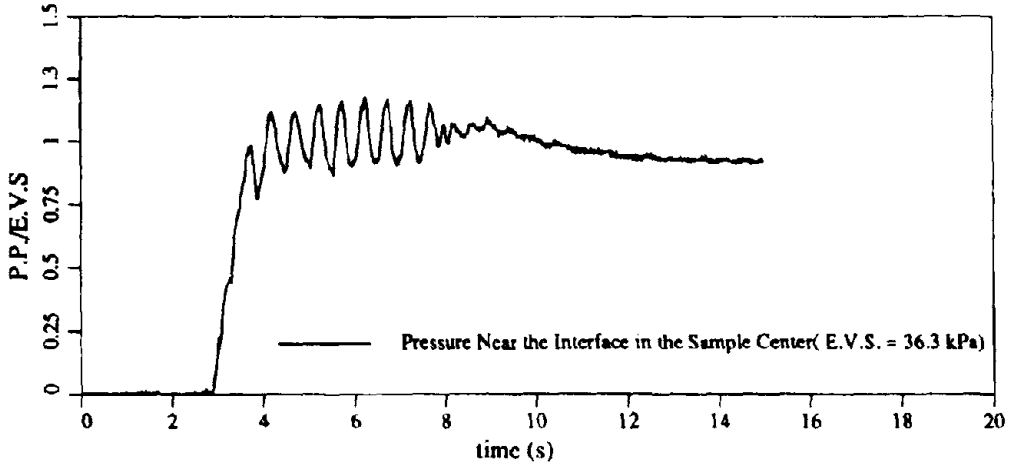

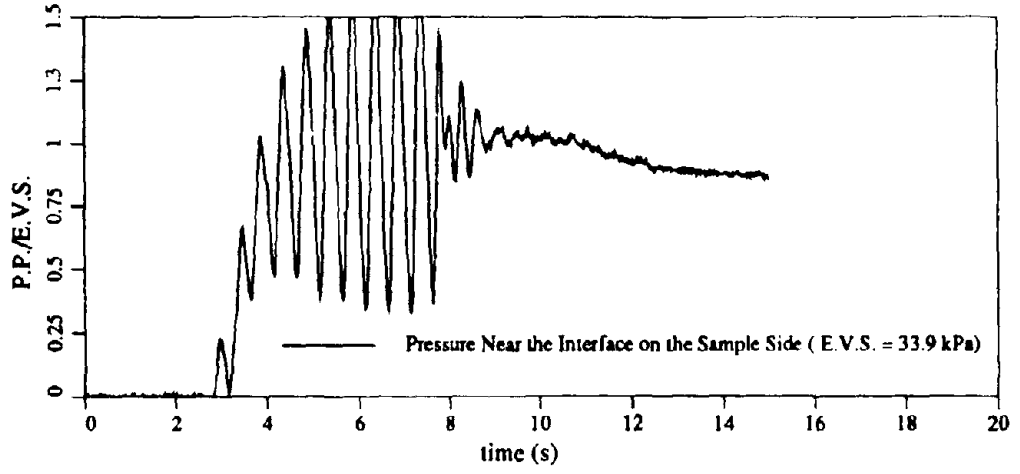

Figure C.19: **Standard VELACS Model Test $75g/II$ Short Term Pore Pressure Ratio Time Histories Comparison Between the Side and the Center of the Testing Box**

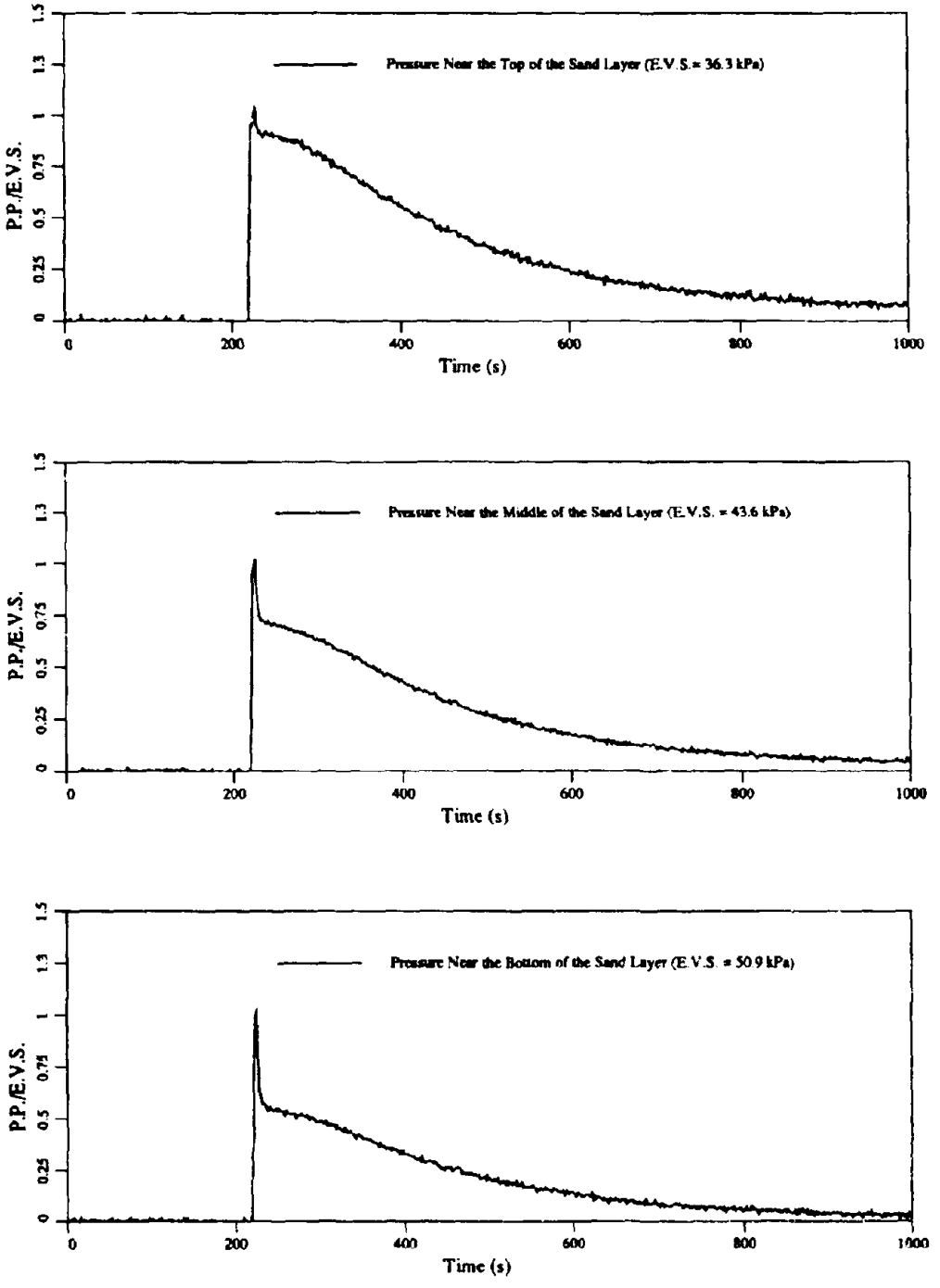

Figure C.20: Standard VELACS Model Test 75g/11 Long Term Pore Pressure Ratio Time Histories

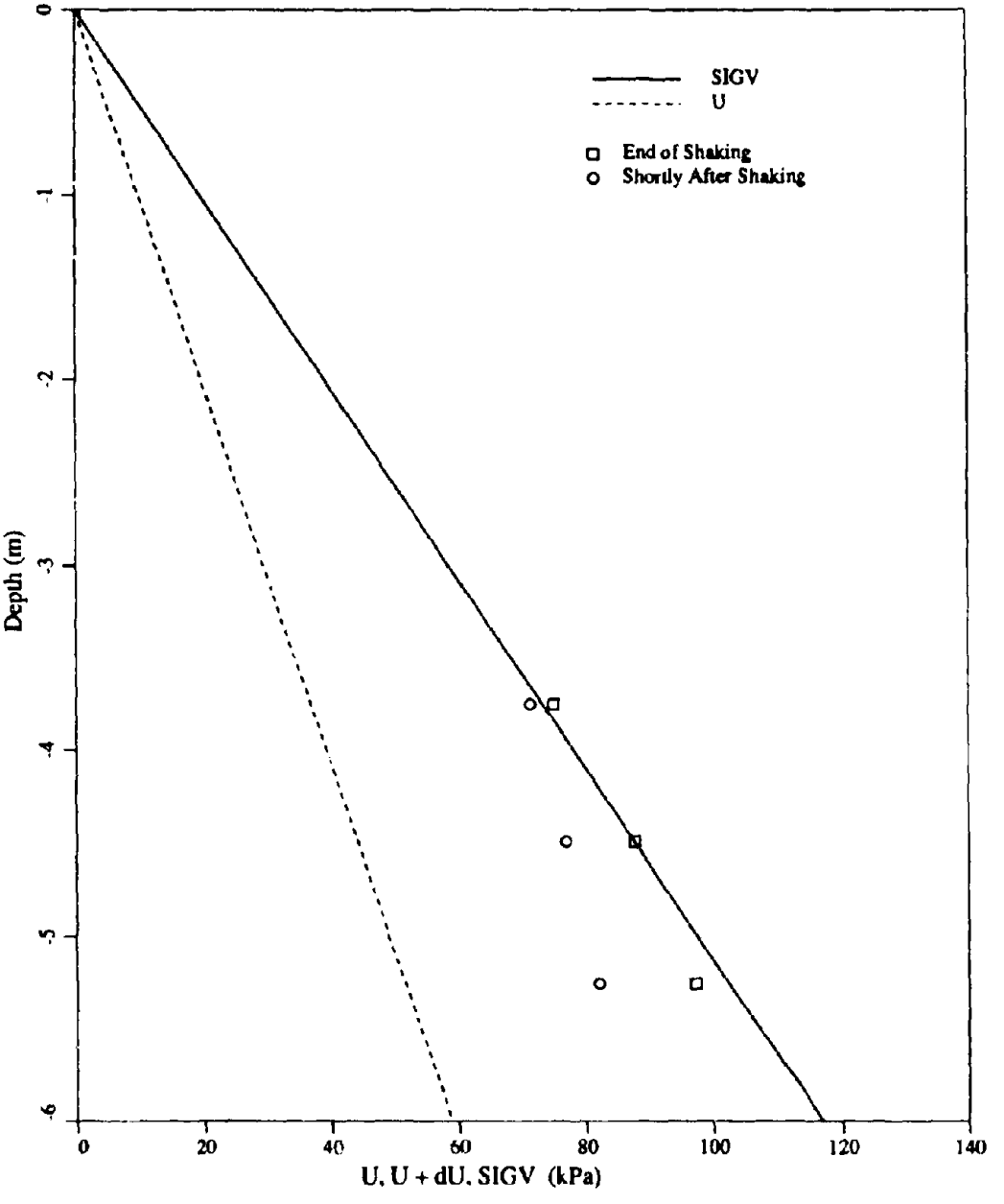

Figure C.21: Standard VELACS Model Test 75*g*/*11* Stress and Pore Pressure Variations With Depth

C.3 Test *75g Glycerin/I*

Test *75g Glycerin/I* was performed on December, 18. 1991 (Figure C.22). In an attempt to study effects of pore fluid viscosity on the pressure dissipation in the sand layer water was mixed with Glycerin in ratio 2 : 1. Ten channels were recorded directly on the Masscomp data acquisition system with a sampling rate of 7500 $[Hz]$. Eight channels were at the same time recorded on the tape recorder, due to the limited capacity of the tape recorder (eight channels), accelerometers A and C were recorded only on the Masscomp.

All pressure transducers were placed with porous stone facing a direction perpendicular to the shaking direction. PT# 4 was not operational during the test.

Input time histories were shown on Figure C.23. Horizontal and vertical acceleration time histories of the silt layer and the silt surface are presented in Figures C.24 and C.25. Pore fluid pressure ratios were shown in Figure C.26.

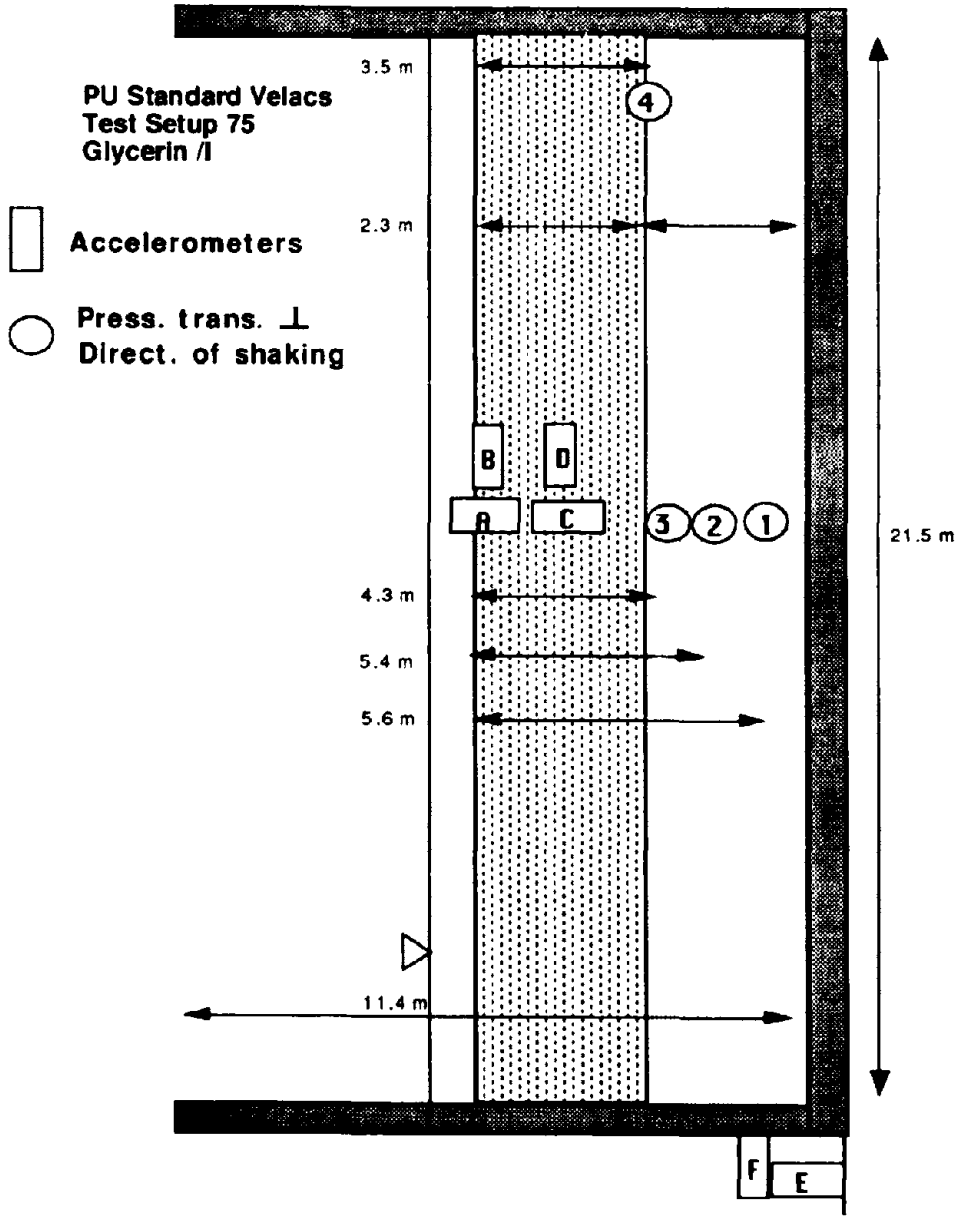

Figure C.22: **Standard Velacs Model Test** *75g Glycerin/I*

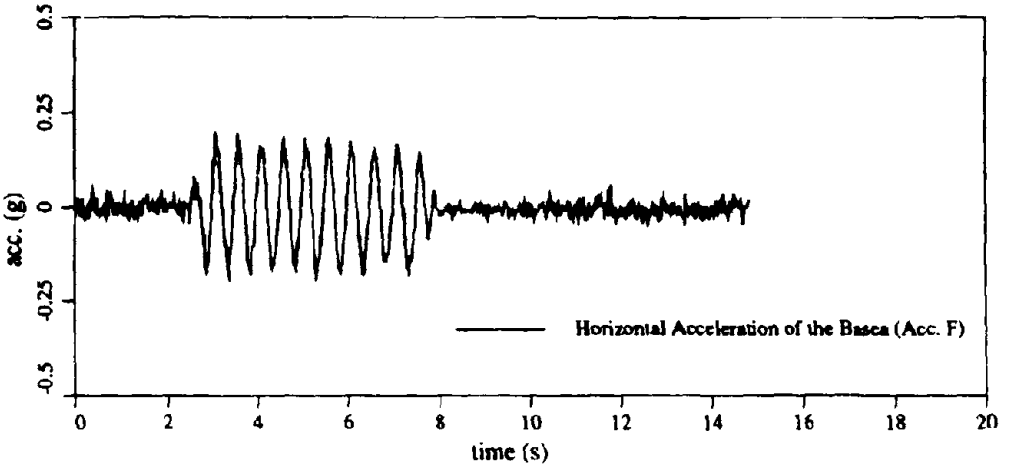

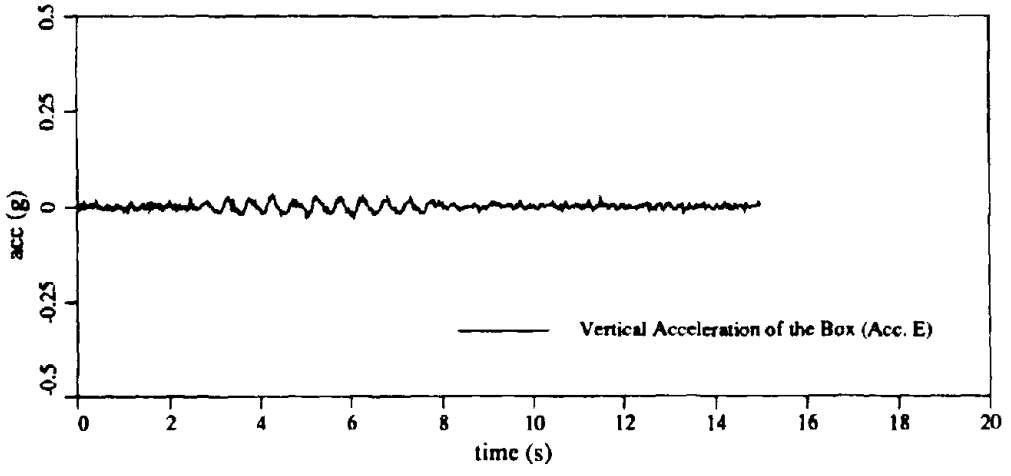

Figure C.23: Standard VELACS Model Test 75*g Glycerin/I* Input Acceleration Time Hystories

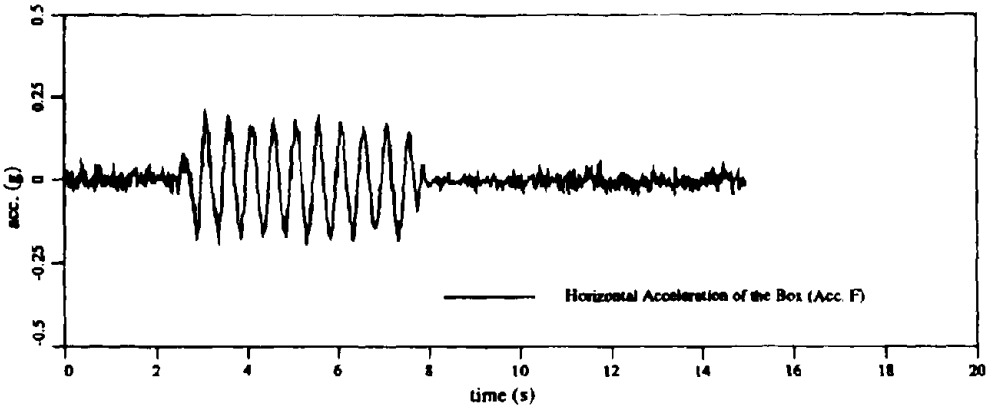

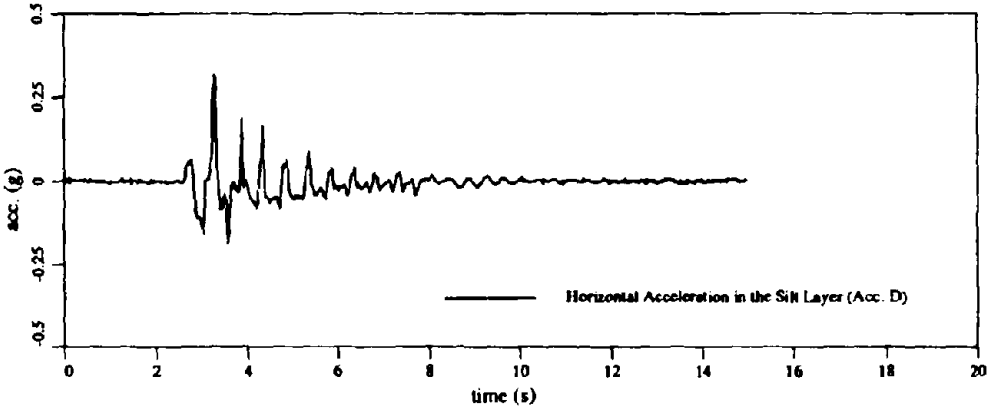

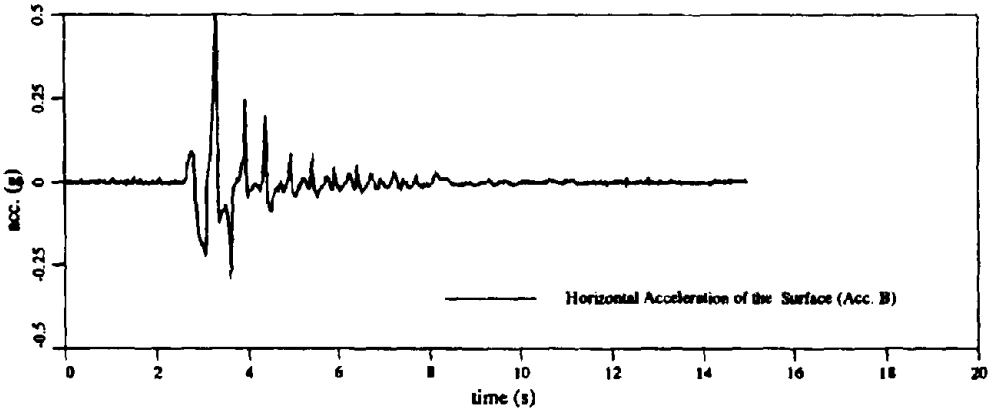

Figure C.24: Standard VELACS Model Test 75*g* *Glycerin/I* Horizontal Acceleration Time Histories

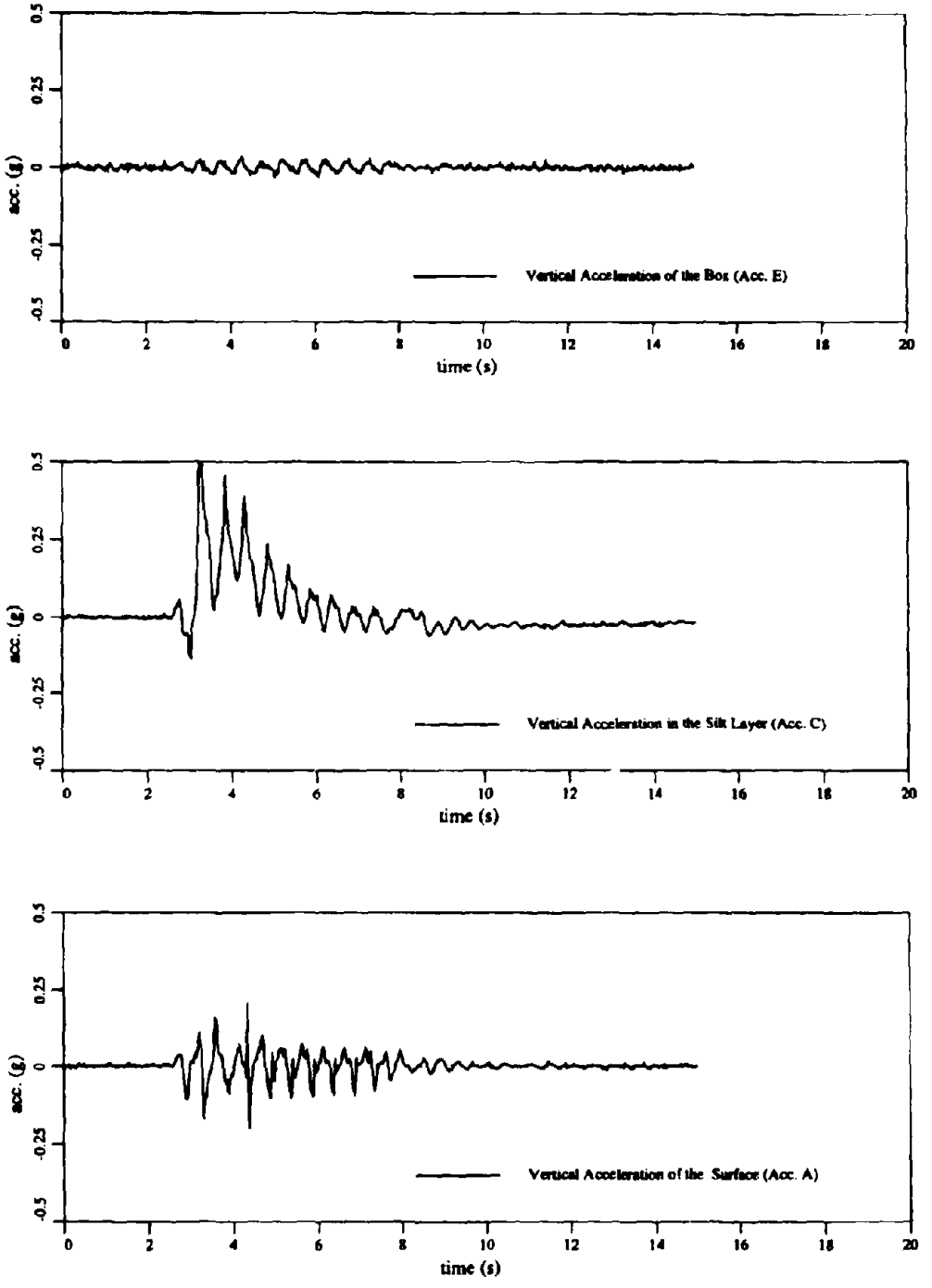

Figure C.25: Standard VELACS Model Test *75g Glycerin/I* Vertical Acceleration Time Histories

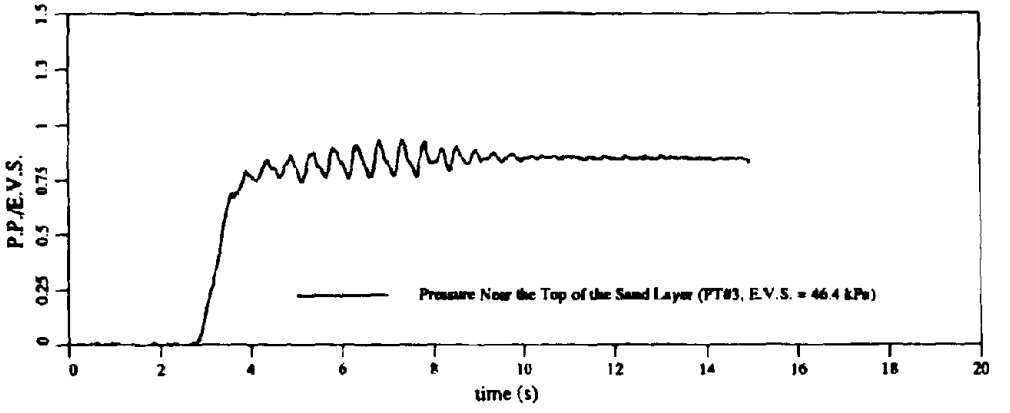

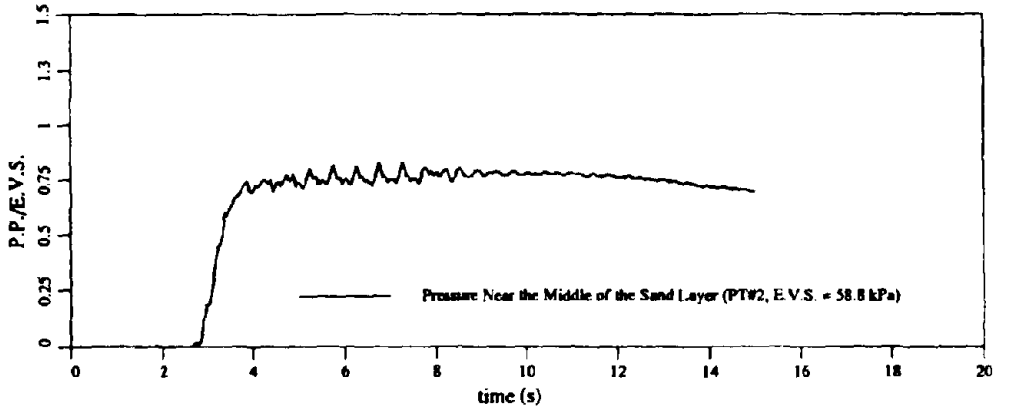

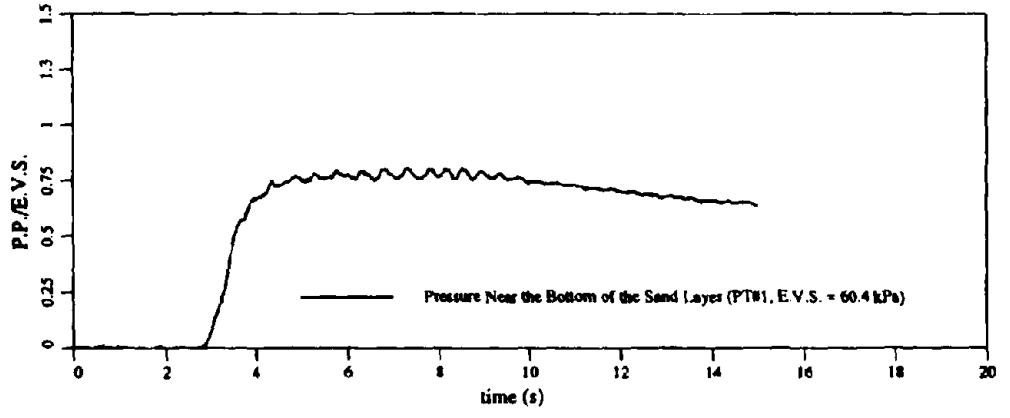

Figure C.26: Standard VELACS Model Test *75gGlycerin/I* Pore Fluid Pressure Ratio Time Histories

C.4 Tests With the Bonnie Silt (Bonnie/I & Bonnie/II)

Another two VELACS check tests were performed during the Spring 1992. It was decided to use Bonnie silt instead of Silica silt which, used in previous tests, proved to be very hard material to work with. The same sample preparation procedure was followed when preparing both samples with the Bonnie silt.

The samples were constructed in two layers. The lower layer consists of approximately 4.0 [cm] of Nevada sand, and the top one consists of 4.0 [cm] of Bonnie silt (both materials were provided by E.T.C.).

During the tests attention was mostly concentrated on the vertical displacements of the silt surface, so only few measurements were taken inside the samples.

Two pressure transducers were placed in the sand layer and one accelerometer in the silt layer (Figures C.27 and C.33). Both samples were allowed to sit 24 hours before they were placed in the centrifuge, and left in flight at 75g for approximately 10 minutes. After the centrifuge was stopped some more silt was added, and the LVDT core support plate and aluminum foil were placed on the samples' surfaces.

The centrifuge was brought up to 75g and readings of both displacement transducers were taken in intervals of 5 minutes. Both tests were performed after the two consecutive readings showed no differential settlements of the silt surface within the instruments' precision. Consolidation period for test Bonnie/I was 15 minutes, and for test Bonnie/II 20 minutes. The sample of the test Bonnie/II was visually checked one more time after the consolidation, and before the shaking, and no LVDT core support sinking was observed.

In spite of the fact that only few measurements inside the samples were taken, results of both tests follow a general trend established by previously performed tests.

In both cases the sand layer was fully liquefied close to the material interface with the silt, which caused significant damping of the silt layer acceleration magnitudes (Figures C.28 to C.36).

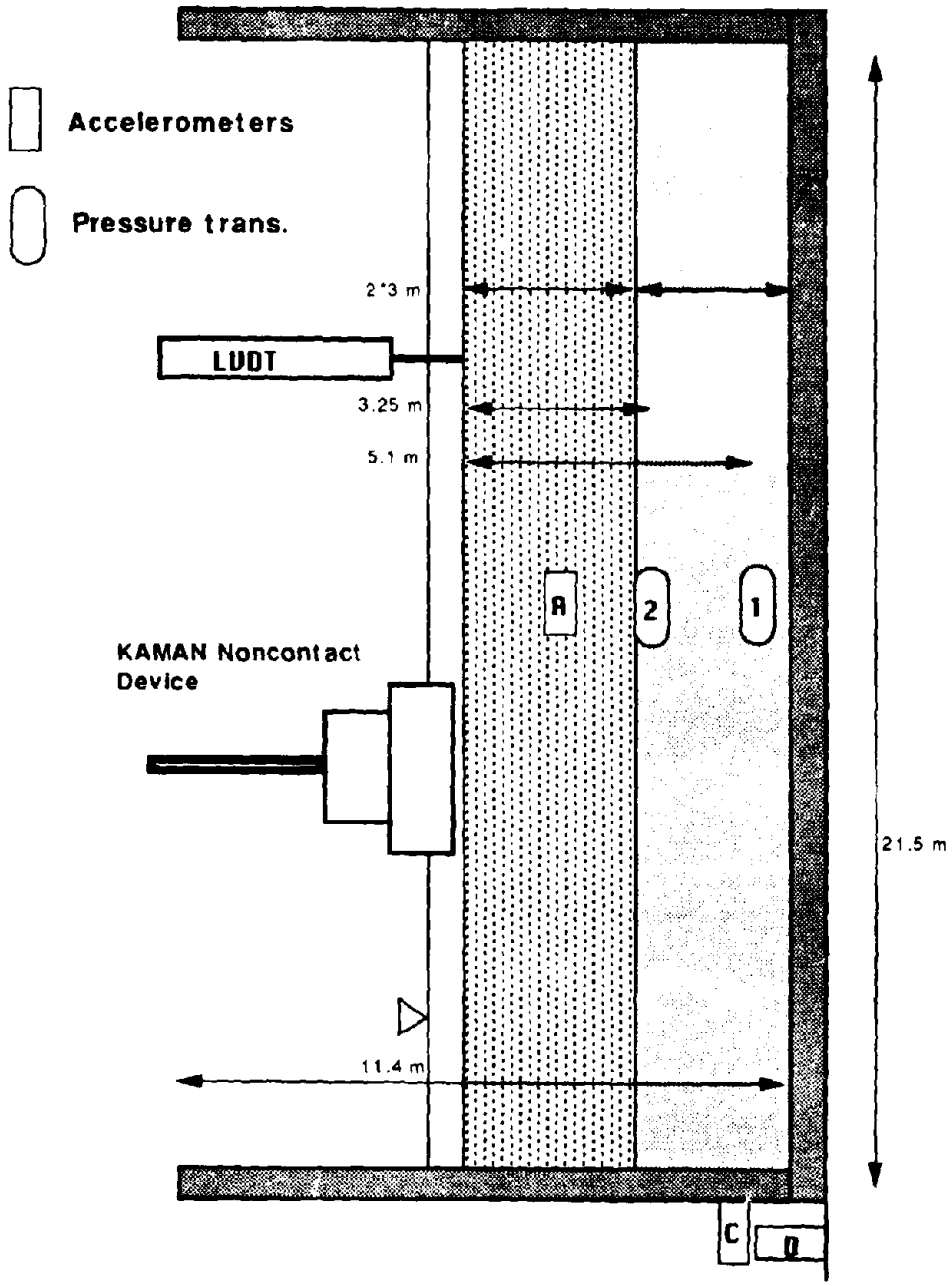

Figure C.27: **Standard Velacs Model Test 75*g* Bonnie/I**

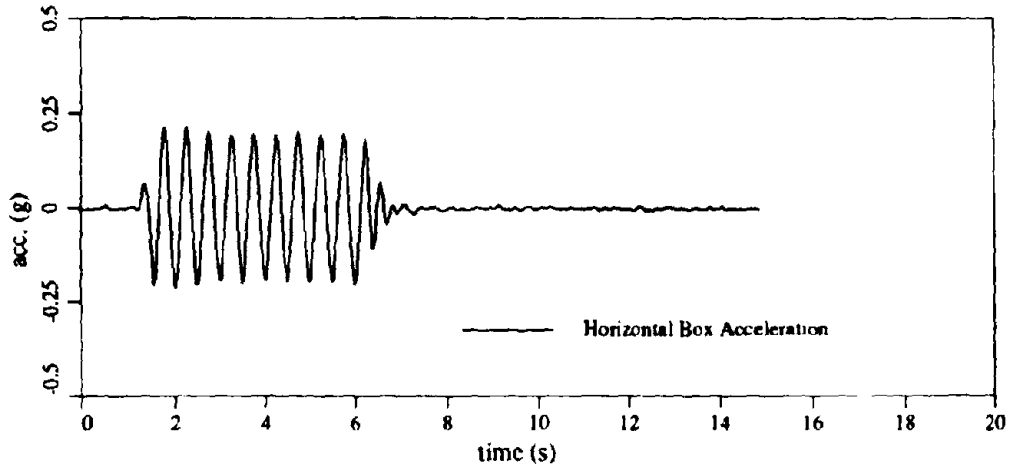

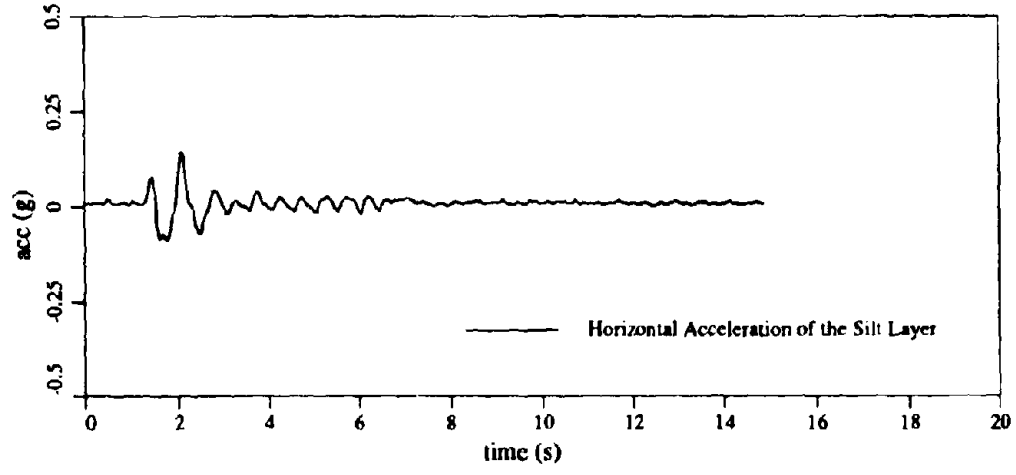

Figure C.28: Standard VELACS Model Test 75g *Bonnie/1* Horizontal Acceleration Time Histories

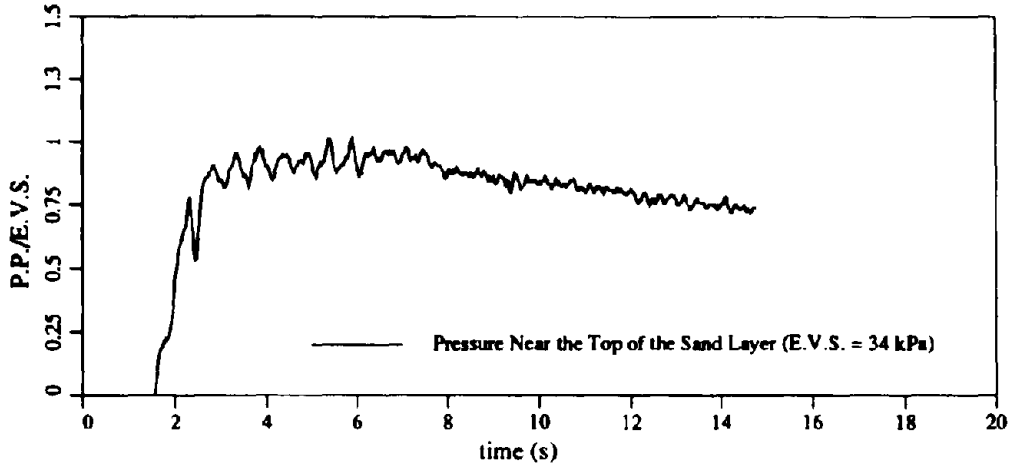

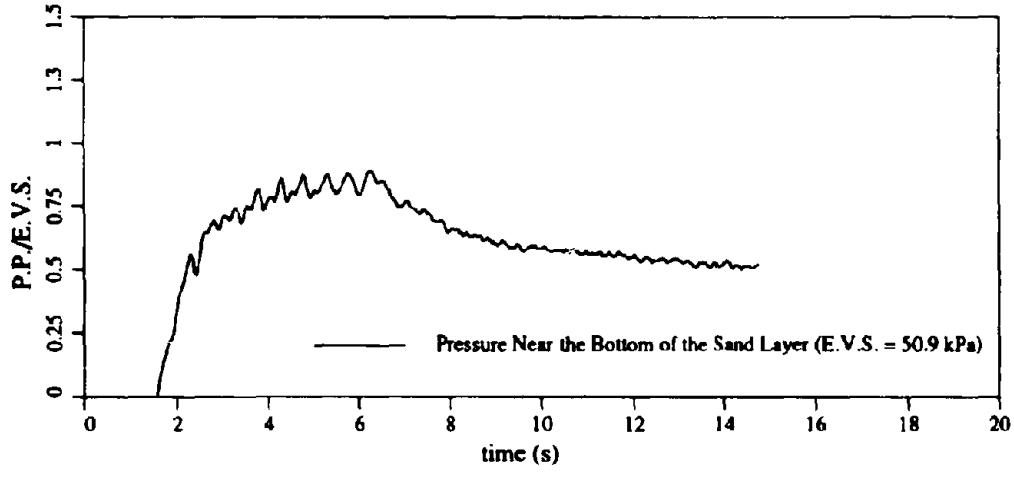

Figure C.29: Standard VELACS Model Test 75*g* *Bonnie/1* Short Term Pore Water Pressure Time Histories

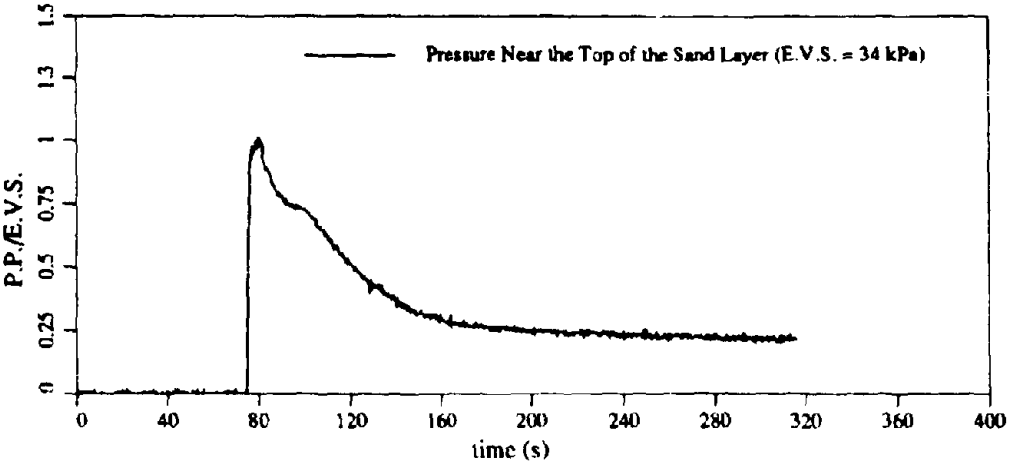

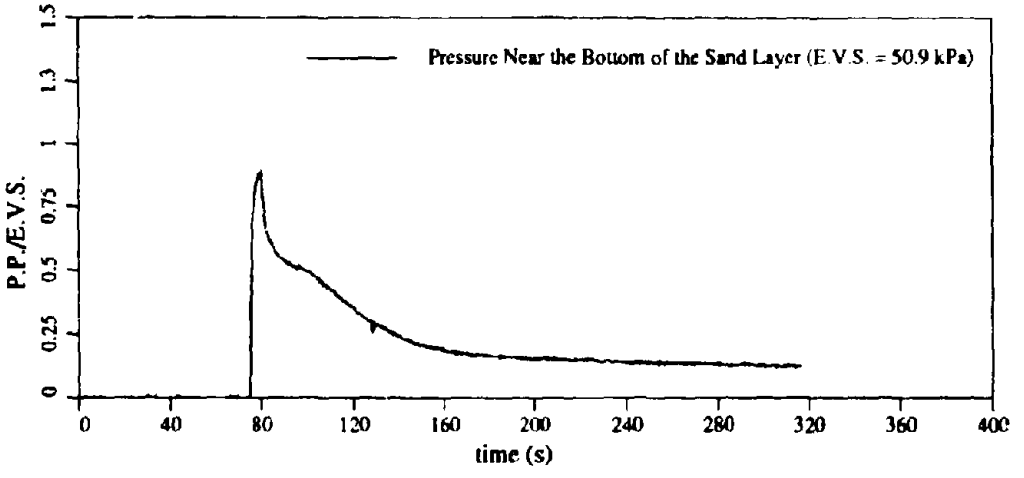

Figure C.30: Standard VELACS Model Test 75*g* *Bonnie/1* Long Term Pore Water Pressure Time Histories

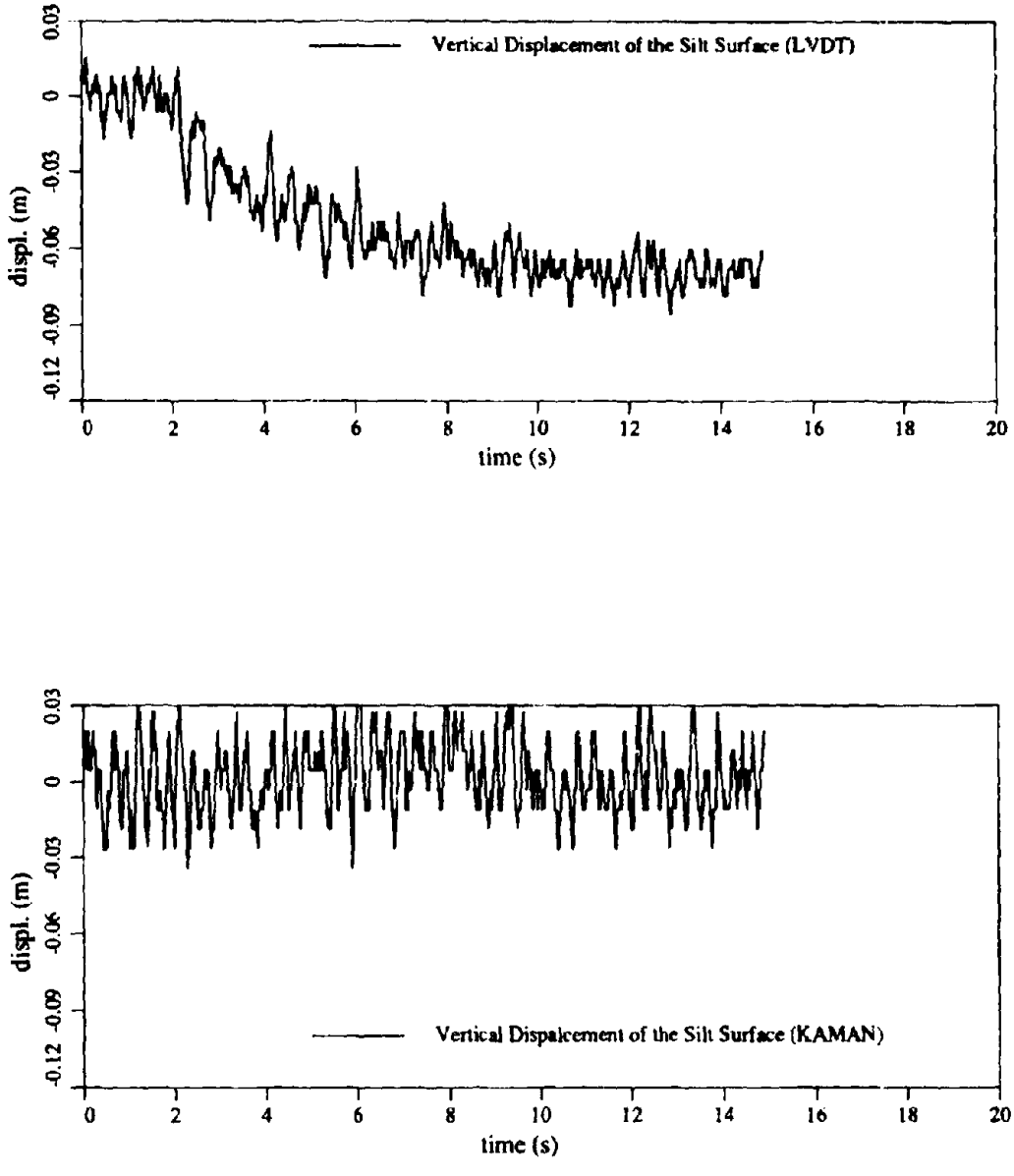

Figure C.31: Standard VELACS Model Test 75*g* *Bonnie/1* Short Term Vertical Displacement Time Histories

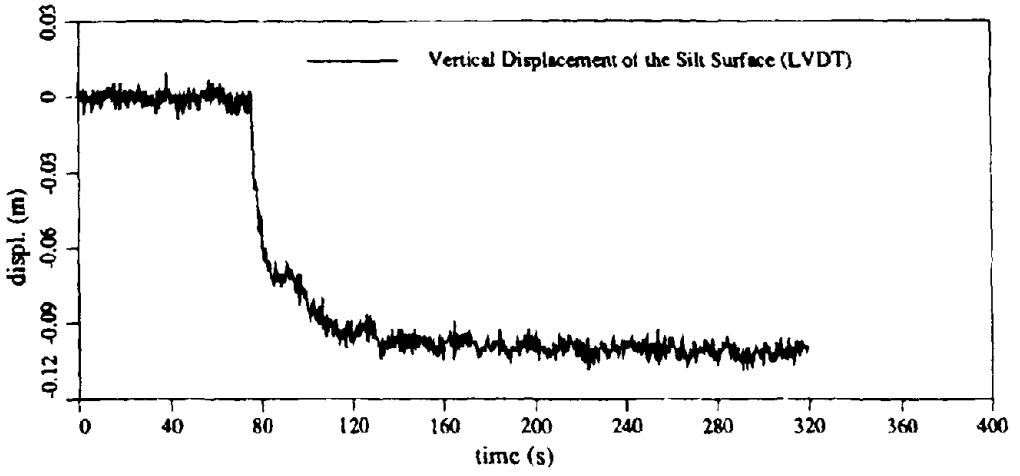

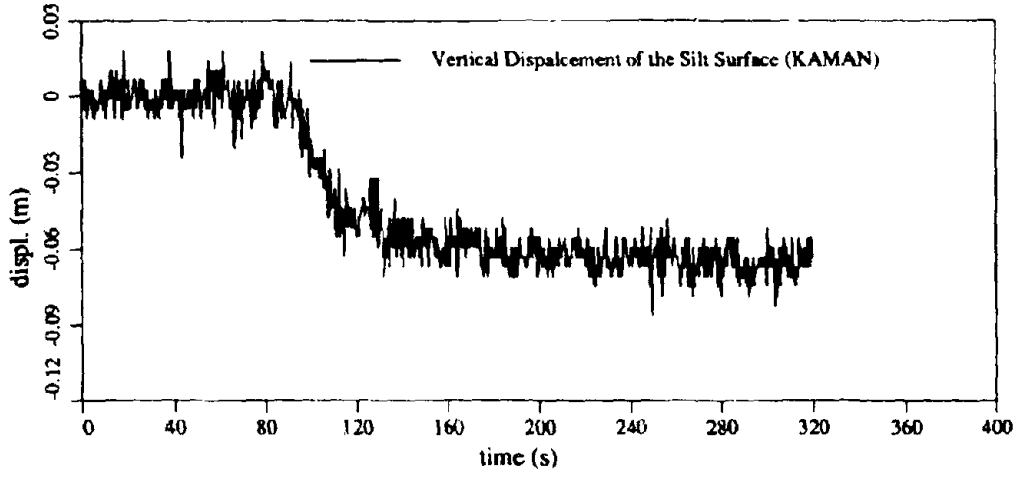

Figure C.32: **Standard VELACS Model Test** *75g Bonnie/1* **Long Term Vertical Displacement Time Histories**

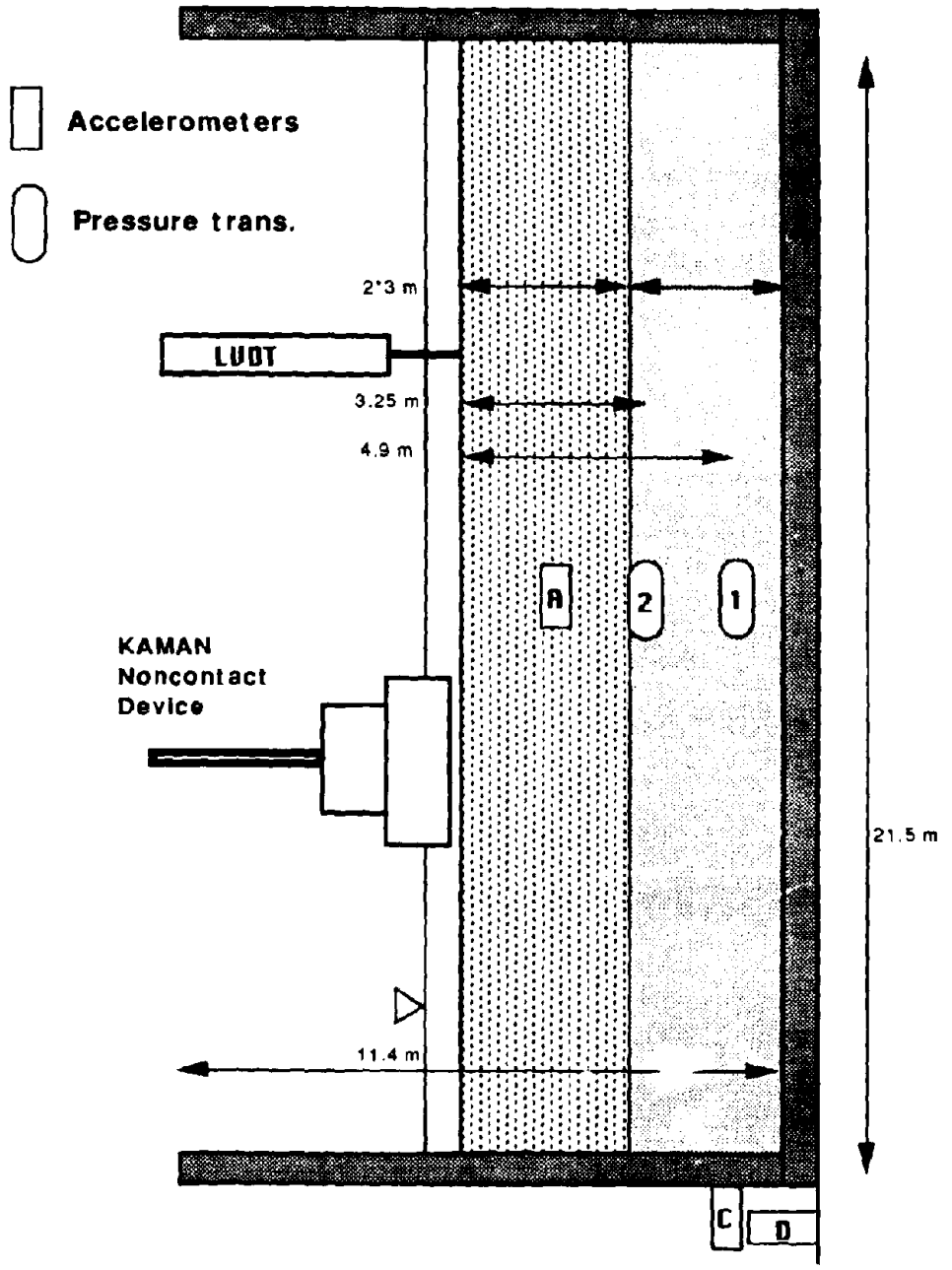

Figure C.33: **Standard Velacs Model Test 75g Bonnie/II**

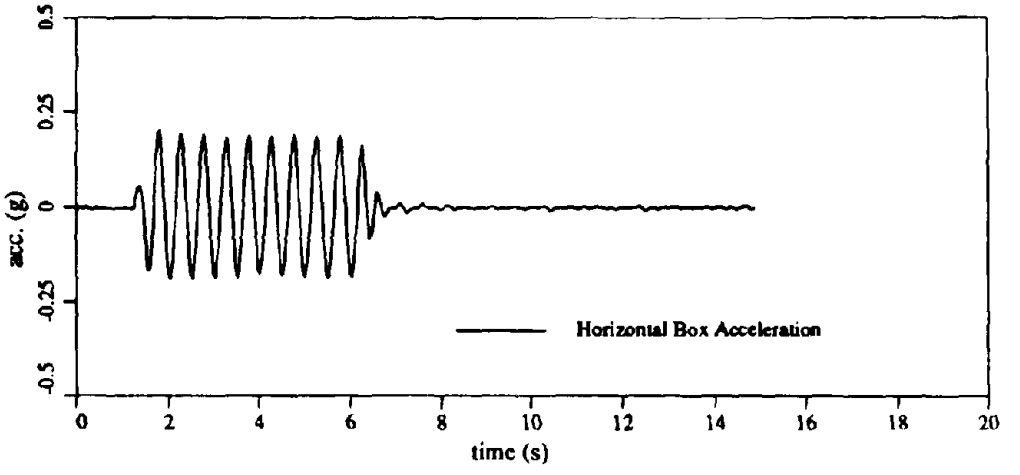

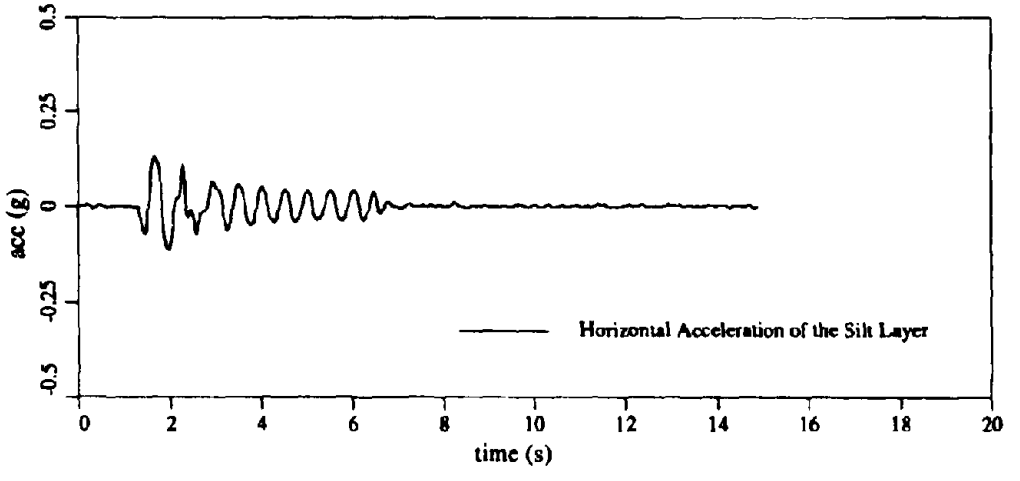

Figure C.34: Standard VELACS Model Test *75g Bonnie/II* Horizontal Acceleration Time Histories

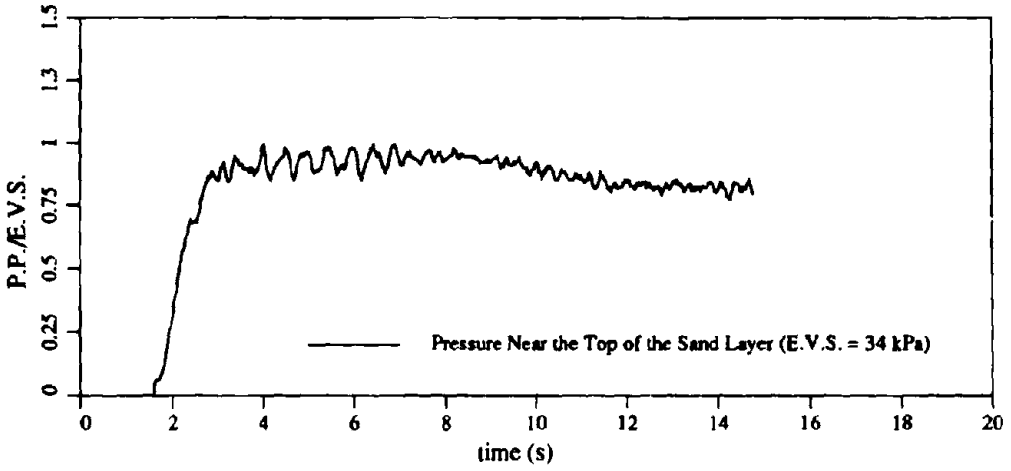

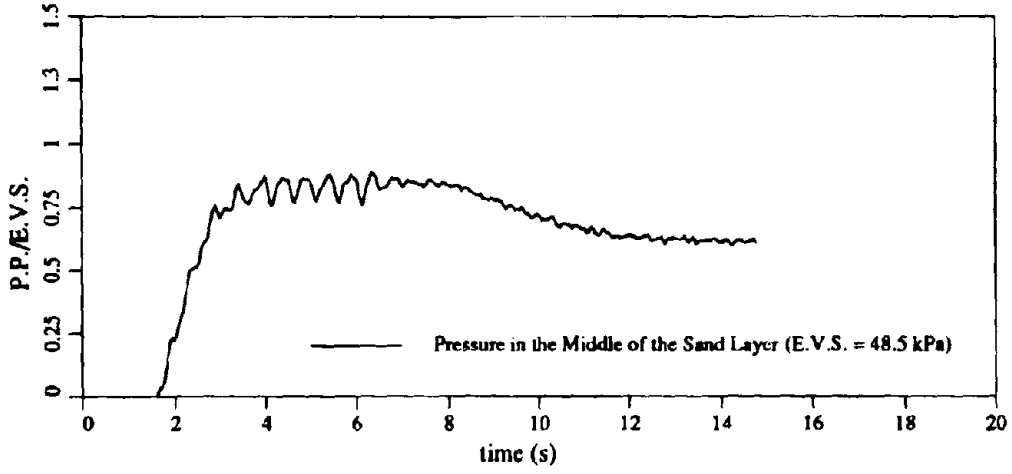

Figure C.35: Standard VELACS Model Test 75*g Bonnie/II* Short Term Pore Water Pressure Time Histories

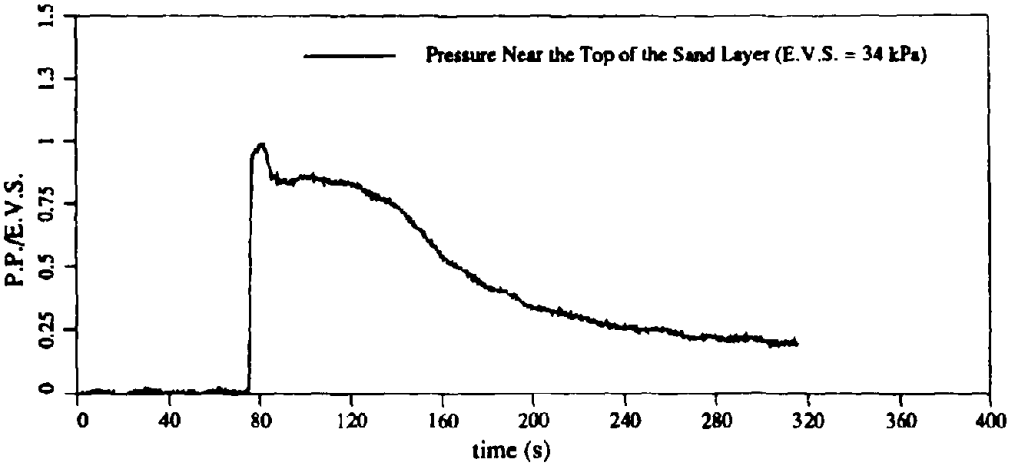

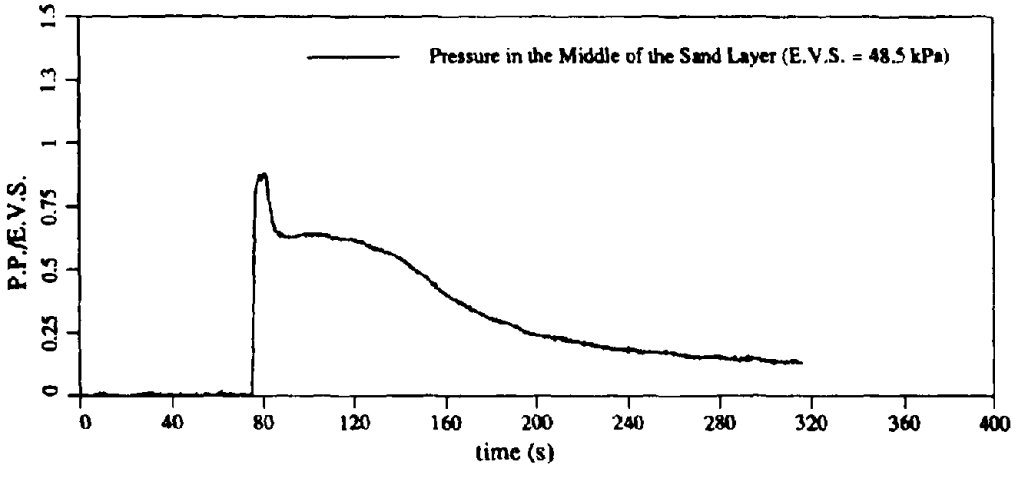

Figure C.36: Standard VELACS Model Test 75*g Bonnie/II* Long Term Pore Water Pressure Time Histories

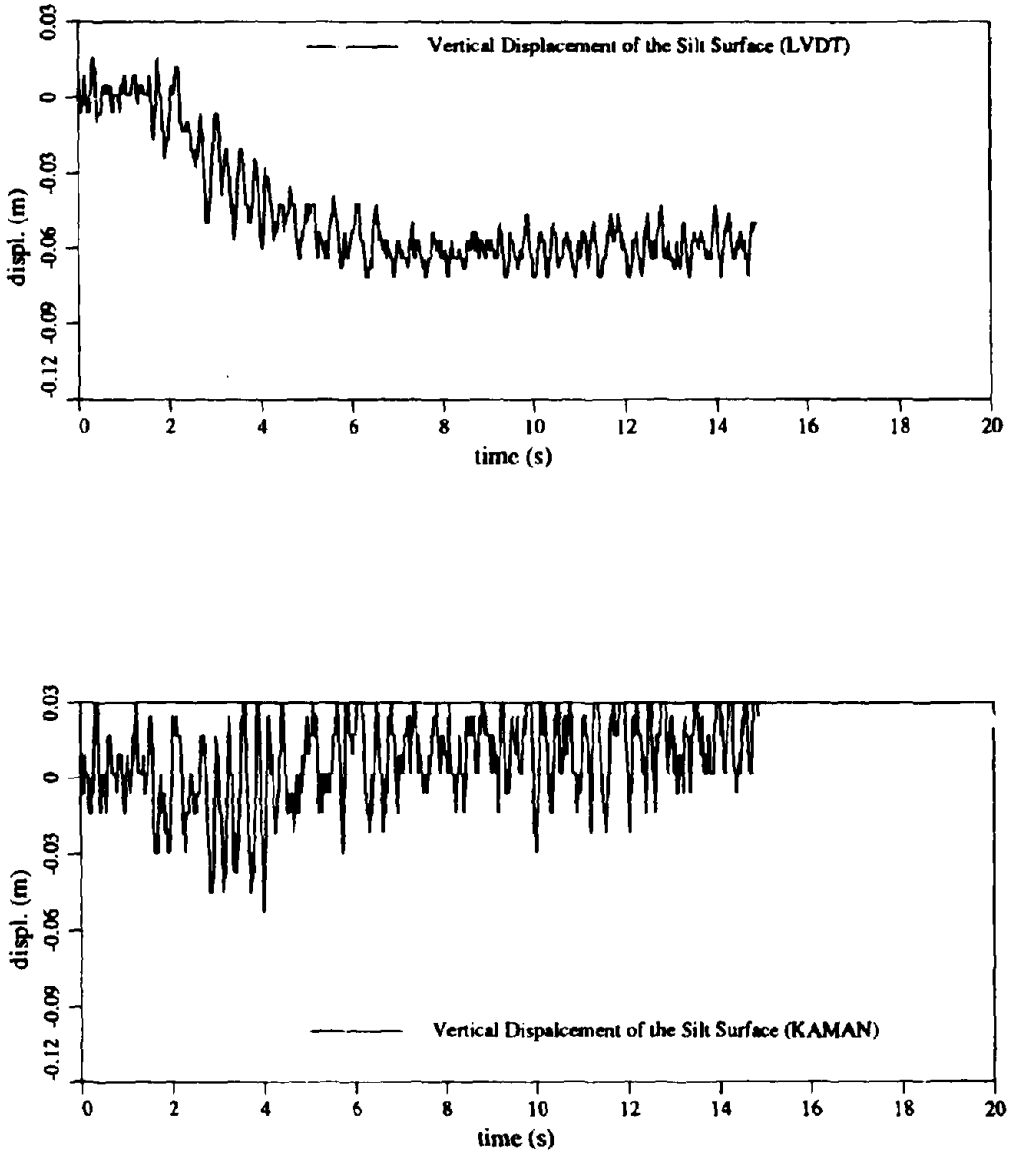

Figure C.37: Standard VELACS Model Test *75g Bonnie/II* Short Term Vertical Displacement Time Histories

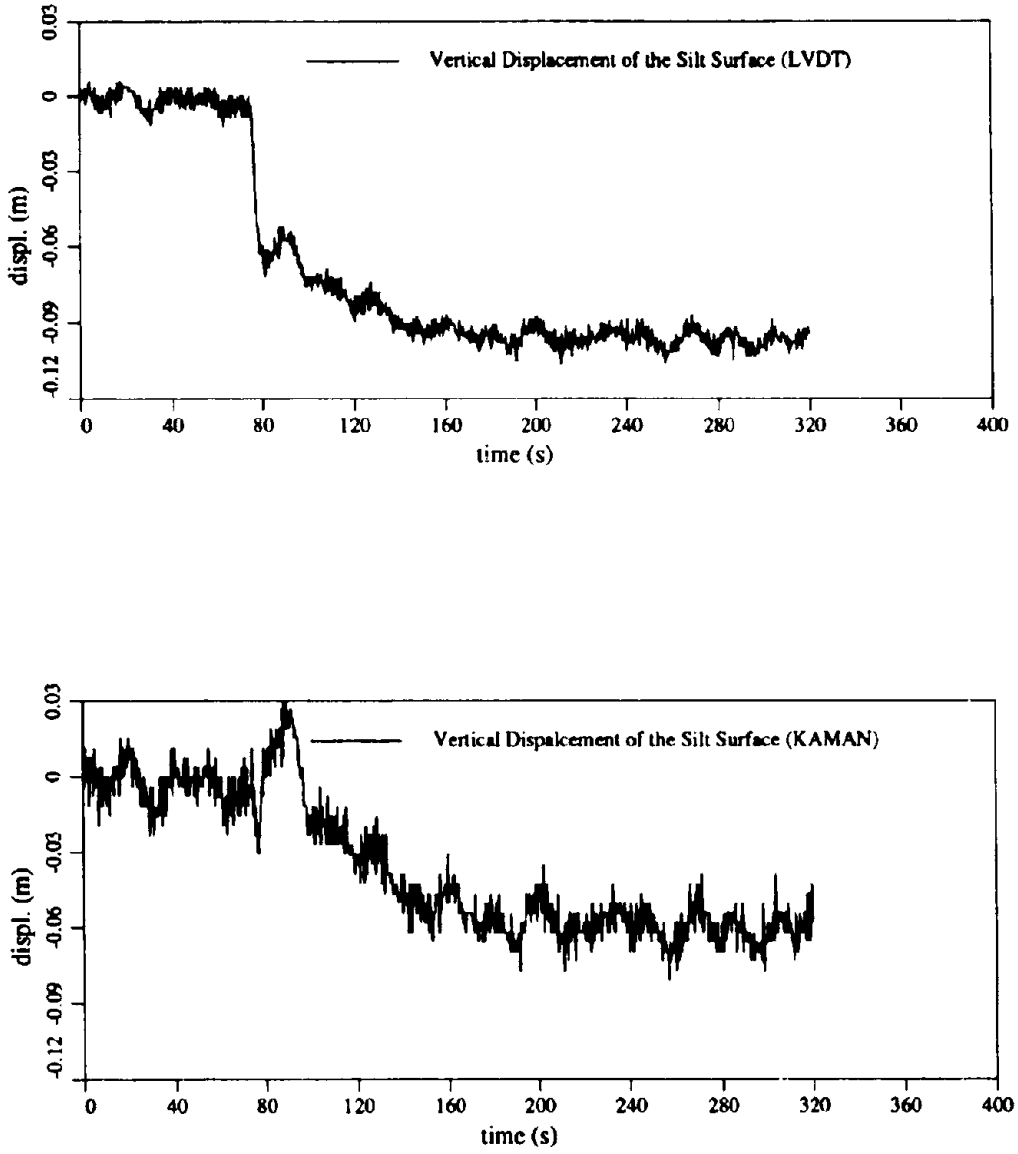

Figure C.38: Standard VELACS Model Test 75*g Bonnie/II* Long Term Vertical Displacement Time Histories

Appendix D

Soil-Structure Interaction Tests

D.1 Test # 1

Test # 1 was performed on April, 9, 1992. Sample box had been redesigned to prevent large deformations of the lexan plate due to the high pressure induced during the test and the vacuum during the sample preparation process. An aluminum bar was placed on the lexan plate to increase the stiffness in the direction of the deformations noticed during the 0^{th} test.

Ten channels were recorded directly on the Masscomp data acquisition system with a sampling rate of 10000 $[Hz]$. Nine channels were at the same time recorded on the tape recorder; accelerometer B (vertical acceleration of the model box) was recorded only on the Masscomp.

The same procedure as the one described for 0^{th} test was followed during the preparation of Test # 1. The aluminum bar performed well, a vacuum introduced during the sand saturation did not deform the lexan plate, and the sample was undisturbed.

It was very difficult to place the structure at the desired level, in this test the structure was put 1.5 [m] below the sand surface.

Two plastic rulers were attached to the structure model for easier monitoring of

the vertical displacements. An optical instrument used for centrifuge balancing was applied as a measuring device for vertical displacement. Initial readings were taken after the sample was placed in the centrifuge bucket.

During the 0^{th} test, the structure leaned on the transducer for measuring horizontal displacements. In this test the goal was to let the structure deform entirely, so displacement transducers were not placed on the structure.

The sample was left in flight at $100g$ for approximately ten minutes before it was stopped and the structure was checked for vertical displacement and standing. Vertical settlement measured following the centrifuge consolidation was $0.2\,[m]$ (prototype), and was equally distributed, in other words, the structure standing was not disturbed.

The centrifuge was spun up again, and ten cycles of sine-like motion with an amplitude of $0.3\,g$ was presented to the soil sample. The vertical displacement was measured after the centrifuge was stopped. The structure had collapsed again, but this time it tipped in the direction of shaking (Figure 5.1). Vertical displacements were $0.2\,[m]$ on the right side and $0.5\,[m]$ on the left side (prototype) with no visible inclination in the direction perpendicular to the shaking direction.

A large vertical displacement of the structure can relocate pore pressure transducers placed under the structure. In order to determine the transducers' positions initial readings were taken after the settlement and prior to the earthquake-like event. Reported are transducers' locations obtained from the initial (static) readings.

During the test, contact on the Masscomp data acquisition cable was lost, so all acceleration time histories, except vertical acceleration of the left structure corner (the side that collapsed), were recovered from the tape recorder.

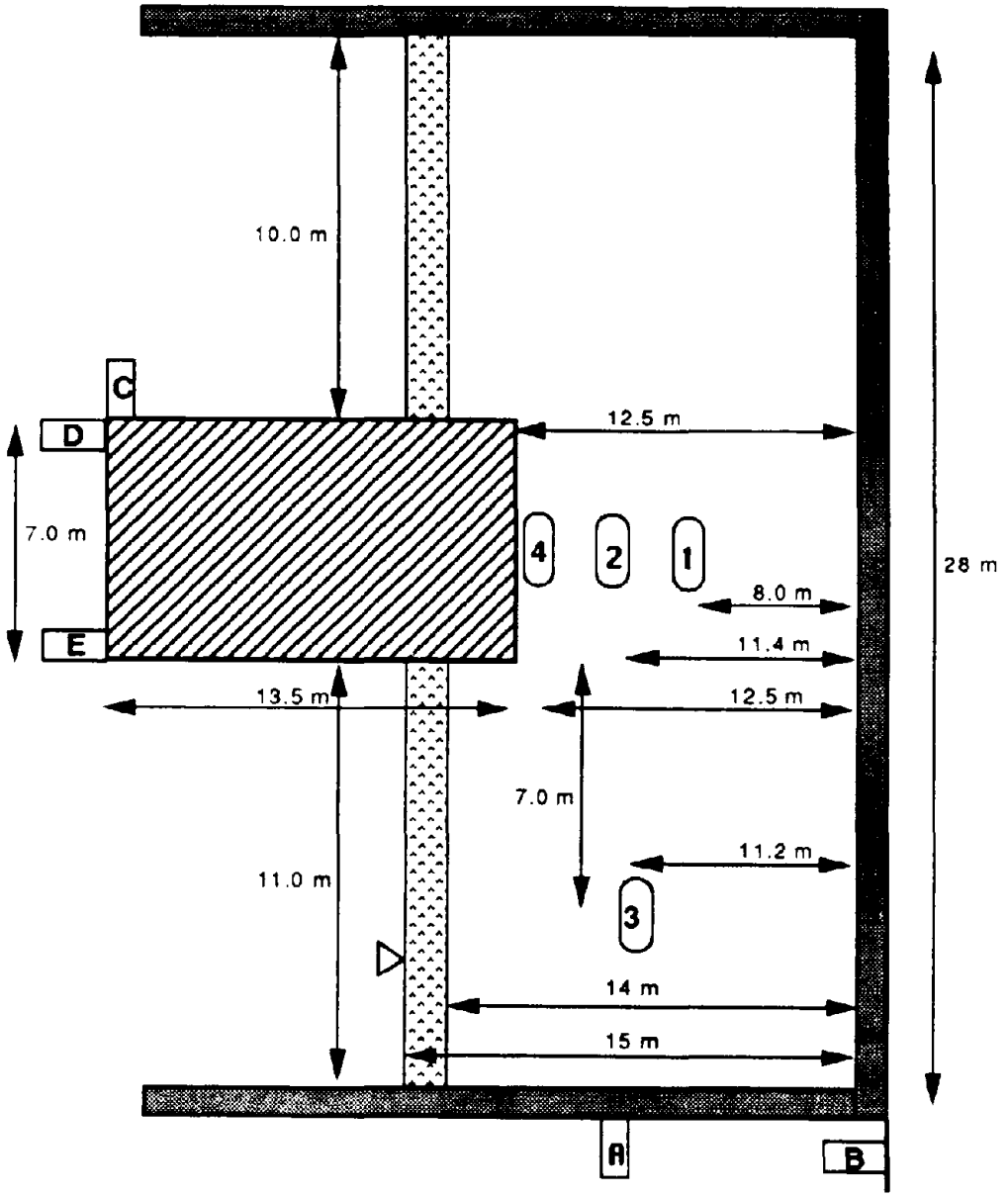

Figure D.1: Soil-Structure Model Test I

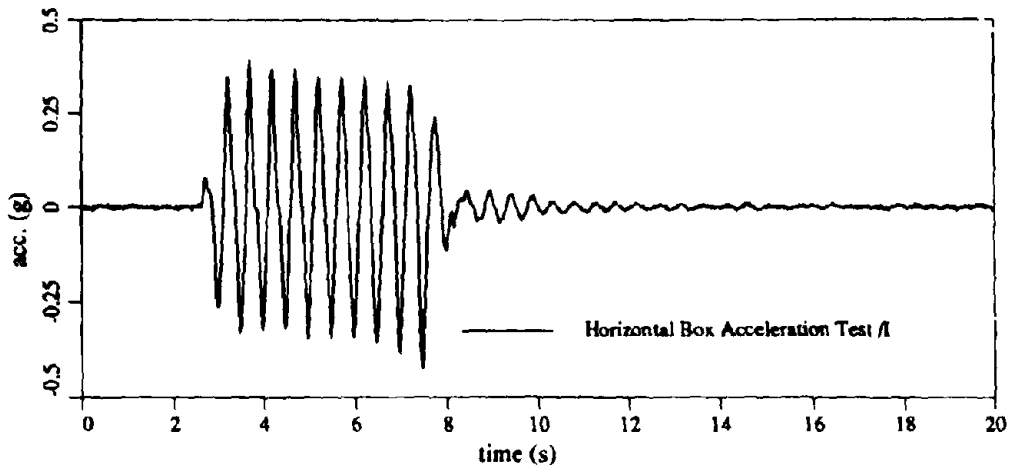

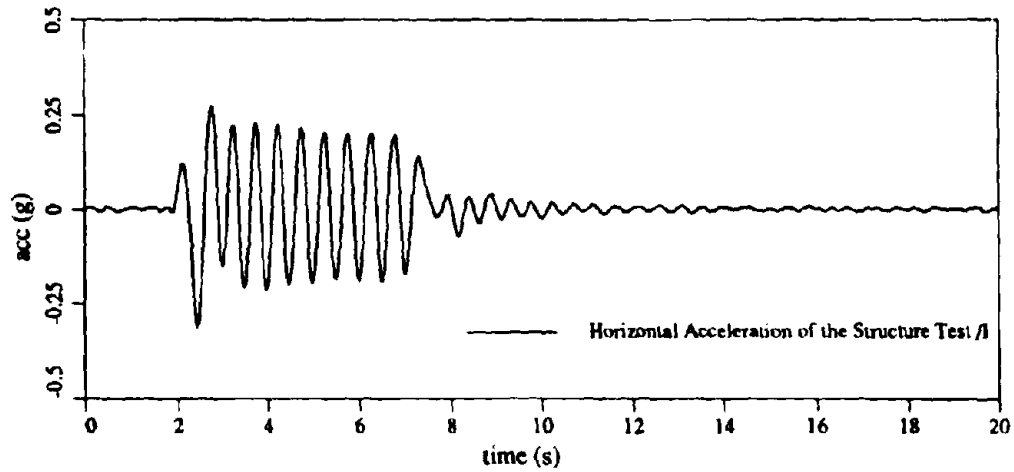

Figure D.2: Soil-Structure Interaction Test I, Horizontal Acceleration Time Histories

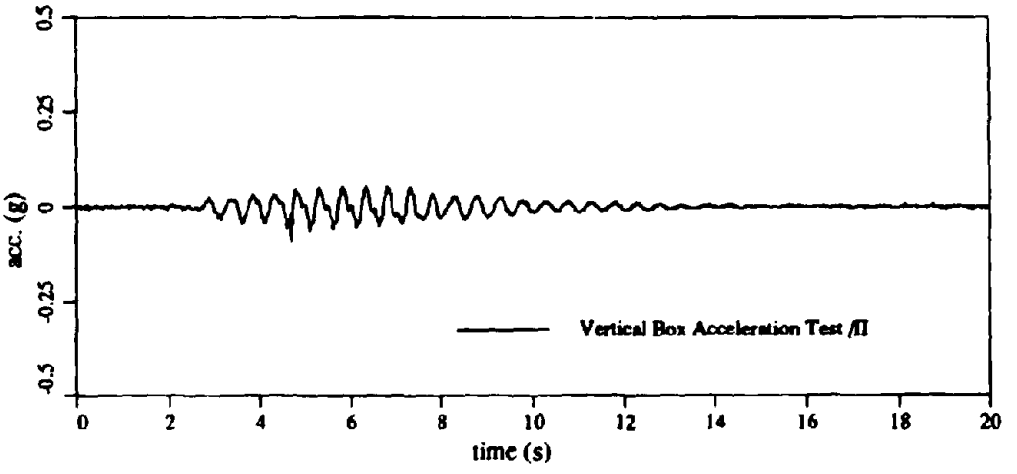

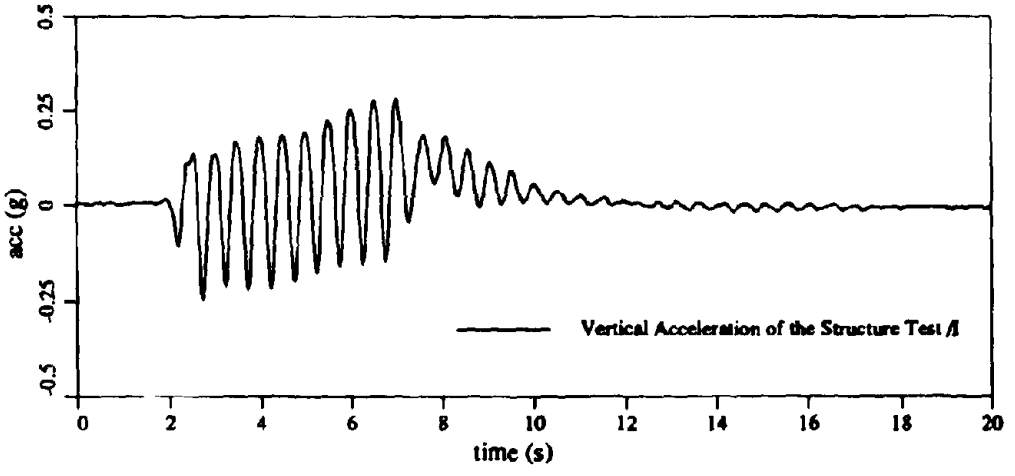

Figure D.3: Soil-Structure Interaction Test I, Vertical Acceleration Time Histories

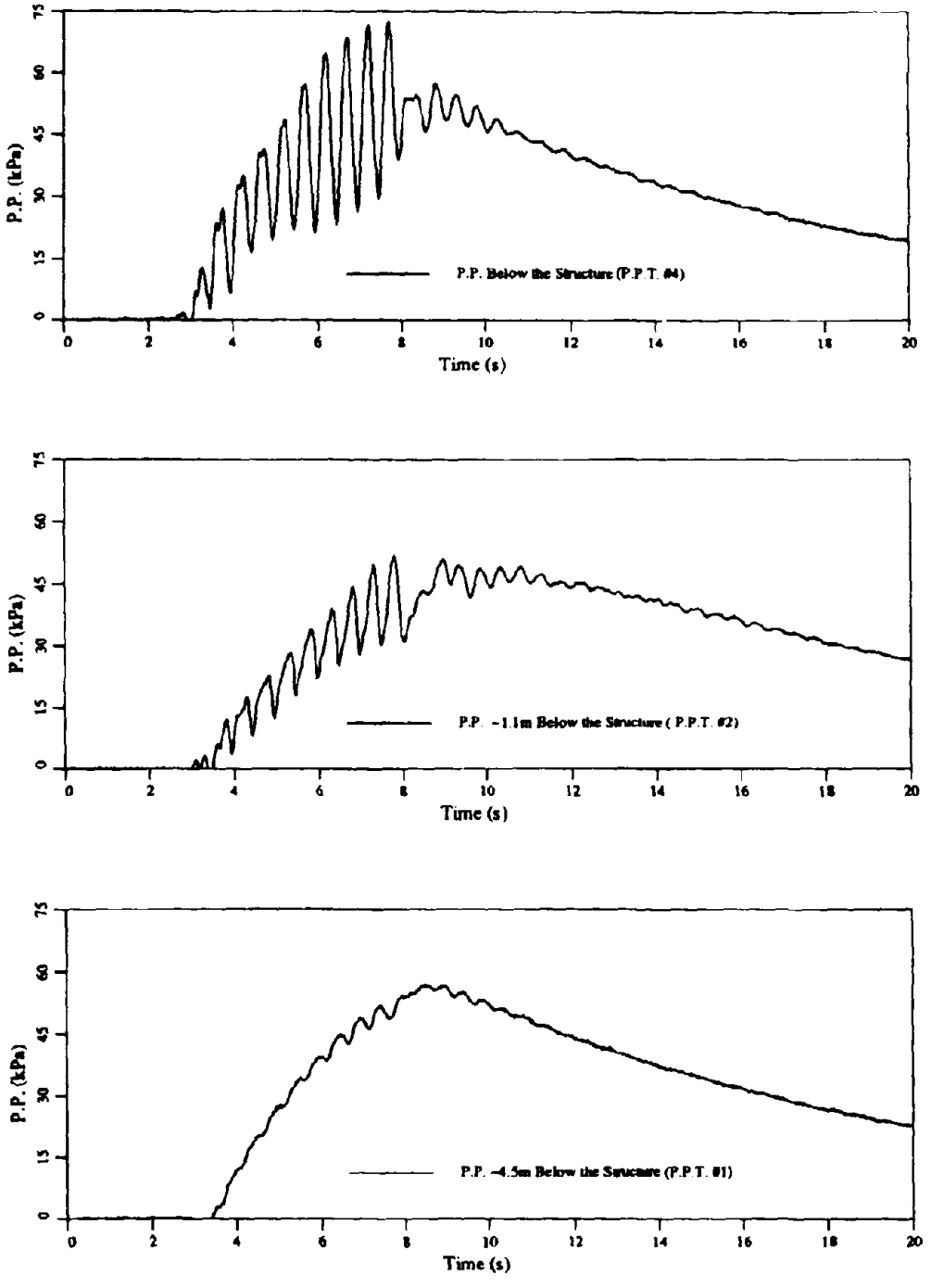

Figure D.4: Soil-Structure Interaction Test I, Excessive Pore Pressure Time Histories Below the Structure

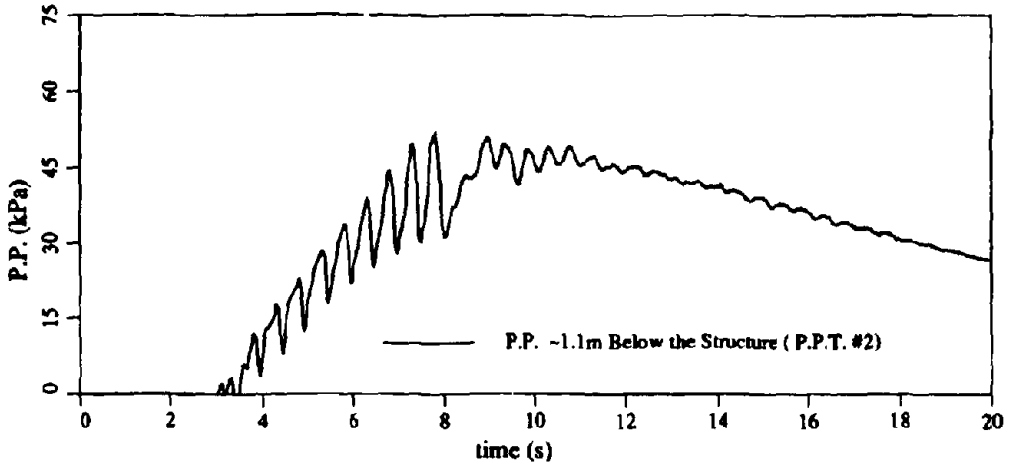

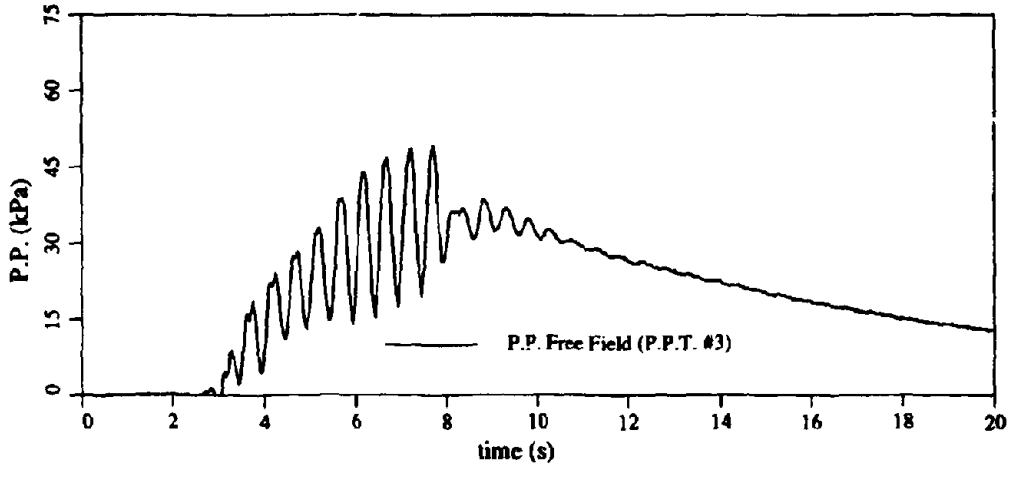

Figure D.5: Soil-Structure Interaction Test I, Excessive Pore Pressure Time Histories Comparison, Free Field Versus Below the Structure

D.2 Test # 2

Test # 2 was performed on April, 9. 1992. Soil-Structure interaction test # 2 was a copy of the test performed on April, 1. 1992. The object was to verify results obtained from the first test.

Ten channels were recorded directly on the Masscomp data acquisition system with a sampling rate of 10000$[Hz]$. Nine channels were at the same time recorded on the tape recorder: due to the limited capacity of the tape recorder (nine channels), accelerometer B was recorded only on the Masscomp.

The same procedure as the one described for 0^{th} and 1^{th} test was followed during the preparation of Test # 2. The aluminum bar again performed well, a vacuum introduced during the sand saturation did not deform the lexan plate, and the sample was undisturbed. Initial readings were taken with the optical instrument after the sample was placed in the centrifuge bucket.

The problem with the structure positioning at a required depth was still not solved, the structure depth for this test was 2 $[m]$. The sample was left in flight at $100g$ for approximately ten minutes before it was stopped and the structure was checked for vertical displacement and standing.

Vertical settlement measured following the centrifuge consolidation was 0.23 $[m]$ (prototype), and was equally distributed, in other words, the structure standing was not disturbed. The centrifuge was spun up again, and ten cycles of sine-like motion with an amplitude of $0.3g$ was presented to the soil sample.

The vertical displacements were measured after the centrifuge was stopped. The structure had collapsed again, once more it tipped in the direction of shaking. Vertical displacements were 0.25 $[m]$ on the right side and 0.6 $[m]$ on the left side (prototype) with no visible inclination in the direction perpendicular to the shaking

direction.

Accelerometer A (horizontal input acceleration) came off during the event. Since the computer set- up was not changed from the one when the first test was performed, it was reasonable to assume that the input acceleration was same as the one in the first test.

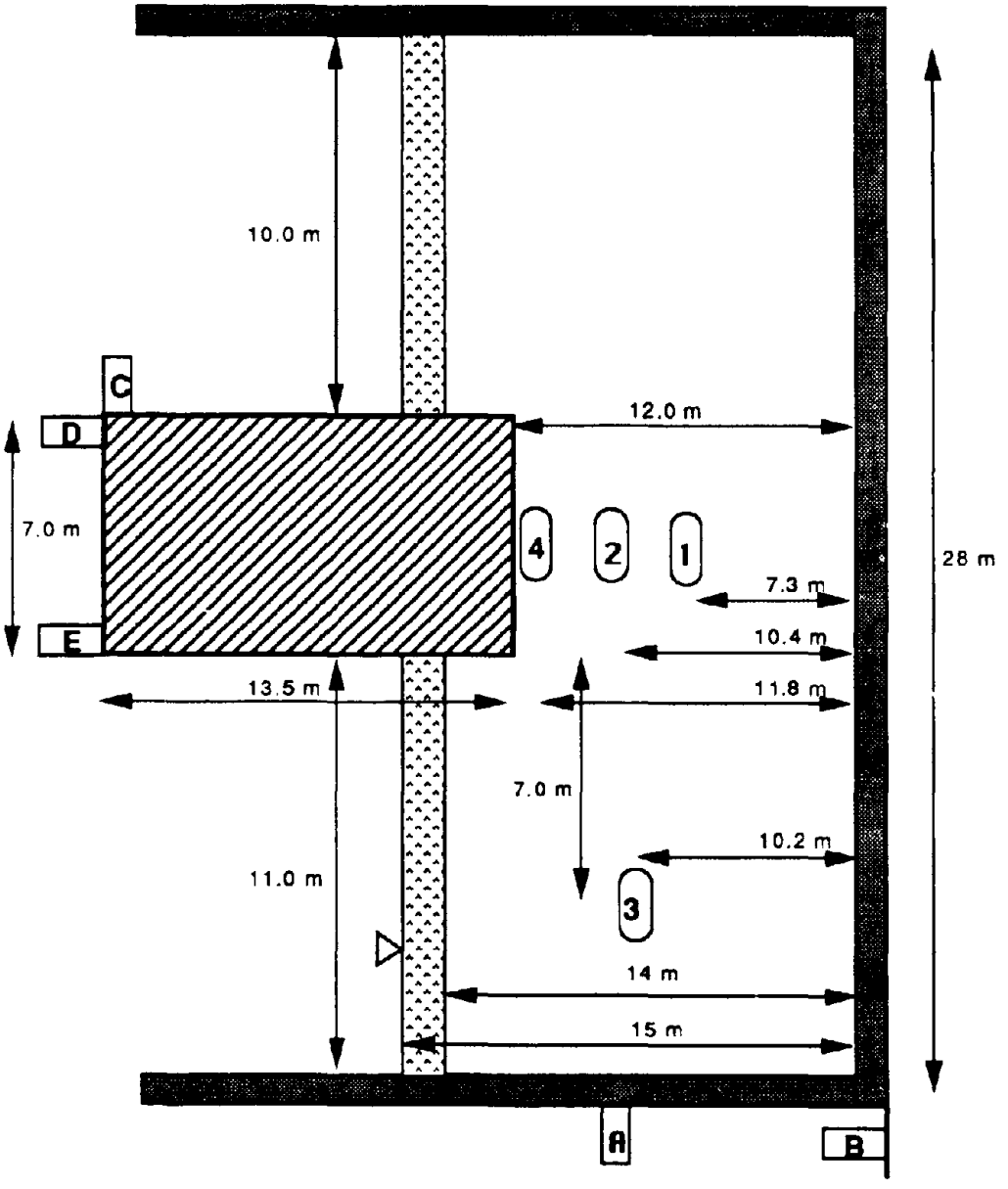

Figure D.6: Soil-Structure Model Test II

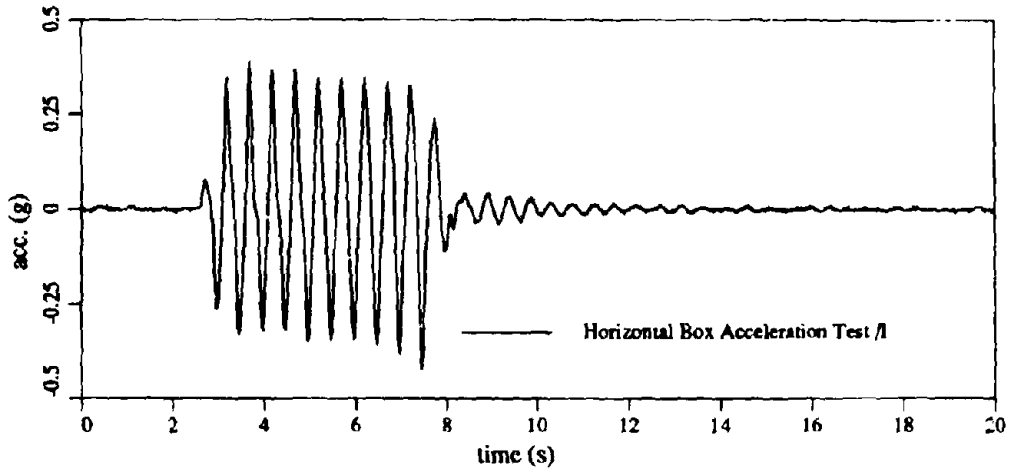

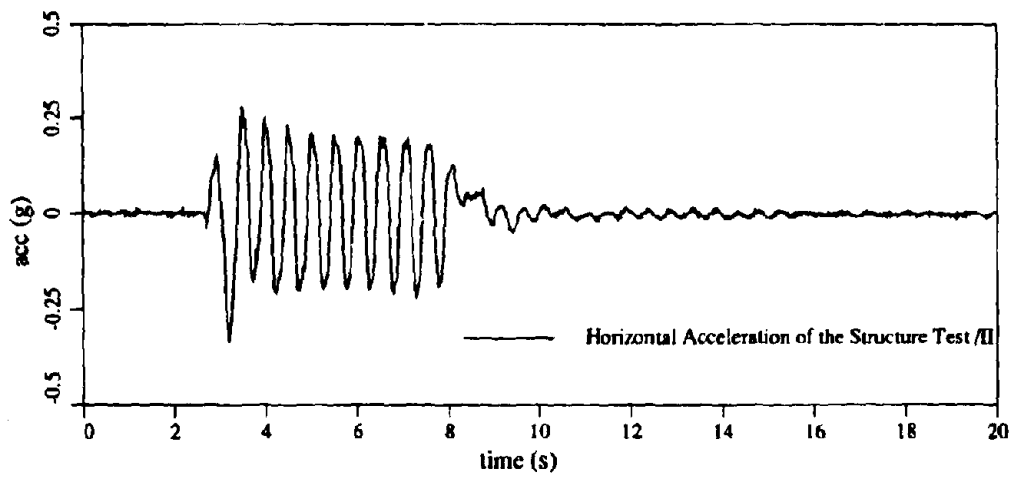

Figure D.7: Soil-Structure Interaction Test II, Horizontal Acceleration Time Histories

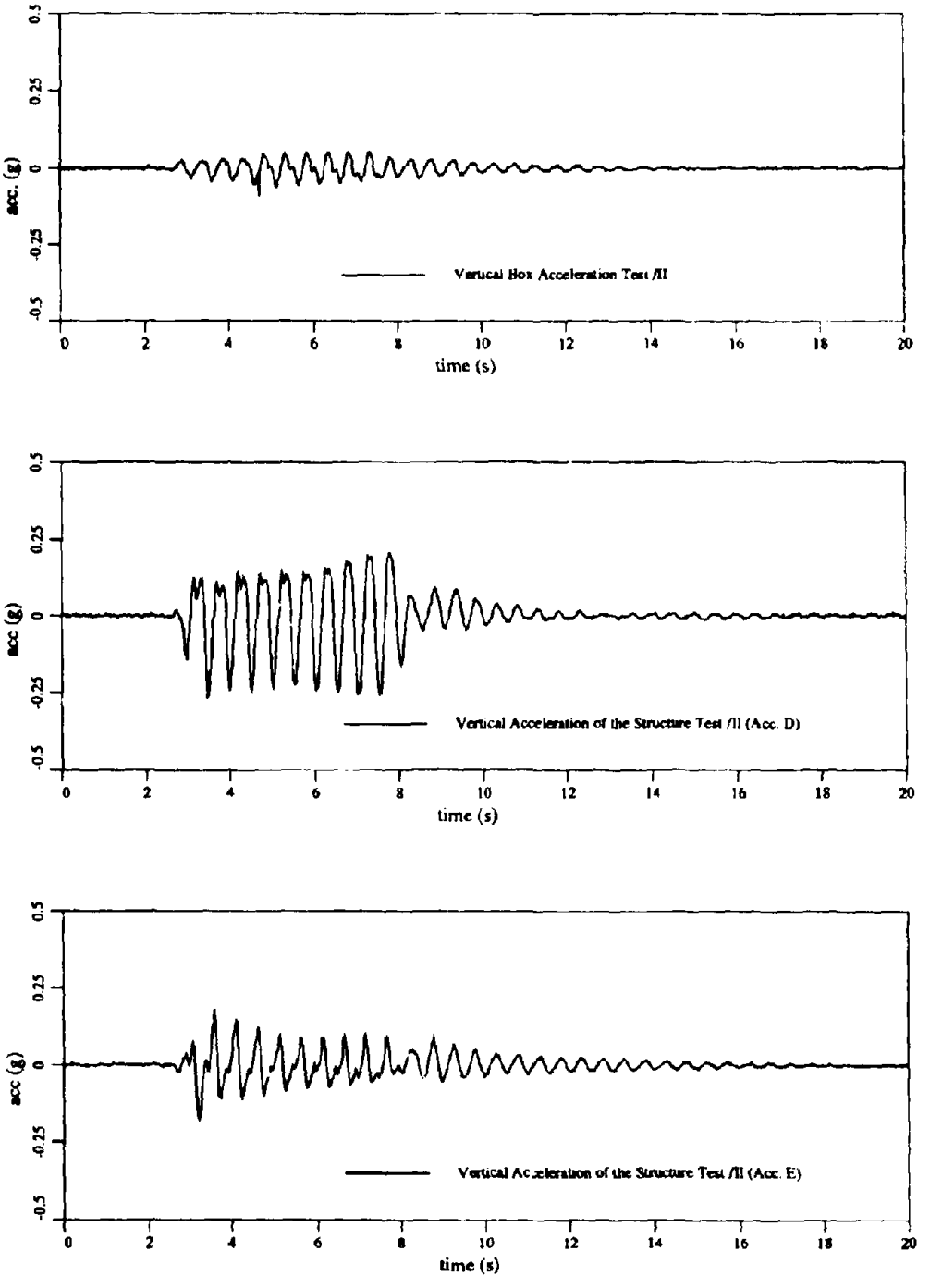

Figure D.8: Soil-Structure Interaction Test II, Vertical Acceleration Time Histories

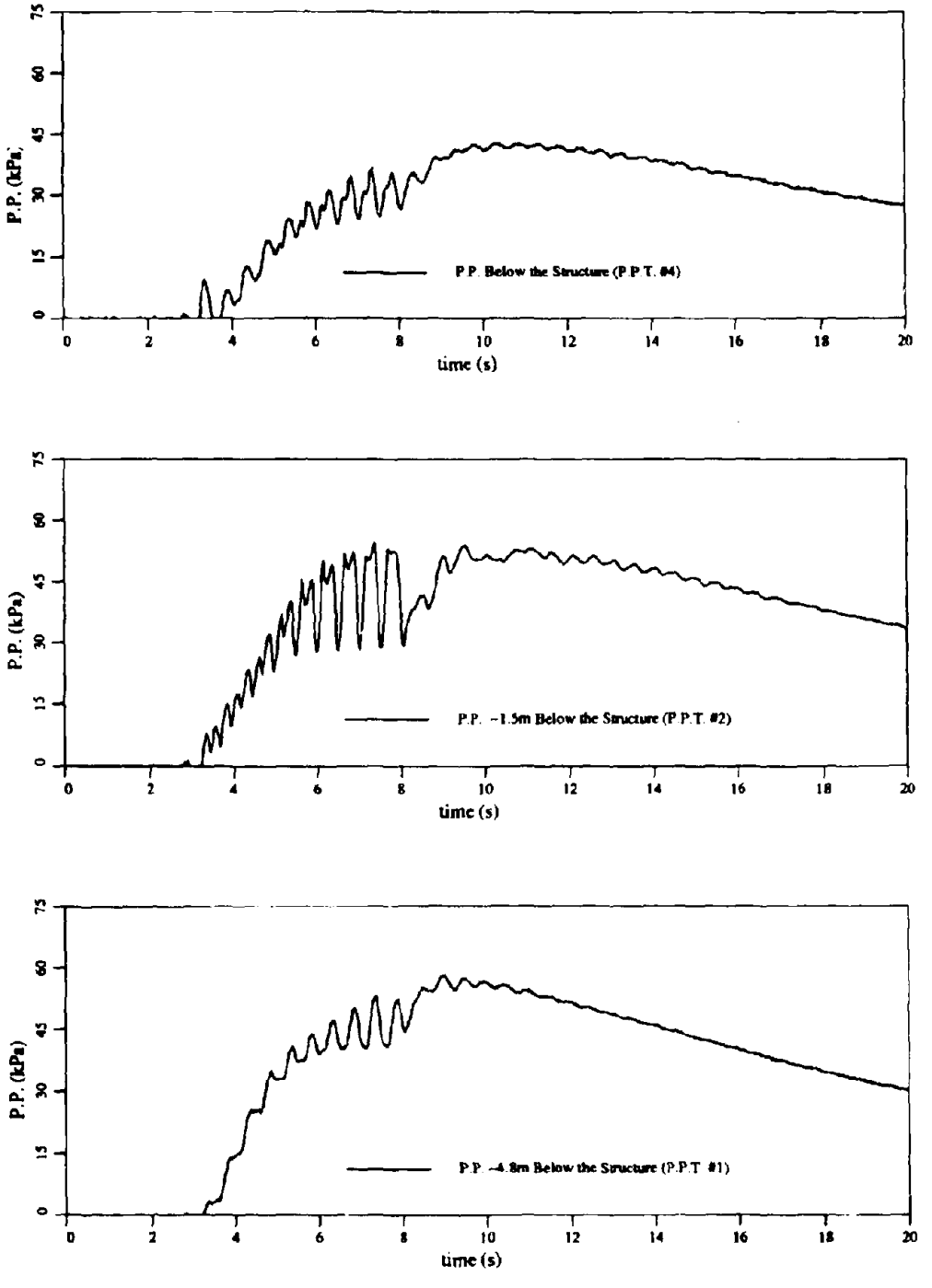

Figure D.9: Soil-Structure Interaction Test II, Excessive Pore Pressure Time Histories Below the Structure

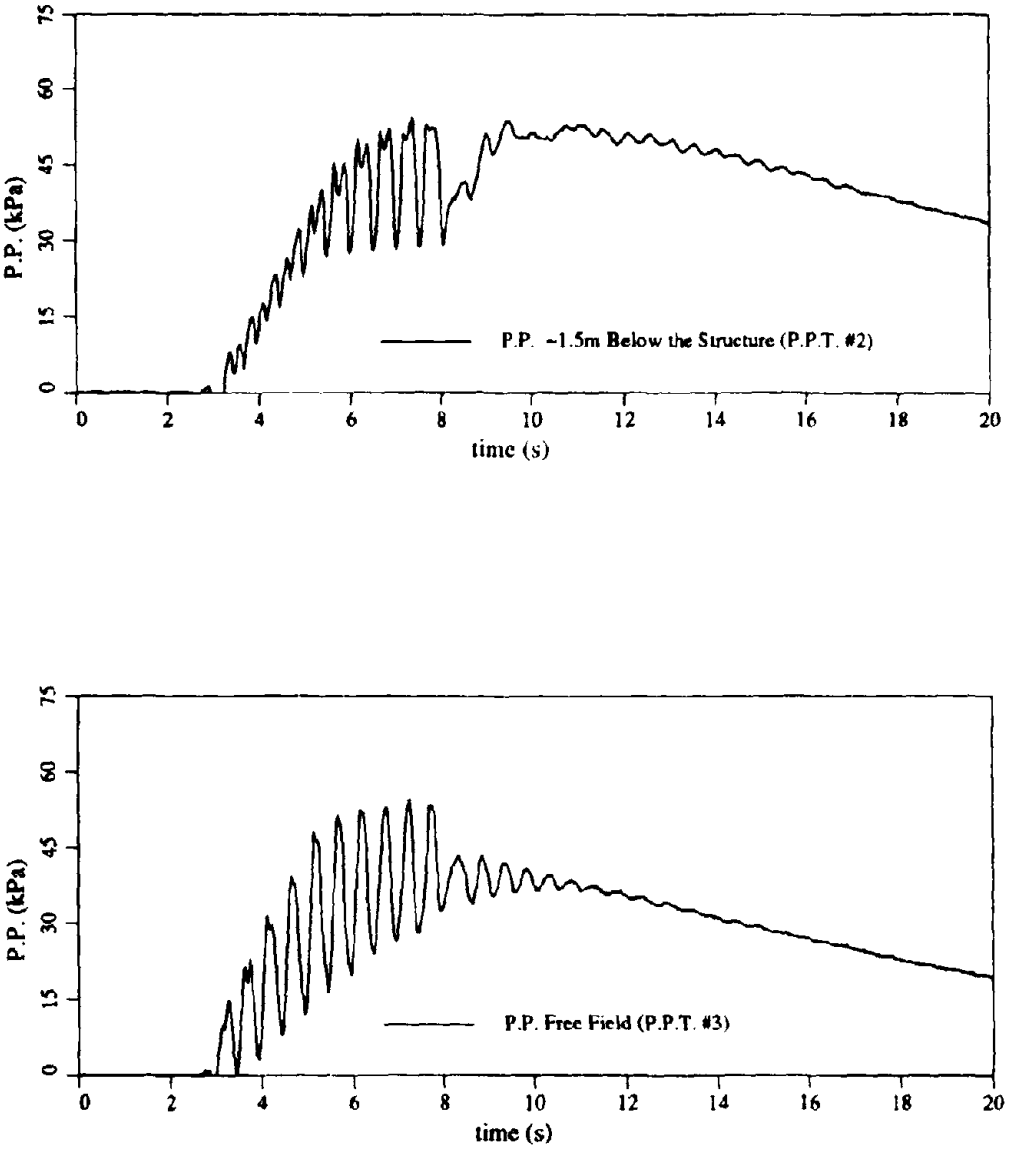

Figure D.10: Soil-Structure Interaction Test II, Excessive Pore Pressure Time Histories Comparison, Free Field Versus Below the Structure

NATIONAL CENTER FOR EARTHQUAKE ENGINEERING RESEARCH
LIST OF TECHNICAL REPORTS

The National Center for Earthquake Engineering Research (NCEER) publishes technical reports on a variety of subjects related to earthquake engineering written by authors funded through NCEER. These reports are available from both NCEER's Publications Department and the National Technical Information Service (NTIS). Requests for reports should be directed to the Publications Department, National Center for Earthquake Engineering Research, State University of New York at Buffalo, Red Jacket Quadrangle, Buffalo, New York 14261. Reports can also be requested through NTIS, 5285 Port Royal Road, Springfield, Virginia 22161. NTIS accession numbers are shown in parenthesis, if available.

NCEER-87-0001 "First-Year Program in Research, Education and Technology Transfer," 3/5/87, (PB88-134275).

NCEER-87-0002 "Experimental Evaluation of Instantaneous Optimal Algorithms for Structural Control," by R.C. Lin, T.T. Soong and A.M. Reinhorn, 4/20/87, (PB88-134341).

NCEER-87-0003 "Experimentation Using the Earthquake Simulation Facilities at University at Buffalo," by A.M. Reinhorn and R.L. Ketter, to be published.

NCEER-87-0004 "The System Characteristics and Performance of a Shaking Table," by J.S. Hwang, K.C. Chang and G.C. Lee, 6/1/87, (PB88-134259). This report is available only through NTIS (see address given above).

NCEER-87-0005 "A Finite Element Formulation for Nonlinear Viscoplastic Material Using a Q Model," by O. Gyebi and G. Dasgupta, 11/2/87, (PB88-213764).

NCEER-87-0006 "Symbolic Manipulation Program (SMP) - Algebraic Codes for Two and Three Dimensional Finite Element Formulations," by X. Lee and G. Dasgupta, 11/9/87, (PB88-218522).

NCEER-87-0007 "Instantaneous Optimal Control Laws for Tall Buildings Under Seismic Excitations," by J.N. Yang, A. Akbarpour and P. Ghaemmaghami, 6/10/87, (PB88-134333). This report is only available through NTIS (see address given above).

NCEER-87-0008 "IDARC: Inelastic Damage Analysis of Reinforced Concrete Frame - Shear-Wall Structures," by Y.J. Park, A.M. Reinhorn and S.K. Kunnath, 7/20/87, (PB88-134325).

NCEER-87-0009 "Liquefaction Potential for New York State: A Preliminary Report on Sites in Manhattan and Buffalo," by M. Budhu, V. Vijayakumar, R.F. Giese and L. Baumgras, 8/31/87, (PB88-163704). This report is available only through NTIS (see address given above).

NCEER-87-0010 "Vertical and Torsional Vibration of Foundations in Inhomogeneous Media," by A.S. Veletsos and K.W. Dotson, 6/1/87, (PB88-134291).

NCEER-87-0011 "Seismic Probabilistic Risk Assessment and Seismic Margins Studies for Nuclear Power Plants," by Howard H.M. Hwang, 6/15/87, (PB88-134267).

NCEER-87-0012 "Parametric Studies of Frequency Response of Secondary Systems Under Ground-Acceleration Excitations," by Y. Yong and Y.K. Lin, 6/10/87, (PB88-134309).

NCEER-87-0013 "Frequency Response of Secondary Systems Under Seismic Excitation," by J.A. HoLung, J. Cai and Y.K. Lin, 7/31/87, (PB88-134317).

NCEER-87-0014 "Modelling Earthquake Ground Motions in Seismically Active Regions Using Parametric Time Series Methods," by G.W. Ellis and A.S. Cakmak, 8/25/87, (PB88-134283).

NCEER-87-0015 "Detection and Assessment of Seismic Structural Damage," by E. DiPasquale and A.S. Cakmak, 8/25/87, (PB88-163712).

NCEER-87-0016 "Pipeline Experiment at Parkfield, California," by J. Isenberg and E. Richardson, 9/15/87, (PB88-163720). This report is available only through NTIS (see address given above).

NCEER-87-0017 "Digital Simulation of Seismic Ground Motion," by M. Shinozuka, G. Deodatis and T. Harada, 8/31/87, (PB88-155197). This report is available only through NTIS (see address given above).

NCEER-87-0018 "Practical Considerations for Structural Control: System Uncertainty, System Time Delay and Truncation of Small Control Forces," J.N. Yang and A. Akbarpour, 8/10/87, (PB88-163738).

NCEER-87-0019 "Modal Analysis of Nonclassically Damped Structural Systems Using Canonical Transformation," by J.N. Yang, S. Sarkani and F.X. Long, 9/27/87, (PB88-187851).

NCEER-87-0020 "A Nonstationary Solution in Random Vibration Theory," by J.R. Red-Horse and P.D. Spanos, 11/3/87, (PB88-163746).

NCEER-87-0021 "Horizontal Impedances for Radially Inhomogeneous Viscoelastic Soil Layers," by A.S. Veletsos and K.W. Dotson, 10/15/87, (PB88-150859).

NCEER-87-0022 "Seismic Damage Assessment of Reinforced Concrete Members," by Y.S. Chung, C. Meyer and M. Shinozuka, 10/9/87, (PB88-150867). This report is available only through NTIS (see address given above).

NCEER-87-0023 "Active Structural Control in Civil Engineering," by T.T. Soong, 11/11/87, (PB88-187778).

NCEER-87-0024 "Vertical and Torsional Impedances for Radially Inhomogeneous Viscoelastic Soil Layers," by K.W. Dotson and A.S. Veletsos, 12/87, (PB88-187786).

NCEER-87-0025 "Proceedings from the Symposium on Seismic Hazards, Ground Motions, Soil Liquefaction and Engineering Practice in Eastern North America," October 20-22, 1987, edited by K.H. Jacob, 12/87, (PB88-188115).

NCEER-87-0026 "Report on the Whittier-Narrows, California, Earthquake of October 1, 1987," by J. Pantelic and A. Reinhorn, 11/87, (PB88-187752). This report is available only through NTIS (see address given above).

NCEER-87-0027 "Design of a Modular Program for Transient Nonlinear Analysis of Large 3-D Building Structures," by S. Srivastav and J.F. Abel, 12/30/87, (PB88-187950).

NCEER-87-0028 "Second-Year Program in Research, Education and Technology Transfer," 3/8/88, (PB88-219480).

NCEER-88-0001 "Workshop on Seismic Computer Analysis and Design of Buildings With Interactive Graphics," by W. McGuire, J.F. Abel and C.H. Conley, 1/18/88, (PB88-187760).

NCEER-88-0002 "Optimal Control of Nonlinear Flexible Structures," by J.N. Yang, F.X. Long and D. Wong, 1/22/88, (PB88-213772).

NCEER-88-0003 "Substructuring Techniques in the Time Domain for Primary-Secondary Structural Systems," by G.D. Manolis and G. Juhn, 2/10/88, (PB88-213780).

NCEER-88-0004 "Iterative Seismic Analysis of Primary-Secondary Systems," by A. Singhal, L.D. Lutes and P.D. Spanos, 2/23/88, (PB88-213798).

NCEER-88-0005 "Stochastic Finite Element Expansion for Random Media," by P.D. Spanos and R. Ghanem, 3/14/88, (PB88-213806).

NCEER-88-0006 "Combining Structural Optimization and Structural Control," by F.Y. Cheng and C.P. Pantelides, 1/10/88, (PB88-213814).

NCEER-88-0007 "Seismic Performance Assessment of Code-Designed Structures," by H.H-M. Hwang, J-W. Jaw and H-J. Shau, 3/20/88, (PB88-219423).

NCEER-88-0008 "Reliability Analysis of Code Designed Structures Under Natural Hazards," by H.H-M. Hwang, H. Ushiba and M. Shinozuka, 2/29/88, (PB88-229471).

NCEER-88-0009 "Seismic Fragility Analysis of Shear Wall Structures," by J-W Jaw and H.H-M. Hwang, 4/30/88, (PB89-102867).

NCEER-88-0010 "Base Isolation of a Multi-Story Building Under a Harmonic Ground Motion - A Comparison of Performances of Various Systems," by F-G Fan, G. Ahmadi and I.G. Tadjbakhsh, 5/18/88, (PB89-122238).

NCEER-88-0011 "Seismic Floor Response Spectra for a Combined System by Green's Functions," by F.M. Lavelle, L.A. Bergman and P.D. Spanos, 5/1/88, (PB89-102875).

NCEER-88-0012 "A New Solution Technique for Randomly Excited Hysteretic Structures," by G.Q. Cai and Y.K. Lin, 5/16/88, (PB89-102883).

NCEER-88-0013 "A Study of Radiation Damping and Soil-Structure Interaction Effects in the Centrifuge," by K. Weissman, supervised by J.H. Prevost, 5/24/88, (PB89-144703).

NCEER-88-0014 "Parameter Identification and Implementation of a Kinematic Plasticity Model for Frictional Soils," by J.H. Prevost and D.V. Griffiths, to be published.

NCEER-88-0015 "Two- and Three- Dimensional Dynamic Finite Element Analyses of the Long Valley Dam," by D.V. Griffiths and J.H. Prevost, 6/17/88, (PB89-144711).

NCEER-88-0016 "Damage Assessment of Reinforced Concrete Structures in Eastern United States," by A.M. Reinhorn, M.J. Seidel, S.K. Kunnath and Y.J. Park, 6/15/88, (PB89-122220).

NCEER-88-0017 "Dynamic Compliance of Vertically Loaded Strip Foundations in Multilayered Viscoelastic Soils," by S. Ahmad and A.S.M. Israil, 6/17/88, (PB89-102891).

NCEER-88-0018 "An Experimental Study of Seismic Structural Response With Added Viscoelastic Dampers," by R.C. Lin, Z. Liang, T.T. Soong and R.H. Zhang, 6/30/88, (PB89-122212). This report is available only through NTIS (see address given above).

NCEER-88-0019 "Experimental Investigation of Primary - Secondary System Interaction," by G.D. Manolis, G. Juhn and A.M. Reinhorn, 5/27/88, (PB89-122204).

NCEER-88-0020 "A Response Spectrum Approach For Analysis of Nonclassically Damped Structures," by J.N. Yang, S. Sarkani and F.X. Long, 4/22/88, (PB89-102909).

NCEER-88-0021 "Seismic Interaction of Structures and Soils: Stochastic Approach," by A.S. Veletsos and A.M. Prasad, 7/21/88, (PB89-122196).

NCEER-88-0022 "Identification of the Serviceability Limit State and Detection of Seismic Structural Damage," by E. DiPasquale and A.S. Cakmak, 6/15/88, (PB89-122188). This report is available only through NTIS (see address given above).

NCEER-88-0023 "Multi-Hazard Risk Analysis: Case of a Simple Offshore Structure," by B.K. Bhartia and E.H. Vanmarcke, 7/21/88, (PB89-145213).

NCEER-88-0024 "Automated Seismic Design of Reinforced Concrete Buildings," by Y.S. Chung, C. Meyer and M. Shinozuka, 7/5/88, (PB89-122170). This report is available only through NTIS (see address given above).

NCEER-88-0025 "Experimental Study of Active Control of MDOF Structures Under Seismic Excitations," by L.L. Chung, R.C. Lin, T.T. Soong and A.M. Reinhorn, 7/10/88, (PB89-122600).

NCEER-88-0026 "Earthquake Simulation Tests of a Low-Rise Metal Structure," by J.S. Hwang, K.C. Chang, G.C. Lee and R.L. Ketter, 8/1/88, (PB89-102917).

NCEER-88-0027 "Systems Study of Urban Response and Reconstruction Due to Catastrophic Earthquakes," by F. Kozin and H.K. Zhou, 9/22/88, (PB90-162348).

NCEER-88-0028 "Seismic Fragility Analysis of Plane Frame Structures," by H.H-M. Hwang and Y.K. Low, 7/31/88, (PB89-131445).

NCEER-88-0029 "Response Analysis of Stochastic Structures," by A. Kardara, C. Bucher and M. Shinozuka, 9/22/88, (PB89-174429).

NCEER-88-0030 "Nonnormal Accelerations Due to Yielding in a Primary Structure," by D.C.K. Chen and L.D. Lutes, 9/19/88, (PB89-131437).

NCEER-88-0031 "Design Approaches for Soil-Structure Interaction," by A.S. Veletsos, A.M. Prasad and Y. Tang, 12/30/88, (PB89-174437). This report is available only through NTIS (see address given above).

NCEER-88-0032 "A Re-evaluation of Design Spectra for Seismic Damage Control," by C.J. Turkstra and A.G. Tallin, 11/7/88, (PB89-145221).

NCEER-88-0033 "The Behavior and Design of Noncontact Lap Splices Subjected to Repeated Inelastic Tensile Loading," by V.E. Sagan, P. Gergely and R.N. White, 12/8/88, (PB89-163737).

NCEER-88-0034 "Seismic Response of Pile Foundations," by S.M. Mamoon, P.K. Banerjee and S. Ahmad, 11/1/88, (PB89-145239).

NCEER-88-0035 "Modeling of R/C Building Structures With Flexible Floor Diaphragms (IDARC2)," by A.M. Reinhorn, S.K. Kunnath and N. Panahshahi, 9/7/88, (PB89-207153).

NCEER-88-0036 "Solution of the Dam-Reservoir Interaction Problem Using a Combination of FEM, BEM with Particular Integrals, Modal Analysis, and Substructuring," by C-S. Tsai, G.C. Lee and R.L. Ketter, 12/31/88, (PB89-207146).

NCEER-88-0037 "Optimal Placement of Actuators for Structural Control," by F.Y. Cheng and C.P. Pantelides, 8/15/88, (PB89-162846).

NCEER-88-0038 "Teflon Bearings in Aseismic Base Isolation: Experimental Studies and Mathematical Modeling," by A. Mokha, M.C. Constantinou and A.M. Reinhorn, 12/5/88, (PB89-218457). This report is available only through NTIS (see address given above).

NCEER-88-0039 "Seismic Behavior of Flat Slab High-Rise Buildings in the New York City Area," by P. Weidlinger and M. Ettouney, 10/15/88, (PB90-145681).

NCEER-88-0040 "Evaluation of the Earthquake Resistance of Existing Buildings in New York City," by P. Weidlinger and M. Ettouney, 10/15/88, to be published.

NCEER-88-0041 "Small-Scale Modeling Techniques for Reinforced Concrete Structures Subjected to Seismic Loads," by W. Kim, A. El-Attar and R.N. White, 11/22/88, (PB89-189625).

NCEER-88-0042 "Modeling Strong Ground Motion from Multiple Event Earthquakes," by G.W. Ellis and A.S. Cakmak, 10/15/88, (PB89-174445).

NCEER-88-0043 "Nonstationary Models of Seismic Ground Acceleration," by M. Grigoriu, S.E. Ruiz and E. Rosenblueth, 7/15/88, (PB89-189617).

NCEER-88-0044 "SARCF User's Guide: Seismic Analysis of Reinforced Concrete Frames," by Y.S. Chung, C. Meyer and M. Shinozuka, 11/9/88, (PB89-174452).

NCEER-88-0045 "First Expert Panel Meeting on Disaster Research and Planning," edited by J. Pantelic and J. Stoyle, 9/15/88, (PB89-174460).

NCEER-88-0046 "Preliminary Studies of the Effect of Degrading Infill Walls on the Nonlinear Seismic Response of Steel Frames," by C.Z. Chrysostomou, P. Gergely and J.F. Abel, 12/19/88, (PB89-208383).

NCEER-88-0047 "Reinforced Concrete Frame Component Testing Facility - Design, Construction, Instrumentation and Operation," by S.P. Pessiki, C. Conley, T. Bond, P. Gergely and R.N. White, 12/16/88, (PB89-174478).

NCEER-89-0001 "Effects of Protective Cushion and Soil Compliancy on the Response of Equipment Within a Seismically Excited Building," by J.A. HoLung, 2/16/89, (PB89-207179).

NCEER-89-0002 "Statistical Evaluation of Response Modification Factors for Reinforced Concrete Structures," by H.H-M. Hwang and J-W. Jaw, 2/17/89, (PB89-207187).

NCEER-89-0003 "Hysteretic Columns Under Random Excitation," by G-Q. Cai and Y.K. Lin, 1/9/89, (PB89-196513).

NCEER-89-0004 "Experimental Study of 'Elephant Foot Bulge' Instability of Thin-Walled Metal Tanks," by Z-H. Jia and R.L. Ketter, 2/22/89, (PB89-207195).

NCEER-89-0005 "Experiment on Performance of Buried Pipelines Across San Andreas Fault," by J. Isenberg, E. Richardson and T.D. O'Rourke, 3/10/89, (PB89-218440). This report is available only through NTIS (see address given above).

NCEER-89-0006 "A Knowledge-Based Approach to Structural Design of Earthquake-Resistant Buildings," by M. Subramani, P. Gergely, C.H. Conley, J.F. Abel and A.H. Zaghw, 1/15/89, (PB89-218465).

NCEER-89-0007 "Liquefaction Hazards and Their Effects on Buried Pipelines," by T.D. O'Rourke and P.A. Lane, 2/1/89, (PB89-218481).

NCEER-89-0008 "Fundamentals of System Identification in Structural Dynamics," by H. Imai, C-B. Yun, O. Maruyama and M. Shinozuka, 1/26/89, (PB89-207211).

NCEER-89-0009 "Effects of the 1985 Michoacan Earthquake on Water Systems and Other Buried Lifelines in Mexico," by A.G. Ayala and M.J. O'Rourke, 3/8/89, (PB89-207229).

NCEER-89-R010 "NCEER Bibliography of Earthquake Education Materials," by K.E.K. Ross, Second Revision, 9/1/89, (PB90-125352).

NCEER-89-0011 "Inelastic Three-Dimensional Response Analysis of Reinforced Concrete Building Structures (IDARC-3D), Part I - Modeling," by S.K. Kunnath and A.M. Reinhorn, 4/17/89, (PB90-114612).

NCEER-89-0012 "Recommended Modifications to ATC-14," by C.D. Poland and J.O. Malley, 4/12/89, (PB90-108648).

NCEER-89-0013 "Repair and Strengthening of Beam-to-Column Connections Subjected to Earthquake Loading," by M. Corazao and A.J. Durrani, 2/28/89, (PB90-109885).

NCEER-89-0014 "Program EXKAL2 for Identification of Structural Dynamic Systems," by O. Maruyama, C-B. Yun, M. Hoshiya and M. Shinozuka, 5/19/89, (PB90-109877).

NCEER-89-0015 "Response of Frames With Bolted Semi-Rigid Connections, Part I - Experimental Study and Analytical Predictions," by P.J. DiCorso, A.M. Reinhorn, J.R. Dickerson, J.B. Radziminski and W.L. Harper, 6/1/89, to be published.

NCEER-89-0016 "ARMA Monte Carlo Simulation in Probabilistic Structural Analysis," by P.D. Spanos and M.P. Mignolet, 7/10/89, (PB90-109893).

NCEER-89-P017 "Preliminary Proceedings from the Conference on Disaster Preparedness - The Place of Earthquake Education in Our Schools," Edited by K.E.K. Ross, 6/23/89, (PB90-108606).

NCEER-89-0017 "Proceedings from the Conference on Disaster Preparedness - The Place of Earthquake Education in Our Schools," Edited by K.E.K. Ross, 12/31/89, (PB90-207895). This report is available only through NTIS (see address given above).

NCEER-89-0018 "Multidimensional Models of Hysteretic Material Behavior for Vibration Analysis of Shape Memory Energy Absorbing Devices, by E.J. Graesser and F.A. Cozzarelli, 6/7/89, (PB90-164146).

NCEER-89-0019 "Nonlinear Dynamic Analysis of Three Dimensional Base Isolated Structures (3D-BASIS)," by S. Nagarajaiah, A.M. Reinhorn and M.C. Constantinou, 8/3/89, (PB90-161936). This report is available only through NTIS (see address given above).

NCEER-89-0020 "Structural Control Considering Time-Rate of Control Forces and Control Rate Constraints," by F.Y. Cheng and C.P. Pantelides, 8/3/89, (PB90-120445).

NCEER-89-0021 "Subsurface Conditions of Memphis and Shelby County," by K.W. Ng, T.S. Chang and H.H.M. Hwang, 7/26/89, (PB90-120437).

NCEER-89-0022 "Seismic Wave Propagation Effects on Straight Jointed Buried Pipelines," by K. Elhmadi and M.J. O'Rourke, 8/24/89, (PB90-162322).

NCEER-89-0023 "Workshop on Serviceability Analysis of Water Delivery Systems," edited by M. Grigoriu, 3/6/89, (PB90-127424).

NCEER-89-0024 "Shaking Table Study of a 1/5 Scale Steel Frame Composed of Tapered Members," by K.C. Chang, J.S. Hwang and G.C. Lee, 9/18/89, (PB90-160169).

NCEER-89-0025 "DYNA1D: A Computer Program for Nonlinear Seismic Site Response Analysis - Technical Documentation," by Jean H. Prevost, 9/14/89, (PB90-161944). This report is available only through NTIS (see address given above).

NCEER-89-0026 "1:4 Scale Model Studies of Active Tendon Systems and Active Mass Dampers for Aseismic Protection," by A.M. Reinhorn, T.T. Soong, R.C. Lin, Y.P. Yang, Y. Fukao, H. Abe and M. Nakai, 9/15/89, (PB90-173246).

NCEER-89-0027 "Scattering of Waves by Inclusions in a Nonhomogeneous Elastic Half Space Solved by Boundary Element Methods," by P.K. Hadley, A. Askar and A.S. Cakmak, 6/15/89, (PB90-145699).

NCEER-89-0028 "Statistical Evaluation of Deflection Amplification Factors for Reinforced Concrete Structures," by H.H.M. Hwang, J-W. Jaw and A.L. Ch'ng, 8/31/89, (PB90-164633).

NCEER-89-0029 "Bedrock Accelerations in Memphis Area Due to Large New Madrid Earthquakes," by H.H.M. Hwang, C.H.S. Chen and G. Yu, 11/7/89, (PB90-162330).

NCEER-89-0030 "Seismic Behavior and Response Sensitivity of Secondary Structural Systems," by Y.Q. Chen and T.T. Soong, 10/23/89, (PB90-164658).

NCEER-89-0031 "Random Vibration and Reliability Analysis of Primary-Secondary Structural Systems," by Y. Ibrahim, M. Grigoriu and T.T. Soong, 11/10/89, (PB90-161951).

NCEER-89-0032 "Proceedings from the Second U.S. - Japan Workshop on Liquefaction, Large Ground Deformation and Their Effects on Lifelines, September 26-29, 1989," Edited by T.D. O'Rourke and M. Hamada, 12/1/89, (PB90-209388).

NCEER-89-0033 "Deterministic Model for Seismic Damage Evaluation of Reinforced Concrete Structures," by J.M. Bracci, A.M. Reinhorn, J.B. Mander and S.K. Kunnath, 9/27/89.

NCEER-89-0034 "On the Relation Between Local and Global Damage Indices," by E. DiPasquale and A.S. Cakmak, 8/15/89, (PB90-173865).

NCEER-89-0035 "Cyclic Undrained Behavior of Nonplastic and Low Plasticity Silts," by A.J. Walker and H.E. Stewart, 7/26/89, (PB90-183518).

NCEER-89-0036 "Liquefaction Potential of Surficial Deposits in the City of Buffalo, New York," by M. Budhu, R. Giese and L. Baumgrass, 1/17/89, (PB90-208455).

NCEER-89-0037 "A Deterministic Assessment of Effects of Ground Motion Incoherence," by A.S. Veletsos and Y. Tang, 7/15/89, (PB90-164294).

NCEER-89-0038 "Workshop on Ground Motion Parameters for Seismic Hazard Mapping," July 17-18, 1989, edited by R.V. Whitman, 12/1/89, (PB90-173923).

NCEER-89-0039 "Seismic Effects on Elevated Transit Lines of the New York City Transit Authority," by C.J. Costantino, C.A. Miller and E. Heymsfield, 12/26/89, (PB90-207887).

NCEER-89-0040 "Centrifugal Modeling of Dynamic Soil-Structure Interaction," by K. Weissman, Supervised by J.H. Prevost, 5/10/89, (PB90-207879).

NCEER-89-0041 "Linearized Identification of Buildings With Cores for Seismic Vulnerability Assessment," by I-K. Ho and A.E. Aktan, 11/1/89, (PB90-251943).

NCEER-90-0001 "Geotechnical and Lifeline Aspects of the October 17, 1989 Loma Prieta Earthquake in San Francisco," by T.D. O'Rourke, H.E. Stewart, F.T. Blackburn and T.S. Dickerman, 1/90, (PB90-208596).

NCEER-90-0002 "Nonnormal Secondary Response Due to Yielding in a Primary Structure," by D.C.K. Chen and L.D. Lutes, 2/28/90, (PB90-251976).

NCEER-90-0003 "Earthquake Education Materials for Grades K-12," by K.E.K. Ross, 4/16/90, (PB91-251984).

NCEER-90-0004 "Catalog of Strong Motion Stations in Eastern North America," by R.W. Busby, 4/3/90, (PB90-251984).

NCEER-90-0005 "NCEER Strong-Motion Data Base: A User Manual for the GeoBase Release (Version 1.0 for the Sun3)," by P. Friberg and K. Jacob, 3/31/90 (PB90-258062).

NCEER-90-0006 "Seismic Hazard Along a Crude Oil Pipeline in the Event of an 1811-1812 Type New Madrid Earthquake," by H.H.M. Hwang and C-H.S. Chen, 4/16/90(PB90-258054).

NCEER-90-0007 "Site-Specific Response Spectra for Memphis Sheahan Pumping Station," by H.H.M. Hwang and C.S. Lee, 5/15/90, (PB91-108811).

NCEER-90-0008 "Pilot Study on Seismic Vulnerability of Crude Oil Transmission Systems," by T. Ariman, R. Dobry, M. Grigoriu, F. Kozin, M. O'Rourke, T. O'Rourke and M. Shinozuka, 5/25/90, (PB91-108837).

NCEER-90-0009 "A Program to Generate Site Dependent Time Histories: EQGEN," by G.W. Ellis, M. Srinivasan and A.S. Cakmak, 1/30/90, (PB91-108829).

NCEER-90-0010 "Active Isolation for Seismic Protection of Operating Rooms," by M.E. Talbott, Supervised by M. Shinozuka, 6/8/9, (PB91-110205).

NCEER-90-0011 "Program LINEARID for Identification of Linear Structural Dynamic Systems," by C-B. Yun and M. Shinozuka, 6/25/90, (PB91-110312).

NCEER-90-0012 "Two-Dimensional Two-Phase Elasto-Plastic Seismic Response of Earth Dams," by A.N. Yiagos, Supervised by J.H. Prevost, 6/20/90, (PB91-110197).

NCEER-90-0013 "Secondary Systems in Base-Isolated Structures: Experimental Investigation, Stochastic Response and Stochastic Sensitivity," by G.D. Manolis, G. Juhn, M.C. Constantinou and A.M. Reinhorn, 7/1/90, (PB91-110320).

NCEER-90-0014 "Seismic Behavior of Lightly-Reinforced Concrete Column and Beam-Column Joint Details," by S.P. Pessiki, C.H. Conley, P. Gergely and R.N. White, 8/22/90, (PB91-108795).

NCEER-90-0015 "Two Hybrid Control Systems for Building Structures Under Strong Earthquakes," by J.N. Yang and A. Danielians, 6/29/90, (PB91-125393).

NCEER-90-0016 "Instantaneous Optimal Control with Acceleration and Velocity Feedback," by J.N. Yang and Z. Li, 6/29/90, (PB91-125401).

NCEER-90-0017 "Reconnaissance Report on the Northern Iran Earthquake of June 21, 1990," by M. Mehrain, 10/4/90, (PB91-125377).

NCEER-90-0018 "Evaluation of Liquefaction Potential in Memphis and Shelby County," by T.S. Chang, P.S. Tang, C.S. Lee and H. Hwang, 8/10/90, (PB91-125427).

NCEER-90-0019 "Experimental and Analytical Study of a Combined Sliding Disc Bearing and Helical Steel Spring Isolation System," by M.C. Constantinou, A.S. Mokha and A.M. Reinhorn, 10/4/90, (PB91-125385).

NCEER-90-0020 "Experimental Study and Analytical Prediction of Earthquake Response of a Sliding Isolation System with a Spherical Surface," by A.S. Mokha, M.C. Constantinou and A.M. Reinhorn, 10/11/90, (PB91-125419).

NCEER-90-0021 "Dynamic Interaction Factors for Floating Pile Groups," by G. Gazetas, K. Fan, A. Kaynia and E. Kausel, 9/10/90, (PB91-170381).

NCEER-90-0022 "Evaluation of Seismic Damage Indices for Reinforced Concrete Structures," by S. Rodriguez-Gomez and A.S. Cakmak, 9/30/90, PB91-171322).

NCEER-90-0023 "Study of Site Response at a Selected Memphis Site," by H. Desai, S. Ahmad, E.S. Gazetas and M.R. Oh, 10/11/90, (PB91-196857).

NCEER-90-0024 "A User's Guide to Strongmo: Version 1.0 of NCEER's Strong-Motion Data Access Tool for PCs and Terminals," by P.A. Friberg and C.A.T. Susch, 11/15/90, (PB91-171272).

NCEER-90-0025 "A Three-Dimensional Analytical Study of Spatial Variability of Seismic Ground Motions," by L-L. Hong and A.H.-S. Ang, 10/30/90, (PB91-170399).

NCEER-90-0026 "MUMOID User's Guide - A Program for the Identification of Modal Parameters," by S. Rodriguez-Gomez and E. DiPasquale, 9/30/90, (PB91-171298).

NCEER-90-0027 "SARCF-II User's Guide - Seismic Analysis of Reinforced Concrete Frames," by S. Rodriguez-Gomez, Y.S. Chung and C. Meyer, 9/30/90, (PB91-171280).

NCEER-90-0028 "Viscous Dampers: Testing, Modeling and Application in Vibration and Seismic Isolation," by N. Makris and M.C. Constantinou, 12/20/90 (PB91-190561).

NCEER-90-0029 "Soil Effects on Earthquake Ground Motions in the Memphis Area," by H. Hwang, C.S. Lee, K.W. Ng and T.S. Chang, 8/2/90, (PB91-190751).

NCEER-91-0001 "Proceedings from the Third Japan-U.S. Workshop on Earthquake Resistant Design of Lifeline Facilities and Countermeasures for Soil Liquefaction, December 17-19, 1990," edited by T.D. O'Rourke and M. Hamada, 2/1/91, (PB91-179259).

NCEER-91-0002 "Physical Space Solutions of Non-Proportionally Damped Systems," by M. Tong, Z. Liang and G.C. Lee, 1/15/91, (PB91-179242).

NCEER-91-0003 "Seismic Response of Single Piles and Pile Groups," by K. Fan and G. Gazetas, 1/10/91, (PB92-174994).

NCEER-91-0004 "Damping of Structures: Part 1 - Theory of Complex Damping," by Z. Liang and G. Lee, 10/10/91, (PB92-197235).

NCEER-91-0005 "3D-BASIS - Nonlinear Dynamic Analysis of Three Dimensional Base Isolated Structures: Part II," by S. Nagarajaiah, A.M. Reinhorn and M.C. Constantinou, 2/28/91, (PB91-190553).

NCEER-91-0006 "A Multidimensional Hysteretic Model for Plasticity Deforming Metals in Energy Absorbing Devices," by E.J. Graesser and F.A. Cozzarelli, 4/9/91, (PB92-108364).

NCEER-91-0007 "A Framework for Customizable Knowledge-Based Expert Systems with an Application to a KBES for Evaluating the Seismic Resistance of Existing Buildings," by E.G. Ibarra-Anaya and S.J. Fenves, 4/9/91, (PB91-210930).

NCEER-91-0008 "Nonlinear Analysis of Steel Frames with Semi-Rigid Connections Using the Capacity Spectrum Method," by G.G. Deierlein, S-H. Hsieh, Y-J. Shen and J.F. Abel, 7/2/91, (PB92-113828).

NCEER-91-0009 "Earthquake Education Materials for Grades K-12," by K.E.K. Ross, 4/30/91, (PB91-212142).

NCEER-91-0010 "Phase Wave Velocities and Displacement Phase Differences in a Harmonically Oscillating Pile," by N. Makris and G. Gazetas, 7/8/91, (PB92-108356).

NCEER-91-0011 "Dynamic Characteristics of a Full-Size Five Story Steel Structure and a 2/5 Scale Model," by K.C. Chang, G.C. Yao, G.C. Lee, D.S. Hao and Y.C. Yeh," 7/2/91, (PB93-116648).

NCEER-91-0012 "Seismic Response of a 2/5 Scale Steel Structure with Added Viscoelastic Dampers," by K.C. Chang, T.T. Soong, S-T. Oh and M.L. Lai, 5/17/91, (PB92-110816).

NCEER-91-0013 "Earthquake Response of Retaining Walls; Full-Scale Testing and Computational Modeling," by S. Alampalli and A-W.M. Elgamal, 6/20/91, to be published.

NCEER-91-0014 "3D-BASIS-M: Nonlinear Dynamic Analysis of Multiple Building Base Isolated Structures," by P.C. Tsopelas, S. Nagarajaiah, M.C. Constantinou and A.M. Reinhorn, 5/28/91, (PB92-113885).

NCEER-91-0015 "Evaluation of SEAOC Design Requirements for Sliding Isolated Structures," by D. Theodossiou and M.C. Constantinou, 6/10/91, (PB92-114602).

NCEER-91-0016 "Closed-Loop Modal Testing of a 27-Story Reinforced Concrete Flat Plate-Core Building," by H.R. Somaprasad, T. Toksoy, H. Yoshiyuki and A.E. Aktan, 7/15/91, (PB92-129980).

NCEER-91-0017 "Shake Table Test of a 1/6 Scale Two-Story Lightly Reinforced Concrete Building," by A.G. El-Attar, R.N. White and P. Gergely, 2/28/91, (PB92-222447).

NCEER-91-0018 "Shake Table Test of a 1/8 Scale Three-Story Lightly Reinforced Concrete Building," by A.G. El-Attar, R.N. White and P. Gergely, 2/28/91, (PB93-116630).

NCEER-91-0019 "Transfer Functions for Rigid Rectangular Foundations," by A.S. Veletsos, A.M. Prasad and W.H. Wu, 7/31/91.

NCEER-91-0020 "Hybrid Control of Seismic-Excited Nonlinear and Inelastic Structural Systems," by J.N. Yang, Z. Li and A. Danielians, 8/1/91, (PB92-143171).

NCEER-91-0021 "The NCEER-91 Earthquake Catalog: Improved Intensity-Based Magnitudes and Recurrence Relations for U.S. Earthquakes East of New Madrid," by L. Seeber and J.G. Armbruster, 8/28/91, (PB92-176742).

NCEER-91-0022 "Proceedings from the Implementation of Earthquake Planning and Education in Schools: The Need for Change - The Roles of the Changemakers," by K.E.K. Ross and F. Winslow, 7/23/91, (PB92-129998).

NCEER-91-0023 "A Study of Reliability-Based Criteria for Seismic Design of Reinforced Concrete Frame Buildings," by H.H.M. Hwang and H.-M. Hsu, 8/10/91, (PB92-140235).

NCEER-91-0024 "Experimental Verification of a Number of Structural System Identification Algorithms," by R.G. Ghanem, H. Gavin and M. Shinozuka, 9/18/91, (PB92-176577).

NCEER-91-0025 "Probabilistic Evaluation of Liquefaction Potential," by H.H.M. Hwang and C.S. Lee," 11/25/91, (PB92-143429).

NCEER-91-0026 "Instantaneous Optimal Control for Linear, Nonlinear and Hysteretic Structures - Stable Controllers," by J.N. Yang and Z. Li, 11/15/91, (PB92-163807).

NCEER-91-0027 "Experimental and Theoretical Study of a Sliding Isolation System for Bridges," by M.C. Constantinou, A. Kartoum, A.M. Reinhorn and P. Bradford, 11/15/91, (PB92-176973).

NCEER-92-0001 "Case Studies of Liquefaction and Lifeline Performance During Past Earthquakes, Volume 1: Japanese Case Studies," Edited by M. Hamada and T. O'Rourke, 2/17/92, (PB92-197243).

NCEER-92-0002 "Case Studies of Liquefaction and Lifeline Performance During Past Earthquakes, Volume 2: United States Case Studies," Edited by T. O'Rourke and M. Hamada, 2/17/92, (PB92-197250).

NCEER-92-0003 "Issues in Earthquake Education," Edited by K. Ross, 2/3/92, (PB92-222389).

NCEER-92-0004 "Proceedings from the First U.S. - Japan Workshop on Earthquake Protective Systems for Bridges," Edited by I.G. Buckle, 2/4/92.

NCEER-92-0005 "Seismic Ground Motion from a Haskell-Type Source in a Multiple-Layered Half-Space," A.P. Theoharis, G. Deodatis and M. Shinozuka, 1/2/92, to be published.

NCEER-92-0006 "Proceedings from the Site Effects Workshop," Edited by R. Whitman, 2/29/92, (PB92-197201).

NCEER-92-0007 "Engineering Evaluation of Permanent Ground Deformations Due to Seismically-Induced Liquefaction," by M.H. Baziar, R. Dobry and A-W.M. Elgamal, 3/24/92, (PB92-222421).

NCEER-92-0008 "A Procedure for the Seismic Evaluation of Buildings in the Central and Eastern United States," by C.D. Poland and J.O. Malley, 4/2/92, (PB92-222439).

NCEER-92-0009 "Experimental and Analytical Study of a Hybrid Isolation System Using Friction Controllable Sliding Bearings," by M.Q. Feng, S. Fujii and M. Shinozuka, 5/15/92, (PB93-150282).

NCEER-92-0010 "Seismic Resistance of Slab-Column Connections in Existing Non-Ductile Flat-Plate Buildings," by A.J. Durrani and Y. Du, 5/18/92.

NCEER-92-0011 "The Hysteretic and Dynamic Behavior of Brick Masonry Walls Upgraded by Ferrocement Coatings Under Cyclic Loading and Strong Simulated Ground Motion," by H. Lee and S.P. Prawel, 5/11/92, to be published.

NCEER-92-0012 "Study of Wire Rope Systems for Seismic Protection of Equipment in Buildings," by G.F. Demetriades, M.C. Constantinou and A.M. Reinhorn, 5/20/92.

NCEER-92-0013 "Shape Memory Structural Dampers: Material Properties, Design and Seismic Testing," by P.R. Witting and F.A. Cozzarelli, 5/26/92.

NCEER-92-0014 "Longitudinal Permanent Ground Deformation Effects on Buried Continuous Pipelines," by M.J. O'Rourke, and C. Nordberg, 6/15/92.

NCEER-92-0015 "A Simulation Method for Stationary Gaussian Random Functions Based on the Sampling Theorem," by M. Grigoriu and S. Balopoulou, 6/11/92, (PB93-127496).

NCEER-92-0016 "Gravity-Load-Designed Reinforced Concrete Buildings: Seismic Evaluation of Existing Construction and Detailing Strategies for Improved Seismic Resistance," by G.W. Hoffmann, S.K. Kunnath, A.M. Reinhorn and J.B. Mander, 7/15/92.

NCEER-92-0017 "Observations on Water System and Pipeline Performance in the Limón Area of Costa Rica Due to the April 22, 1991 Earthquake," by M. O'Rourke and D. Ballantyne, 6/30/92, (PB93-126811).

NCEER-92-0018 "Fourth Edition of Earthquake Education Materials for Grades K-12," Edited by K.E.K. Ross, 8/10/92.

NCEER-92-0019 "Proceedings from the Fourth Japan-U.S. Workshop on Earthquake Resistant Design of Lifeline Facilities and Countermeasures for Soil Liquefaction," Edited by M. Hamada and T.D. O'Rourke, 8/12/92, (PB93-163939).

NCEER-92-0020 "Active Bracing System: A Full Scale Implementation of Active Control," by A.M. Reinhorn, T.T. Soong, R.C. Lin, M.A. Riley, Y.P. Wang, S. Aizawa and M. Higashino, 8/14/92, (PB93-127512).

NCEER-92-0021 "Empirical Analysis of Horizontal Ground Displacement Generated by Liquefaction-Induced Lateral Spreads," by S.F. Bartlett and T.L. Youd, 8/17/92, (PB93-188241).

NCEER-92-0022 "IDARC Version 3.0: Inelastic Damage Analysis of Reinforced Concrete Structures," by S.K. Kunnath, A.M. Reinhorn and R.F. Lobo, 8/31/92, (PB93-227502, A07, MF-A02).

NCEER-92-0023 "A Semi-Empirical Analysis of Strong-Motion Peaks in Terms of Seismic Source, Propagation Path and Local Site Conditions, by M. Kamiyama, M.J. O'Rourke and R. Flores-Berrones, 9/9/92, (PB93-150266).

NCEER-92-0024 "Seismic Behavior of Reinforced Concrete Frame Structures with Nonductile Details, Part I: Summary of Experimental Findings of Full Scale Beam-Column Joint Tests," by A. Beres, R.N. White and P. Gergely, 9/30/92, (PB93-227783, A05, MF-A01).

NCEER-92-0025 "Experimental Results of Repaired and Retrofitted Beam-Column Joint Tests in Lightly Reinforced Concrete Frame Buildings," by A. Beres, S. El-Borgi, R.N. White and P. Gergely, 10/29/92, (PB93-227791, A05, MF-A01).

NCEER-92-0026 "A Generalization of Optimal Control Theory: Linear and Nonlinear Structures," by J.N. Yang, Z. Li and S. Vongchavalitkul, 11/2/92, (PB93-188621).

NCEER-92-0027 "Seismic Resistance of Reinforced Concrete Frame Structures Designed Only for Gravity Loads: Part I - Design and Properties of a One-Third Scale Model Structure," by J.M. Bracci, A.M. Reinhorn and J.B. Mander, 12/1/92.

NCEER-92-0028 "Seismic Resistance of Reinforced Concrete Frame Structures Designed Only for Gravity Loads: Part II - Experimental Performance of Subassemblages," by L.E. Aycardi, J.B. Mander and A.M. Reinhorn, 12/1/92.

NCEER-92-0029 "Seismic Resistance of Reinforced Concrete Frame Structures Designed Only for Gravity Loads: Part III - Experimental Performance and Analytical Study of a Structural Model," by J.M. Bracci, A.M. Reinhorn and J.B. Mander, 12/1/92, (PB93-227528, A09, MF-A01).

NCEER-92-0030 "Evaluation of Seismic Retrofit of Reinforced Concrete Frame Structures - Part I - Experimental Performance of Retrofitted Subassemblages," by D. Choudhuri, J.B. Mander and A.M. Reinhorn, 12/8/92.

NCEER-92-0031 "Evaluation of Seismic Retrofit of Reinforced Concrete Frame Structures - Part II - Experimental Performance and Analytical Study of a Retrofitted Structural Model," by J.M. Bracci, A.M. Reinhorn and J.B. Mander, 12/8/92.

NCEER-92-0032 "Experimental and Analytical Investigation of Seismic Response of Structures with Supplemental Fluid Viscous Dampers," by M.C. Constantinou and M.D. Symans, 12/21/92, (PB93-191435).

NCEER-92-0033 "Reconnaissance Report on the Cairo, Egypt Earthquake of October 12, 1992," by M. Khater, 12/23/92, (PB93-188621).

NCEER-92-0034 "Low-Level Dynamic Characteristics of Four Tall Flat-Plate Buildings in New York City," by H. Gavin, S. Yuan, J. Grossman, E. Pekelis and K. Jacob, 12/28/92, (PB93-188217).

NCEER-93-0001 "An Experimental Study on the Seismic Performance of Brick-Infilled Steel Frames With and Without Retrofit," by J.B. Mander, B. Nair, K. Wojtkowski and J. Ma, 1/29/93, (PB93-227510, A07, MF-A02).

NCEER-93-0002 "Social Accounting for Disaster Preparedness and Recovery Planning," by S. Cole, E. Pantoja and V. Razak, 2/22/93, to be published.

NCEER-93-0003 "Assessment of 1991 NEHRP Provisions for Nonstructural Components and Recommended Revisions," by T.T. Soong, G. Chen, Z. Wu, R-H. Zhang and M. Grigoriu, 3/1/93, (PB93-188639).

NCEER-93-0004 "Evaluation of Static and Response Spectrum Analysis Procedures of SEAOC/UBC for Seismic Isolated Structures," by C.W. Winters and M.C. Constantinou, 3/23/93, (PB93-198299).

NCEER-93-0005 "Earthquakes in the Northeast - Are We Ignoring the Hazard? A Workshop on Earthquake Science and Safety for Educators," edited by K.E.K. Ross, 4/2/93.

NCEER-93-0006 "Inelastic Response of Reinforced Concrete Structures with Viscoelastic Braces," by R.F. Lobo, J.M. Bracci, K.L. Shen, A.M. Reinhorn and T.T. Soong, 4/5/93, (PB93-227486, A05, MF-A02).

NCEER-93-0007 "Seismic Testing of Installation Methods for Computers and Data Processing Equipment," by K. Kosar, T.T. Soong, K.L. Shen, J.A. HoLung and Y.K. Lin, 4/12/93, (PB93-198299).

NCEER-93-0008 "Retrofit of Reinforced Concrete Frames Using Added Dampers," by A. Reinhorn, M. Constantinou and C. Li, to be published.

NCEER-93-0009 "Seismic Applications of Viscoelastic Dampers to Steel Frame Structures," by K.C. Chang and T.T. Soong, to be published.

NCEER-93-0010 "Seismic Performance of Shear-Critical Reinforced Concrete Bridge Piers," by J.B. Mander, S.M. Waheed, M.T.A. Chaudhary and S.S. Chen, 5/12/93, (PB93-227494, A08, MF-A02).

NCEER-93-0011 "3D-BASIS-TABS: Computer Program for Nonlinear Dynamic Analysis of Three Dimensional Base Isolated Structures," by S. Nagarajaiah, C. Li, A.M. Reinhorn and M.C. Constantinou, 8/2/93.

NCEER-93-0012 "Effects of Hydrocarbon Spills from an Oil Pipeline Break on Ground Water," by O.J. Helweg and H.H.M. Hwang, 8/3/93.

NCEER-93-0013 "Simplified Procedures for Seismic Design of Nonstructural Components and Assessment of Current Code Provisions," by M.P. Singh, L.E. Suarez, E.E. Matheu and G.O. Maldonado, 8/4/93.

NCEER-93-0014 "An Energy Approach to Seismic Analysis and Design of Secondary Systems," by G. Chen and T.T. Soong, 8/6/93.

NCEER-93-0015 "Proceedings from School Sites: Becoming Prepared for Earthquakes - Commemorating the Third Anniversary of the Loma Prieta Earthquake, Edited by F.E. Winslow and K.E.K. Ross, 8/16/93, to be published.

NCEER-93-0016 "Reconnaissance Report of Damage to Historic Monuments in Cairo, Egypt Following the October 12, 1992 Dahshur Earthquake," by D. Sykora, D. Look, G. Croci, E. Karaesmen and E. Karaesmen, 8/19/93.

NCEER-93-0017 "The Island of Guam Earthquake of August 8, 1993," by S.W. Swan and S.K. Harris, 9/30/93.

NCEER-93-0018 "Engineering Aspects of the October 12, 1992 Egyptian Earthquake," by A.W. Elgamal, M. Amer, K. Adalier and A. Abul-Fadl, 10/7/93.

NCEER-93-0019 "Development of an Earthquake Motion Simulator and its Application in Dynamic Centrifuge Testing," by I. Krstelj, Supervised by J.H. Prevost, 10/23/93.

B86
9

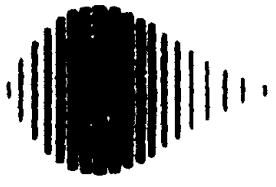

National Center for Earthquake Engineering Research
State University of New York at Buffalo